

# UNIVERSIDAD NACIONAL DE COLOMBIA

LEOPOLDO MÚNERA RUIZ  
RECTOR

JUAN CAMILO RESTREPO GUTIÉRREZ  
VICERRECTOR · SEDE MEDELLÍN

GUILLERMO LEÓN VÁSQUEZ VELÁSQUEZ  
DECANO · FACULTAD DE CIENCIAS AGRARIAS

## COMITÉ CIENTÍFICO INTERNACIONAL

<b>Rita M. Ávila de Hernández</b> , Ph.D. Universidad Centroccidental Lisandro Alvarado Barquisimeto, Lara, Venezuela. ritaavila@ucla.edu.ve	<b>Walter Motta Ferreira</b> , D.Sc. Universidade Federal de Minas Gerais. Belo Horizonte, Brasil. pereira3456@hotmail.com
<b>Felipe Bravo Oviedo</b> , D.Sc. Universidad de Valladolid. Valladolid, España. fbravo@pvs.uva.es	<b>Tomas Norton</b> , Ph.D. University of Leuven. Leuven, Flanders, Bélgica. tnorton@harper-adams.ac.uk
<b>José Rafael Córdova</b> , Ph.D. Universidad Simón Bolívar y Universidad Central de Venezuela. Baruta, Venezuela. jcordova45@yahoo.com	<b>Pepijn Prinsen</b> , Ph.D. University of Amsterdam. Holanda. pepijnprinsen33@hotmail.com
<b>José Luis Crossa</b> , Ph.D. Centro Internacional de Mejoramiento de Maíz y Trigo (CIMMYT). Texcoco, México. j.crossa@cgiar.org	<b>Aixa Ofelia Rivero Guerra</b> , Ph.D. Centro Europeo de Estadística Aplicada. Sevilla, España. rivero-guerra@hotmail.com
<b>Mateo Itzá Ortiz</b> , D.Sc. Universidad Autónoma de Ciudad Juárez Chihuahua, México. mateo.itz@uacj.mx	<b>Antonio Roldán Garrigos</b> , Ph.D. Consejo Superior de Investigaciones Científicas. Murcia, España. aroldan@cebas.csic.es
<b>Juan Pablo Damián</b> , Ph.D. Universidad de la República, Uruguay. jpablodamian@gmail.com	<b>Elhadi M. Yahia</b> , Ph.D. Universidad Autónoma de Querétaro. Querétaro, México. elhadiyahia@hotmail.com
<b>Moncef Chouaibi</b> , Ph.D. Higher School of Food Industries of Tunisia (ESIAT), Tunisia. moncef.chouaibi@yahoo.com.au	<b>Meisam Zargar</b> , Ph.D. RUDN University, Rusia. zargar_m@pfur.ru

## COMITÉ EDITORIAL

Período 2022-2024

<b>Carlos Julio Márquez Cardozo</b> , Ph.D. Editor en Jefe	Universidad Nacional de Colombia. Colombia cymarque@unal.edu.co
<b>Flavio Alves Damasceno</b> , Ph.D.	Universidade Federal de Lavras. Brasil flavioua@gmail.com
<b>Luz Estela González de Bashan</b> , Ph.D.	The Bashan Institute of Science, USA legonzal04@cibno.mx
<b>Juan Diego León Peláez</b> , Ph.D.	Universidad Nacional de Colombia. Colombia jdleon@unal.edu.co
<b>Deyanira Lobo Luján</b> , Ph.D.	Universidad Central de Venezuela. Venezuela lobo.deyanira@gmail.com
<b>Sara Márquez Girón</b> , Ph.D.	Universidad de Antioquia. Colombia saramariamarquezg@gmail.com
<b>Jousset Alexandre</b> , Ph.D.	Utrecht University. Países Bajos A.L.C.Jousset@uu.nl
<b>Juan Gonzalo Morales Osorio</b> , Ph.D.	Universidad Nacional de Colombia. Colombia jgmorealeso@unal.edu.co
<b>Jaime Parra Suescún</b> , Ph.D.	Universidad Nacional de Colombia. Colombia jeparrasu@unal.edu.co
<b>Camilo Ramírez Cuartas</b> , Ph.D.	Universidad de Antioquia. Colombia camilo.ramirez@udea.edu.co
<b>lang Schroniltgen Rondon B.</b> M.Sc. Ph.D(c)	Universidad del Tolima. Colombia isrondon@ut.edu.co
<b>Paola Andrea Sotelo Cardona</b> , Ph.D.	World Vegetable Center (WorldVeg). Taiwan paola.sotelo@worldveg.org

## EDICIÓN TÉCNICA

Mario Alejandro Vallejos Jiménez - Ingeniero Biológico. M.Eng. Química  
mavallejosj@unal.edu.co

**Periodicidad:** Cuatrimestral  
Vol. 77 No. 3 - 2024

**Admitida en las Bases**

**Bibliográficas:** Scopus  
Scielo (Scientific Electronic Library Online)  
ISI-Scielo Citation Index  
REDIB (Red Iberoamericana e innovación y conocimiento científico)  
Cabi (www.cabi.org)  
EBSCO Host  
Google Scholar  
DOAJ (Directory of Open Access Journals)  
Ulrich's Periodicals Directory (Global Serials Directory)  
Redalyc (Red de Revistas Científicas de América Latina, el Caribe, España y Portugal)  
Latindex (Sistema Regional de Información en Línea para Revistas Científicas de América Latina, el Caribe, España y Portugal)  
ProQuest  
Teeal (The Essential Electronic Agricultural Library)  
WZB (Berlin Social Science Center)  
Cross ref  
Cornell University  
Field Crop Abstracts  
Forestry Abstracts  
Plant Breeding Abstracts  
Índice Agrícola de América Latina y el Caribe  
Índice Bibliográfico Nacional  
Minciencias - Publindex  
AGRIS-FAO

**Portada:** Ocaso en el Norte Antioqueño - Yuliana María Cruz Cardona  
- Universidad Nacional de Colombia Sede Medellín, Colombia.  
ymcruz@unal.edu.co

**Contraportada:** Klara Torres Restrepo

**Dirección postal:** Apartado Aéreo 568, Medellín, Colombia

**Dirección electrónica:** rfnagron\_med@unal.edu.co

**Página Web:** <http://www.revistas.unal.edu.co/index.php/refame>

**Teléfono:** (\*4) 430 90 06; Fax: (\* 4) 230 04 20

**Diagramación:** Miryam Ospina Ocampo


**Marcación:** LandSoft S.A.

**Diseño e Impresión:** Centro de Publicaciones UN, Medellín.

**Primera edición:** Año 1939

**ISSN:** 0304-2847

**ISSN formato web:** 2248-7026

**doi:**  am

**Licencia Ministerio de Gobierno:** 275/64

- 10797 First report of bacteria associated with soft rot in yellow pitahaya (*Selenicereus megalanthus* haw.) in Colombia crops**

Primer reporte de bacterias asociadas a pudrición blanda en pitahaya amarilla en cultivos de Colombia (*Selenicereus megalanthus* haw.)

Luz Marina Lizarazo-Forero / Julián Esteban Másmela-Mendoza

- 10811 Soil quality indicators related to the deterioration of Kikuyu grass *Cenchrus clandestinus* (Hochst. ex Chiov.) Morrone**

Indicadores de calidad del suelo relacionados con el deterioro del pasto kikuyo *Cenchrus clandestinus* (Hochst. ex Chiov.) Morrone

Jorge Mario Noreña-Grisales / Ramiro Ramírez Pisco / Nelson Walter Osorio Vega

- 10827 Influence of indole-butyric acid and substrate type on vegetative propagation of native Peruvian blueberry (*Vaccinium* sp.)**

Influencia del ácido indol butírico y del tipo de sustrato en la propagación vegetativa del arándano nativo peruano (*Vaccinium* sp.)

Tito Sanchez-Santillan / Henry Santillan-Culquimboz / María Huamán Vela

- 10833 Sulfuric acid as a germination stimulator in forage soybean seeds (*Neonotonia wightii*)**

Ácido sulfúrico como estimulante de la germinación en semillas de soja forrajera (*Neonotonia wightii*)

Jhusua David Reina-García / Gustavo Almaguer-Vargas / Juan Guillermo Cruz-Castillo / Diana Guerra-Ramírez / Álvaro Castañeda-Vildozola

- 10839 Enzymatic biocatalysis processes on the semicrystalline and morphological order of native cassava starches (*Manihot esculenta*)**

Procesos de biocatálisis enzimática sobre el orden semicristalino y morfológico de los almidones nativos de mandioca (*Manihot esculenta*)

Jorge Figueroa-Flórez / Edith Cadena-Chamorro / Jairo Salcedo-Mendoza / Eduardo Rodríguez-Sandoval / Héctor Ciro-Velásquez / Tiana Serna-Fadul

- 10853 Coating of oxidized banana starch and olive oil for the preservation of cherry tomatoes (*Solanum lycopersicum* cv. Cerasiforme)**

Recubrimiento de almidón oxidado de plátano y aceite de oliva para la conservación de tomates cherry (*Solanum lycopersicum* cv. Cerasiforme)

Luis A. Cedeño Sares / Alicia Casariego Año / Mario A. García Pérez / Ney D. Jumbo-Peña / Jennifer V. Machuca Román

- 10865 Promoting food security and sustainability with a transportable indirect evaporative solar pre-cooler**

Promoción de la seguridad alimentaria y la sostenibilidad con un preenfriador solar evaporativo indirecto transportable

Nabil Shaban Mahmoud Elkaoud / Ragab Kassem Mahmoud / Hassan Hafiz Tarabye / Mahmoud Saad Adam

**10877 Artificial neural networks in the retention of anthocyanins and total phenolics in the osmotic pre-treatment of Biloxi variety blueberry (*Vaccinium corymbosum* L.) jam**

Redes neuronales artificiales en la retención de antocianinas y fenoles totales en el pre-tratamiento osmótico de mermelada de arándano (*Vaccinium corymbosum* L.) variedad Biloxi

Jesús Alfredo Obregón Domínguez / Carlos Alberto Minchón Medina  
/ Gabriela del Carmen Barraza-Jáuregui

**10887 Starch from *Colocasia esculenta* (L.) Schott of purple and white esculenta varieties: Thermal, technological properties, and morphological study**

Almidón de *Colocasia esculenta* (L.) Schott de variedades esculenta morada y blanca: Estudio de Propiedades térmicas, tecnológicas y morfológicas

José Trujillo-Ccanahuire / Elizabeth S. Ordoñez  
/ Darlym Reategui / Melchor Soria Iturri

**10899 Broiler feed proposal with vinasse**

Propuesta de alimento con vinaza para pollos de engorde

Nicolle Giraud / María Alejandra Rodríguez

**10907 Leaf spectrum analysis of three tropical timber species: Diomate (*Astronium graveolens*), Choibá (*Dipteryx oleifera*), and Algarrobo (*Hymenaea courbaril*)**

Análisis del espectro foliar de tres especies tropicales maderables: Diomate (*Astronium graveolens*), Choibá (*Dipteryx oleifera*), y Algarrobo (*Hymenaea courbaril*)

Estefany Johana Alzate-Marin / Luis Jairo Toro-Restrepo / July Andrea Suárez-Gómez

The ideas expressed in the articles published in this volume are exclusively those of the authors and do not necessarily reflect the opinion of the Facultad de Ciencias Agrarias

Las ideas de los trabajos publicados en esta entrega, son de exclusiva responsabilidad de los autores y no reflejan necesariamente la opinión de la Facultad de Ciencias Agrarias



## EVALUADORES

El Comité Editorial dentro de sus políticas, envía los artículos a especialistas, con el fin de que sean revisados.

Sus observaciones en adición a las que hacen los editores, contribuyen a la obtención de una publicación de reconocida calidad en el ámbito de las Ciencias Agrarias. Sus nombres son mencionados como una expresión de agradecimiento.

**Alio Sanda M. Djibrilla.** Faculty of Science and Technique, Abdou Moumouni University, Niamey, Niger. asmdjibrilla@gmail.com

**Jose Miguel Soto.** Universidad Nacional Agraria La Molina, Perú. jmsoto@lamolina.edu.pe

**Ana Cruz Morillo-Coronado.** Universidad Pedagógica y Tecnológica de Colombia, Colombia. ana.morillo@uptc.edu.co

**Juan Edson Villanueva Tiburcio.** Universidad Nacional Hermilio Valdizan, Perú. juanedvi@unheval.edu.pe

**Cesar García.** Universidad del Valle, Colombia. cesar.edwin.garcia@correounivalle.edu.co

**Juan Manuel Rojo Bedoya.** Universidad de Antioquia, Colombia. manuel.rojo@udea.edu.co

**Daimy Costales-Menéndez.** Instituto Nacional de Ciencias Agrícolas (INCA), Cuba. daimycostales@nauta.cu

**Juan Manuel Tito Humpiri.** Universidad Nacional de Juliaca, Perú. jtito@unaj.edu.pe

**Daryoush Babazadeh.** Faculty of Veterinary Medicine, Shiraz University, Iran. daryoush.babazadeh@shirazu.ac.ir

**Juan Martínez Solís.** Universidad Autónoma Chapingo, México. jmartinezs@chapingo.mx

**Diana M. Torres-Novoa.** Universidad Nacional Abierta y a Distancia (UNAD), Colombia. milena.torres@unad.edu.co

**Julio Echeverri Gómez.** Universidad de Antioquia, Colombia. julio.echeverri@udea.edu.co

**Elamin Mohamed Arif Abdel Hameed.** Agricultural Engineering Research Institute, Agriculture Research Center, Egypt. elaminarif@yahoo.com

**Laura Machado de Faria.** Federal University of Rio de Janeiro, Brazil. lauramdf@gmail.com

**Elizabeth Pérez-Soto.** Instituto de Ciencias Agropecuarias, Universidad Autónoma del Estado de Hidalgo, México. epsoto@uaeh.edu.mx

**Luz M. Zapata.** Universidad Nacional de Entre Ríos, Facultad Ciencias de la Alimentación, Argentina. luzmarina.zapata@uner.edu.ar

**Elsa Díaz-Montes.** Unidad Profesional Interdisciplinaria de Biotecnología, Instituto Politécnico Nacional, México. elsadimo123@gmail.com

**Marcos Alejandro Robles Lora.** Universidad Nacional de Trujillo, Perú. maroblesl@unitru.edu.pe

**Everaldo Silvino dos Santos.** Federal University of Rio Grande do Norte, Brazil. everaldo@eq.ufrn.br

**María Laura Foresti.** Instituto de Tecnología en Polímeros y Nanotecnología (ITPN), Universidad de Buenos Aires, Argentina. mforesti@fi.uba.ar

**Hassan AbdEl-Mawla.** Al-Azhar University, Assiut Branch, Egypt. HassanAbdEl-Mawla.50@azhar.edu.eg

**Néstor González-Aleman.** Facultad de Recursos Naturales y Medio Ambiente (FARENA), Bluefields Indians & Caribbean University (BICU), Nicaragua. ngonzalezaleman@yahoo.es

**Pedro Saldívar-Iglesias.** Facultad de Ciencias Agrícolas, Universidad Autónoma del Estado de México, México. psaldivari@yahoo.com.mx

**Rafael Olivero Verbel.**  
Universidad del Atlántico, Colombia.  
rafaelolivero@mail.uniatlantico.edu.co

**Rodobaldo Ortiz-Pérez.** Instituto Nacional de Ciencias Agrícolas (INCA), Cuba. rodo2110@yahoo.com.mx

**Rodrigo Alberto Hoyos Sanchez.**  
Universidad Nacional de Colombia Sede Medellín, Colombia. rhoyos@unal.edu.co

**S.P. Singh.** UGC-CAS Department of Biosciences, Saurashtra University, India. satyapsingh125@gmail.com

**Sergio Ruffo Roberto.**  
State University of Londrina, Brazil. sroberto@uel.br

**Shela Gorinstein.** Faculty of Medicine, The Hebrew University of Jerusalem, Jerusalem, Israel. gorin@cc.huji.ac.il

**T. V. Ramana Rao.** Sardar Patel University, Vallabh Vidyanagar, India. tadapanenirao@yahoo.com

**Teresa A. Coutinho.** Forestry and Agricultural Biotechnology Institute (FABI), University of Pretoria, South Africa. teresa.coutinho@fabi.up.ac.za

**Verónica Botero Fernández.** Universidad Nacional de Colombia Sede Medellín, Colombia. vbotero@unal.edu.co

**Wael Abo El-Magd Mahmoud.** Al-Azhar University, Assiut Branch, Egypt. WaelShaban.50@azhar.edu.eg

**Walter Motta Ferreira.** Department of Animal Science, Federal University of Minas Gerais, Brazil. waltermf@ufmg.br



### **The Crucial Role of Agriculture in the Colombian Economy: Challenges and Opportunities**

### **El Papel Crucial de la Agricultura en la Economía Colombiana: Retos y Oportunidades**

In Colombia's vast economic landscape, agriculture emerges as a fundamental pillar, with a significant impact on national development and the well-being of its citizens. This activity not only supports millions of rural families but also plays a crucial role in the country's trade balance and economic growth. As Colombia faces global and local challenges, it is imperative to recognize and strengthen the role of agriculture in the national economy, which has become one of its foundational pillars. According to recent data from the National Administrative Department of Statistics (DANE), the agricultural sector contributes approximately 6% of the country's Gross Domestic Product (GDP) and employs around 16% of the labor force. This significant participation demonstrates that agriculture is not only vital for food supply but also as an economic engine for society.

Colombia is a country with diverse geography that allows for the cultivation of a wide variety of products. From coffee, avocado, and cocoa in the Andean region's mountains to bananas in the Caribbean region, each area has its own specialties contributing to the country's agricultural wealth. Coffee, for example, is not only one of the main export products but also a cultural symbol of Colombian identity.

The economic impact of agriculture in Colombia is manifested in multiple ways. First, through job creation. In rural areas, agriculture is often the primary source of income. Coffee plantations, avocados, fruit trees, sugar cane, and flowers, among other products, provide employment to thousands of Colombians, often in areas where other job opportunities are scarce. Additionally, agriculture contributes to the country's trade balance. Agricultural exports represent a significant portion of Colombia's foreign trade. In 2023, exported agricultural products totaled approximately \$8.2 billion, with coffee, bananas, and flowers standing out as the main export products. This flow of foreign currency is crucial for the country's economic stability and financing imports.

However, despite its importance, agriculture in Colombia faces numerous challenges that threaten its stability and growth. Among these are insecurity in rural areas, deforestation, and climate change. Violence in some regions prevents the full development of agricultural activities and affects the safety of workers. Deforestation, partly driven by the expansion of the agricultural frontier, is destroying vital ecosystems and affecting biodiversity. Climate change is another critical challenge. Changes in precipitation patterns and extreme temperatures affect agricultural production, reducing the quality and quantity of crops. Farmers face prolonged droughts and intense rains, affecting not only crop yields but also the economic stability of rural families.

Despite the challenges, there are opportunities to transform Colombian agriculture into a more resilient and sustainable sector. The adoption of modern technologies and sustainable agricultural practices is essential to improve productivity and profitability. For example, the adoption and implementation of plant biotechnology techniques, considered a pillar of agricultural innovation. We are talking about using biological techniques necessary to improve plants in terms of yield, resistance, and food quality. Techniques such as in vitro cell and tissue culture, developing new plants through plant genetic engineering, molecular marker-assisted selection, and, lately, the gene editing. This scientific approach has revolutionized global agriculture and is beginning to show its potential in Colombia. For example, biotechnology allows for the development of crops that are more productive, disease-resistant, and

adapted to adverse climatic conditions. Genetically modified crops such as corn, cotton, and soybeans have proven more resistant to insects and diseases. Other crops, such as flowers, avocados, rice, cocoa, and sugar cane, have also been improved through plant biotechnology. (In Colombia, cocoa is one of the most profitable crops in the long term and one of the crops whose production has increased year after year, according to Eduardo Baquero López, executive president of the National Federation of Cocoa Growers of Colombia (Fedecacao), who mentions that “17 years ago, 30,000 tons were produced annually, and today around 63,416 are produced”). The banana industry expects a 5% increase by 2024, and it is reported that “during the last season (2023), accumulated exports were 106 million boxes worth USD 969 million, compared to the 2022 season, where 108 million boxes were sold for USD 891 million. The producing regions of Colombia are Urabá with 64 million boxes and Magdalena and Guajira with 42 million boxes.”

It is also necessary to mention that implementing efficient irrigation systems, using climate-resilient crop varieties, and adopting conservation tillage techniques can help mitigate some of the negative impacts. Additionally, boosting agricultural research and development can provide new solutions and improve existing practices. Partnerships between the public sector, private sector, and academic institutions can foster innovation and promote the development of new technologies that benefit farmers and the environment.

For Colombian agriculture to face its challenges and seize its opportunities, effective public policy support is essential. The Colombian government must continue strengthening support programs for farmers, ensuring they have access to financing, technical assistance, and risk insurance. Subsidy policies and soft loans can facilitate the adoption of more sustainable technologies and practices. It is also crucial to implement strategies to improve rural infrastructure, such as roads and markets, to facilitate market access and reduce transportation costs. Investment in infrastructure can improve the competitiveness of Colombian products in the international market and increase farmers' incomes.

The future of agriculture in Colombia depends on the country's ability to adapt to global and local changes. Promoting sustainable agricultural practices and including farmers in decisions affecting the sector are crucial steps to ensure balanced development. The participation of rural communities in policy and strategy formulation can ensure that their needs and perspectives are considered. Agriculture is not just an economic activity; it is a way of life for millions of Colombians. Strengthening this sector is essential for the country's economic development and improving quality of life in rural areas. With a combination of innovation, institutional support, and effective policies, Colombia can face current challenges and ensure a prosperous future for its agriculture.

**Rodrigo Alberto Hoyos Sánchez**  
Ph.D. Associate Professor  
Facultad de Ciencias Agrarias,  
Universidad Nacional de Colombia  
Sede Medellín  
rhoyos@unal.edu.co

---

# First report of bacteria associated with soft rot in yellow pitahaya (*Selenicereus megalanthus* haw.) in Colombia crops

Primer reporte de bacterias asociadas a pudrición blanda en pitahaya amarilla en cultivos de Colombia (*Selenicereus megalanthus* haw.)

<https://doi.org/10.15446/rfnam.v77n3.111234>

Luz Marina Lizarazo-Forero<sup>1</sup> and Julián Esteban Másmela-Mendoza<sup>1\*</sup>

## ABSTRACT

### Keywords:

Dragon fruit  
*Enterobacter*  
*Pantoea*  
*Pectobacterium*  
Phytopathogens

Colombia is the ninth largest producer of dragon fruit in the world and the department of Boyacá is the largest with 440 hectares planted. Bacterial phytopathogens can cause pitahaya fruit losses and low yields by producing stem soft rot. This research aimed to study and identified possible agents of bacterial diseases of pitahaya in Boyacá, Colombia. Thirteen farms in the region were selected to take 20 samples by means of a targeted and random sampling of stem and fruit tissues with soft rot symptoms in the early stages of the disease. A process of microbiological isolation, biochemical and molecular taxonomic identification of the isolated bacteria. The 16s rRNA gene sequences of the V2-V5 region were edited by removing the primers, assembling and obtaining the consensus sequence of the primers 1100R-337F and 800R -518F. The phylogenetic analysis was performed by BLAST at NCBI, using the "Classifier" and "SeqMatch" tools from the RDP website, and phylogenetic trees were created by multiple alignment using the MUSCLE algorithm and the Tamura Nei distance method was performed. Signs like blisters and mucilaginous fluids, symptoms like yellow and brown chlorotic spots, soft rot, and liquefaction were identified, and possible vectors like flies and ants were report. Twenty-five bacterial morphotypes were identified classified in 4 phyla, 9 families and 13 genera. The analysis of the 16S rRNA gene sequences of the bacterial strains showed a 98 to 100% identity with *Enterobacter cloacae*, *Pectobacterium carotovora* and *Paenibacillus glucanolyticus*, reported in other studies as causing the soft rot of the pitahaya stem and fruit. New species were reported as possible pathogenic bacteria of pitahaya: *Pantoea cypripedii*, *Kluyvera intermedia* and *Klebsiella oxytoca*. Infectivity assays did not have positive results. The microbiota identified in the stages of the necrotrophic phase or final stage of soft rot of the stem belong to the genera *Achromobacter*, *Sphingobacterium*, *Pseudomonas*, *Klebsiella*, *Paenibacillus*, *Bacillus*, *Stenotrophomonas* and *Microbacterium*. In the fly *Leptoglossus zonatus* associated with the crop were identified *Pseudomonas fulva* and *Lysinibacillus fusiformis* were identified. This is also the first official report of a complex of possible phytopathogen bacteria of the order Enterobacterales (Enterobacteriaceae, Erwiniaceae and Pectobacteriaceae family) in symptoms by bacterial disease on pitahaya Colombian crops. Identification of the bacteria in a pathogenic system can guide chemical and biological control practices in order to increase the productive and export potential of exotic and orphan crops from small local farmings.

## RESUMEN

### Palabras clave:

Pitahaya  
*Enterobacter*  
*Pantoea*  
*Pectobacterium*  
Fitopatógenos

Colombia es el noveno productor de pitahaya amarilla en el mundo y el Departamento de Boyacá es el mayor productor con 440 hectáreas plantadas. Los fitopatógenos bacterianos pueden causar pérdidas de frutos de pitahaya y bajos rendimientos al producir la pudrición blanda de los tallos. El objetivo de esta investigación fue estudiar e identificar posibles agentes de enfermedades bacterianas de la pitahaya en Boyacá, Colombia. Trece (13) fincas de la región fueron seleccionadas para la toma de 20 muestras mediante un muestreo dirigido y al azar de tejidos de tallo y frutos con síntomas de pudrición blanda en estadios iniciales de la enfermedad. Se realizó un proceso de aislamiento microbiológico, identificación bioquímica y taxonómica molecular de las bacterias aisladas. Las secuencias del gen ARNr 16s de la región V2-V5 fueron editadas mediante la eliminación de los primers, ensamblaje y obtención de la secuencia consenso de los primers 1100R-337F y 800R -518F. El análisis filogenético fue hecho por BLAST en el NCBI, por las herramientas "Classifier" y "SeqMatch", del sitio Web del RDP y se realizaron árboles filogenéticos mediante alineamiento múltiple usando el algoritmo MUSCLE y el método de distancias de Tamura Nei. Se registraron signos como ampollas y fluidos mucilaginosos, síntomas como manchas cloróticas amarillas y marrones, pudrición blanda y licuefacción, y se reportaron posibles vectores como moscas y hormigas. Veinticinco (25) morfotipos de bacterias fueron clasificados en 4 filos, 8 familias y 13 géneros. El análisis de las secuencias del gen ARNr 16S de las cepas bacterianas mostró una identidad del 98 al 100% con *Enterobacter cloacae*, *Pectobacterium carotovora* y *Paenibacillus glucanolyticus*, reportados en otros estudios como causantes de la pudrición blanda del tallo y fruto de pitahaya. Se reportaron nuevas especies como posibles bacterias patógenas de pitahaya: *Pantoea cypripedii*, *Kluyvera intermedia* y *Klebsiella oxytoca*. Los ensayos de infectividad no arrojaron resultados positivos. La microbiota identificada en los estadios de la fase necrotrofa o final de la pudrición blanda del tallo podría estar conformada por los géneros *Achromobacter*, *Sphingobacterium*, *Pseudomonas*, *Klebsiella*, *Paenibacillus*, *Bacillus*, *Stenotrophomonas* y *Microbacterium*. En la mosca *Leptoglossus zonatus* asociada al cultivo se identificó *Pseudomonas fulva* y *Lysinibacillus fusiformis*. Este es el primer registro oficial de un complejo de posibles bacterias fitopatógenas del orden Enterobacterales (familia Enterobacteriaceae, Erwiniaceae y Pectobacteriaceae) en síntomas por enfermedad bacteriana en cultivos colombianos de pitahaya. La identificación de las bacterias de un pato-sistema puede orientar las prácticas de control químico y biológico con el fin de incrementar el potencial productivo y de exportación de los cultivos exóticos y huérfanos de las pequeñas fincas locales.

<sup>1</sup>Grupo Biología Ambiental, Universidad Pedagógica y Tecnológica de Colombia, Tunja, Colombia. [luz.lizarazo@uptc.edu.co](mailto:luz.lizarazo@uptc.edu.co) , [Julian.masmela@udea.edu.co](mailto:Julian.masmela@udea.edu.co) 

\*Corresponding author

The pitahaya is a cactus, native to the Andean region of the tropics and subtropics of Central and South America, mainly cultivated in Bolivia, Ecuador, Colombia, and Brazil (Vilaplana et al. 2018).

Pitahaya cultivation in Colombia has a high commercial value as an export crop because it is an exotic fruit known as dragon fruit in markets such as Japan, Europe, the United States, and Canada (Agronet 2022). The yellow pitahaya is a fruit with a high demand for its unique appearance, flavor, quality, and nutritional properties in vitamins, antioxidants, high fiber, flavonoids, and phenol contents (Ibrahim et al. 2018; Betancur et al. 2020; Pásko et al. 2021; Da Graca et al. 2023).

Colombia is the ninth supplier of this exotic fruit worldwide. The country has 827 planted areas, it produced 124.5 million tons and 17 thousand tons which represented 38% of the total international exports (Agronet 2022). In 2009, Colombia was the main producer of pitahaya in the world (FAO 2009). The Boyacá's department is the main producer with about 440 hectares planted. Hence, in the municipality of Miraflores, in Boyacá there are 53 farms producing pitahaya, with a cultivated area of 42 hectares (Morillo-Coronado et al. 2022).

The most widely planted genotypes currently in production systems of Boyacá, Colombia is the yellow pitahaya, *Hylocereus megalanthus* known as *Selenicereus megalanthus* (Morillo-Coronado et al. 2021). One of the limiting factors in the production of the pitahaya crop is the diseases caused by phytopathogens and can cause losses in productivity because the bacteria can infect plants during processes of establishment and growth of the crop. The phytopathogens can infect stems, developing fruits, and post-harvest fruits (Balendres and Bengoa 2019; Lozada et al. 2022). However, there are few official reports on the composition of the bacterial community in pitahaya diseases (Peng et al. 2022). The pitahaya is vulnerable to bacteria, fungi, viruses, and some insect pests and it has been reported 17 genera and 25 species of phytopathogens. The bacterial phytopathogens identified are *Enterobacter cloacae*, *Enterobacter hormaechei* and *Paenibacillus polymixa* (Balendres and Bengoa 2019). *Enterobacter cloacae* has been reported to cause disease in Malaysian crops (Masyahit et al. 2009), while *Paenibacillus polymixa* was identified as the cause of soft rot in China (Zhang et al. 2017). *Enterobacter cloacae* has

been detected in *H. undatus* in Peru (Soto et al. 2019). The first report of stem rot in *H. costaricensis* for Costa Rica identified the bacterial isolation of *Enterobacter hormaechei* (Retana et al. 2019).

Although the main producer of pitahaya in Colombia is the department of Boyacá, there is a lack of technical and scientific research studies that can improve the agronomic practices of farmers in the sector (Gaona et al. 2015). Likewise, there are no official reports of the disease-causing agents for pitahaya crops in the country. Agronomic practices are based on the empirical knowledge of the farmer and the conversion to techniques of integrated disease management can be a solution to the problems (Gaona et al. 2015). In Colombia, phytosanitary problems have been described such as basal rot of the stem and fruit caused by *Fusarium oxysporum*, dry rot of the stalk caused by *Dreschlera cactivora*, Anthracnose caused by the fungus *Colletotrichum*, bacteriosis presumably associated with *Erwinia*, and the nematodes *Meloidogyne* (Burgos 2013; Gaona et al. 2015; Salazar-González et al. 2016). There are no official reports of the identification of bacteria isolated from signs and symptoms of soft rot for the region. Due to the lack of official publications, this research aimed to analyze the etiology of the disease, identify and characterize the composition of the cultivable bacterial community associated with soft in yellow dragon fruit (*Selenicereus megalanthus* haw.) of Boyacá, Colombia.

## MATERIALS AND METHODS

### Sampling locations

The study was done in 13 yellow pitahaya farms with open field production systems and covered crops (*S. megalanthus*) located in the Municipality Miraflores, Department of Boyacá (Colombia) (05°14'121" N; 073°11'949" W). The region has an average annual temperature of 19.5 °C and a relative humidity of 88.9%.

The soil fertilization management is rich in major elements. The farmers do a chemical control of diseases with Oxychloride (80 g 20 L<sup>-1</sup>), the curative and preventive contact iodine liquid Baladine® (100 mL 20 L<sup>-1</sup>) or powder (80 g 20 L<sup>-1</sup>). Diseases with high incidence included basal rot, fungal symptoms and signs with unidentified microbial agents, and pests included the flower bud fly (*Dasiops saltans*) and the potato bug (*Leptoglossus zonatus*).



### Sampling

Pitahaya plants in the initial stage of flowering and full fruit production were sampled. The sampling was random, selecting material according to the observation of signs and symptoms in the tissues. A minimum of 20 samples were collected per farm. Samples of stems and fruits with chlorosis, yellow to brown halos, and aqueous tissues due to rotting, were collected mainly in the initial stages of the disease. The plant material was placed in plastic bags and placed in portable refrigerators (0 to 4 °C) and taken to the laboratory. Photographs were made during the sample collection process, identifying the signs and symptoms of bacterial disease.

### Isolation of bacteria associated with symptoms

Bacterial isolations using cultivable microbiological techniques were obtained from the symptomatic cladodes and fruits showing lesions. The surface of the tissues was disinfected with 70% alcohol for 1 min and rinsed with sterile water. Pieces approximately 1 mm wide and no more than 3 mm long were cut from the lesion and mixed with a few drops of sterile distilled water for 2 to 4 min to allow bacteria to flow into the fluid. Likewise, the tissues were placed in a sterile 0.85% saline solution and vortexed for 2 min. The aliquotes were taken from this suspension with a bacteriological loop and streak plates of nutrient agar (Merck®) [Composition: Peptone (5 g L<sup>-1</sup>), meat extract (3 g L<sup>-1</sup>), NaCl (8 g L<sup>-1</sup>), bacteriological agar (15 g L<sup>-1</sup>)]. A 100 µL aliquot was also taken and streaked with a Drigalsky loop. The plates were incubated at 30 °C for 24 to 48 h. Controls were set up to discriminate epiphytic microbiota. Sterile swabs were passed over the surface of the tissue and immersed in 0.85% saline solution. 100 µL aliquots were plated on nutrient agar and incubated at 37 °C during 48 h. Epiphytic colonies were discriminated from the isolates obtained in diseased tissues. Five samples of diseased tissue per farm were analyzed. Five pieces were taken from each sample of diseased tissue and planted in triplicate. In total, 65 samples were analyzed and around 200 culture media were planted. The different colonies were plated again on nutrient agar plates and this process was repeated until purified bacterial cultures with homogeneous colony morphology were obtained.

### Biochemical and molecular identification of bacterial isolates

Microscopic morphology was performed using Gram

staining and Gram-negative colonies were cultured in MacConckey medium (Merck®). Biochemical identification was performed using the API 20NE® and API20 E® technique (BioMérieux, France) according to the manufacturer's instructions. The following biochemical tests were made: fermentation or oxidation of carbohydrates such as glucose, mannitol, sorbitol, sucrose, arabinose, and rhamnose. It also includes gelatin, tryptophan to produce indole-acetic acid, cytochrome oxidase, arginines, urease test, and the production of acetoin (Voges-Proskauer), among others. The results obtained from the negative or positive reactions were transformed into a 7-digit code called numerical profile entered into the Apiweb® [CD-ROM] BioMérieux software (2010). For the identifications, the Percent Probability of Identity and the T probability value were evaluated. The bacterial strains were preserved in 20% glycerol at -20 °C and in cryovial with conservation beads.

For molecular characterization and identification, the selected bacterial strains were subjected to analyses of 16S ribosomal RNA gene by V2-V5 region sequencing. The selected bacterial strains were grown in trypticase soy agar (Merck®), and the DNA was extracted using DNeasy UltraClean Microbial Kit MoBio®. The 16S rRNA genes were amplified by PCR using the 337F (5' GACTCCTACGGGAGGCWGCAG 3'), 518F (5' CCAGCAGCCGCGGTAATACG 3'), 800R (5' TACCAGGGTATCTAATCC 3'), and 1100R (5' GGGTTGCGCTCGTTG 5'). The amplification of the V2-V5 region of the 16S rRNA gene was done in a final volume of 20 µL, using 100 ng of genomic DNA as a template, and with a concentration of: 0.5 mM of each of the oligonucleotides, 200 µM of each of the 4 dNTPs (dATP, dGTP, dCTP, and dTTP), 1X GoTaq Flexi Buffer, 2.5 mM MgCl<sub>2</sub>, and 1 U of GoTaq® Taq Polymerase. The PCR cycle was made in an ESCO® SWT-MXB-1 thermocycler under the following conditions: i) One denaturation cycle of 1 min at 94 °C, ii) 30 amplification cycles: 30 s at 94 °C, 30 s at 55 °C and 1 min at 72 °C and iii) final extension of 10 min at 72 °C. The purification process of the PCR fragments and sequencing was done using the Sanger method. The 16s rRNA gene sequences of the V2-V5 region were edited by removing the primers, assembling and obtaining the consensus sequence. The DNA sequences obtained were analyzed with the basic sequence alignment (BLAST) run against the database from the National Center for

Biotechnology Information Blast ([www.ncbi.nlm.nih.gov/BLAST](http://www.ncbi.nlm.nih.gov/BLAST)). The taxonomic analysis of the sequence was made using the “Classifier” and “SeqMatch” tools, hosted on the RDP (Ribosomal Data Project) website (<https://bio.tools/rdp>). Next, the multiple alignment was made using the Multiple Sequence Comparison by Log-Expectation (MUSCLE) algorithm with the thirty most similar bacterial sequences reported by Basic Local Alignment Search Tool (BLAST) in NCBI, for the generation of a phylogenetic tree using the model of Tamura-Nei genetic distance, with the “Neighbor-Joining” method and the “Bootstrap” method with a thousand replicates. The phylogenetic analysis was done by multiple alignment using the MUSCLE algorithm and the Tamura Nei distance method in the statistical program Geneious prime (2024.0.5).

#### ***In-vitro* pathogenicity assay and bacteria in insect vector**

A pathogenicity assay was done to evaluate Koch's postulates to determine the causal agents of the observed symptoms. The cultures of the *Pectobacterium* and *Enterobacter* cultured in nutritive agar medium (Merck®) were suspended in sterilized water ( $10^8$  CFU mL<sup>-1</sup>). Four pitahaya stems 4 to 6 cm in diameter were inoculated with 20 µL bacterial suspension on each stem by injection at two opposite locations with a depth of 2 mm. For the control, stems were injected with sterilized water. The inoculated stems were wrapped in clear plastic and incubated at 26 °C for 5 days before the observation of rotting symptoms. Since no pathogenic response was obtained with the first infection procedure, a second infection test was performed. Healthy pitahaya stems were cut, washed with sterile distilled water, disinfected with 1% sodium hypochlorite and finally rinsed with sterile distilled water. The stems were placed in Petri dishes and pierced in several places with toothpicks impregnated with the bacteria. Control stems were pierced with the tips of toothpicks containing Nutrient Agar only. They were sealed and incubated at 30 °C for 72 h.

To verify a possible relationship between insects as vectors of phytopathogenic bacteria, a direct collection of 10 insects of the species *Leptoglossus zonatus* (Dallas) (Hemiptera: Coreidae) was made up. This insect causes damage to the flower buds and cladode in yellow pitahaya (Medina and Kondo 2012). Each collected insect was deposited alive in sterile glass jars. In a laminar flow chamber, live insects

were picked up with sterile forceps from the midsection (between the thorax and the abdomen) and their legs were brought into contact with the Trypticase soy agar culture medium. The plates were incubated at 28 °C and examined daily for bacterial growth that occurred at 48 h.

## **RESULTS AND DISCUSSION**

### **Description of signs and symptoms of the bacterial disease**

The affected plants with brown and yellow spots were observed more frequently. Some cladodes show liquefaction, with strong bacterial odors, and postharvest fruits with yellow-brown lesions (Figure 1). The symptoms can begin with small chlorosis of the stems, and it can spread throughout the entire area of the cactus pads, to later generate softening of the stem, dark brown coloration with odors of bacterial rot.

From the observations and photographs, the possible development initial stages of the disease were reconstructed (Figure 1). The bacteria enter the peduncles through a vector during the first stages related to the biotrophic phase of the microorganism. The microorganisms could enter by small drops of water or by exposure to the mucilage of another diseased plant, and forming symptoms like yellowish chlorotic halos on the stems (Figure 1A). Initial yellow spots have been described as the initial symptoms when injecting *Enterobacter* pathogens into Pitahaya, which can take on yellow and orange colors after eight days of infection (Retana et al. 2019). The yellowish colorations or chlorotic symptoms spread along the surface of the stem with black borders on the outside of the diseased tissue (Figure 1B, C). Valencia et al. (2003) reported an unidentified Enterobacteriaceae as the causal agent that in the initial stages produces a yellow chlorotic halo. The starting point of chlorotic spots can be in the center of the stem or edges. For example, Soto et al. (2019) describe that initial yellowish or chlorotic spots may begin on the protruding edges of the stem and may extend to the center of the stem.

Subsequently, the injured tissue becomes inflamed, forming a blister that accumulates a translucent liquid, with a mucilaginous appearance or mucus. The fluid is secreted and can run down the entire surface of the stem. This fluid may be a mechanism of persistence and dispersion of the bacteria (Figure 1D, F). Meanwhile,



Masyahit et al. (2009) describe several isolates of the Enterobacteriaceae family such as *Enterobacter*, *Pantoea*, *Klebsiella* in symptoms of yellow chlorosis that the

symptoms caused by *Enterobacter* do not affect vascular bundles, but yellow and dark brown chlorotic halos can develop.

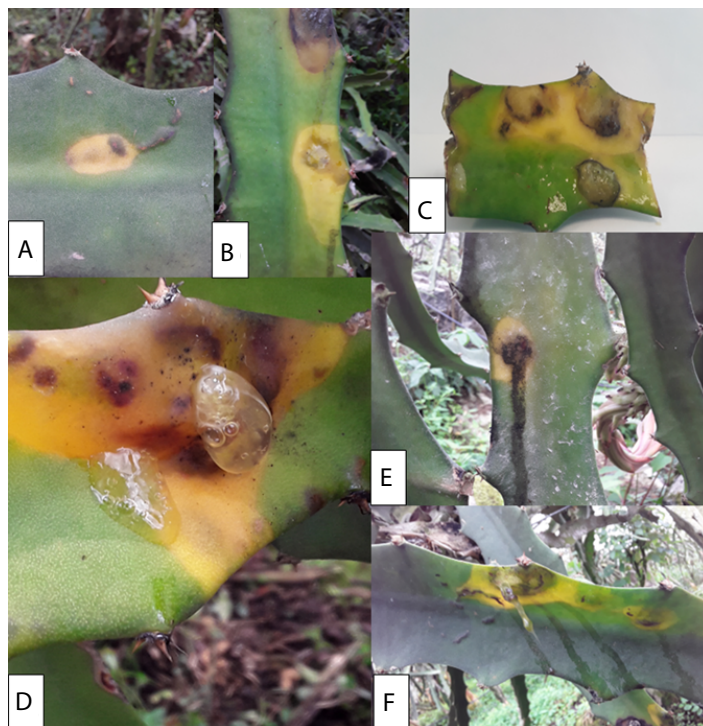


**Figure 1.** Initial stages of symptoms associated to bacterial disease in Pitahaya (*Selenicereus megalanthus* Haw.). A-B) First symptoms of the disease, with forms of yellow chlorotic halos can start in a black spot. C) Blister formed from the disease. D) The clearest sign of the disease is the discharge of a mucilaginous fluid developed in the symptoms of chlorosis and blisters. E-F) Mucilage can run down the stem and flows from the lesions.

In the final phases of the development of the disease, the tissue can show liquefaction, strong odors related to bacterial growth, and extensive decomposition in the tissue. It would be the final necrotrophic phase of the bacteria. In the final symptoms of the disease, some cladodes stop the progression of the disease, while in others the necrosis is total (Soto et al. 2019). The arrest of symptoms in a stem can be caused by the high calcium contents that the plant can store in the form of oxalate (Faheed et al. 2013; Retana et al. 2019). Furthermore, Soto et al. (2019) describes a decomposed stems with strong bacterial odors detach from healthy tissue under their own weight, and the plants can keep vascular bundles and epidermis intact attached to healthy stems.

#### Bacteria identified in soft rot

A total of 25 bacterial isolates were cultured. Microscopic morphology was performed by Gram stain, described

16 strains corresponding to Gram-negative bacilli, and these were cultured twice in MacConkey agar and conducted biochemical tests using API 20E® and API 20NE® kit (BioMérieux, France) (Table 1). Genera such as *Enterobacter*, *Erwinia*, *Pseudomonas*, and *Pantoea* were identified with a high percentage of identity from the biochemical tests According to the API code (Table 1). The *Enterobacter* strains can produce  $\beta$ -galactosidase, arginine dehydrolase, ornithine decarboxylase and gelatinase in this metabolism. Likewise, the *Enterobacter* strain produce acetoin and can oxidize or ferment citrates, glucose, mannitol, inositol, rhamnose, cellobiose and arabinose. This metabolic versatility could be used by the phytopathogen in the biotrophic phases to penetrate cell walls by liquefaction of pectins and in the necrotrophic phase to take advantage of the photosynthate organic compounds of pitahaya. Aerobic chemoheterotrophy and oxydative functional group have been identified in

the core microbiome of soft rot by metagenomic function prediction, suggesting that plant pathogenic bacteria need

to break down tissue organic matter in the early stages of plant-pathogen interaction (Peng et al. 2022).

**Table 1.** Biochemical characteristics of the bacteria isolated in the symptoms for bacterial disease.

Isolates	Medium MK <sup>1</sup> lactose	Taxonomic identification by API web	API code-numeric profile	ID (%) <sup>2</sup>	T <sup>3</sup>
1.1 A1	+	<i>Enterobacter cloacae</i>	3307573	94.10	0.67
1.1 A2	+/-	<i>Erwinia</i> spp	1006573	73.2	0.67
1.1 A3	+	<i>Enterobacter cloacae</i>	3307573	94.01	0.67
3.1 A1	+	<i>Enterobacter cloacae</i>	1105053	40	0.38
		<i>Enterobacter amnigenus</i>		43	
3.1 A2	+	<i>Enterobacter amnigenus</i>	1101153	68.3	0.38
		<i>Enterobacter cloacae</i>	1105153	40	
3.1 A3	+	<i>Enterobacter cloacae</i>	3305577	98.6	0.22
			3301577		
F4 C1-9	-	<i>Pseudomonas luteola</i>	3003000	99.2	0.36
F4 C1-12 AN	+	<i>Enterobacter</i> spp	3003100		
F7 C3-19 AN	+/-	<i>Pantoea</i> spp	3377777	90	0.67
		<i>Erwinia</i> spp			
F7 C3-1	-	<i>Aeromonas hydrophyla</i>	2007333	97.8	0.22
			3047122		
8.1 A	-	<i>Erwinia carotovora</i>	3247123	85.60	0.51
8.1 A	-	<i>Pantoea</i>	1207333	84	0.73
F8 C4-21	+	<i>Pantoea</i> spp	1206333	62.6	0.6
F8 C4-3	+	<i>Pantoea</i> spp	1206333	62.6	0.6
9.1 A	-	<i>Erwinia</i> spp	1003133	99.7	0.54
		<i>Erwinia carotovora</i> sub. <i>carotovora</i>			
F9 C5-19 A	-	<i>Morganella morganii</i>	0175000	99.6	0.5
10.1 AN	+	<i>Enterobacter cloacae</i>	3301573	98.6	0.72

<sup>1</sup>MacConkey's Medium; <sup>2</sup>ID%: Identity Probability Percentage; <sup>3</sup>T: Probability T value.

The cultivable microbiota of the pitahaya's soft rot in Boyacá, Colombia is composed by 25 morphotypes grouped into 4 phyla (Firmicutes, Actinobacteriota, Bacteroidota, Proteobacteria or Pseudomonadota), 6 classes, 8 orders, 9 families, 13 genera and 25 morphotypes (Figure 2). Bacteria identified by ARNr 16S gene sequencing were clustered with 97-99% relationship with other type strain or ATCC reference sequences from the gene bank based on the phylogenetic and taxonomic analysis by BLAST in NCBI and the Ribosomal Data Project (Figure 2). Four strains studied corresponded to the genus *Enterobacter* (two *E. cloacae*, and species like *E. ludwigii*). *Enterobacter* strains were

isolated from stem lesions and postharvest fruit. The two strains *Pectobacterium carotovora* were isolated from diseased stems. Likewise, *Paenibacillus glucanolyticus* is identified in the symptoms of chlorosis in stems and soft rot of fruits.

This study demonstrated the association of three bacterial species with the disease symptoms reported in the literature with soft rot of the Pitahaya stem: *Enterobacter cloacae*, *Pectobacterium carotovora* and *Paenibacillus glucanolyticus*. In addition, two new species are reported as possible phytopathogenic bacteria of pitahaya: *Pantoea cypripedii* and *Enterobacter ludwigii*. It is important to

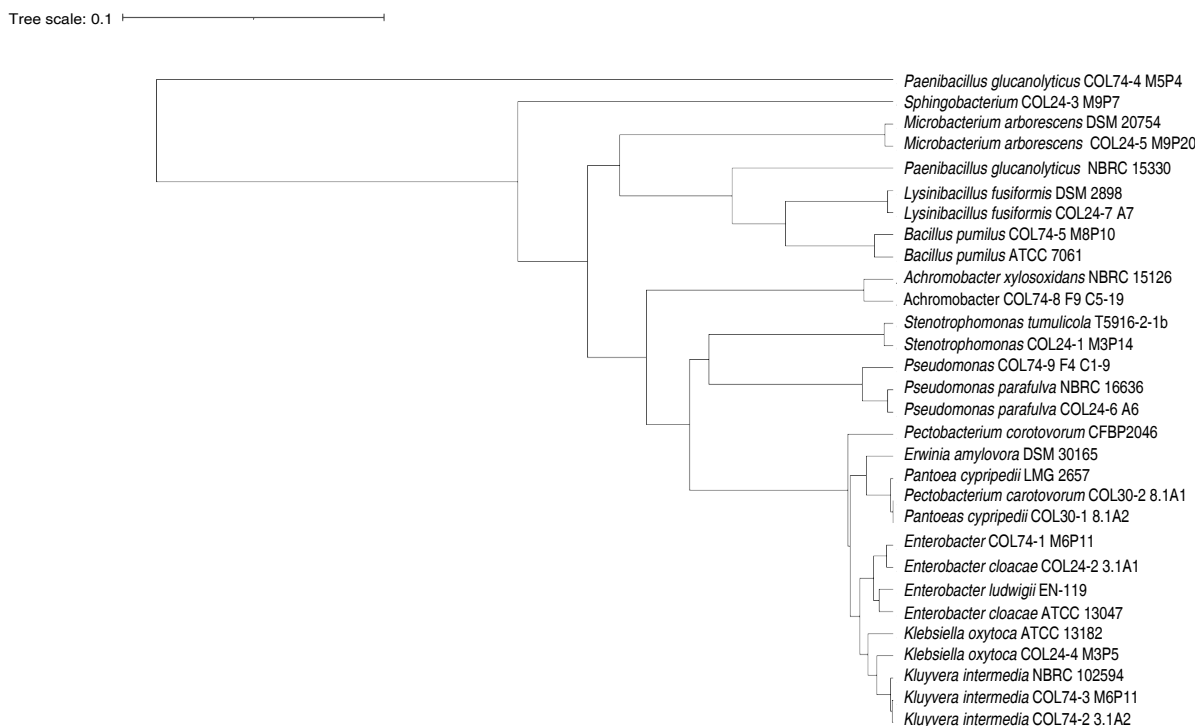


**Figure 2.** Phylogenetic tree based on 16S rRNA gene sequences of bacteria isolated in signs and symptoms of soft rot from *Selenicereus megalanthus* crops from Boyacá, Colombia. The COL initials of the strain identification code refer to the bacteria isolates for Colombia. The Variable regions of the 16S rRNA gene were sequenced with primers 1100R-337F and 800R-518F. The tree was constructed using the genetic distance model of Tamura Nei and UPGMA Tree building method.

highlight how four genera of bacteria (*Enterobacter*, *Pantoea*, *Kluyvera*, *Erwinia* and *Pectobacterium*) belonging to the Enterobacteriales order were identified in the symptoms of the bacterial disease in Pitahaya. The three closely related families (Enterobacteriaceae, Erwiniaceae and Pectobacteriaceae) are part of Enterobacteriales, assigned from the very close phylogenetic clades of *Enterobacter*-*Escherichia*, *Erwinia*-*Pantoea*, *Pectobacterium*-*Dickeya* (Adeolu et al. 2016). This result may suggest an enterobacterial complex causes diseases Pitahaya crops and a possible coevolutionary relationship in the plant-pathogen interaction. Enterobacteriaceae soft rot (ESR) has been identified by different genera according to the taxonomic assignments made for some strains, from *Erwinia* (in 1917) to some strains classified as *Pectobacterium* and *Dickeya* (in 1945) and currently as *Pantoea* (Brady et al. 2010; Charkowski et al. 2014; Adeolu et al. 2016). Different bacterial isolates classified in the three genera have been reported as causative agents of soft rot in tubers, rice, corn and brassicas (Charkowski et al. 2014).

The *Enterobacter* strains have been frequently reported as a phytopathogen of pitahaya. Masyahit et al. (2009) isolated *Enterobacter cloacae* from pitahaya stem infected with soft rot. Isolates bacterial of *Enterobacter cloacae*, *Enterobacter nimipressuralis*, and *Enterobacter pyrinus* have been identified in soft rot of *Hylocereus undatus* from China (Lin et al. 2015). In Costa Rica for *Hylocereus costaricensis* and *Hylocereus undatus* in Peru, *Enterobacter hormaechei* and *Enterobacter cloacae* was isolated as the causal agent soft rot, respectively (Retana et al. 2019; Soto et al. 2019). In the study by Peng et al. (2022), samples of soft rot symptoms in *Hylocereus* were analyzed using metagenomic libraries of the 16s rRNA gene. These researchers have detected a high abundance of operational taxonomic units (OTU) of *Enterobacter* and *Pseudomonas* as predominant genera in the development of the disease. Similarly, *Enterobacter* strains have been identified as endophytic bacteria in pitahaya seedlings that can induce typical soft rot symptoms (Lin et al. 2015). It is interesting how *Enterobacter* species have been reported

as plant growth-promoting bacteria (Ogbo and Okonkwo 2012), as commensal and beneficial endophytic bacteria (Grimont and Grimont 2006). However, they have also been reported as phytopathogenic bacteria (Soto et al. 2019). The change of a bacteria between two behavioral states (asymptomatic endophyte and pathogenic) is interesting because a microbial group can transit in the middle of a commensalistic relationship with the plant (Stengel et al. 2022). This theory can be explained by the concept of continuum endophyte. Certain bacterial taxonomic groups can exhibit pathogenic or mutualistic traits depending on the environmental niche, the phenological state of the plant, and the association with the host (Stengel et al. 2022). This theory can be explored in the future research in the ecological system of pitahaya-*Enterobacter*.

The genera *Achromobacter*, *Pseudomonas*, *Klebsiella*, *Stenotrophomonas*, *Microbacterium*, and *Sphingobacterium* were identified by molecular techniques like the microbiota associated with stem symptoms, possibly as endophytes, phytopathogenic, necrotrophic or environmental bacteria (Figure 2). Pierangeli (2019) also identified three endophytic bacteria that reside on host plants without causing symptoms like *Microbacterium* (*M. arborescens*, *M. testaceum* and *M. imperial*), *Pseudomonas rhodesiae*, *Enterobacter asburiae*, and *Bacillus altitudinis* by the Maldi-TOF MS technique in fresh pitahaya pulp (*Hylocereus undatus*) with lesions of gelatinous spots. This genera are considered biological control agent and/or plant growth promoting bacteria. These microorganisms are beneficial to the plant and can establish mutualistic interactions like endophytic bacteria; however, during the development of a disease, in tissue decomposition, they can take advantage of nutritional resources such as carbon and energy sources to proliferate in lesions. Further study of the interaction of these strains in the development of the disease is necessary, since genera such as *Pseudomonas*, *Paenibacillus*, *Microbacterium* and *Sphingobacterium* have been reported as the most abundant in the bacterial community of the disease during the late stages or necrotrophic phase (Peng et al. 2022). This suggests a role like pathogens or opportunistic copiotrophic bacteria. Equally, in pitahaya stem tissues affected by soft rot caused by *Enterobacter*, non-pathogenic bacteria have also been identified such as *Klebsiella mobilis*, *K. oxytoca* and *Pantoea dispersa* (Masyahit et al. 2009). In this research, *Achromobacter*, *Pseudomonas*, *Klebsiella*,

*Stenotrophomonas*, and *Microbacterium* were identified as endophytic microbiota accompanying the development of the disease, and they could be heterotrophic, opportunistic, and copiotrophic bacteria that appear in the decomposition process in the necrotrophic phase of the soft rot. In addition to the isolated bacteria, fungi of the special *Fusarium fujikoro* Complex (in the publication process) were isolated from some of the liquefied lesions and it is a pending report to be made.

It is interesting how some genera identified in this study could play an important role in infectivity. For example, *Sphingomonas*, *Enterobacter* and *Pseudomonas* could play an important role in the biotrophic stage of the disease. Their increase is related to chemo-heterotrophy, heterotrophy and symbiotic or parasitic interaction with the plant. During the development of the disease there is a change in the composition of the disease. *Enterobacter* is the genus that could be guiding or modulating the response of the pathogenic functional groups (Peng et al. 2022). The role of *Pseudomonas* is still not clear, since in healthy pitahaya it has been reported as abundant together with the *Enterococcus* genus (Peng et al. 2022). It would be interesting in future works to evaluate strains of these genera as biological control agent of soft rot.

#### Analysis of phylogenetic relationships of the bacterial genera identified in stem rot

The results of the taxonomic analysis for *Paenibacillus*'s DNA sequence against the NCBI ref\_seq database, indicate that it has 99% identity in 97% of its length, with 16S ribosomal gene sequences, belonging to the species *P. glucanolyticus* and *P. lautus*. The distance tree (unpublished results) constructed from the thirty closest culturable microorganism sequences available in the NCBI RefSeq\_RNA database shows clusters with sequences from the species *Paenibacillus glucanolyticus*. There is previous evidence of the participation of *Paenibacillus polymyxa* in lesions of the pitahaya species *Hylocereus undulatus*, eventually turn yellow and brown color, where finally the fleshy stems completely decompose, leaving only the woody pith stem center (Zhang et al. 2017).

This study could be considered the first scientific proof of *Pectobacterium carotovora* in soft stalk rot in yellow pitahaya in Colombia. *Pectobacterium* is known to cause destructive soft rot disease in many economically important



vegetables such as carrots, cabbage, cucumbers, onions, pepper, potatoes, and tomato (Adeolu et al. 2016). Likewise, the *Pectobacterium* genus could be causing secondary infections because it is a necrotrophic bacterium actively kills host tissue as it colonizes and thrives on the contents of dead or dying cells (Davidsson et al. 2013).

A bacterial isolate identified as *Pectobacterium* spp. by biochemical test and RDP was classified within Erwiniaceae family (Figure 3), with a high identity percentage, possibly classified as an *Erwinia amylovora* species. The assembled test sequence presents greater homology with sequences from the genus *Erwinia* spp. However, the results of the taxonomic analysis of the 1,487 bp assembled query sequence against the NCBI ref\_seq database indicate that it has a 99% identity belonging to the species *Pantoea cyripedii*, previously taxonomically classified as *Pectobacterium cyripedi*. It is considered the first report of the possible phytopathogenic strain of *Pantoea cyripedii* for Colombia identified in Pitahaya. It is necessary to deepen the investigation of this species and to review their taxonomic assignments. Brady et al. (2010) described the *Pantoea* genus became part of the *Erwinia herbicola*–*Enterobacter agglomerans* complex, with more phylogenetically close *Pectobacterium cyripedii* strains such as *Pantoea*. However, the *Pectobacterium cyripedii* species became part of *Pantoea*, as *Pantoea cyripedii*. This is an example of how the molecular taxonomic identification of phytopathogenic strains can change depending on the genomic databases used and the taxonomic reassignments of the genera studied. For a more robust taxonomic and phylogenetic analysis and to distinguish between species of *Pantoea*, sequence analysis of other genes (rpoB gen, gyrB gen, atpD gen) is necessary in an Assessment of Multilocus Sequence Analysis (MLSA). The phylogenetic relationships of the order Enterobacteriales are still not clear, within the order Enterobacteriales there are three close families: Enterobacteriaceae, Erwiniaceae and Pectobacteriaceae (Adeolu et al. 2016). The taxonomic reassignments of the strains belonging to the genera *Pectobacterium* as *Pantoea*, and the classification of some strains of *Erwinia* like *Pantoea* have been described, and it is related with the formation of different clades between *Erwinia*-*Pantoea* and the *Pectobacterium*-*Dickeya* clade (Adeolu et al. 2016). Described and discussed above, the strain identified in this study corresponds to *Pantoea cyripedii*. The genus

*Pantoea* has not been detected as a pathogenic bacterium for pitahaya Colombian crops, and it may be part of the endophyte bacterium and accompanying microbiota of bacterial symptoms (Masyahit et al. 2009). However, *Pantoea* species are pathogenic of corn, onion, rice, and eucalyptus and can proliferate in various niches and cause diseases in a wide range of hosts (Weller-Stuart et al. 2017). The above discussion can be observed in Figure 2. The *Pantoea* and *Pectobacterium* isolates recorded in this research in Colombia have a phylogenetic closeness as they are grouped in the same clades together with reference strains of the same genus and *Erwinia*.

### Pathogenicity tests

None of the plants inoculated with *Enterobacter cloacae* and *Pectobacterium carotovora* and bacteria or with sterile water had any malformation symptoms. Although Koch's postulates could not be effective to relate as a causal agent of the symptoms of bacterial disease, some of the bacterial genera identified in this study have been reported as causal agents of the disease in different dragon fruit crops. Likewise, in most inoculation assays of phytopathogenic bacteria in pitahaya, it has not been possible to achieve adequate development of symptoms and infectivity because the environmental factors involved in the phytopathogen system are still unknown (Salazar-González et al. 2016; Peng et al. 2022). Likewise, the infectivity protocols have been used in assays with dragon fruit of the genus *Hylocereus* and have not been described for *Selenicereus* infectivity assays. It is necessary to design new infectivity protocols, changing variables such as the density of the bacterial inoculum, temperature, humidity, and inoculation mechanisms. In the literature there is little evidence of positive results in a different species of pitahaya. Thus, the *in vitro* pathogenicity test in *Hylocereus* spp. was positive in caused soft rot symptoms for *Enterobacter cloacae* (Masyahit et al. 2009). The symptoms appeared 24 and 48 h after inoculation in fruit and stem. The pathogenicity test was 100% incidence in stems infected by *E. cloacae* and *E. hormaechei* for *H. undatus* and *H. costaricensis*, respectively (Masyahit et al. 2009; Retana et al. 2019; Soto et al. 2019).

For future research, it would be important to evaluate inoculations with consortia of phytopathogens. Possibly in the development of the disease is caused by communities of microorganisms that infect together. Also, is important

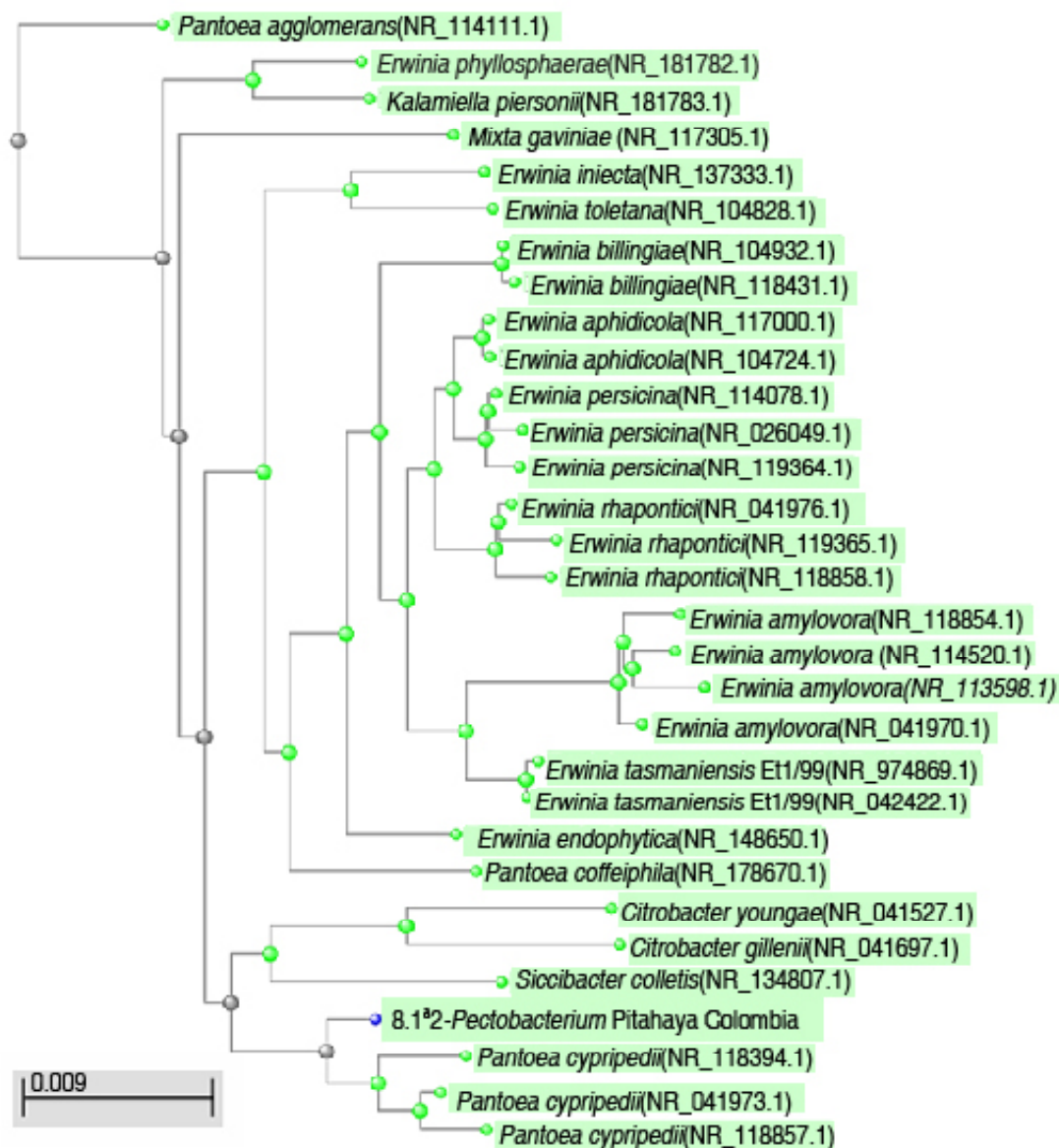


**Figure 3.** Phylogenetic tree obtained from pairwise alignment between the V2-V5 region of 16s rRNA gene sequence for the *Pectobacterium* isolate from Colombia and the NCBI BLAST 16s rRNA gene database sequences.

to improve the conditions of infectivity with plant growth rooms in greenhouses with environmental conditions of humidity, temperature and simulated rainfall, and test other inoculation techniques like the wounds caused by possible vectors.

#### Agronomic practices and vectors of bacterial diseases

All bacterial isolates were obtained from production systems under a plastic cover, in a greenhouse-type

design, regardless of whether the plants were planted in stone, cement, or wood systems. An interesting fact was not identifying signs, symptoms, or achieving isolates in those farms with good cultural management of diseases such as removal of plant material with symptoms, burning and burial with dolomite lime of diseased plant material. A good practice identified was the use of liquid biofertilizers called "mountain microorganisms", mainly based on *Trichoderma* and *Beauveria*'s fungic inoculant. In crops with this biological

control practice there was a low incidence of the disease. Cultural management and biological control of a disease are important as strategies within the intergrade management of the crop that can reduce the incidence and severity of bacterial disease in a crop (Balendres and Bengoa 2019).

The predominance of the disease in some crops can be caused by mechanical wounds to the stems from agricultural tools, insect bites, or the environment (Masyahit et al. 2009). These lesions are an entry point for bacteria that infect the plants. In environments with greater atmospheric humidity and nutrient-rich soils or with crops with foliar fertilizations, these are ideal conditions to increase bacterial growth. Mainly, most of the plant material studied presented open lesions generated by the pruning of the stems. The

identified bacteria may be in the crop environment such as water and soil and could enter open lesions through contaminated work materials. Likewise, bacteria can be transmitted by vectors such as flying insects.

Possible vectors of bacterial disease in pitahaya (*Selenicereus megalanthus* Haw.) are described in Figure 4. The Diptera are attracted to and feed on mucus or mucilage (Figure 4A). Likewise, the ants walk through the chlorotic stains and secretions and feed on the mucilage (Figure 4B). An unidentified larval stage inside the stems during the initial stages of the disease was observed. Small galleries and paths of the larva can be observed in the symptoms of bacterial disease (Figure 4D, E).

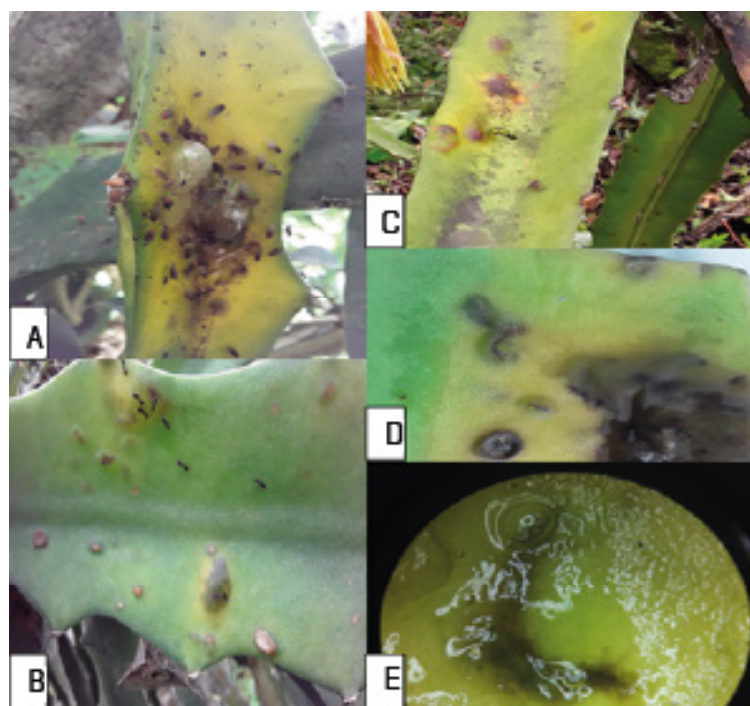


**Figure 4.** Possible vectors of bacterial disease in pitahaya (*Selenicereus megalanthus* Haw.). A) Diptera, flower bud fly (*Dasiops saltans*) are attracted to and feed on mucus or mucilage, and the fluid is one of the symptoms of bacterial disease. B) The ants walk through the chlorotic stains and excretions and feed on the mucilage that is excreted in the symptoms. C) Diptera feeds on the blisters in the early stages of the disease. D-E) Stereoscopic view (10x) of the unidentified larval stage inside the stems during the initial stages of the disease. Small galleries and paths of the larva can be observed in the symptoms of bacterial disease such as spots of chlorosis, blisters, small translucent drops, and mucoid.

For Colombian crops, the stink bug *Leptoglossus zonatus* (Dallas) (Hemiptera: Coreidae) and the pitahaya's flower bud fland *Dasiops saltans* Townsend (Diptera: Lonchaeidae) have been identified as possible vectors of the disease or it can be insects that cause wounds

that facilitate the infection by phytopathogens (Burgos 2013). Likewise, the fly *Neosilba* could be a vector of basal rot of the fruit, and for future publication in this study *Fusarium oxysporum* was detected in basal rot of stem (unpublished data).

Two types of morphotypes were isolated of the leg's insect *Leptoglossus zonatus*. By molecular technique, the species *Pseudomonas fulva* and *Lysinibacillus fusiformis* were identified. Associated insects of the Order Diptera, flies belonging to the family Lonchaeidae, and ants of the family Formicidae have been identified in pitahaya crops in Colombia, with a positive correlation of the number of insects with the number of cladodes and the number of fruits of yellow pitahaya, adapting to microclimates thanks to the forms of the plant. Therefore, proper pruning must be maintained, removal of diseased material and avoid leaving open wounds on the stems of the plants as a prevention strategy and phytosanitary management, especially in periods of high precipitation (Medina and Kondo 2012; González-Trujillo et al. 2019).

## CONCLUSION

This study describes the etiology and bacteria associated with the symptoms of soft rot of pitahaya stems from Boyacá, Colombia. Twenty-five bacterial morphotypes were isolated, identified and grouped into 13 genera. Most bacterial isolates belong to the order Enterobacterales suggesting a possible complex of bacteria in the phytopathogenic system. Within the group of Enterobacteria, *Kluyvera*, *Enterobacter*, *Klebsiella*, *Pantoea*, *Pectobacterium* and *Erwinia* were identified. This is the first report in Colombia of *Enterobacter cloacae*, *Pectobacterium carotovora* and *Paenibacillus glucanolyticus*, associated with the soft rot of the pitahaya stem and as potential phytopathogens in pitahaya, since the pathogenicity tests did not obtain positive results for *in vitro* infection. The genera *Achromobacter*, *Pseudomonas*, *Klebsiella*, *Stenotrophomonas*, *Microbacterium*, and *Sphingobacterium* were identified by molecular techniques like the microbiota associated with stem symptoms, possibly as endophytes, necrotrophic bacteria, or commensal bacteria. The etiology of the disease is also described in the field, identifying the signs and symptoms such as small chlorosis of the stems, and it can spread throughout the entire area of the cactus pads, to later generate softening of the stem, dark brown coloration with odors of bacterial rot. Different management practices such as preventive pruning, the use of microbiological control agent and organic management of the farm, cleaning, and disinfection of material as a cultural control practice could work to control the disease. The yellow pitahaya constitutes an exotic, "orphan" crop and valuable crop chain that justifies research and innovation

investment to assure competitiveness and socio-cultural and environmental preservation values. Likewise, the identification of the phytopathogens and the preservation of the strains allow the study of chemical and biological control agents as an alternative in the management of the disease.

## ACKNOWLEDGMENTS

This project has received funding from Patrimonio Autónomo Fondo Nacional de Financiamiento para la Ciencia, la Tecnología y la Innovación Francisco José de Caldas- MinCiencias. Gobernación de Boyacá". Code: 110986575466, Colombia.

## REFERENCES

- Adeolu M, Alnajjar S, Naushad S and Gupta RS (2016) Genome-based phylogeny and taxonomy of the 'Enterobacterales': Proposal for Enterobacterales ord. nov. divided into the families Enterobacteriaceae, Erwiniaceae fam. nov., Pectobacteriaceae fam. nov., Yersiniaceae fam. nov., Hafniaceae fam. nov., Morganellaceae fam. nov., and Budviciaceae fam. nov. International Journal of Systematic and Evolutionary Microbiology 66: 5575-5599. <https://doi.org/10.1099/ijsem.0.001485>
- Agronet - Red de información y comunicación del sector agropecuario colombiano (2022) Reporte: Área, Producción y Rendimiento Nacional para el cultivo de Pitahaya. <https://www.agronet.gov.co/estadistica/Paginas/home.aspx?cod=1>
- Balendres MA and Bengoa JC (2019) Diseases of dragon fruit (*Hylocereus* species): Etiology and current management options. Crop Protection 126: 104920. <https://doi.org/10.1016/j.cropro.2019.104920>
- Betancur JA, Muriel SB and González EP (2020) Morphological characterization of the red dragon fruit-*Selenicereus undatus* (Haw.) D.R. Hunt—under growing conditions in the municipality of San Jerónimo (Antioquia, Colombia). Revista Facultad Nacional de Agronomía Medellín 73: 9019-9027. <https://doi.org/10.15446/rfnam.v73n1.77735>
- Brady CL, Cleenwerck I, Venter SN et al (2010) Emended description of the genus *Pantoea*, description of four species from human clinical samples, *Pantoea septica* sp. nov., *Pantoea eucrina* sp. nov., *Pantoea brenneri* sp. nov. and *Pantoea conspicua* sp. nov., and transfer of *Pectobacterium cyripedii* (Hori 1911) Brenner et al. 1973 emend. Hauben et al. 1998 to the genus as *Pantoea cyripedii* comb. nov. International Journal of Systematic and Evolutionary Microbiology 60: 2430-2440. <https://doi.org/10.1099/ijms.0.017301-0>
- Burgos CC (2013) Manual técnico: Tecnología para el manejo de pitaya amarilla *Selenicereus megalanthus* (K. Schum. ex Vaupel) Moran en Colombia. Primera edición. Corporación colombiana de investigación agropecuaria – AGROSAVIA, Valle del Cauca (Colombia). 96 p.
- Charkowski AO, Lind J and Rubio-Salazar I (2014) Genomics of plant-associated bacteria: The soft rot Enterobacteriaceae. pp. 37-58. In: Gross D, Lichens-Park A, Kole C (Eds.) Genomics of plant-associated bacteria. Springer. First edition, Berlin, Heidelberg.



[https://doi.org/10.1007/978-3-642-55378-3\\_2](https://doi.org/10.1007/978-3-642-55378-3_2)

Da Graca T, Rodrigues LJ, de Almeida F et al (2023) Physicochemical characteristics and volatile profile of pitaya (*Selenicereus setaceus*). South African Journal of Botany 154: 88-97. <https://doi.org/10.1016/j.sajb.2023.01.020>

Davidsson PR, Kariola T, Niemi O and Palva ET (2013) Pathogenicity of and plant immunity to soft rot pectobacteria. Frontiers in Plant Science 4: 1-13. <https://doi.org/10.3389/fpls.2013.00191>

Faheed F, Mazen A and Abd Elmohsen S (2013) Physiological and ultrastructural studies on calcium oxalate crystal formation in some plants. Turkish Journal of Botany 37: 139-152. <https://doi.org/10.3906/bot-1112-19>

FAO - Food and Agriculture Organization, FAOSTAT Statistics Database (2009) Estadísticas de producción de pitahaya a nivel mundial. <http://www.fao.org/corp/statistics/es/>

Gaona AA, Castellanos EM and Fonseca LO (2015) Sistema productivo del cultivo de pitaya amarilla (*Selenicereus megalanthus*) en Boyacá-Colombia. Espacio I+ D, Innovación más Desarrollo 4(9): 155-170. <https://doi.org/10.31644/IMASD.9.2015.a07>

González-Trujillo MM, Peraza-Arias A and Brochero HL (2019) Insects associated to yellow pitaya crops (*Selenicereus megalanthus*) on Inzá Cauca, Colombia. Revista Colombiana de Entomología 45: 1-8. <http://doi.org/10.25100/socolen.v45i2.7961>

Grimont F and Grimont PAD (2006) The Genus *Enterobacter*. pp. 197-214. In: Dworkin M, Falkow s, Rosenberg E, Schleifer K, Stackebrandt E (Eds.) The Prokaryotes. Sixth edition. Springer, New York, NY. [https://doi.org/10.1007/0-387-30746-X\\_9](https://doi.org/10.1007/0-387-30746-X_9)

Ibrahim SRM, Mohamed GA, Khedr AIM et al (2018) Genus *Hylocereus*: Beneficial phytochemicals, nutritional importance, and biological relevance—A review. Journal of Food Biochemistry 42(2): e12491. <https://doi.org/10.1111/jfbc.12491>

Lin W, Liao F, Chen X et al (2015) Isolation and identification of the pathogen causing soft rot in *Hylocereus undatus*. Acta Phytopathologica Sinica 45(2): 220-224.

Lozada LF, Aguilar CN, Vargas CL et al (2022) Biological control for basal rot in yellow pitahaya fruits (*Selenicereus megalanthus*): Ex vivo trials. Journal of King Saud University-Science 34(5): 102042. <https://doi.org/10.1016/j.jksus.2022.102042>

Masyahit M, Sijam K, Awang Y et al (2009) First report on bacterial soft rot on dragon fruit (*Hylocereus* spp.) caused by *Enterobacter cloacae* in Peninsular Malaysia. International Journal of Agriculture & Biology.11: 659-666.

Medina J and Kondo T (2012) Listado taxonómico de organismos que afectan la pitaya amarilla, *Selenicereus megalanthus* (K. Schum. ex Vaupel) Moran (Cactaceae) en Colombia. Ciencia y Tecnología Agropecuaria 13: 41-46. [https://doi.org/10.21930/rcta.vol13\\_num1\\_art:238](https://doi.org/10.21930/rcta.vol13_num1_art:238)

Morillo-Coronado AC, Manjarres Hernández EH and Forero-Mancipe L (2021) Phenotypic diversity of morphological characteristics of pitahaya (*Selenicereus megalanthus* Haw.) germplasm in Colombia. Plants 10: 2255. <https://doi.org/10.3390/plants10112255>

Morillo-Coronado AC, Manjarres-Hernández EH, Saenz-Quintero OJ and Morillo-Coronado Y (2022) Morphoagronomic evaluation of yellow Pitahaya (*Selenicereus megalanthus* Haw.) in Miraflores, Colombia. Agronomy 12: 1582. <http://doi.org/10.3390/agronomy12071582>

Ogbo F and Okonkwo J (2012) Some characteristics of a plant growth promoting *Enterobacter* sp. isolated from the roots of maize. Scientific Research 2: 368-374. <http://doi.org/10.4236/aim.2012.23046>

Pásco P, Galanty A, Zagrodzki P et al (2021) Bioactivity and cytotoxicity of different species of pitaya fruits- a comparative study with advanced chemometric analysis. Food Bioscience 40: 1-8. <https://doi.org/10.1016/j.fbio.2021.100888>

Peng Z, Guan J, Mou D et al (2022) Analysis of bacterial community composition and ecological function during soft rot process in pitaya (*Hylocereus* spp.) stems. Journal of Chemistry 2022(1): 9169433. <https://doi.org/10.1155/2022/9169433>

Pierangeli C (2019) Espécies de fungos e bactérias associados à cultura da pitaya e avaliação de estádios de maturação na qualidade do fruto (Doutorado em Agronomia/Fitotecnia). Universidade Federal de Lavras, Lavras. Brasil. 74 p. <http://repositorio.ufla.br/jspui/handle/1/35146>

Retana Sánchez K, Castro-Zúñiga O, Blanco-Meneses M et al (2019) Etiología de las pudriciones en el tallo de *Hylocereus costaricensis*, provocadas por *Enterobacter hormaechei*, en Costa Rica. Agronomía Costarricense 43(2): 61-73. <http://doi.org/10.15517/rac.v43i2.37949>

Salazar-González C, Serna-Cock L and Gómez-López E (2016) Molecular characterization of *Fusarium* associated with basal rot of the fruit of pitahaya (*Selenicereus megalanthus*). Agronomía Mesoamericana 27(2): 277-285. <https://doi.org/10.15517/am.v27i2.21269>

Soto J, Cadenas C, Mattos L et al (2019) First report of *Enterobacter cloacae* as a causative agent of soft rot in dragon fruit (*Hylocereus undatus*) stems in Peru. Peruvian Journal of Agronomy 3(3): 144-152. <https://doi.org/10.21704/pja.v3i3.1367>

Stengel A, Drijber R, Carr E et al (2022) Rethinking the roles of pathogens and mutualists: exploring the continuum of symbiosis in the context of microbial ecology and evolution. Phytobiomes Journal 6(2): 108-117. <https://doi.org/10.1094/PBIOMES-05-21-0031-P>

Valencia A, Cruz H and Rodriguez C (2003) Avances en la etiología y manejo de la pudrición blanda de tallos de pitahaya, *Hylocereus undatus* H. (Cactaceae). Fitosanidad 7: 11-17. ISSN: 1562-3009

Vilaplana R, Alba P and Valencia-Chamorro S (2018) Sodium bicarbonate salts for the control of postharvest black rot disease in yellow pitahaya (*Selenicereus megalanthus*). Crop Protection 114: 90-96. <https://doi.org/10.1016/j.cropro.2018.08.021>

Weller-Stuart T, De Maayer P and Coutinho T (2017) *Pantoea ananatis*: genomic insights into a versatile pathogen. Molecular Plant Pathology 18: 1191-1198. <https://doi.org/10.1111/mp.12517>

Zhang RY, Zhao SX, Tan ZQ et al (2017) First report of bacterial stem rot disease caused by *Paenibacillus polymyxa* on *Hylocereus undulatus* in China. Plant Disease 101: 1031-1031. <https://doi.org/10.1094/PDIS-11-16-1577-PDN>



# Soil quality indicators related to the deterioration of Kikuyu grass *Cenchrus clandestinus* (Hochst. ex Chiov.) Morrone

Indicadores de calidad del suelo relacionados con el deterioro del pasto kikuyo *Cenchrus clandestinus* (Hochst. ex Chiov.) Morrone

<https://doi.org/10.15446/rfnam.v77n3.109829>

Jorge Mario Noreña-Grisales<sup>1\*</sup>, Ramiro Ramírez Pisco<sup>1</sup> and Nelson Walter Osorio Vega<sup>1</sup>

## ABSTRACT

### Keywords:

Degraded pastures  
High Andean tropics  
Principal component analysis  
Soil chemical properties  
Soil physical properties  
Soil quality index

Inadequate grassland management has resulted in the degradation of extensive areas, loss of productivity and sustainability of many of them, reflecting a common reality among livestock farmers in Colombia. Therefore, at the Paysandú Agricultural Station of the Universidad Nacional de Colombia, located in the Santa Elena township of the city of Medellín, a study was carried out to determine a soil quality index (SQI) by evaluating the physical and chemical indicators that were most related to the deterioration and dry matter production of kikuyu grass (*Cenchrus clandestinus*). A minimum data set (MDS) was established for the most sensitive indicators, selected by principal component analysis (PCA), and a nonlinear scoring function was used to obtain the SQI. Statistical differences were found between all the treatments in relation to dry matter production ( $P < 0.05$ :  $1.91 \times 10^{-32}$ ). The most sensitive indicators were bulk density BD > total porosity TP > macropores MAC > micropores MIC > penetration resistance PR > effective cation exchange capacity ECEC > pH. As a result, the following formula was obtained:  $SQI = (0.225 \times BD) + (0.224 \times TP) + (0.220 \times MAC) + (0.218 \times MIC) + (0.113 \times PR) + (0.0879 \times ECEC) + (0.0877 \times pH)$ . This index should be tested in kikuyu grass-dominated pastures located in the Colombian high tropics. The baseline is critical at values > 0.58 Mg m<sup>-3</sup> for BD and > 2.25 MPa for PR. In addition, the optimum pH range for kikuyu grass development was between 5.4 and 6.4.

## RESUMEN

### Palabras clave:

Pasturas degradadas  
Trópico alto andino  
Análisis de componentes principales  
Propiedades químicas del suelo  
Propiedades físicas del suelo  
Índice de calidad del suelo

El manejo inadecuado de los pastizales ha provocado la degradación de extensas áreas, la pérdida de productividad y sostenibilidad de muchas de ellas, reflejando una realidad común entre los ganaderos de Colombia. Por ello, en la Estación Agraria Paysandú de la Universidad Nacional de Colombia, ubicada en el corregimiento de Santa Elena de la ciudad de Medellín, se realizó una investigación para determinar un índice de calidad del suelo (SQI) mediante la evaluación de los indicadores físicos y químicos más relacionados con el deterioro y producción de materia seca del pasto kikuyo (*Cenchrus clandestinus*). Se estableció un conjunto mínimo de datos (MDS) para los indicadores más sensibles, elegidos mediante el análisis de componentes principales PCA, y se utilizó una función de puntuación no lineal para obtener el SQI. Se encontraron diferencias estadísticas entre todos los tratamientos y la producción de materia seca ( $P < 0.05$ :  $1.91 \times 10^{-32}$ ). Los indicadores más sensibles fueron: densidad aparente DR > porosidad total TP > macroporos MAC > microporos MIC > resistencia a la penetración PR > capacidad de intercambio catiónico efectiva ECEC > pH. Como resultado, se obtuvo el siguiente  $SQI = (0.225 \times BD) + (0.224 \times TP) + (0.220 \times MAC) + (0.218 \times MIC) + (0.113 \times PR) + (0.0879 \times ECEC) + (0.0877 \times pH)$ . Se sugiere probar el índice en praderas dominadas por pasto kikuyo ubicadas en el trópico alto colombiano. La línea de base es crítica a valores > 0,58 Mg m<sup>-3</sup> para BD y > 2,25 MPa para PR. Además, el intervalo de pH óptimo para el desarrollo del pasto kikuyo se situó entre 5,4 y 6,4.

<sup>1</sup>Universidad Nacional de Colombia Sede Medellín, Colombia. [jmnorena@unal.edu.co](mailto:jmnorena@unal.edu.co) , [r Ramirez@unal.edu.co](mailto:r Ramirez@unal.edu.co) , [nwosorio@gmail.com](mailto:nwosorio@gmail.com) 

\*Corresponding author

**K**ikuyu grass *Cenchrus clandestinus* (Hochst. ex Chiov.) Morrone is native to tropical Africa (northeast, east, central west and south) (USDA 2024). It was introduced into Colombia just before 1930. It is a perennial herbaceous, stoloniferous and rhizomatous plant. The stolons –aerial, creeping stems– can exceed 3 m in length, while the rhizomes – underground stems– can reach 1 m deep. Sometimes it develops aquatic stolons (floating or submerged). These characteristics allow it to colonize extensive areas superficially as well as underground, which is desirable during establishment. However, this can become a negative aspect, since stolons and rhizomes can reach a high level of deterioration when the pasture is improperly managed. This detriment, although it does not affect the persistence of the species, does reduce the productive potential of the crop and as a consequence, the quality of the forage.

In the Colombian high tropics, kikuyu grass typically represents between 65-95% of the botanical composition of herbaceous plants commonly found in the pastures, constitutes the main forage source and is the most used species in specialized dairy production systems in the country's dairy belt. However, inadequate management of the species has led to the degradation of extensive areas, the loss of productivity and a decrease in the environmental and economic sustainability of a large number of hectares, reflecting a reality that ranchers in the tropical high Andean regions of the country commonly face.

Pasture mulching is the result of the progressive deterioration of the different vegetative structures of a plant, mainly its leaves and stems. Consequently, it is common to observe limited growth of the aerial part (dwarfism); significant shortening of the distance between knots; lignification of stems, and death or senescence of leaves located in lower positions. This detriment can also occur in subterranean stems (rhizomatous mulching), which sometimes exceeds 1 m in depth; or it can also be observed, as typical, in aerial stems, including stolons (stoloniferous mulching). This degenerative condition is one of the most influential aspects in the loss of quality and productivity of kikuyu grass. In summary, when the deterioration is superficial, small plants can present a high degree of lignification (especially favored by continuous overgrazing) or a higher cushion, generated by undergrazing. On the contrary, when it grows underground, a network of rhizomes can be observed.

Grasslands are at risk of degradation due to unsustainable management practices and climate change (Milazzo et al. 2023). Therefore, evaluating grazing management practices on soil quality is essential for ensuring the sustainability of pastures, which represent the largest land use in world agroecosystems (Amorim et al. 2020). To this end, soil quality indices are widely used as comprehensive tools of soil function for grouping and assessing multiple soil properties (Chaudhry et al. 2024).

Soil quality is defined as the ability of soil to perform ecological functions, provide ecosystem services in order to maintain biological productivity, and environmental quality, and improve plant and animal health (Joimel et al. 2017). External factors such as parent material, climate, topography, or hydrology can alter soil properties, making it impossible to establish universal values of soil quality (Bünemann et al. 2018). A common approach to determining them is through the selection of physical, chemical and biological indicators (Milazzo et al. 2023; Koureh et al. 2020; Valle and Carrasco 2018).

These indicators are used as parameters to assess soil quality. However, the evaluation of soil quality cannot be performed based on a single parameter. Thus, the need arises to establish a minimum data set (MDS) including physical, chemical and biological variables (Joimel et al. 2017). However, the difficulty is when the indicator does not have an optimal reference value for a specific soil type and use. Consequently, an indicator is useful if the value can be interpreted unambiguously and the reference values are available.

The present study aims to establish soil quality indicators related to pasture degradation and forage yield of kikuyu grass (*Cenchrus clandestinus*).

## MATERIALS AND METHODS

### Description of the study site

The research was carried out at the Paysandú Agricultural Station of the Universidad Nacional de Colombia, located in the Santa Elena township, to the east of the city of Medellín, Department of Antioquia, at a distance of approximately 18 km from the downtown area (Figure 1). It is located on Andisols in the very humid low montane forest (bmh-MB) life zone, at an altitude of 2,530-2,640 m, average annual temperature of 16.6 °C, and average annual precipitation of

2,950 mm. It has a total area of 139.3 ha and geographical coordinates 6°12'25" north latitude and 75°30'08" west longitude. The main land use is intensive dairy farming

under the rotational grazing model in meadows with steep slopes, gentle hills and small plateaus dominated by kikuyu grass (*Cenchrus clandestinus*).

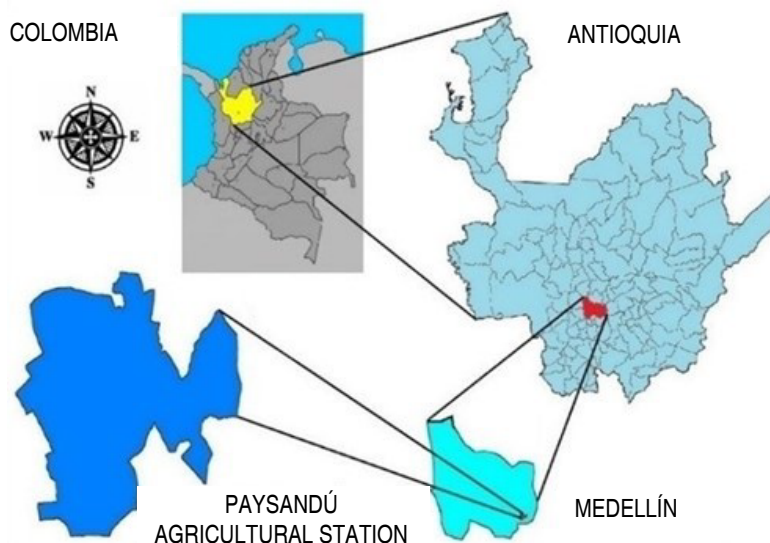


**Figure 1:** Location of the experiment site.

A 0.5-hectare paddock was selected, which is part of the dairy cattle strip rotation system in which 20 Holstein cows between 525±43.3 kg of liveweight grazed. They entered the paddock every 40 days to consume the forage, interacting with the physical and chemical properties of the soil through trampling and the deposition of urine and excretion.

Afterward, 25 plots of 1 m<sup>2</sup> dominated by kikuyu grass were selected. For this purpose, a scale was used according to forage yield from 1 to 5, with 5 being those sites with the highest production and 1 being those with the least forage biomass. These plots were used to establish five treatments (T1: low; T2: medium-low; T3: medium; T4: medium-high; T5: high) (Figure 2). At



**Figure 2:** Example of treatment selection.



each site, a set of physical and chemical variables was evaluated and their relationship with DM production was quantified. Each variable was measured at the Soil Laboratory of Universidad Nacional de Colombia, Medellín Headquarters, except for penetration resistance and forage production. The first was measured in the

field at a depth of 10 cm, and the second was cut one day before the animals entered.

### Methods and techniques for assessing soil quality indicators

The methods and techniques are described in Table 1.

**Table 1.** Methods and techniques used to assess soil quality indicators.

Soil quality attribute	Method/Extraction/Technique
<b>Physical indicators</b>	
Texture (%).	NTC 6299 2018/DTD/Bouyoucos
Bulk density ( $\text{Mg m}^{-3}$ ).	Waxed lump
Real density ( $\text{Mg m}^{-3}$ ).	Pycnometer
Gravimetric humidity (%).	Gravimetric/N.A./Kiln dried
Total porosity (%).	$[1 - (\text{BD}/\text{RD})] \times 100$
Penetration resistance (MPa). 10 cm	Cone penetrometer
<b>Chemical indicators</b>	
pH	NTC 5264 2018/Water 1:1/Potentiometry
Electrical conductivity ( $\text{dS m}^{-1}$ ).	NTC 5596 2008/Ext. of Sat./Potentiometry
Organic matter in the soil (%).	NTC 5526 2007/Oxid. Wet way/Volumetry
Exchangeable Al ( $\text{cmol} + \text{kg}^{-1}$ )	NTC 5263 2017/KCL 1 N/Volumetry
Ca, Mg, K and Na ( $\text{cmol} + \text{kg}^{-1}$ )	NTC 5349 2016/Ammonium acetate pH 7/Atom. Abs.
ECEC ( $\text{cmol} + \text{kg}^{-1}$ )	NTC 5268 2014/Ammonium acetate pH 7/Volumetry
P ( $\text{mg kg}^{-1}$ ).	Internal method/Bray II/Colorimetry
S ( $\text{mg kg}^{-1}$ ).	NTC 5402 2006/Monoammonium phosphate 0.08M/Turbidimetry
Fe, Mn, Cu and Zn ( $\text{mg kg}^{-1}$ ).	NTC 5526 2007/DTPA/Atomic absorption
B ( $\text{mg kg}^{-1}$ ).	Internal method/ Hot water/Atomic emission

## RESULTS AND DISCUSSION

### Descriptive statistics

Descriptive statistics of soil quality indicator values are summarized in Table 2.

The bulk density fluctuated from 0.4 to 0.8  $\text{Mg m}^{-3}$ , which is consistent with that reported in Andisols with a predominance of allophane in the clay complex considered by the taxonomy for this order of soils ( $<0.9 \text{ Mg m}^{-3}$ ) (Soil Survey Staff 2022). Furthermore, they have high porosity, increased by particularly high soil water retention (Hewitt et al. 2021). However, cattle trampling commonly alters this variable. The penetration resistance presented values

of 1.6-3.4 MPa, close to 2 MPa, i.e., the critical limit proposed by Barbosa (2019), over which root growth can be restricted. The porosity ranged from 61.4 to 79.6%, which is reportedly high for Andisols. This high porosity is related to a structural assemblage of poorly crystalline and non-crystalline secondary minerals into stable (sand- and silt-sized) aggregates. Allophanic and non-allophanic Andisols can accumulate large amounts of organic matter. However, non-allophanic andisols also form highly porous aggregates and have a high-water retention capacity (Delmelle et al. 2015). Gravimetric moisture retention ranged from 119.9 to 199.8% between saturation and 15 bar (Table 2).

The pH value fluctuated between 5.0 and 7.2 and was within the recommendations for many grasses, including kikuyu. However, according to Läuchli (2017), acidic soils (pH<5.5) and alkaline soils (pH>7.5) fall outside the optimal pH range and can generate low nutrient availability, ionic toxicities and nutritional imbalances. The values of Ca, Mg, and K (Table 2) exceeded the required ranges in pastures according to Rodelo-Torrente et al. (2022); especially K, which can become a problem in bovine productivity (Swanepoel et al. 2014). Although phosphate retention values of  $\geq 25\%$  or  $\geq 85\%$  are common in Andisols (Soil Survey Staff 2022), P and S sufficiency was found due to the continuous input of chemical fertilizers. Sufficiency was established according to the ranges proposed by Siatwiinda et al. (2024) and Hazelton and Murphy (2016).

The ECEC fluctuated from 9.0 to 46.8 cmol kg<sup>-1</sup>, with an average of 21.47 cmol kg<sup>-1</sup> (considered high), where the Ca made the greatest contribution, and the Ca/Mg ratio was 5.5 on average. Regarding minor elements, only Cu (0.86 mg kg<sup>-1</sup>) presented deficiency according to the theoretical optimum suggested by Siatwiinda et al. (2024). In parallel, a high average soil organic matter was found (SOM=17.49%), which is typical of Andisols with <25% organic carbon (Soil Survey Staff 2022). This high content of surface organic matter is a consequence of the humid cold climate of the area and the formation of organometallic complexes that protect it from mineralization (Pérez et al. 2017). A high amount of organic matter can improve soil functionality, and its ability to provide essential ecosystem services and soil health (Lal 2020).

**Table 2.** Descriptive statistics of physical and chemical indicators of soil quality.

Soil quality attribute	Mean	SEM	CV	Minimum	Maximum
<b>Physical indicators</b>					
Bulk density <b>BD</b> (Mg m <sup>-3</sup> )	0.58	0.08	13.86	0.4	0.8
Real density <b>RD</b> (Mg m <sup>-3</sup> )	1.97	0.1	4.92	1.81	2.27
Penetration resistance <b>PR</b> (MPa)	2.37	0.41	17.23	1.60	3.45
Total porosity <b>TP</b> (%)	70.64	3.85	5.44	61.35	79.6
Macropores <b>MAC</b> >100 um (%)	26.1	10.54	40.37	0.8	47.37
Mesopores <b>MES</b> 10-100 um (%)	37.13	7.27	19.58	18.09	61.09
Micropores <b>MIC</b> <10 um (%)	36.77	5.8	15.78	27.28	53.66
<b>Chemical indicators</b>					
pH (1:1)	5.9	0.51	8.72	5	7.2
Exchangeable Al (Cmol <sup>+</sup> kg <sup>-1</sup> )	0.16	0.3	186.43	0	1
Exchangeable Ca (Cmol <sup>+</sup> kg <sup>-1</sup> )	16.52	7.27	43.99	7.1	35.10
Exchangeable Mg (Cmol <sup>+</sup> kg <sup>-1</sup> )	2.99	1.19	39.85	1.1	5.6
Exchangeable K (Cmol <sup>+</sup> kg <sup>-1</sup> )	0.67	0.39	58.66	0.14	1.78
Exchangeable Na (Cmol <sup>+</sup> kg <sup>-1</sup> )	0.15	0.11	74.54	0.03	0.76
Exchangeable ECEC (Cmol <sup>+</sup> kg <sup>-1</sup> )	21.47	9.67	45.02	9	46.8
P (mg kg <sup>-1</sup> )	61.54	54.76	88.98	7	232
S (mg kg <sup>-1</sup> )	17.79	6.72	37.76	10	39
Fe (mg kg <sup>-1</sup> )	78.22	44.9	57.4	18	176
Mn (mg kg <sup>-1</sup> )	2.05	1.01	49.14	0.6	5
Cu (mg kg <sup>-1</sup> )	0.86	0.59	68.21	0.2	3
Zn (mg kg <sup>-1</sup> )	6.56	3.85	58.67	0.9	16
B (mg kg <sup>-1</sup> )	0.44	0.11	25.97	0.2	0.8
Dry matter <b>DM</b> (kg ha <sup>-1</sup> year <sup>-1</sup> )	3863.9	2352.9	60.9	296.3	10790.5

SEM = standard error of the mean, CV = coefficient of variation (%).

### Correlations

The correlation analysis between (physical and chemical) soil indicators and DM production showed that the variables with the highest positive correlation

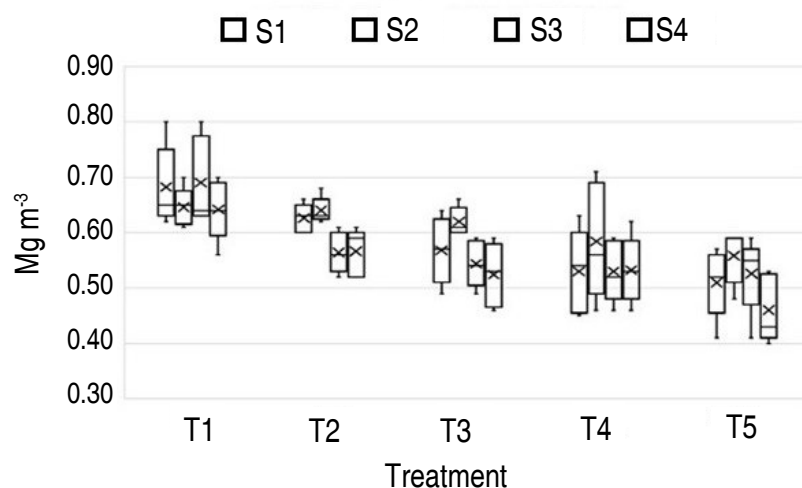
were K (0.62), Mg (0.54), ECEC (0.50), TP (0.48), Na (0.47) and Ca (0.39). In turn, those with the highest negative correlation were BD (-0.52) and PR (-0.49) (Table 3).

**Table 3.** Correlation between soil quality indicators and dry matter production.

IQS	DM	BD	PR	TP	MAC	MIC	pH	Al	Ca	Mg	K	Na	ECEC	P	S	Fe	Mn	Cu	Zn	B
DM	1	-	-	-	-	-	-	-	-	-	-	-	-	-	-	-	-	-	-	-
BD	<b>-0.52</b>	1	-	-	-	-	-	-	-	-	-	-	-	-	-	-	-	-	-	-
PR	<b>-0.49</b>	0.34	1	-	-	-	-	-	-	-	-	-	-	-	-	-	-	-	-	-
TP	<b>0.48</b>	-0.93	-0.32	1	-	-	-	-	-	-	-	-	-	-	-	-	-	-	-	-
MAC	-0.06	-0.30	0.02	0.34	1	-	-	-	-	-	-	-	-	-	-	-	-	-	-	-
MIC	-0.08	0.22	-0.13	-0.17	-0.76	1	-	-	-	-	-	-	-	-	-	-	-	-	-	-
pH	0.32	-0.03	-0.15	0.19	-0.05	-0.08	1	-	-	-	-	-	-	-	-	-	-	-	-	-
Al	-0.30	-0.08	0.25	-0.08	0.12	0.00	-0.76	1	-	-	-	-	-	-	-	-	-	-	-	-
Ca	<b>0.39</b>	-0.06	-0.10	0.09	-0.39	0.18	0.66	-0.55	1	-	-	-	-	-	-	-	-	-	-	-
Mg	<b>0.54</b>	-0.23	-0.38	0.23	-0.29	0.22	0.61	-0.59	0.70	1	-	-	-	-	-	-	-	-	-	-
K	<b>0.62</b>	-0.38	-0.42	0.45	-0.26	0.19	0.53	-0.48	0.59	0.63	1	-	-	-	-	-	-	-	-	-
Na	<b>0.47</b>	-0.42	-0.10	0.35	0.11	-0.18	-0.11	0.05	0.02	0.17	0.14	1	-	-	-	-	-	-	-	-
ECEC	<b>0.50</b>	-0.18	-0.29	0.21	-0.38	0.22	0.68	-0.55	0.86	0.87	0.62	0.06	1	-	-	-	-	-	-	-
P	<b>0.40</b>	-0.16	-0.16	0.07	-0.48	0.38	0.01	0.01	0.42	0.55	0.24	0.24	0.57	1	-	-	-	-	-	-
S	<b>0.39</b>	-0.03	-0.17	0.03	-0.42	0.35	0.19	-0.23	0.42	0.48	0.34	0.16	0.43	0.61	1	-	-	-	-	-
Fe	-0.06	-0.17	-0.06	-0.04	0.03	0.07	-0.75	0.59	-0.33	-0.17	-0.34	0.32	-0.26	0.34	0.10	1	-	-	-	-
Mn	0.24	0.09	-0.11	-0.13	-0.39	0.28	0.15	-0.21	0.47	0.47	0.25	0.25	0.55	0.60	0.59	0.21	1	-	-	-
Cu	0.25	0.20	0.09	-0.20	-0.58	0.35	0.34	-0.30	0.68	0.49	0.26	0.04	0.62	0.64	0.60	-0.12	0.71	1	-	-
Zn	0.50	-0.12	-0.20	0.08	-0.55	0.36	0.35	-0.31	0.80	0.72	0.45	0.17	0.81	0.77	0.65	0.06	0.72	0.82	1	-
B	0.09	-0.02	-0.13	-0.07	-0.06	-0.02	0.12	-0.04	0.24	0.44	0.00	-0.06	0.40	0.39	0.19	0.21	0.31	0.23	0.38	1

BD presented a negative correlation with DM productivity (-0.52). Therefore, the BD values in which the mean was higher, corresponded to the most mulched plots where DM production was lower (T1), and the opposite

for T5. The results of the mean BD values for the treatments T1, T2, T3, T4, and T5 were 0.665, 0.599, 0.564, 0.544, and 0.514  $\text{Mg m}^{-3}$ , respectively (Figure 3).

**Figure 3.** Bulk Density vs Treatment. S: sample.



A negative correlation was found between PR and DM (-0.49). Therefore, higher mean PR values usually corresponded to treatments where biomass was lower (T1), and vice versa. Increases in PR explained 49% of the reduction in productivity (Figure 4). Additionally, a positive correlation was obtained between BD and PR (0.34). Consequently, soil compaction leads to reduced plant productivity, mainly due to poor root density, low elongation rates, and limited access to water and nutrients (Colombi and Keller 2019). This is because compaction produces low connectivity and continuity of the pore space, reducing the air and water transport capacity of the soil (Keller et al. 2017). Blanco-Sepúlveda et al. (2024) evaluated different physical properties of soils (bulk density, total porosity, field capacity, infiltration, and aggregate stability). They found that bulk

density and infiltration are the most useful parameters to identify areas affected by cattle trampling and that bulk density is the key property for analyzing the impact of cattle with respect to increased stocking rates. They also concluded that the relationship between physical soil degradation and stocking rate is not linear because it also depends on environmental factors.

A value of 2 MPa has been estimated as the threshold that limits root growth when soil compaction is evaluated using a penetrometer (Barbosa 2019). In all the treatments (T1, T2, T3, T4, and T5), the mean values exceeded this limit (2.73, 2.59, 2.20, 2.17, and 2.15 MPa, respectively). High mean PR values corresponded, in general, to the treatments that produced less dry mass (T1) (Figure 4).

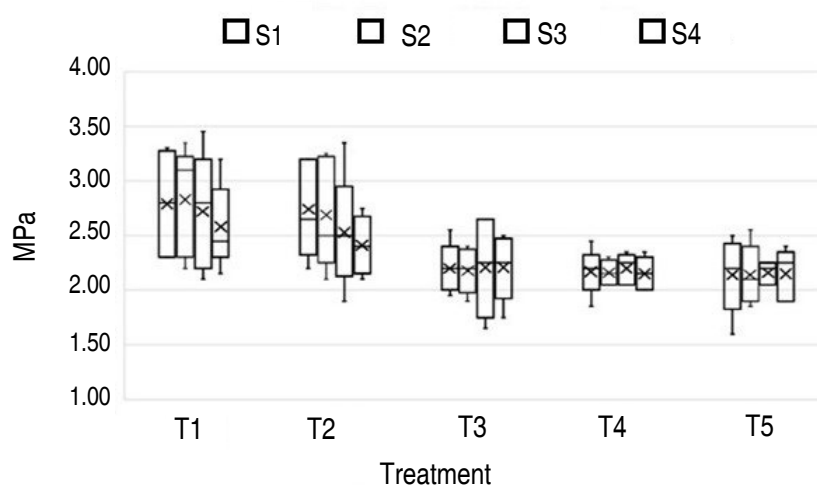


**Figure 4.** Penetration Resistance vs Treatment. S: sample.

A positive correlation was obtained between TP and DM production (0.48). Therefore, increases in TP explained 48% of the increase in dry forage produced. The higher the TP, the higher the forage yield (Figure 5). The mean TP values (67.2, 69.1, 70.6, 72.5 and 73.9%) produced with treatments T1, T2, T3, T4 and T5, respectively, can be classified as high (Hazelton and Murphy 2016). But more important than the TP value is establishing the percentage of macropores, mesopores and micropores. Macropores presented the widest range (0.8-47.4%) compared to mesopores (18.1-61.1%) and micropores (27.3-53.7%). When the percentage of macropores was

calculated, it was found that, in 10% of the cases, it was <10%. Rabot et al. (2018) discussed ideal percentages in the first 20 to 30 cm of depth: micropores: 20-30% (<0.2  $\mu\text{m}$ ), mesopores: 40-60% (0.2-50  $\mu\text{m}$ ) and macropores: 10-20% (>50  $\mu\text{m}$ ). Therefore, imbalances were observed in this study.

Using analysis of variance, the difference between treatments with respect to dry matter production was evaluated and found to be statistically significant ( $P$ -value:  $1.911372 \times 10^{-32}$ ). Therefore, there is evidence to reject that they are equal. In this regard, the means were T1=790 kg;

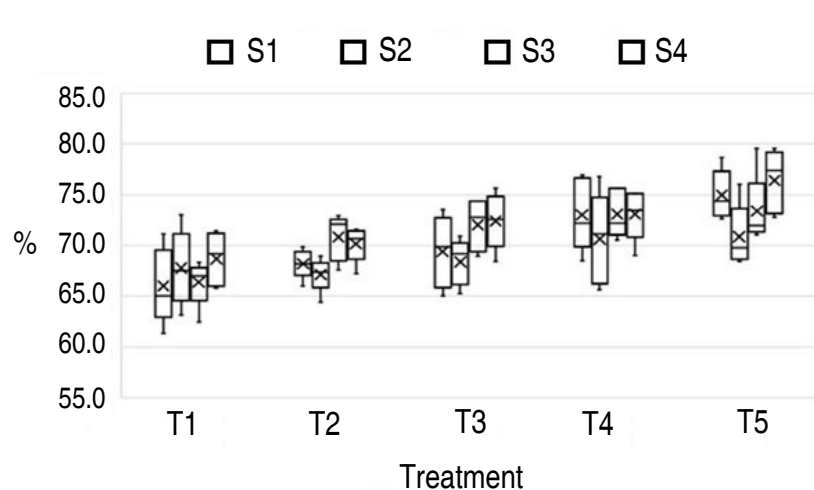


**Figure 5.** Total Porosity vs Treatment. S: sample.

T2=2,468 kg; T3=4,005 kg; T4=5,264 kg and T5=6,792 kg. The grand mean was 3,863 kg in 40 days. Meanwhile, the

total effects were T1= -3073.7 kg; T2= -1396.1 kg; T3=141.4 kg; T4=1399.9 kg, and T5= 2928.5 kg (Figure 6).

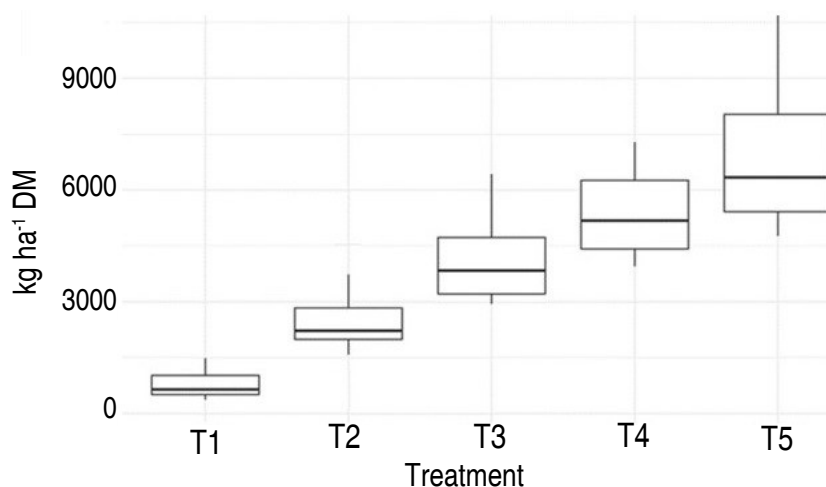


**Figure 6.** Dry Matter vs Treatment.

DM production was 35.3 tons  $\text{ha}^{-1} \text{yr}^{-1}$ , which is below that achieved by Villalobos-Villalobos and WingChing-Jones (2023), who reached 42.4 tons of  $\text{DM ha}^{-1} \text{yr}^{-1}$ , and above that reported by Gómez et al. (2014), who obtained 34.3 tons of  $\text{DM ha}^{-1} \text{yr}^{-1}$ . However, it should be noted that the cutting or grazing cycles were every 40, 36 and 45 days, respectively. Therefore, the DM production  $\text{ha}^{-1}$  per cycle was 4,184 kg, which is above that obtained by Villalobos-

Villalobos and WingChing-Jones (2023), who achieved 3,517 kg  $\text{DM ha}^{-1}$  per cycle and below that found by Gómez et al. (2014), who achieved 4,230 kg  $\text{DM ha}^{-1}$  per cycle. It is important to stress that the total dry matter production was obtained by multiplying the average production of each stratum by 20%, but, for greater precision, the percentage of participation of each stratum should be determined by estimating the botanical composition.

**Selection of soil quality indicators for an MDS**

An individual PCA was performed for physical and chemical properties. The selection criterion was PCs with an eigenvalue >1. This was met by the first two

and three PCs of the physical and chemical properties, respectively, showing a cumulative variance percentage of 79.04 and 72.88%, respectively, as can be seen in Table 4.

**Table 4.** Eigenvalues, variance (%), and variance cumulative (%) explained by the principal components within each group.

Component	Eigenvalues	Variance (%)	Var. cumulative (%)
<b>Physical indicators</b>			
Comp 1	2.51	50.15	50.15
Comp 2	1.44	28.89	<b>79.04</b>
<b>Chemical indicators</b>			
Comp 1	6.44	45.97	45.97
Comp 2	2.61	18.65	64.63
Comp 3	1.16	8.26	<b>72.88</b>

Once the PCs were determined, those that presented the highest correlation coefficients (regardless of whether they were positive or negative) were preselected in each component. Therefore, TP was selected as the most representative physical indicator of the first PC; and

MIC, for the second PC. Among the chemical indicators, the ECEC exhibited the highest coefficient for the first PC, Fe for the second PC, and Na for the third PC (Table 5). These indicators, despite being selected, can be discarded in the MDS.

**Table 5.** Eigenvectors, principal components (PC), and communality estimate of the physical and chemical indicators, ranked according to the magnitude of the vector within each group.

Eigenvector	PC1	PC2	PC3	Communality	Magnitude of vector
<b>Physical indicators</b>					
Bulk density <b>BD</b> (Mg m <sup>-3</sup> )	0.867	0.373	-	<b>0.891</b>	<b>0.225</b>
Total Porosity <b>TP</b> (%)	<b>-0.872</b>	-0.355	-	<b>0.886</b>	<b>0.224</b>
Macropores <b>MAC</b> (%)	-0.668	0.649	-	<b>0.868</b>	0.220
Micropores <b>MIC</b> (%)	0.588	<b>0.717</b>	-	<b>0.861</b>	0.218
Penetration resistance <b>PR</b> (MPa)	0.452	0.493	-	0.447	0.113
<b>Chemical indicators</b>					
Exchangeable ECEC (cmol + kg <sup>-1</sup> )	<b>0.933</b>	-0.109	-0.118	<b>0.897</b>	<b>0.088</b>
pH (1:1)	0.680	-0.654	-0.067	<b>0.895</b>	<b>0.088</b>
Zn (mg kg <sup>-1</sup> )	0.895	0.305	-0.012	0.895	0.088
Fe (mg kg <sup>-1</sup> )	-0.252	<b>0.882</b>	-0.059	0.845	0.083
Exchangeable Ca (cmol + kg <sup>-1</sup> )	0.882	-0.163	-0.025	0.805	0.079
Exchangeable Mg (cmol + kg <sup>-1</sup> )	0.855	-0.057	-0.101	0.744	0.073
P (mg kg <sup>-1</sup> )	0.598	0.618	0.062	0.743	0.073
Cu (mg kg <sup>-1</sup> )	0.826	0.212	0.034	0.728	0.071
Exchangeable Na (cmol + kg <sup>-1</sup> )	0.097	0.201	<b>0.780</b>	0.658	0.064
B (mg kg <sup>-1</sup> )	0.448	0.235	-0.624	0.646	0.063
Mn (mg kg <sup>-1</sup> )	0.678	0.411	0.099	0.639	0.063
Exchangeable Al (cmol + kg <sup>-1</sup> )	-0.563	0.527	-0.181	0.628	0.062
Exchangeable K (cmol + kg <sup>-1</sup> )	0.627	-0.330	0.234	0.557	0.055
S (mg kg <sup>-1</sup> )	0.556	0.438	0.151	0.524	0.051

The indicators with the greatest magnitude within each group (BD and ECEC) were selected for the MDS. When these presented the same value, the one with the highest communality was chosen. A high communality indicates that a large part of the variance is explained by said component. Nevertheless, because they explain more than 79% of the variance in the physical variables, TP, MAC and MIC were also selected. In addition, pH was selected because it explains more than 72% of the variance in the chemical indicators (Table 4).

All these variables presented the highest magnitude and communality within each group. The previous selection

was also based on the weight of the variables and using as a criterion that it be >10% (for that reason, PR was also chosen in the physical variables). Although none of the chemical variables reached that value, those closest to 10% were selected (Table 6).

### Scoring the selected indicators

Nonlinear scoring functions were used to transform the soil properties in the MDS to values between 0 and 1 (Figure 7). "Less is better" functions were used for scoring BD and PR; "more is better" functions for ECEC; and the "mid-point optimum" function for TP, MAC, MIC, and pH.

**Table 6.** Weight of physical and chemical indicators.

Physical		Chemical	
Indicator	Weight (%)	Indicator	Weight (%)
BD	22.5	ECEC	8.79
TP	22.4	pH	8.77
MAC	22.0	-	-
MIC	21.8	-	-
PR	11.3	-	-

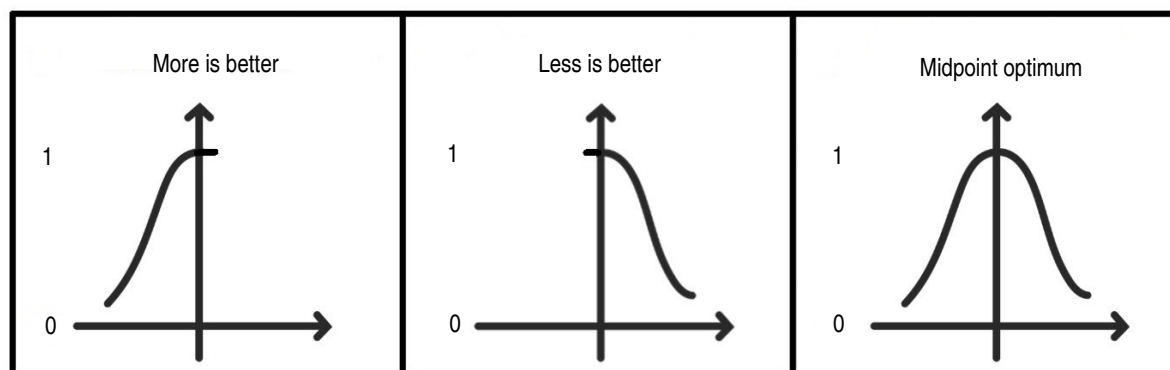


**Figure 7.** Representations of nonlinear scoring functions.

BD was represented using a decreasing score curve (less is better). Therefore, a BD of  $0.4 \text{ Mg m}^{-3}$  presented a higher score than a BD of  $0.8 \text{ Mg m}^{-3}$ . The cumulative normal distribution of BD shows that most data fell in the range  $0.4\text{--}0.6 \text{ Mg m}^{-3}$  (explaining a high probability of occurrence), while  $0.7 \text{ Mg m}^{-3}$  is already very close to the lower asymptote (Figure

8). However, by determining the baseline, it can be established that a BD above  $0.58 \text{ Mg m}^{-3}$  is related to scores below 0.5, which is undesirable with respect to production. Therefore, the best scores are observed at a BD below  $0.58 \text{ Mg m}^{-3}$  down to  $0.40 \text{ Mg m}^{-3}$ , where they stabilize and reach a constant value, favoring dry matter productivity.

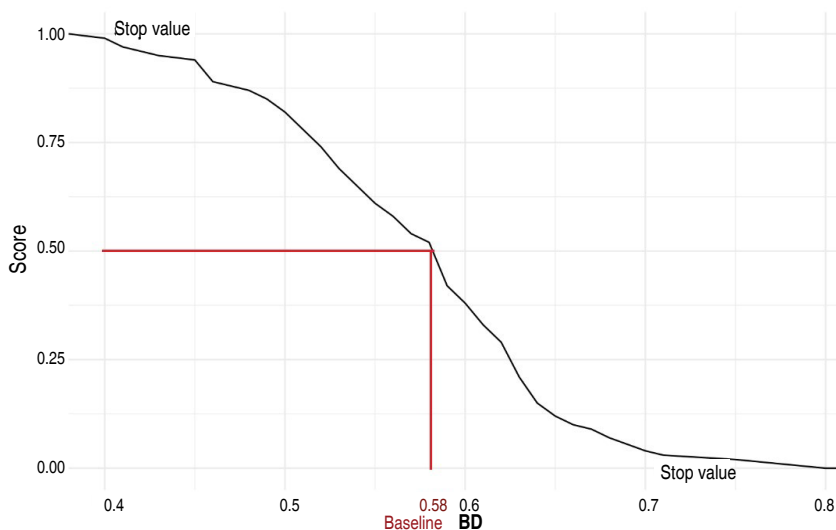


**Figure 8.** Scoring curve of Bulk Density (BD).

Likewise, PR presented a decreasing score curve (less is better). The cumulative normal distribution of PR indicates that most data have a high probability of falling between 2.0 and 3.5 kPa, which is undesirable (Figure 9). Furthermore, by determining the baseline, it can be established that a PR above 2.25 kPa is

related to scores below 0.5, which is also undesirable with respect to production. On the one hand, the best PR scores are observed below 2.25 kPa, which favors dry biomass productivity. On the other hand, values greater than the optimum impair the productivity and functions of the soil.

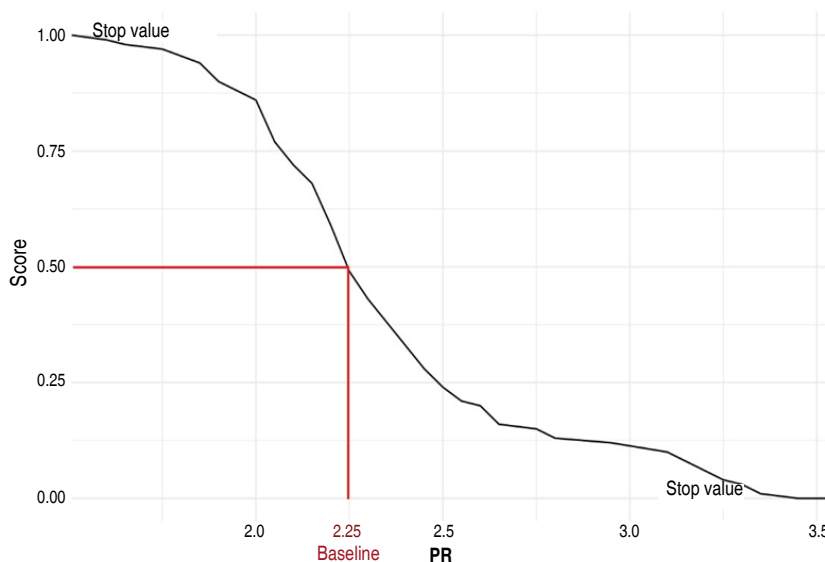


**Figure 9.** Scoring curve of Penetration Resistance (PR).

TP and pH presented optimal plateau score curves (Figures 10 and 11). Regarding the former, a TP of approximately 70% presented the highest score. The cumulative normal

distribution of TP shows that most pores are in the 66-75.2% range and that values less than 60% and greater than 80% have a very low probability of occurrence and

may be undesirable (Figure 10). Nevertheless, a proper distribution between MAC and MIC is no less important. Similarly, pH exhibited an optimal plateau, indicating a

high probability of values close to 5.8, which favors forage production. It was found that the most favorable pH range is between 5.4 and 6.4 (Figure 11).

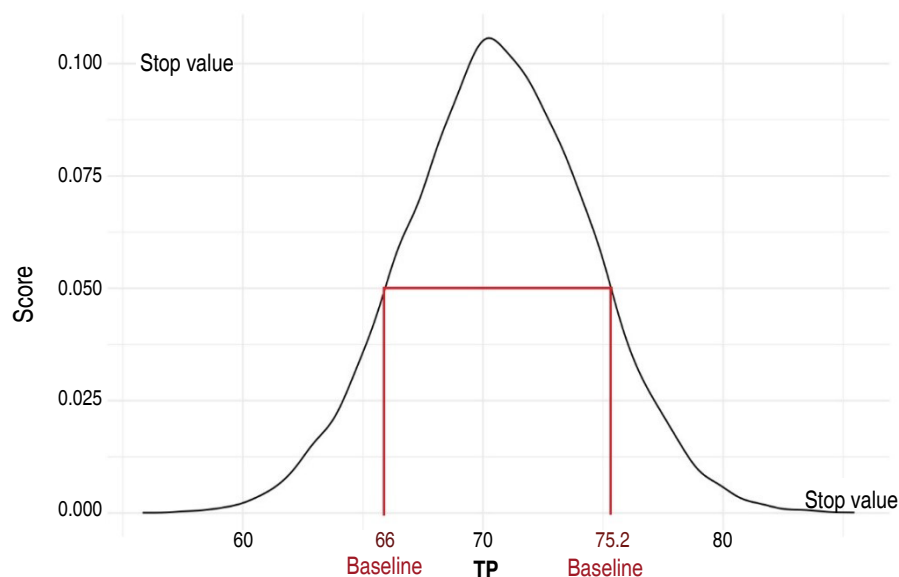


**Figure 10.** Scoring curve of Total Porosity (TP).

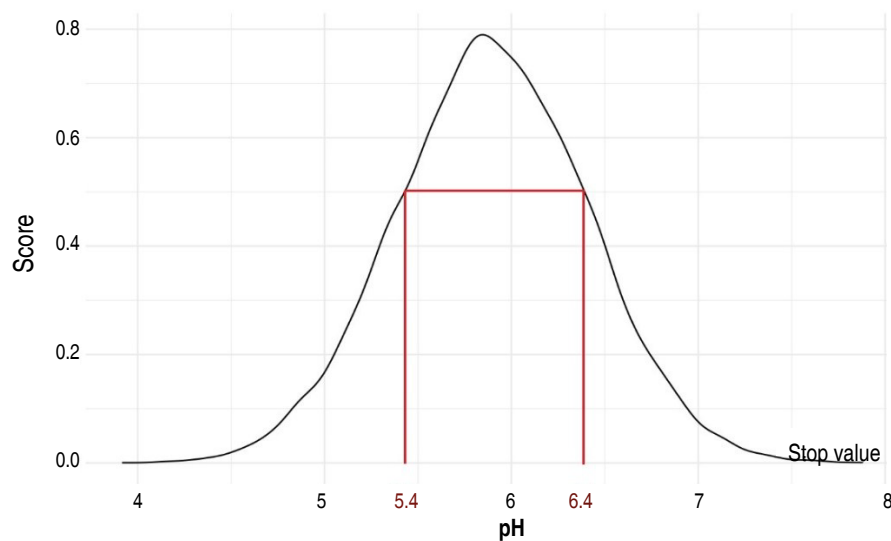


**Figure 11.** Scoring curve of pH.

ECEC presented a “more is better” scoring curve, showing a higher probability of occurrence for values above 18.5 (Figure 12). If the ECEC is above 18.5,

there is a score above 50%, which is desirable for the pasture. ECEC is especially favored by high concentrations of Ca.

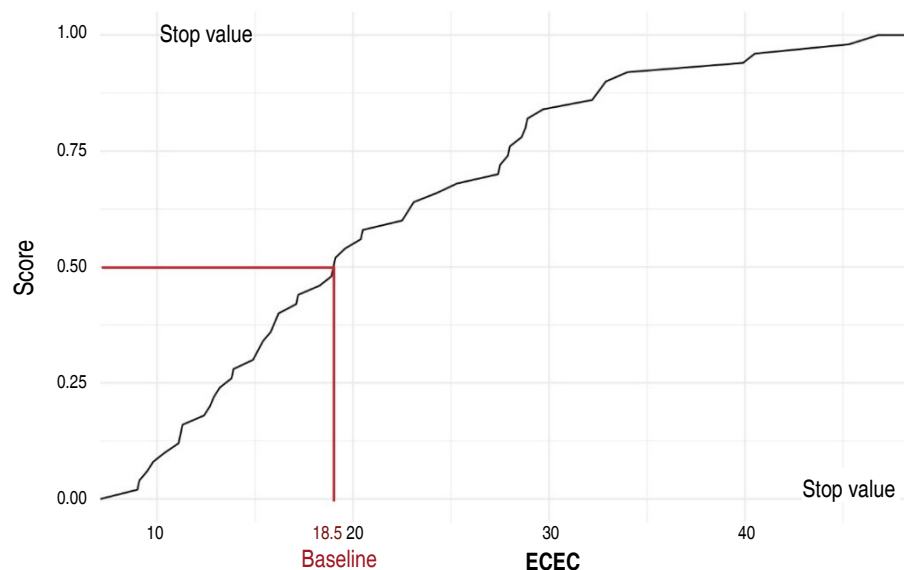


**Figure 12.** Scoring curve of Effective Cation Exchange Capacity (ECEC).

### A soil quality model/index

The data in the MDS were re-evaluated by PCA to obtain vector magnitudes for all the soil components. These values were used to calculate the weights of the different soil quality indicators. As a result (Table

6), a soil quality index (SQI) was obtained (Equation 1). The weight of the indicators ranged between 8.7 and 22.5%, while the variables BD, TP, and MAC contributed the most to the model, with 22.5, 22.4, and 22.0%, respectively.

$$SQI = (0.225 \times BD) + (0.224 \times TP) + (0.220 \times MAC) + (0.218 \times MIC) + (0.113 \times PR) + (0.0879 \times ECEC) + (0.0877 \times pH) \quad (1)$$

Swanepoel et al. (2014), who studied kikuyu and ryegrass pastures in South Africa, evaluated an MDS using PCA and obtained the magnitudes of the soil components, which they used to select the PCs with the highest weight. When they determined the SQI, they found that gravel (16%), moisture retention capacity (15%), and PR (13%) were the most relevant physical indicators; P (17%) and Mn (12%) were the most important chemical indicators; and SOM (13%) was the most influential biological indicator. Thus, the only variable in common between their study and this investigation was PR (13 vs 11.3%). On the other hand, Sharma et al. (2014) evaluated *Pennisetum americanum* grass and found the key soil quality indicators and their contributions to the SQI: organic carbon (19%), available N (20%), exchangeable Ca (3%), available Zn (4%) and Cu (17%), labile carbon (20%), and mean weight diameter of soil aggregates (17%).

It was found that the physical variables presented the greatest contribution to the SQI compared to their chemical counterparts, and a more marked trend was observed when the index was determined separately. The physical variables showed a decreasing trend, contrary to the chemical properties, which exhibited high sufficiency values. However, no determining correlation was found between the total SQI and the forage yield of the crop.

### CONCLUSION

A Soil Quality Index (SQI) was established as a baseline for assessing the degradation and forage yield of kikuyu grass at the Paysandú Agricultural Station. This index can also be used as a reference for similar studies in the high Andean tropics of Colombia. Principal Component Analysis (PCA) facilitated the identification of key indicators that are most influential in the soil quality of kikuyu grasslands, and it



was used to develop the SQI. The most sensitive indicators identified here were bulk density (BD)>total porosity (TP)>macropores (MAC)>micropores (MIC)>penetration resistance (PR)>effective cation exchange capacity (ECEC)>pH. The SQI was calculated using Equation (1):  $SQI = (0.225 \times BD) + (0.224 \times TP) + (0.220 \times MAC) + (0.218 \times MIC) + (0.113 \times PR) + (0.0879 \times ECEC) + (0.0877 \times pH)$ .

The physical variables were found to contribute more significantly to the SQI than their chemical counterparts. This index offers a valuable tool for preventing grassland degradation because it is based on the most sensitive indicators and provides guidance for effective management. These findings can serve as a reference for establishing SQIs at a regional level in the municipalities in the dairy belt of eastern and northern Antioquia.

For bulk density (BD), the baseline threshold is critical at values exceeding  $0.58 \text{ Mg m}^{-3}$ . For penetration resistance (PR), the baseline threshold is critical at values greater than 2.25 MPa. Additionally, the optimal pH range for the development of kikuyu grass is between 5.4 and 6.4.

## ACKNOWLEDGMENTS

The authors thank Professor Ramiro Ramírez Pisco for his accurate and timely academic contributions. They are also grateful to Universidad Nacional de Colombia (Medellín Headquarters) for allowing them to conduct this study at the Paysandú Agricultural Experiment Station and use the Soil Physics Laboratory to evaluate the samples.

## REFERENCES

- Amorim H, Ashworth A, Moore P et al (2020) Soil quality indices following long-term conservation pasture management practices. *Agriculture, Ecosystems and Environment* 301: 107060. <https://doi.org/10.1016/j.agee.2020.107060>
- Barbosa L, Magalhães P, Bordonal R et al (2019) Soil physical quality associated with tillage practices during sugarcane planting in south-central Brazil. *Soil and Tillage Research* 195: 104383. <https://doi.org/10.1016/j.still.2019.104383>
- Blanco-Sepúlveda R, Gómez-Moreno ML and Lima F (2024) An approach to the key soil physical properties for assessing soil compaction due to livestock grazing in Mediterranean Mountain Areas. *Sustainability* 16(10): 4279. <https://doi.org/10.3390/su16104279>
- Bünemann E, Bongiorno G, Bai Z et al (2018) Soil quality: A critical review. *Soil Biology and Biochemistry* 120: 105-125. <https://doi.org/10.1016/j.soilbio.2018.01.030>
- Chaudhry H, Vasava H, Chen S et al (2024) Evaluating the soil quality index using three methods to assess soil fertility. *Sensors* 24(864): 1-15. <https://doi.org/10.3390/s24030864>
- Colombi T and Keller T (2019) Developing strategies to recover crop productivity after soil compaction: A plant eco-physiological perspective. *Soil and Tillage Research* 191: 156-161. <https://doi.org/10.1016/j.still.2019.04.008>
- Delmelle P, Opfergelt S, Cornelis J and Ping C-L (2015) Chapter 72 - Volcanic Soils. *The Encyclopedia of Volcanoes* (Second edition), pp 1253-1264. In: *The Encyclopedia of Volcanoes*. <https://doi.org/10.1016/B978-0-12-385938-9.00072-9>
- Gómez A, Silva A, Salazar J et al (2014) Producción de materia seca y calidad del pasto kikuyo *P. clandestinum* en diferentes niveles de fertilización nitrogenada y en asocio con aliso *Alnus acuminata* en el trópico alto colombiano. En: *Anais do 1o Simpósio Internacional de Arborização de Pastagens em Regiões Subtropicais*. <https://ainfo.cnptia.embrapa.br/digital/bitstream/item/123660/1/p32-41-Doc.-268-Anais.pdf>
- Hazelton P and Murphy B (2016) Interpreting soil test results: what do all the numbers mean? Third edition. CSIRO Publishing. Australia. <http://doi.org/10.1071/9781486303977>
- Hewitt A, Balks M and Lowe D (2021) The soils of Aotearoa New Zealand. *World Soils Book Series*. USA, 332 p. <https://doi.org/10.1007/978-3-030-64763-6>
- Joimel S, Schwartz C, Hedde M et al (2017) Urban and industrial land uses have a higher soil biological quality than expected from physicochemical quality. *Science of The Total Environment* 584-585: 614-621. <https://doi.org/10.1016/j.scitotenv.2017.01.086>
- Keller T, Colombi T, Ruiz S et al (2017) Long-term soil structure observatory for monitoring post-compaction evolution of soil structure. *Vadose Zone Journal* 16(4): 1-13. <https://doi.org/10.2136/vzj2016.11.0118>
- Koureh H, Asgarzadeh H, Mosaddeghi M et al (2020) Critical values of soil physical quality indicators based on vegetative growth characteristics of spring wheat (*Triticum aestivum* L.). *Journal of Soil Science and Plant Nutrition* 20(2): 493-506. <https://doi.org/10.1007/s42729-019-00134-8>
- Lal R (2020) Soil organic matter content and crop yield. *Journal of Soil and Water Conservation* 75(2): 27A-32A. <https://doi.org/10.2489/jswc.75.2.27A>
- Läuchli A and Grattan S (2017) Plant stress under non-optimal soil pH. pp 201-216. In: Shabala S (eds.). *Plant stress physiology*. Second edition. Ediciones S. Shabala. USA 362 p. <https://doi.org/10.1079/9781780647296.0201>
- Milazzo F, Francksen R, Abdalla M et al (2023) An overview of permanent grassland grazing management practices and the impacts on principal soil quality indicators. *Agronomy* 13(5): 1-16. <https://doi.org/10.3390/agronomy13051366>
- Pérez N, Jaramillo D, Ruiz O et al (2017) Caracterización de un Andisol de la cuenca alta de la quebrada Santa Elena, oriente antioqueño, Colombia. *Revista de la Facultad de Ciencias* 6(1): 24-38. <https://doi.org/10.15446/rev.fac.cienc.v6n1.60628>
- Rabot E, Wiesmeier M, Schlüter S et al (2018) Soil structure as an indicator of soil functions: A review. *Geoderma*, 314: 122-137. <https://doi.org/10.1016/j.geoderma.2017.11.009>
- Rodelo-Torrente S, Torregroza-Espinosa A, Moreno M et al (2022) Soil fertility in agricultural production units of tropical áreas. *Global Journal of Environmental Science and Management* 8(3): 403-418.
- Sharma K, Grace J, Chandrika S et al (2014) Effects of soil management practices on key soil quality indicators and indices in pearl millet (*Pennisetum americanum* (L.) Leeke)-based system



in hot semi-arid inceptisols. Communications in Soil Science and Plant Analysis 45(6): 785-809. <https://doi.org/10.1080/00103624.2013.867048>

Siatwiinda S, Ros G, Yerokun O et al (2024) Options to reduce ranges in critical soil nutrient levels used in fertilizer recommendations by accounting for site conditions and methodology: A review. Agronomy for sustainable development 44 (9): 1-22. <https://doi.org/10.1007/s13593-023-00943-3>

Soil Survey Staff (2022) Keys to soil taxonomy, 13th edition. USDA-Natural Resources Conservation Service. <https://www.nrcs.usda.gov/sites/default/files/2022-09/Keys-to-Soil-Taxonomy.pdf>

Swanepoel P, du Preez C, Botha P et al (2014) Soil quality characteristics of kikuyu-ryegrass pastures in South Africa. Geoderma

232-234: 589-599. <https://doi.org/10.1016/j.geoderma.2014.06.018>

USDA, Agricultural Research Service, National Plant Germplasm System (2024) Germplasm resources information network (GRIN Taxonomy). National Germplasm Resources Laboratory, Beltsville, Maryland. <https://npgsweb.ars-grin.gov/gringlobal/taxon/taxonomydetail?id=464260>

Valle S and Carrasco J (2018) Soil quality indicator selection in Chilean volcanic soils formed under temperate and humid conditions. Catena 162: 386-395. <https://doi.org/10.1016/j.catena.2017.10.024>

Villalobos-Villalobos L and WingChing-Jones R (2023) Forage biomass estimated with a pre-calibrated equation of a rising platometer in pastures grown in tropical conditions. Grasses 2(2):127-141. <https://doi.org/10.3390/grasses2020011>



# Influence of indole-butyric acid and substrate type on vegetative propagation of native Peruvian blueberry (*Vaccinium* sp.)

Influencia del ácido indol butírico y del tipo de sustrato en la propagación vegetativa del arándano nativo peruano (*Vaccinium* sp.)

<https://doi.org/10.15446/rfnam.v77n3.109393>

Tito Sanchez-Santillan<sup>1\*</sup>, Henry Santillan-Culquimboz<sup>2</sup> and María Huamán Vela<sup>3</sup>

## ABSTRACT

### Keywords:

Auxin  
Coconut fiber  
Microtunnel  
Native fruit tree  
Rooting of cuttings

In the Amazon region of Peru, native blueberries are found in high Andean areas, where they are associated with small shrubs and mosses. These blueberries prefer shallow soils with a sandy-clay texture and low fertility. However, their population is threatened by their limited regenerative capacity and various anthropogenic factors. The aim of this study was to evaluate the influence of indole butyric acid and substrate type on the vegetative propagation of native Peruvian blueberry (*Vaccinium* sp.) grown in microtunnel. The experiment was conducted under a complete randomized design with the factorial arrangement; A: substrate (sand 100%, sand + coconut fiber 1:1 v/v and coconut fiber 100%) and B: AIB concentrations (1, 2 and 3 g L<sup>-1</sup>) and control (0 g L<sup>-1</sup>), giving 12 treatments, three replicates and 36 experimental plots. In the field, apical shoots of blueberry with semi-lignified and vigorous stems were collected. In the laboratory, they were disinfected with fungicide and cut to a size of 7 cm. Subsequently, they were treated with AIB and planted in prepared substrates. After 120 days in the microtunnel, it was observed that blueberry cuttings showed higher survival in sand + coconut fiber (94.7%), rooting (73.8%), root number (6.9), and root growth (9.2). AIB concentrations at 2 and 3 g L<sup>-1</sup> had a greater effect on rooting, with values above 60%. The use of suitable substrates and auxin concentrations significantly favors the vegetative propagation of native blueberries. This propagation technique is postulated as a promising alternative for the mass propagation of this species for the conservation and rehabilitation of degraded ecosystems.

## RESUMEN


### Palabras clave:

Auxina  
Fibra de coco  
Microtúnel  
Frutal nativo  
Clonación

En la región Amazonas del Perú, los arándanos nativos se encuentran en zonas altoandinas, donde se asocian con pequeños arbustos y musgos. Estos arándanos prefieren suelos poco profundos con textura arcillo-arenosa y de baja fertilidad. Sin embargo, su población se ve amenazada por su limitada capacidad regenerativa y diversos factores antropogénicos. El objetivo de este estudio fue evaluar la influencia del ácido indol butírico y del tipo de sustrato en la propagación vegetativa del arándano nativo peruano (*Vaccinium* sp.) cultivado en microtúnel. El experimento se realizó bajo un diseño completo al azar con arreglo factorial; A: sustrato (arena 100%, arena + fibra de coco 1:1 v/v y fibra de coco 100%) y B: concentraciones de AIB (1, 2 y 3 g L<sup>-1</sup>) y un testigo (0 g L<sup>-1</sup>), dando 12 tratamientos, 3 repeticiones y 36 unidades experimentales. En el campo, se recolectaron brotes apicales de arándano con tallos semi-lignificados y vigorosos. En el laboratorio, fueron desinfectados con fungicida y cortados a un tamaño de 7 cm. Posteriormente, se trataron con AIB y se plantaron en sustratos preparados. Tras 120 días en el microtúnel, se observó que los esquejes de arándano mostraron una mayor supervivencia en arena + fibra de coco (94,7%), enraizamiento (73,8%), número de raíces (6,9) y crecimiento radicular (9,2). Las concentraciones de AIB a 2 y 3 g L<sup>-1</sup> tuvieron un mayor efecto en el enraizamiento, con valores superiores al 60%. El uso de sustratos y concentraciones adecuadas de auxina favorece significativamente la propagación vegetativa del arándano nativo. Esta técnica de propagación se postula como una alternativa prometedora para la propagación masiva de esta especie con fines de conservación y rehabilitación de ecosistemas degradados.

<sup>1</sup>Research Institute for the Sustainable Development of Ceja de Selva, Universidad Nacional Toribio Rodríguez de Mendoza de Amazonas, Chachapoyas, Peru. [titosanchezsantillan@gmail.com](mailto:titosanchezsantillan@gmail.com) 

<sup>2</sup>Professional School of Agricultural Engineering, Universidad Nacional Toribio Rodríguez de Mendoza de Amazonas, Chachapoyas, Peru. [henry280401@gmail.com](mailto:henry280401@gmail.com) 

<sup>3</sup>Graduate School of the Universidad Nacional Toribio Rodríguez de Mendoza de Amazonas, Chachapoyas, Peru. [marihuamanv170@gmail.com](mailto:marihuamanv170@gmail.com) 

\*Corresponding author

In recent years, berries in Peru have become very important in the food trade. Such is the case of the blueberry, which includes several species and hybrids of the genus *Vaccinium* (García et al. 2013). The latter is home to about 500 species with a wide geographic distribution, reported mainly throughout the Americas (Mendoza et al. 2020).

The Peruvian native blueberry (*Vaccinium* sp.) is a perennial species of the Ericaceae family (Mostacero et al. 2015). Currently, this fruit presents a growth in its consumption due to its nutraceutical qualities, mainly its high percentage of antioxidants and its low levels of sugars (Tejada Alvarado et al. 2019). It also possesses bioactive compounds that prevent the risk of degenerative and cardiovascular diseases (Hernández et al. 2017). These aspects allowed it to take on greater importance, amplifying its development prospects, which has motivated the establishment of plantations in the Amazon region.

According to Mendoza et al. (2020), blueberry propagation can be done by botanical seed and vegetative seed. Regarding the first method, this species presents limitations, in terms of seed availability, added to the high dormancy of seeds (Suárez-Ballesteros et al. 2018; Jiménez-Bonilla and Abdelnour 2018). On the other hand, with vegetative seeds, it turns out to be a more advantageous technique, since seeds can be available all year round and genotypes with superior agronomic characteristics can be propagated (Mendoza et al. 2020).

In vegetative propagation, there are endogenous and exogenous factors that favor root formation in cuttings (Castro-Garibay et al. 2019). Saini et al. (2013), mention that auxins have important functions in cuttings, these act in biosynthesis, transport, and signaling during the rooting phase. The most widely used auxin is indole butyric acid (IBA), due to its stability and easy translocation in plants, and can be applied in wide ranges of doses in a large number of species (Báez-Pérez et al. 2015).

Another relevant factor in rooting is the substrate, thanks to its textural properties that allow it to retain temperature, humidity, and porosity during root formation and growth (Yukari et al. 2013). According to Castrillón et al. (2008), the most used substrates for rooting stakes are agricultural

soil, sand, peat, vermiculite, pumice, compost, coconut fiber, and rice husk, all with different effects depending on the species. Frías-Moreno et al. (2021) mentioned that to propagate species of the Ericaceae family, it is necessary to use substrates rich in organic matter (Frías-Moreno et al. 2021).

In research conducted on blueberries, Tejada Alvarado et al. (2019), reported that auxin AIB at a concentration of 100 to 200 mg L<sup>-1</sup>, generated better rooting and root growth percentage. In the same line, Tejada-Alvarado et al. (2021), tested the effect of AIB concentrations and different genotypes of native blueberry, achieving and higher rooting with the concentration of 2,000 mg L<sup>-1</sup>.

To find effective techniques for the multiplication of native species in a vulnerable state, the aim of this study is to evaluate the influence of indole butyric acid and the type of substrate on the vegetative propagation of the native Peruvian blueberry (*Vaccinium* sp.) grown in microtunnel.

## MATERIALS AND METHODS

### Collection of biological material

Blueberry cuttings were collected from remnant plants in natural forests in the province of Rodríguez de Mendoza. These plants had an average height of 0.40 m and were branched. In the early morning hours, apical shoots of 10 cm in length were cut. They were then covered with kraft paper and placed in a properly labeled and conditioned technopor box. In addition, the samples were moistened with a hand sprayer to keep the vegetative material turgid and immediately transferred to the laboratory.

### Preparation and sowing of planting material

In the laboratory, the cuttings were standardized to a size of 7 cm. They were then subjected to a disinfection process with a fungicide (mancozeb + propineb at 1 g L<sup>-1</sup> of water) and left to rest for 3 minutes. Subsequently, the cuttings were prepared for auxin treatment by removing the basal leaves to expose the stem to 1.5 cm. A straight cut was made and the cuttings were immersed in an auxin solution of Indole-butyric acid with a purity of 98% diluted in 96 ° alcohol at various concentrations (1, 2, and 3 g L<sup>-1</sup>) along with a control (0 g L<sup>-1</sup>). The excess solution was removed, and the cuttings were allowed to volatilize for 6 to 10 min at a constant temperature of 20 °C.

At the same time, the substrates were prepared (sand 100%, sand + coconut fiber 1:1 v/v, and coconut fiber 100%), disinfected in an autoclave at 121 °C for 3 h, then allowed to dry and eliminate the excess water, until leaving it in field capacity; these substrates were placed in germination trays of 72 cavities, properly distributed according to design.

The cuttings were placed by introducing the auxin-treated base at a depth of no more than 1.5 cm, then a slight pressure was applied to the substrate to put it in direct contact with the cuttings and also to avoid leaving air chambers.

The trays were finally placed in a microtunnel of 3.0x1.0x0.90 m, in which the temperature (>18 °C) and relative humidity (>80%) were controlled and a nebulized irrigation system with forget-type nozzles was incorporated.

#### Variables studied

After 120 days, the following variables were evaluated: rooting, number of roots, and root size for each factor and the interaction of these.

#### Experimental design and data analysis

The experiment was conducted under a completely

randomized design with a bifactorial. Factor A corresponded to the substrate, with three levels: sand, sand + coconut fiber, and coconut fiber. Factor B was the IBA dose, with four levels: 0, 1, 2, and 3 g L<sup>-1</sup>. The data complied with the assumptions of normality and homogeneity of variances, therefore, an analysis of variance ( $\alpha=5\%$ ) was performed. Processing of all data was performed with InfoStat Statistical Software version 2020.

#### RESULTS AND DISCUSSION

In the overall analysis, significant differences were identified between substrates in rooting ( $P<0.05$ ), as well as in survival, number, and length of roots ( $P<0.01$ ). Both the percentage of rooted cuttings and the number of roots showed a high significant difference ( $P<0.01$ ) between the different doses of AIB; in addition, a significant difference ( $P<0.05$ ) was observed in survival. However, no significant effects were found in the interaction between both factors (Table 1). On the other hand, Yukari et al. (2013) mentioned that the factors substrate and AIB doses act independently in the rooting process, suggesting that the type of substrate and AIB doses do not affect the percentage of rooted cuttings of *Rubus* spp. and that the application of AIB is even unnecessary.

**Table 1.** Probability *P* value in the rooting of native blueberry mini-shoots with different substrates and AIB concentrations.

Source of variation	<i>P</i> -value			
	Survival (%)	Rooted cuttings (%)	Number of roots	Root length
Substrate	0.0008**	0.0107*	0.0023**	0.0040**
Dose	0.0237*	0.0001**	0.0039**	0.6349
Substrate*Dose	0.1562	0.5297	0.0000	0.2039

\*=significant ( $P<0.05$ ); \*\*=highly significant ( $P<0.01$ ).

The 5% Tukey test (Table 2) was performed for both factors. In the variables of the substrate factor, two ranges of significance were registered; where the sand + coconut fiber substrate registered a statistical difference concerning the other treatments, presenting a higher percentage of survival and rooting; with 94.7 and 63.8%, respectively, as well as a greater number (6.9) and length of roots (9.2 cm). Research conducted by Frías-Moreno et al. (2021) in raspberry, showed that organic matter substrates presented greater efficiency in propagation with an increase in the survival of the number of plants, and also mentioned that substrates with a high content of organic matter and

adequate nutrient composition favor vegetative growth. Regarding AIB doses, a statistical difference was observed in the survival percentage at the 3 mg L<sup>-1</sup> concentration compared to the other doses, also showing the lowest survival percentage (72.92%), which contrasts with the results of Marangon and Biasi (2013), who suggest that an increase in AIB concentration results in a reduction in the percentage of dead cuttings. To rooting percentage, two significant ranges were identified that can be associated with two groups: doses of 0 and 1 g L<sup>-1</sup> form one group, while 2 and 3 g L<sup>-1</sup> constitute another group. Although no statistical differences were found within each group,



both groups differed from each other, with the second group (2 and 3 g L<sup>-1</sup>) showing the best rooting results. Therefore, the choice of dose for rooting will depend on factors internal or external to the study.

In support of these findings, Marangon and Biasi (2013) note that the highest rooting percentages in different

blueberry varieties were obtained with concentrations of 2 g L<sup>-1</sup>. This concentration also yielded promising results in microscopic cutting of the apical portion of branches of the Climax variety (Schuch et al. 2007). Regarding root number, the 1 g L<sup>-1</sup> concentration of AIB showed the best results with a significant statistical difference. However, no significant effects on root length were observed (Table 2).

**Table 2.** Multiple comparisons of means according to Tukey post-hoc test ( $\alpha=5\%$ ) for rooting variables of native blueberry mini shoots.

Factor	Survival (%)	Rooting (%)	NR	LR
<b>Substrate</b>				
Sand	76.6 <sup>b</sup>	51.3 <sup>b</sup>	5.6 <sup>b</sup>	6.6 <sup>b</sup>
Sand + coconut fiber	94.7 <sup>a</sup>	63.8 <sup>a</sup>	6.9 <sup>a</sup>	9.2 <sup>a</sup>
Coconut fiber	4.2 <sup>b</sup>	52.2 <sup>b</sup>	5.8 <sup>b</sup>	7.1 <sup>b</sup>
<b>Dose de AIB (ppm)</b>				
0	95.5 <sup>a</sup>	45.4 <sup>b</sup>	5.6 <sup>b</sup>	7.9 <sup>a</sup>
1,000	80.8 <sup>ab</sup>	47.1 <sup>b</sup>	7.2 <sup>a</sup>	8.2 <sup>a</sup>
2,000	77.1 <sup>ab</sup>	64.6 <sup>a</sup>	5.8 <sup>b</sup>	7.7 <sup>a</sup>
3,000	72.9 <sup>b</sup>	65.8 <sup>a</sup>	5.9 <sup>b</sup>	7.0 <sup>a</sup>

NR: number of roots; LR: root length; Means with equal letters do not differ statistically from each other ( $\alpha=0.05$ ).

According to Castrillón et al. (2008), the most important factors in seedling formation are: sources of vegetative material, rooting media, treatments with rooting stimulators, and environmental conditions. In the Tukey test in the interaction of factors (substrate \* AIB dose), the best results in the variable number of roots were obtained with the 1 g L<sup>-1</sup> dose of AIB in the Sand + coconut fiber substrate, possibly due to its ability to

retain adequate moisture and help in the interaction with AIB. Less encouraging results were observed in the sand substrate without the application of AIB, while the average in the coconut fiber substrate decreased more than the control group at the 2 g L<sup>-1</sup> AIB dose (Figure 1).

In the root length variable, a significant effect was observed in the Sand + coconut fiber substrate with a dose of

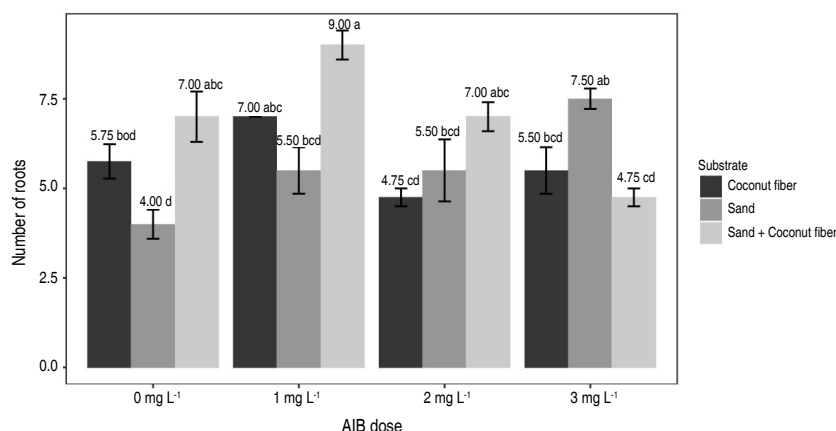


**Figure 1.** Effect of the interaction between substrate and AIB dose factors on the number of roots of *Vaccinium* sp.

1 g L<sup>-1</sup> of AIB, showing better results. In the Sand + coconut fiber substrates, no statistical differences were found in any AIB dose (Figure 2). However, Báez-Pérez

et al. (2015) indicate that the rooting process occurs at the expense of the vegetative material, i.e., the presence or absence of nutrients in a substrate will not affect the

rooting power of a cutting, but is subject to the vigor of the mother plant.

The substrate sand + coconut fiber gave the best results in the variables number and length of roots at a concentration of  $1 \text{ g L}^{-1}$  (Figures 1 and 2). This substrate presents characteristics of good aeration, structure, moisture retention capacity, and drainage, among others (Picolotto et al. 2013); which maximize the effects of the AIB hormone. Likewise, Kumar et al. (2022)

mentioned that exposure to high auxin concentrations produces inhibitory effects on root number and length, which would explain the downward trend in the means of the variables with increasing doses of AIB. On the other hand, the sand substrate, having a lower moisture retention capacity and therefore higher porosity, seems to suppress the effects of AIB, presenting an increasing trend with increasing doses of AIB; that is, in the results shown, the substrate variable is a factor that conditions the effects of Auxin.

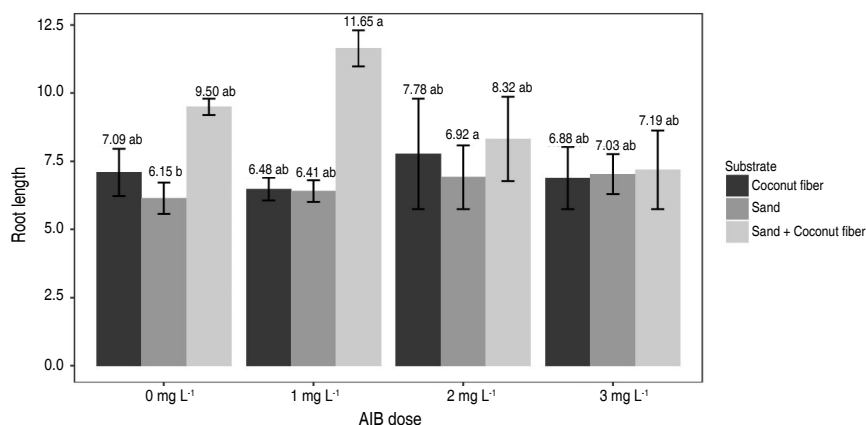


**Figure 2.** Effect of the interaction between substrate factors and AIB dose on root length of *Vaccinium* sp.

Figure 3 illustrates the clonal propagation process of native blueberries, depicting the blueberry mother plants in the field and the rooting of minicutting at 120 days, utilizing various substrates and AIB doses. These findings underscore the importance of meticulously selecting

substrates and AIB doses to ensure a successful rooting process during the clonal propagation of native blueberries. Considering these variables is crucial for achieving optimal plant development and ensuring success in the clonal reproduction of this species.

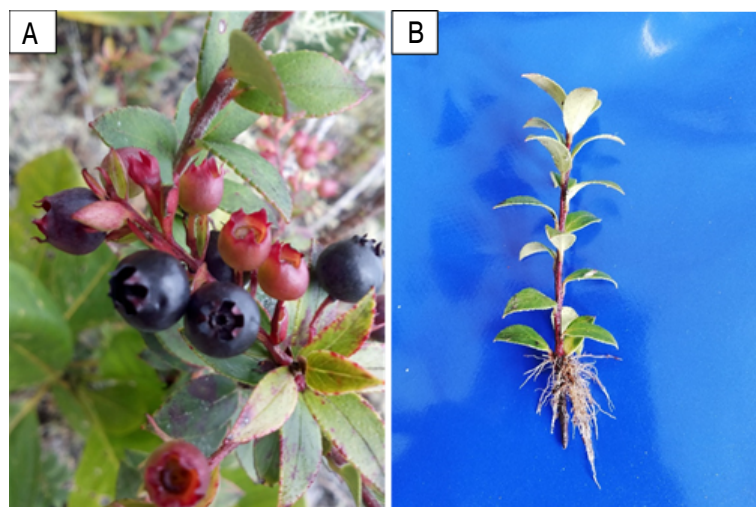


**Figure 3.** Clonal propagation of native blueberry; A. Blueberry mother plants in the field; B. Rooting of minicutting at 120 days, with different substrates and AIB doses.

## CONCLUSION

The substrates used in the study had different effects on the native blueberry mini-stakes. The sand-based substrate favored survival and, in combination with coconut fiber, favored the rooting of the cuttings. AIB auxin, used at a concentration of 2 g L<sup>-1</sup>, considerably improved the rhizogenic capacity of the cuttings. This study demonstrates the feasibility of propagating native blueberries using available substrates and effective auxins. The developed technique turns out to be a promising alternative for the mass reproduction of native species for the conservation and rehabilitation of degraded ecosystems.

## REFERENCES

- Báez-Pérez A, González-Molina L, Solís Moya E et al (2015) Effect of the application of indole-3-butyric acid in production and quality of wheat (*Triticum estivum* L.). *Revista Mexicana de Ciencias Agrícolas* 6(3): 523–537. <https://www.scielo.org.mx/pdf/remexca/v6n3/v6n3a7.pdf>
- Castrillón JC, Carvajal E, Ligarreto, G and Magnitskiy S (2008) El efecto de auxinas sobre el enraizamiento de las estacas de agraz (*Vaccinium meridionale* Swartz) en diferentes sustratos. *Agronomía Colombiana* 26(1): 16-22. <http://scielo.org.co/pdf/agc/v26n1/v26n1a03.pdf>
- Castro-Garibay SL, Villegas-Monter A and Contreras-Garibay Maya R (2019) Enraizamiento de estacas en tres cultivares de arándano (*Vaccinium corymbosum* L.). *Agroproductividad* 12(3): 63-68. <https://doi.org/10.32854/agrop.v0i0.1328>
- Frías-Moreno MN, Olivas Orozco GI, González Aguilar GA, Jacobo Cuellar JL et al (2021) Sustratos y ácido indol-3-butírico en la propagación de frambuesa. *Terra Latinoamericana* 39: 1-10. <https://doi.org/10.28940/terra.v39i0.753>
- García Rubio J, García González de Lena G and Giordina Ara M (2013) Situación actual del cultivo del arándano en el mundo. *Tecnología Agroalimentaria: Boletín informativo del SERIDA*.
- Hernández Hernández I, Benito Bautista P and Arellanes Juárez N (2017) Evaluación de calidad del fruto de arándano (*Vaccinium corymbosum* L.) var. Biloxi, en dos regiones del estado de Oaxaca. *Universidad & Ciencia* 6: 256-273.
- Jiménez-Bonilla V and Abdelnour Esquivel A (2018) Protocolo de micropropagación de arándano nativo de Costa Rica (*Vaccinium consanguineum*). *SciELO* 31(1): 144-159.
- Kumar P, Patel PK and Sonkar MK (2022) Propagation through juvenile shoot cuttings in difficult-to-root *Dalbergia latifolia* – examining role of endogenous IAA in adventitious rooting. *Plant Physiology Reports* 27(2): 242–249. <https://doi.org/10.1007/s40502-022-00664-x>
- Marangon MA and Biasi LA (2013) Estaquia de mirtilo nas estações do ano com ácido indolbutírico e aquecimento do substrato. *Pesquisa Agropecuária Brasileira* 48(1): 25-32. <https://doi.org/10.1590/S0100-204X2013000100004>
- Mendoza W, , López-Medina S, Mostacero-León J et al (2020) Determinación de las concentraciones adecuadas de 2,4 diclorofenoxiacético y Kelpak en el enraizamiento de estacas de *Vaccinium floribundum* Kunth “pushgay”. *Manglar* 17(1): 21-25. <http://doi.org/10.17268/manglar.2020.004>
- Mostacero León J, Rázuri González T and Gil Rivero AE (2015) Fitogeografía y morfología de los *Vaccinium* (Ericaceae) “arándanos nativos” del Perú. *INDES Revista de Investigación para el Desarrollo Sustentable* 3(1): 43-52.
- Picolotto L, Dos Santos Pereira I, Kleinick Vignolo G et al (2013) Enraizamiento de Mirtilero em diferentes substratos. *Congrega Urcamp*. <https://ainfo.cnptia.embrapa.br/digital/bitstream/item/91645/1/25.pdf>
- Saini S, Sharma I, Kaur N and Kumar Pati P (2013) Auxin: a master regulator in plant root development. *Plant Cell Reports* 32: 741-757. <https://doi.org/10.1007/s00299-013-1430-5>
- Schuch MW, De Rossi A, Damiani CR and Campos Soares G (2007) Iba and substrate in the plantlets production of blueberry cv. ‘Climax’ through microcuttings. *Ciência Rural* 37(5): 1446-1449. <https://doi.org/10.1590/S0103-84782007000500036>
- Suárez-Ballesteros CI, Calderón-Hernández M and Mancipe-Murillo C (2018) Propagación sexual y tolerancia a la desecación del agraz (*Vaccinium meridionale* Sw) de tres fuentes semilleras localizadas en Ráquira, San Miguel de Sema (Boyacá) y Gachetá (Cundinamarca). *Revista De La Academia Colombiana De Ciencias Exactas, Físicas y Naturales* 42(163): 207-215. <https://doi.org/10.18257/raccefyn.614>
- Tejada Alvarado JJ, Oliva M, Collazos Silva R, Vilca Valqui NC and Huaman Huaman E (2019) Efecto del ácido indolbutírico (AIB) sobre el enraizamiento y adaptabilidad de segmentos nodales de arándano (*Vaccinium corimbosum* L.). *Revista de Investigación de Agroproducción Sustentable* 3(3): 24-29. <https://www.semanticscholar.org/reader/465f2e2d5e67866190298853c1ba44e973caed72>
- Tejada-Alvarado JJ, Meléndez-Mori JB, Vilca-Valqui NC, Huaman-Huaman E and Oliva M (2021) Enraizamiento de esquejes de arándanos silvestres (*Vaccinium* spp.) del noreste peruano. *Acta Agrobotánica* 74 (7413). <https://doi.org/10.5586/aa.7413>
- Yukari Yamamoto L, Koyama R, Silva Borge WF et al (2013) Substratos no enraizamento de estacas herbáceas de amora-preta Xavante. *Ciência Rural* 43(1): 15-20. <https://doi.org/10.1590/S0103-84782012005000135>

# Sulfuric acid as a germination stimulator in forage soybean seeds (*Neonotonia wightii*)

Ácido sulfúrico como estimulante de la germinación en semillas de soja forrajera (*Neonotonia wightii*)

<https://doi.org/10.15446/rfnam.v77n3.109179>

Jhusua David Reina-García<sup>1</sup>, Gustavo Almaguer-Vargas<sup>2\*</sup>, Juan Guillermo Cruz-Castillo<sup>3</sup>, Diana Guerra-Ramírez<sup>4</sup> and Álvaro Castañeda-Vildozola<sup>5</sup>

## ABSTRACT

### Keywords:

Immersion time  
Latency  
Scarification  
Seminal cover

Forage soybean (*Neonotonia wightii*) is a legume frequently used as a cover crop in field crops. However, as a species of the *Phaseoloideae* subfamily, it is characterized by the physical latency of the seed, which makes it difficult to obtain a high, homogeneous, and rapid germination. The aim of the present study was to determine which method of scarification stimulates the germination process to a greater extent. The following immersion times were evaluated: 5 to 20 minutes in 98% sulfuric acid, 24 hours in 5.4% sodium hypochlorite, water, and gibberellic acid [100 ppm], 15 minutes of treatment with sandpaper and the combination of these last two. They were distributed in a completely randomized experimental design, where eight treatments and a control were evaluated, with three replicates each and 200 seeds as experimental units, subjected to controlled conditions (germination chambers at constant temperatures and a relative humidity of 27 °C and 70%, respectively) during the spring of 2022. The results were favorable, a high germination percentage was obtained from seeds subjected to a 20-minute immersion time in sulfuric acid (90% germination and an average of six germinated seeds per day) and this was significantly higher than the rest, making it an effective method to break the physical latency of the seeds, as it removes the impermeable cover allowing inhibition and consequently the activation of the seed's metabolism.


## RESUMEN

### Palabras clave:


Tiempo de inmersión  
Latencia  
Escarificación  
Cubierta seminal

La soja forrajera (*Neonotonia wightii*) es una leguminosa frecuentemente utilizada como cubierta en cultivos de campo. Sin embargo, al ser una especie de la subfamilia *Phaseoloideae*, se caracteriza por la latencia física de la semilla, lo que dificulta obtener una germinación alta, homogénea y rápida. El objetivo del presente estudio fue determinar cuál método de escarificación estimula en mayor medida el proceso de germinación, se evaluaron tiempos de inmersión desde los 5 hasta los 20 minutos en ácido sulfúrico (98%), 24 horas en inmersión en hipoclorito de sodio (5,4%), agua y ácido giberélico [100 ppm], 15 minutos con lija y el combinado de estas dos últimas, las cuales fueron distribuidas en un diseño experimental completamente al azar, donde se evaluaron ocho tratamientos y un testigo, tres repeticiones cada uno y 200 semillas como unidades experimentales, sometidas en condiciones controladas (cámaras de germinación a temperaturas y humedad relativa constantes de 27 °C y 70%, respectivamente) durante la primavera del 2022. Los resultados fueron favorables, un alto porcentaje de germinación se obtuvo de las semillas sometidas a un tiempo de inmersión de 20 minutos en ácido sulfúrico (90% de germinación y un promedio de germinación de seis semillas germinadas por día) y fue significativamente mayor que el resto. Este método resulta efectivo para romper la latencia física de las semillas, debido a la remoción de la cubierta impermeable, permitiendo la inhibición en agua y consecuentemente la activación del metabolismo de la semilla.


<sup>1</sup>Universidad de los Llanos, Escuela de Ingeniería en Ciencias Agrícolas, Programa Ingeniería Agronómica, Villavicencio, Meta, Colombia.

jhsuadavid11@hotmail.com 

<sup>2</sup>Universidad Autónoma Chapingo (UACH), Departamento de Fitotecnia, México. galmaguerv@chapingo.mx 

<sup>3</sup>UACH, Centro Regional Universitario Oriente, Huatusco, Veracruz, México. jcruz@chapingo.mx 

<sup>4</sup>Laboratorio de Productos Naturales, Departamento de Preparatoria Agrícola, UACH, México. dguerr@chapingo.mx 

<sup>5</sup>Facultad de Ciencias Agrícolas, Universidad Autónoma del Estado de México, Campus "El Cerrillo", México. acastanedav@uaemex.mx 

\*Corresponding author

Currently, the use of legumes as living soil covers has proved to be a socially, economically, and environmentally viable alternative for integrated soil management, due to its interrelation with atmospheric nitrogen-fixing bacteria (Bécquer and Prévost 2016). In addition, they conserve soil moisture, improve water absorption, reduce erosion by runoff or leaching, and increase soil conservation. They also suppress the weed population and reduce the spread of pathogens (Labrada 2004).

Conventionally, current agricultural systems eliminate the weeds that grow in crops and most of the time the soil remains completely open and exposed to environmental factors (sun, wind, rain, etc.) (Cotler et al. 2020) causing to a greater or lesser extent fertility loss and erosion, which involves the detachment, transport, and deposition of soil particles due to water or wind; it is a natural process that depends on climate, soil type, topography, and vegetation (García 2016). In response to these problems, sustainable alternatives have emerged such as agroforestry techniques, crop rotation, and the use of covers, among others. Their purpose is to avoid soil degradation and increase yields.

Regarding the use of covers, *Neonotonia wightii* has established itself as one of the main plants of the Fabaceae family. Because of its African origin, it can withstand periods of drought, and due to its perennial, voluble, and branched habit it contributes to weed control in subtropical and tropical perennial fruit crops (Jannoyer et al. 2011; Morris et al. 2013). This makes it an environmentally viable strategy for the control of weed populations.

However, its conventional propagation method (by seed) has inhibited its establishment in the field due to the presence of an impermeable seed coat that acts as a physical barrier and limits the diffusion of water and gases into the seed, which prevents a uniform development and germination of embryos in a shorter period of time even when the conditions are favorable (physical latency) (Acosta et al. 2020).

Given the particular nature of this seed, the effectiveness of various chemical and mechanical scarification methods has been tested. Their purpose was to break the impermeable layer that surrounds it (Baskin and Baskin 2014) and increase the percentage of germination. The treatments

used include sulfuric acid, sandpaper, and hot water, among others (De Morais et al. 2014).

This study aim was to determine which scarification method stimulates the germination process to a greater extent. Different immersion times were evaluated, from 5 to 20 minutes in sulfuric acid, 24 hours in sodium hypochlorite, water and gibberellic acid, 15 minutes of treatment with sandpaper, and a combination of the last two.

## MATERIALS AND METHODS

### Study area

The study was conducted at the Fruit Crop Nutrition laboratory at Chapingo Autonomous University, Mexico, in the summer of 2022.

### Plant material

Forage soybean seeds (*Neonotonia wightii* var. Cooper) obtained from dry pods containing 5-6 dark brown seeds, selected from random plants from the municipality of Álamo Temapache-Veracruz, Mexico, were used; located between parallels 20°47' and 21°12' N, meridians 97°30' and 97°56' W, and at an altitude between 10 to 500 meters above sea level (masl), in the spring of 2022.

### Experimental design

A germination assay was performed where the treatments described in Table 1 were arranged in a completely randomized design with three replicates, using 200 seeds per experimental unit.

### Management of the experiment

Seeds that were treated with chemical scarification methods were washed with abundant distilled water, subsequently, 100 were placed in each Petri dish (diameter 100 mm) with moist filter paper, kept in darkness for 2 days at room temperature and moistened once a day. Afterwards, they were kept in germination chambers (SEEDBURO brand) at a constant temperature of  $27 \pm 2$  °C and moistened daily with distilled water by means of a syringe (from 3 to 13 mL as the seeds germinated) during the runtime of the assay.

### Evaluated variables

Seed germination was visually assessed every 2 days, until 15 days after sowing. Through daily observations it was possible to evaluate the variables that make up the germination process such as:



**Table 1.** Pregerminated treatments on forage soybean seeds (*Neonotonia wightii* var. Cooper).

No	Scarificación	Treatments	Immersion Time
1	Chemical	Sulfuric Acid (98%) (H <sub>2</sub> SO <sub>4</sub> )	5 min
2			10 min
3			15 min
4			20 min
5		Gibberellic acid [100 ppm] (AG <sub>3</sub> )	24 h
6		Sodium hypochlorite (NaClO)	24 h
7	Mechanical	Sandpaper #1,200	15 min
8	Chemical + mechanical	Gibberellic acid [100 ppm] + Sandpaper #1,200	24 h + 15 min
9		Control (imbibition in water)	24 h

**Germination percentage (GP):** Number of germinated seeds/total seeds, expressed as a percentage (%). A seed is considered germinated when the radicle emerges from the testa (Maqueira-López et al. 2021).

**Mean germination speed (MGS):** expressed in seeds germinated per day (González-Amaya et al. 2018).

**Mean germination time (MGT):** considering the days needed for 50% of the total of germinated seeds to germinate (González-Amaya et al. 2018).

### Data analysis

After the assessments, the germination percentage (GP), mean germination speed (MGS) and mean germination time (MGT) were calculated. The response variables of

GP and MGS were square root-transformed because the data were not normally distributed according to the Shapiro-Wilk test ( $P \leq 0.05$ ). An ANOVA and Tukey's multiple-means comparison test were performed, with a 5% probability of error using the statistical program Infostat version 2020 (Di Rienzo et al. 2020).

### RESULTS AND DISCUSSION

Analyses were performed for data collected over a 15-day period. Mean comparisons showed significant differences for the variables under study, except for Mean Germination Time (MGT), indicating differential responses of soybean seeds to each pre-germination treatment (Table 2).

**Table 2.** Mean values ( $\pm$  standard error) and Tukey's mean comparison for the variables germination in soybean seeds subjected to different scarification methods.

Treatments	Description	GP (%)	MGS	MGT
1	H <sub>2</sub> SO <sub>4</sub> T5'	5.6 $\pm$ 0.3 <sup>c</sup>	1.43 $\pm$ 0.06 <sup>c</sup>	5.5 $\pm$ 0.14 <sup>a</sup>
2	H <sub>2</sub> SO <sub>4</sub> T10'	7.33 $\pm$ 0.06 <sup>bc</sup>	1.9 $\pm$ 0.0 <sup>bc</sup>	5.38 $\pm$ 0.69 <sup>a</sup>
3	H <sub>2</sub> SO <sub>4</sub> T15'	8.73 $\pm$ 0.21 <sup>ab</sup>	2.27 $\pm$ 0.06 <sup>ab</sup>	4.14 $\pm$ 0.21 <sup>a</sup>
4	H <sub>2</sub> SO <sub>4</sub> T20'	9.47 $\pm$ 0.15 <sup>a</sup>	2.43 $\pm$ 0.06 <sup>a</sup>	4.08 $\pm$ 0.56 <sup>a</sup>
5	AG <sub>3</sub> [100 ppm]	2.0 $\pm$ 0.95 <sup>d</sup>	0.53 $\pm$ 0.25 <sup>d</sup>	2.15 $\pm$ 1.30 <sup>a</sup>
6	NaClO (5.4%)	1.17 $\pm$ 0.45 <sup>d</sup>	0.30 $\pm$ 0.1 <sup>d</sup>	3.25 $\pm$ 0.98 <sup>a</sup>
7	N°1,200 Sandpaper	2.37 $\pm$ 0.83 <sup>d</sup>	0.60 $\pm$ 0.26 <sup>d</sup>	3.17 $\pm$ 0.87 <sup>a</sup>
8	N°1,200 Sandpaper+100ppm AG <sub>3</sub>	2.6 $\pm$ 1.01 <sup>d</sup>	0.63 $\pm$ 0.25 <sup>d</sup>	3.03 $\pm$ 1.19 <sup>a</sup>
9	Control	1.97 $\pm$ 0.71 <sup>d</sup>	0.50 $\pm$ 0.20 <sup>d</sup>	6.39 $\pm$ 3.84 <sup>a</sup>
	HSD	1.78	0.48	1.08
	CV (%)	13.6	14.3	19.1

Germination Percentage (GP), Mean Germination Speed (MGS) and Mean Germination Time (MGT).

Means with the same letter do not differ significantly. ( $P \leq 0.05$ ); T: Treatments; HSD: Honestly Significant Difference; CV: coefficient of variation.

The 20 min immersion time in sulfuric acid (T4) was statistically superior in the variables Percentage and Mean Germination Speed with respect to the control and the seeds subjected to sodium hypochlorite, sandpaper #1200, gibberellic acid and the combination of the latter two.

However, in terms of Mean Germination Time (MGT) there were no significant differences between treatments. It should be noted that there were no significant differences between the immersion times (10, 15 and 20 min), but there were significant differences with respect to T1 ( $H_2SO_4$  T5').

These differences can be explained by the fact that, by not altering the seed coat as occurred in the control treatment, the embryo failed to activate, thereby inhibiting germination. This happens because the embryo is enclosed within an impermeable cover (Varela and Arana 2011) that prevents the passage of water (called physical latency). When it gets damaged by artificial methods of chemical or mechanical scarification, which weaken or break the teguments, it allows greater water entry and gas exchange, facilitating the expansion of the embryo and the exit of the radicle.

This indicates that, as the seed's exposure time to sulfuric acid increases, the seminal coat or testa is weakened by the corrosive action of the acid, resulting in an increase in the permeability of the seed coat, and therefore in the proportion of the variable GP, going from 1.17 in sodium hypochlorite to 7.3, 8.73 and almost 9.47 in T2, T3 and T4, respectively, exceeding those reported by Febles and Padilla (1977), who immersed *Neonotonia wightii* seeds in concentrated sulfuric acid for 60 min and obtained a 31% germination rate, while in the control it was only 1%. Another study reported a 50% germination rate in seeds immersed in the same acid at 98% for 30 min, compared to zero percent in seeds that were in hot water immersion at 70 and 80 °C for 10 and 15 min, respectively (Tauro et al. 2009). On the other hand, Lima et al. (2019) found that there were no significant differences in seed germination of three forage species (*Avena strigosa* Schreb, *Calopogonium mucunoides*, and *Neonotonia wightii*, all collected from animal feces at intervals of 6 up to 48 h after ingestion, and where only 5% of germinated seeds were obtained in *Neonotonia*.

The results with another legume species (*Amburana cearensis*) showed that immersion in sulfuric acid for 10

min stimulated germination, resulting in a higher proportion of PG (0.9 to 1) compared to other treatments (immersion in distilled water at 40, 60, 80, and 100 °C for 2 min) (0.2 to 0.6) (Galíndez et al. 2015).

The presence of an impermeable seed coat (generating physical latency) is typical of some forage legumes (Camacho 2011). Therefore, when the testa is partially or totally damaged, it is easier for water to pass through these tissues, activating enzymes and protein synthesis, and hydrolyzing starches, lipids and endosperm proteins into sugars, fatty acids, and amino acids, necessary at the growing points of the embryonic axis for cell expansion and mitotic division, until the radicle and plumule appear (Finch-Savage and Leubner-Metzger 2006). Thus, acid immersion time is a key factor in stimulating germination in seeds with physical latency, since not all seeds have a favorable response to acid immersion.

Due to the scarcity of updated information on germination tests with sulfuric acid and immersion times and other scarification methods in this family, the decision was made to compare with other species. Merino-Valdés et al. (2018) found that, in seeds of *Capsicum pubescens*, the presence of  $H_2SO_4$  at concentrations of 100, 75 and 60% with an immersion time of 30 min, had a negative effect on germination, it caused the seminal coat to rupture, which lead to the destruction of the embryo.

The seeds that were treated with #1200 sandpaper were statistically equal to the control in the GP variable, but inferior to those subjected to sulfuric acid, including those reported by Flores et al. (2020), where a 90% germination rate was obtained using an equipment set at 1,330 rpm with #60 sandpaper for 2 min and friction for 5 min with #125 sandpaper, respectively.

Similarly, for treatments T5, T6 and T8, the rates were significantly lower. Castillo-Quiroz et al. (2018) found that immersion in 3% NaClO for 8 min favored germination in *Nolina cespitifera*, which, like soybean seeds, is characterized by physical latency, obtaining 49.3%, indicating that NaClO is indeed a germination-inducing agent in this species. The longer exposure time (24 h) and higher concentration (5.4%) may have had a negative effect on the germination percentage, as the result in this study was lower than the one reported by this author.

In the case of gibberellic acid, which is characterized as a phyto-regulatory hormone that is directly involved in the control and promotion of seed germination, it can break seed latency and replace the need for environmental stimuli, such as light and temperature (Araya et al. 2000). Saldívar-Iglesias et al. (2010) found that by applying 250 mg L<sup>-1</sup> of this acid, they obtained an -87% germination rate of *Jaltomata procumbens* (Cav.) J. L. Gentry, which is higher than what was reported in this study, as the concentration used here was lower (100 mg L<sup>-1</sup>).

As a result, the slowest germination speeds (germinated seeds per day) occurred in these treatments compared to seeds that were subjected to different immersion times with 98% sulfuric acid (5, 10, 15 and 20 min).

## CONCLUSION

The presence of an impermeable coating inhibits germination in soybean seeds. This was determined as treatments removed the coating. Therefore, immersion in sulfuric acid for different periods of time was more effective than the rest of the treatments, favoring the germination process of the seeds. However, it was not possible to conclude or demonstrate in what time it is possible to obtain a 100% germination rate, therefore, it is recommended for future research to continue with this treatment reaching up to 35 min of immersion in this acid.

## ACKNOWLEDGMENTS

The contribution to the National Council of Humanities, Sciences and Technologies (CONAHcyT spanish acronym) and to the Chapingo Autonomous University (UACH) of is appreciated.

## REFERENCES

- Acosta Y, Santiago F, Escalante D, Mazorra C, Cejas I et al (2020) Cryo-exposure of *Neonotonia wightii* wight and Am seeds enhances field performance of plants. *Acta Physiologiae Plantarum* 42 (13): 1-6. <https://doi.org/10.1007/s11738-019-3010-y>
- Araya E, Gómez L, Hidalgo N and Valverde R (2000) Efecto de la luz y del ácido giberélico sobre la germinación *in vitro* de Jaul (*Alnus acuminata*). *Agronomía Costarricense* 24(1): 75-80. <https://www.redalyc.org/pdf/436/43624108.pdf>
- Baskin CC and Baskin JM (2014) Seeds: Ecology, biogeography, and evolution of dormancy and germination. Second edition. Academic Press, San Diego, 150-162.
- Bécquer CJ and Prévost D (2016) Nodule formation potential in forage and grain legumes from *Rhizobia indigenous* to Sancti Spiritus, Cuba. *Cuban Journal of Agricultural Science* 48(3). <https://cjasience.com/index.php/CJAS/article/view/589>
- Camacho MF (2011) Capítulo 1: Definición y constitución de las semillas. En: Dormición de semillas: causas y tratamientos. Segunda edición. Editorial Trillas, 16-20.
- Castillo-Quiroz D, Antonio-Bautista A, Ávila-Flores DY, Sáenz-Reyes JT and Castillo-Reyes F (2018) Tratamientos químicos y biológicos para estimular la germinación en semillas de *Nolina cespitífera* Trel. *Polibotánica* 45: 147-156. <https://doi.org/10.18387/polibotanica.5.11>
- Cotler H, Corona JA and Galeana-Pizaña JM (2020) Erosión de suelos y carencia alimentaria en México: una primera aproximación. *Investigaciones Geográficas* (101). <https://doi.org/10.14350/ig.59976>
- De Moraes LF, Deminiciis BB, De Pádua FT, Morenz MJ et al (2014) Methods for breaking dormancy of seeds of tropical legumes. *American Journal of Plant Sciences* 5: 1831-1835. <http://doi.org/10.4236/ajps.2014.513196>
- Di Rienzo JA, Casanoves F, Balzarini MG et al (2020) InfoStat versión 2020. Centro de Transferencia InfoStat, FCA, Universidad Nacional de Córdoba, Argentina. <http://www.infostat.com.ar>
- Febles G and Padilla C (1977) Effect of sulphuric acid on the germination and establishment of *Glycine wightii*. *Cuban Journal of Agricultural Science* 11: 105.
- Finch-Savage WE and Leubner-Metzger G (2006) Seed dormancy and the control of germination. *New Phytologist* 171: 501-523. <https://doi.org/10.1111/j.1469-8137.2006.01787.x>
- Flores ME, Cáceres WE, Aguirre TL and Castillo MS (2020) Efecto de la escarificación en la germinación de semillas de soja forrajera perenne (*Neonotonia wightii*). *Revista de Investigaciones Veterinarias del Perú* 31(3). <http://www.scielo.org.pe/pdf/rivep/v31n3/1609-9117-rivep-31-03-e16728.pdf>
- García VA (2016) La vegetación como factor de control de la erosión. *Repertorio Científico* 19(1) 13-17. <https://revistas.uned.ac.cr/index.php/repertorio/article/view/2529/3217>
- Galíndez G, Malagrina G, Ceccato D, Ledesma T, Lindow-López L and Ortega-Baes P (2015) Dormición física y conservación *ex situ* de semillas de *Amburana cearensis* y *Myroxylon peruiferum* (Fabaceae). *Boletín de la Sociedad Argentina de Botánica* 50(2): 153-161. <http://www.scielo.org.ar/pdf/bsab/v50n2/v50n2a03.pdf>
- González-Amaya LJ, Pita BE, Pinzón-Sandoval EH, Cely GE and Serrano PA (2018) Effect of pre-germination treatments in *Dianthus barbatus* L. seeds cv. 'Purple' under controlled conditions. *Revista de Ciencias Agrícolas* 35(1): 58-68. <https://doi.org/10.22267/rcia.183501.83>
- Jannoyer ML, Le Bellec F, Lavigne C, Achard R and Malézieux E (2011) Choosing cover crops to enhance ecological services in orchards: A multiple criteria and systemic approach applied to tropical areas. *Procedia Environmental Sciences* 9: 104-112. <https://doi.org/10.1016/j.proenv.2011.11.017>
- Labrada R (2004) Manejo de malezas para países en desarrollo. Addendum 1. Capítulo 3. Opciones de manejo y perspectivas. Organización de las Naciones Unidas para la Agricultura y la Alimentación (FAO). <https://www.fao.org/4/y5031s/y5031s00.htm>
- Lima ED, Quintanilha SC, Deminiciis BB, Souza VA, Valente TN et al (2019) Germination of forage seeds through cattle as a natural propagator. *Journal of Agricultural Science*. <https://doi.org/10.5539/jas.v11n1p231>
- Maqueira-López LA, Roján-Herrera O, Solano-Flores J and

Milagros-Santana I (2021) Germination of bean seeds (*Phaseolus vulgaris* L.) at different temperatures. *Cultivos Tropicales* 42(2). [http://scielo.sld.cu/pdf/ctr/v42n2/en\\_1819-4087-ctr-42-02-e03.pdf](http://scielo.sld.cu/pdf/ctr/v42n2/en_1819-4087-ctr-42-02-e03.pdf)

Merino-Valdés M, Andrés-Meza P, Leyva O, Sánchez H, Murguía-González J et al (2018) Influencia de tratamientos pregerminativos en semillas de chile manzano (*Capsicum pubescens* Ruiz & Pav.). *Acta Agronómica* 67(4): 531-537. <https://doi.org/10.15446/acag.v67n4.73426>

Morris JB, Wang ML and Tonniss B (2013) Variability for phenotype, anthocyanin indexes, and flavonoids in accessions from a close relative of soybean, *Neonotonia wightii* (Wight & Arn JA Lackey) in the U.S. Germplasm Collection for potential use as a health forage. *Soybean–Bio-Active Compounds*. Manhattan, NY: InTech,

375-386. <http://doi.org/10.5772/53102>

Saldivar-Iglesias P, Laguna-Cerda A, Gutiérrez-Rodríguez F and Domínguez-Galindo M (2010) Ácido giberélico en la germinación de semillas de *Jaltomata procumbens* (Cav.) J. L. Gentry. *Agronomía Mesoamericana* 21(2): 327-331. <https://www.scielo.sa.cr/pdf/am/v21n2/a12v21n2.pdf>

Tauro TP, Nezomba H, Mtambanengwe F and Mapfumo P (2009) Germination, field establishment patterns and nitrogen fixation of indigenous legumes on nutrient-depleted soils. *Simbiosis* 48: 92-101. <https://doi.org/10.1007/BF03179988>

Varela SA and Arana MV (2011) Latencia y germinación de semillas. *Tratamientos pregerminativos*. EEA Bariloche, INTA. <https://repositorio.inta.gob.ar/xmlui/handle/20.500.12123/11393>

# Enzymatic biocatalysis processes on the semicrystalline and morphological order of native cassava starches (*Manihot esculenta*)

Procesos de biocatálisis enzimática sobre el orden semicristalino y morfológico de los almidones nativos de mandioca (*Manihot esculenta*)

<https://doi.org/10.15446/rfnam.v77n3.111270>

Jorge Figueroa-Flórez<sup>1\*</sup>, Edith Cadena-Chamorro<sup>2</sup>, Jairo Salcedo-Mendoza<sup>1</sup>, Eduardo Rodríguez-Sandoval<sup>2</sup>, Héctor Ciro-Velásquez<sup>2</sup> and Tiana Serna-Fadul<sup>1</sup>

## ABSTRACT

### Keywords:

Amorphous zone  
Amylases  
Biocatalysis  
Exo-erosion  
Semi-crystalline order  
Starch




Enzymatic biocatalysis has emerged as a green technology in starch modification with divergent results at the morphological level depending on the origin of the starch source. Therefore, various enzymatic biocatalysts were implemented to evaluate their effect on the morphological and semi-crystalline characteristics of native cassava starches. The degree of affinity of the biocatalysts and the conversion rate on native cassava starches were determined by kinetic parameters such as the Michaelis-Menten constant, whose results revealed the following order of affinity from highest to lowest:  $\alpha$ -amylase, amyloglucosidase, pullulanase, and  $\beta$ -amylase. In addition, greater biocatalytic activity of  $\alpha$ -amylase and  $\beta$ -amylase was evidenced on the amorphous zones of the polymer associated with the decrease in the amylose content and a significant increase in the degree of relative crystallinity. According to morphological analyses and XDR, the action of amyloglucosidase promoted exo-erosion phenomena and the appearance of lacerations on the granular surface of starch with the consequent decrease in the semicrystalline order. The pullulanase caused slightly eroded fragmented granules with greater biocatalytic activity on the crystalline lamellae, associated with a significant increase in the apparent amylose content. FTIR analysis in the 1,200-900  $\text{cm}^{-1}$  region, corresponding to the starch fingerprint, allowed us to detect notable changes in the degree of molecular order after the enzymatic attack; this result was consistent with the degree of relative crystallinity estimated by X-ray diffraction. Likewise, the results allowed us to notice significant changes in the semi-crystalline order and morphological characteristics during the modification with  $\alpha$ -amylase (AAM) and amyloglucosidase (AMG) associated with their greater affinity and preferential action on the amorphous structures located on the granular surface of native cassava starch.




## RESUMEN

### Palabras clave:

Zona amorfa  
Amilasas  
Biocatálisis  
Exo-erosión  
Orden semicristalino  
Almidón

La biocatálisis enzimática ha surgido como una tecnología verde en la modificación de almidones con resultados divergentes a nivel morfológico en función de procedencia de la fuente amilácea. Por consiguiente, diversos biocatalizadores enzimáticos fueron implementados para evaluar su efecto sobre las características morfológicas y semicristalinas en almidones nativos de yuca. El grado de afinidad de los biocatalizadores y la tasa de conversión sobre almidones nativos de yuca fueron determinados mediante parámetros cinéticos como la constante de Michaelis-Menten, cuyos resultados revelaron el siguiente orden de afinidad de mayor a menor:  $\alpha$ -amilasa, amiloglucosidasa, pululanasa y  $\beta$ -amilasa. Además, se evidenció una mayor actividad biocatalítica de la  $\alpha$ -amilasa y  $\beta$ -amilasa sobre las zonas amorfas del polímero debido a la disminución del contenido de amilosa y un aumento significativo en el grado de cristalinidad relativa. Según los análisis morfológicos y DRX, la acción de la amiloglucosidasa promovió fenómenos de exoerosión y la aparición de laceraciones en la superficie granular del almidón con la consiguiente disminución del orden semicristalino. La pululanasa provocó la obtención de gránulos fragmentados levemente erosionados con una mayor actividad biocatalítica en las zonas cristalinas asociada con el aumento significativo del contenido de amilosa aparente. El análisis de FTIR en la región 1.200-900  $\text{cm}^{-1}$ , correspondiente a la huella digital del almidón, permitió determinar cambios notorios en el grado del orden molecular después del ataque enzimático, este resultado fue coherente con el grado de cristalinidad relativo estimador por difracción de rayos-X. Asimismo, los resultados permitieron identificar cambios significativos en el orden semicristalino y características morfológicas durante la modificación con  $\alpha$ -amilasa (AAM) y amiloglucosidasa (AMG) asociado a su mayor afinidad y acción preferencial sobre las estructuras amorfas ubicadas en la superficie granular del almidón nativo de yuca.

<sup>1</sup>Facultad de Ingeniería, Universidad de Sucre, Sincelejo, Colombia. [jorge.figueroa@unisucra.edu.co](mailto:jorge.figueroa@unisucra.edu.co) , [jairo.salcedo@unisucra.edu.co](mailto:jairo.salcedo@unisucra.edu.co) , [tiana.serna@unisucra.edu.co](mailto:tiana.serna@unisucra.edu.co) 

<sup>2</sup>Facultad de Ciencias Agrarias, Universidad Nacional de Colombia, Medellín, Colombia, [emcadenac@unal.edu.co](mailto:emcadenac@unal.edu.co) , [edrodriguez@unal.edu.co](mailto:edrodriguez@unal.edu.co) , [hjciro@unal.edu.co](mailto:hjciro@unal.edu.co) 

\*Corresponding author



**S**tarch is a polysaccharide macromolecule product of biosynthesis in the form of semi-crystalline granules stored in plant cells as an energy source (Li et al. 2017; Li et al. 2023). Structurally, it consists of linear amylose formed by  $\alpha$ -D-glucan-(1,4) bonds but slightly branched (ca. 3-5%), and amylopectin molecule of higher molecular weight organized by  $\alpha$ -D-glucan-(1,4)-bonds with a highly branched structure consisting of  $\alpha$ -D-glucan-(1,6)-bonds (Li et al. 2023). Short- and long-range molecular studies deduce that single amylose helices generally form intermixed amorphous domains together with branched amylopectin groups, whereas regular packing of amylopectin or amylose-amylopectin double helices forms the crystalline domain (Ma et al. 2019). Amylose provides heterogeneity and significantly influences the structural and retrogradation properties of the granule, negatively affecting the quality and texture of the starch-formulated product (Keeratiburana et al. 2020). Therefore, to achieve the desired properties and meet the requirements of food applications, it is necessary to modify the structure and/or morphology of the granule in its native state.

Enzymatic modification emerges as a green technology to develop clean label products with desired properties such as solubility, retrogradation, and improved thermal stability (Miao et al. 2015). It has gained relevance, especially when performed below the gelatinization temperature, because of its lower energy cost and higher yields (Yang et al. 2019). Granular modification performed by biocatalytic processes can change the physicochemical nature of starch, product of the alteration of morphological properties and semicrystalline order, due to the cleavage of  $\alpha$ -D-(1,4) or  $\alpha$ -D-(1,6) glycosidic bonds on amylose or amylopectin chains (Li et al. 2017; Gao et al. 2023). Starch is generally hydrolyzed by the exogenous or endogenous action of amylolytic enzymes such as  $\alpha$ -amylase (AAM),  $\beta$ -amylase (BAM), amyloglucosidase (AMG), and pullulanase (PUL). AAM is an endo-amylase capable of cleaving  $\alpha$ -D-glucan-(1,4) linkages and yielding glucose, maltose, and oligosaccharides (DP<5), as well as branched-limit dextrin of configuration alpha ( $\alpha$ ) (Gui et al. 2021; Zhou et al. 2021; Gao et al. 2023). BAM and AMG are exo-amylases; BAM cleaves every two units of glucose from the non-reducing end to obtain maltose and branched-limiting dextrin of configuration ( $\beta$ ) (Gui et al. 2021; Li et al. 2023), while AMG is capable of hydrolyzing

as many  $\alpha$ -(1,4) and  $\alpha$ -(1,6) glycosidic linkages to maltose and glucose units, excluding the production of boundary dextrin (Yang et al. 2019; Zhou et al. 2021). PUL is a debranching enzyme, capable of producing partially linear short chains (Li et al. 2017; Ma et al. 2019; Semwal and Meera 2023). Thus, the use of polypeptides with amylolytic action has been subordinated to hydrolysis of polymeric chains to obtain soluble starches, granules with porous structures, and slow-digesting starches.

Polymer degradation during enzymatic modification is usually performed on granules in their native state instead of starch paste, processes characterized by low degrees of hydrolysis due to the semi-crystalline structure, which makes it difficult for enzymes to access the substrate. This poses a difficult challenge for enzymatic action, involving diffusion of the enzyme on the granular surface, followed by adsorption of the polypeptide within the granule, and finally initiating the biocatalytic process (Blazek and Gilbert 2010; Almeida et al. 2019; Almeida et al. 2022). Moreover, the exo- and endo-amylolytic action depends on the type of starch due to the intrinsic semicrystalline structure of the granules that confer a certain degree of molecular resistance (Miao et al. 2015). In addition, it has been reported that the rate and extent of depolymerization of starch chains depend not only on the characteristics of the polysaccharide material but also on the preferential and differentiated activities of each enzyme (Blazek and Gilbert 2010; Benavent-Gil and Rossell 2017).

In starch granules from cereals, it has been found that enzymatic hydrolysis starts preferentially by the amorphous growth ring, given the appearance of cracks and lacerations on the granular surface (exo-erosion), and that the inherent micro- and nano-porous structure of the granule influences the opportunity of the enzyme to access the substrate (endo-erosion) (Lin et al. 2016). In contrast, enzymatic action on tuber starches reveals confounding results, where surface exo-erosion phenomena predominate, with no noticeable porosities internally (Blazek and Gilbert 2010; Benavent-Gil and Rossell 2017). Some authors report that the enzymatic action on native starches is dependent on amylose/amylopectin packing, the interaction of close double helices, and the redistribution of amylose in the macromolecular structure of the granule (Lin et al. 2016; Zhou et al. 2021; Li et al. 2023). However, there is limited information about the mechanisms of endo- and

exo-amylolytic action of different enzymatic catalysts on tuber-derived starches, especially on native cassava starches; likewise, the effect of various mechanisms of enzymatic action on the amorphous regions in tuber starches has been poorly discussed. In this sense, it is hypothesized that the semicrystalline order and morphological characteristics in hydrolyzed cassava starches depend on the differential action of amylolytic enzymes. Consequently, this research aims to analyze the morphological and structural changes during enzymatic attack on native cassava starch granules using commercial biological catalysts with differentiated mechanisms of action.

## MATERIALS AND METHODS

### Materials

Native cassava (*Manihot esculenta* cv M-TAI) starch was supplied by Almidones de Sucre S.A.S (Sincelejo, Colombia).  $\alpha$ -amylase from *Bacillus licheniformis* (Lyquozyme Supra 2.2X®, Denmark),  $\beta$ -amylase from *Hordeum vulgare* (Optimalt®BBA, China), amyloglucosidase from *Aspergillus niger* (Dextrozyme®GA, Denmark) and pullulanase from *Bacillus licheniformis* (Optimax® L-1000, China) were donated by Dupont® and Novozymes®.

### Determination of enzymatic activity

Biocatalytic activity was determined using the protocol described by De Schepper et al. (2021) with slight modifications. A 30 mg sample of starch was suspended in 10 mL of buffer solution at a defined pH (Table 1). The hydrolytic reaction was made in 15 mL hermetic tubes under stirring at 150 rpm for 15 min at a fixed temperature. Enzyme activity was estimated as a function of the concentration of reducing sugars released during hydrolysis based on the 3,5-dinitrosalicylic acid method (Salcedo-Mendoza et al. 2018). The protein concentration of the enzyme in the preservation medium was evaluated by the Bradford method using BSA as a standard (0-0.5 mg mL<sup>-1</sup>) to determine the specific activity. One enzyme unit (U) was defined as the enzyme quantity necessary to release 1.0  $\mu$ mol of reducing sugar per minute in the assay conditions (Frota et al. 2020). In Equation 1,  $U_a$  is the enzyme activity ( $\mu$ M min<sup>-1</sup> mL<sup>-1</sup>),  $[g]$  is the reducing sugar concentration (g L<sup>-1</sup>),  $V_s$  is the volume of solution (L),  $M_w$  is the molar mass of glucose g mol<sup>-1</sup>,  $V_e$  is the volume of the enzyme, and  $t$  the hydrolysis time (min).

$$U_a = \frac{[g] * V_s}{M_w * V_e * t} \quad (1)$$

**Table 1.** Established operational parameters to estimate enzyme activity.

Enzyme	Operational parameters		
	pH <sup>1</sup>	Temperature (°C)	Concentration <sup>2</sup> ( $\mu$ L mg <sup>-1</sup> )
$\alpha$ -amylase (AAM)	4-9	50-90	0.45
$\beta$ -amylase (BAM)	3-8	40-70	0.90
Amyloglucosidase (AMG)	3-7	50-80	0.40
Pullulanase (PUL)	3-7	50-75	0.75

<sup>1</sup>Buffer solutions: 0.1 M citrate (pH=3-6), 0.1 M phosphate (pH=7-8). <sup>2</sup>Enzyme concentration used by recommendation of the commercial house and expressed as  $\mu$ L enzyme/mg starch.

### Determination of kinetic parameters

The enzymatic activity was determined as a function of the substrate concentration (S) corresponding to starch solutions in a range from 0.1 to 100 mM. Hydrolysis under the enzyme concentrations presented in Table 1 was carried out for 15 min under constant stirring at 150 rpm, and at optimum pH and temperature conditions. Reducing sugars released during hydrolysis were determined by the 3,5-dinitrosalicylic acid method using glucose as standard (0.0-2.0 g L<sup>-1</sup>). The molecular weight of native cassava

starch was determined by size exclusion-high-performance liquid chromatography (SEC-HPLC) coupled to multi-angle laser light scattering detectors (Wyatt Technology Inc., Dawn 8+ Heleos, USA) and refractive index (Agilent, G1362A, UK) using pullulan as standard, eluting the samples in ammonium formate (10 mM) with a flow rate of 0.5 mL min<sup>-1</sup> (Keeratiburana et al. 2020).  $V_{max}$  and  $k_m$  as kinetic parameters were estimated using Lineweaver-Burk and Langmuir linearization methods (Torabizadeh et al. 2014).

### Starch granule modification

Suspensions of native cassava starch at 100 mg mL<sup>-1</sup> in citrate buffer were subjected to enzymatic hydrolysis using commercial polypeptides such as  $\alpha$ -amylase,  $\beta$ -amylase, amyloglucosidase, and pullulanase under a specific activity of 10 U mg<sup>-1</sup> at 60 °C for 24 h (Figueroa-Flórez et al. 2023). The pH was adjusted to the optimal conditions of maximum biocatalytic activity for each enzyme (Figure 1). At the end of the hydrolysis time, the supernatant was separated by centrifugation, and the sediment corresponding to modified starch samples was dried by forced convection for 8 h at 35 °C to be macerated, stored, and subsequently characterized. To evaluate the enzymatic kinetics of native cassava starch granules over time, hydrolysates were sampled every 15 min during the first 2 h, and then every hour until 24 h of hydrolysis were completed. The sugar release behavior over time was fitted to two-parameter nonlinear empirical models using SigmaPlot software (Systat Software Inc., Germany) (Lin et al. 2016). In Equation 2,  $t$  is the time (h),  $G$  is the concentration of sugar released (M),  $A$  is the maximum asymptote (M), and  $B$  is the time to reach half of the maximum asymptote (A).

$$G = \left[ \frac{A * t}{B + t} \right] \quad (2)$$

In Equation 3,  $t$  is the hydrolysis time (h),  $G$  is the concentration of glucose released (M) at time  $t$ , and  $k$  is the hydrolysis rate constant (h<sup>-1</sup>). The absolute value of  $a$  can be assumed to be the specific biocatalysis coefficient of an enzyme.

$$G = [a - e^{kt}] \quad (3)$$

### Morphological characteristics

The morphological characteristics of native and modified starch were analyzed by scanning electron microscopy (JEOL, JSU LV-5600, Japan) on samples previously fixed on electro-conductive carbon strips, coated with a platinum/gold alloy (Almeida et al. 2022). Photomicrographs were acquired at 15 kV and 30 mA, using magnification approaches at 1,000 and 3,000X.

### Amylose content

Starch samples were dissolved in 95% DMSO solution and then precipitated in 90% alcohol. Amylose content

was determined using the iodine staining method and estimating the absorbance in a UV-Vis spectrometer at 620 nm by preparing a calibration curve (0-100% w/v) using potato amylose and corn amylopectin (Sigma Aldrich, USA) (Li et al. 2017).

### Molecular order by spectroscopy FT-IR

The FTIR-ATR spectra were acquired by single rebound attenuated total reflectance spectroscopy using a diamond crystal with a diameter of 1.5 mm (UATR, PerkinElmer, USA). Samples were processed in triplicate and each spectrum was recorded with a resolution of 4.0 cm<sup>-1</sup> and 64 readings in the range of 600 to 4,500 cm<sup>-1</sup> (Gao et al. 2023). Spectra were processed including baseline correction, automatic smoothing, and normalization of absorbance with respect to the starch fingerprint in the 1,100-900 cm<sup>-1</sup> region. The band ratios 1,047/1,022 cm<sup>-1</sup> and 995/1,022 cm<sup>-1</sup> were used to estimate the short-range ordered starch structure (OM<sub>1</sub> and OM<sub>2</sub>, respectively), expressed as percentages according to Ma et al. (2019).

### Diffraction patterns and crystallinity degree (CD)

X-ray diffraction patterns were obtained using a diffractometer (Panalytical, X'Pert MPD, Switherland) operated at 1.8 kW and 40 mA. The diffractograms were acquired over a range of 4-40°, at a scan rate of 2.0° min<sup>-1</sup> and a sampling interval of 0.02° (Davoudi et al. 2022; Figueroa-Flórez et al. 2023). The data were then smoothed using the Savitzky-Golay algorithm and the deconvolution process was developed using the Gaussian function in the 5-30° region. The degree of crystallinity (CD) was estimated as the ratio of the areas of the crystalline peaks over the total area of the diffractogram, using numerical integration methods and MATLAB software (MathWorks, R2019a, USA).

### Data analysis

The results were expressed as mean values of five replicates  $\pm$  standard deviation. Data were analyzed using the analysis of variance procedure and Tukey's multiple range test with a significance level of 95% using Statgraphics Centurion software (Statgraphics Inc., version XVI, USA).

## RESULTS AND DISCUSSION

### Enzymatic activity of biocatalysts: pH and temperature

The activity of commercial enzymes using native cassava starch as substrate was evaluated as a function of pH and temperature (Figure 1). Bacterial AAM presented higher

enzymatic activity in a wide pH range from 6-8 and reached the best conditions at pH=6. Plant BAM presented a wide plateau of maximum values of biocatalytic activity in a pH range from 5-7, and the best conditions were found at pH=7. Polypeptides such as AMG and PUL presented higher enzymatic activities in the pH range from 4-5, reaching a maximum peak of activity at pH=4.5. It is evident that AAM presents higher stability to acidic conditions in the pH

range from 5-8 compared to the rest of the polypeptides. In addition, the concentration of  $H^+$  ions altered the alkaline-tolerant stability of the enzymes, affecting their enzymatic activity. This behavior is consistent with that reported by Kikani and Singh (2015), who demonstrated that pH changes altered the protein structure, affecting the three-dimensional shape of the enzymes—with the consequent deformation of catalytic sites—and its biocatalytic activity.

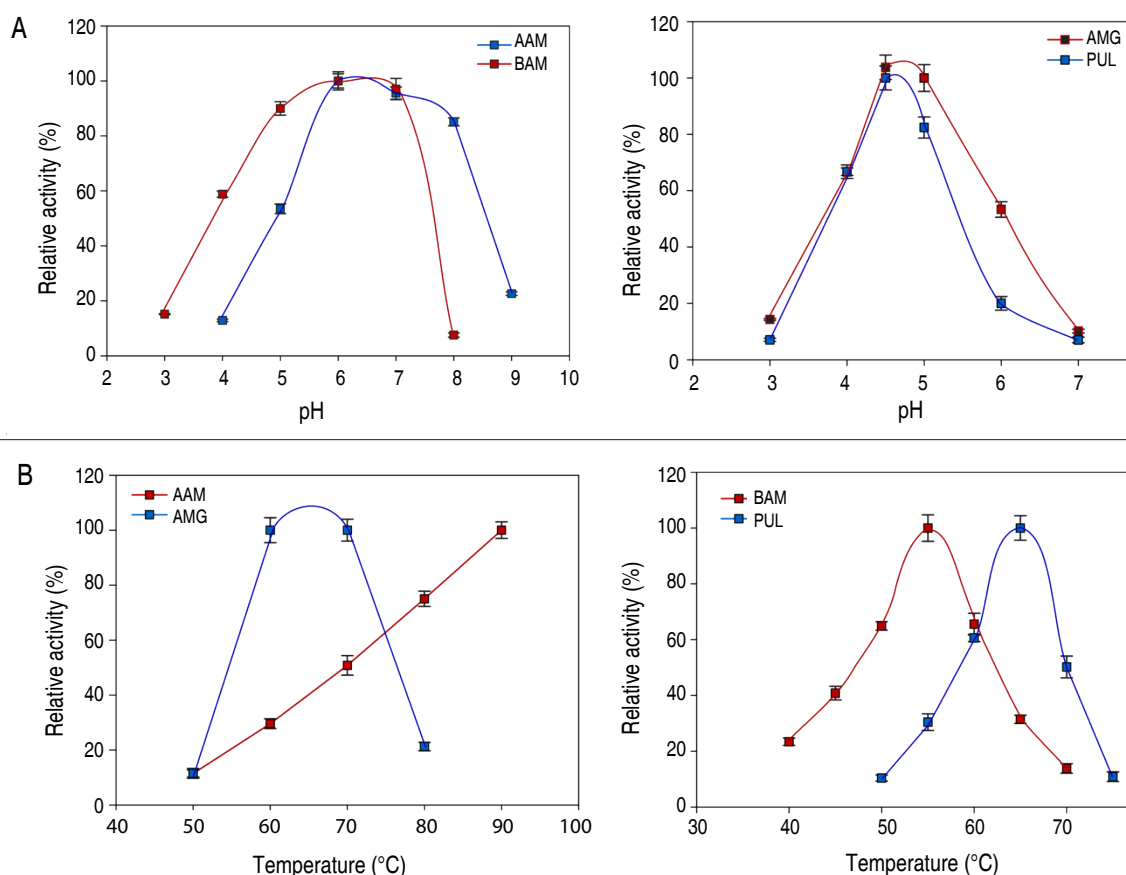


**Figure 1.** Enzyme activity profile as a function of pH (A) and temperature (B). AAM:  $\alpha$ -amylase; BAM:  $\beta$ -amylase; AMG: amyloglucosidase; PUL: pullulanase.

Concerning temperature, AAM showed higher enzymatic activity under thermal conditions above 70 °C, possibly linked to its thermal resistance. AMG presented high enzymatic activity in the range from 60-70 °C with a maximum at 65 °C (Figure 1), bacterial PUL showed similar behavior, while plant BAM presented higher enzymatic activities between 50 and 60 °C with a maximum at 55 °C. Under thermal conditions above

80 °C, a decrease in enzymatic activity is observed (except for AAM); it could be due to thermal stress promoted during heating that leads to molecular disorder and subsequent denaturation of the polypeptide structure (Sagu et al. 2015). The molecular stability of bacterial AAM could be due to genetic adaptability, intrinsic to the conditions of the bacterial habitat where it performs its metabolic activities (Liu et al. 2017). In contrast, the reduction of

enzyme activity at temperatures below 40 °C is probably due to insufficient kinetic energy stimulating collisions or ionic interactions between substrate molecules and the enzyme active site (Fitter et al. 2001). Results show that pH and temperature can increase or decrease biocatalytic activities related to the effect they promote on the affinity of the catalytic site to the substrate.

### Analysis of enzyme kinetics on native starch

The biocatalytic activity presented a gradual increase in glucose release with increasing substrate concentration, governed by a first-order exponential behavior, with subsequent inhibition at substrate concentrations above 70 mM. Kinetic parameters such as  $v_{\max}$  and  $k_m$  were estimated from the Lineweaver-Burk method (Figure 2A, Table 2) due to a better regression fit ( $r^2 > 0.90$ ) compared to the Langmuir method. The results revealed that AAM and AMG presented lower  $k_m$  values with respect to BAM and PUL, thus showing a higher affinity of the catalytic sites of AAM and AMG on native cassava starch granules. This result is consistent with the morphological changes evidenced on the granular surface using SEM. It justifies the higher values in the

releasing rate of reducing sugars over time (Figure 2B). The low catalytic activity of BAM is possibly associated with low adsorption capacity, characteristic of enzymatic polypeptides extracted from plant sources, which slow down catalytic activity processes (Lahmar et al. 2018). In addition, Zareian et al. (2010) report a decrease in enzymatic activity in bacterial pullulanase using soluble starch compared to pullulan; it is associated with the adsorption capacity of the enzyme to the substrate and the molecular size of the polymeric substance. Nevertheless, the estimated values for  $v_{\max}$  and  $k_m$  are close to those reported in other studies using bacterial AAM (Torabizadeh et al. 2014), fungal AMG (Gupta et al. 2015), plant BAM (Vajravijayan et al. 2018), and bacterial PUL (Li et al. 2018; Zeng et al. 2019) biocatalysts in the presence of soluble starch as substrate. However, the values differ significantly from the kinetic parameters reported by other authors, who claim that such discrepancies depend on the type of substrate, the source, and the type of enzymatic extraction, as well as its purification process (Gupta et al. 2015; Chen et al. 2015; Liu et al. 2017; Wang et al. 2019).

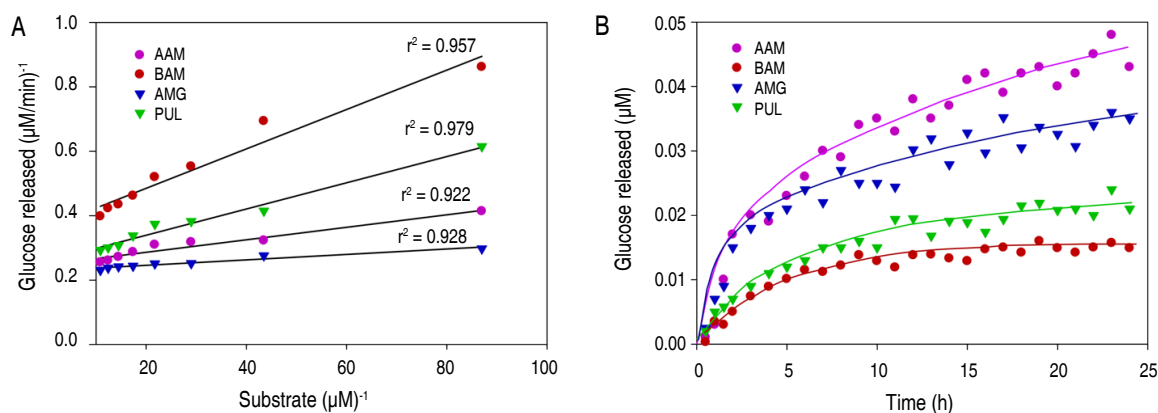


**Figure 2.** The behavior of enzyme kinetics on native cassava starch granules. Lineweaver-Burk linearization method (A), kinetics as a function of hydrolysis time (B). AAM:  $\alpha$ -amylase; BAM:  $\beta$ -amylase; AMG: amyloglucosidase; PUL: pullulanase.

Figure 2B details the enzymatic hydrolysis behavior of native cassava starch, depending on the type of enzyme and based on the release of reducing sugars. The type of hydrolysis was biphasic, with a high rate of conversion in the first 5-6 h, followed by a progressive decrease in the degradation rate up to 24 h. The kinetics of the degradation rate were found to be similar to those of the

enzyme. Similar depolymerization kinetics have been found in hydrolysis with  $\alpha$ -amylase on waxy maize starch (Lin et al. 2016), amyloglucosidase on barley granules (Li et al. 2004), and  $\beta$ -amylase on soluble maize starch particles (Miao et al. 2015). This biphasic behavior is probably due to the type of substrate available—polymeric chains—in different areas of the granule, depending on



their molecular structure and granular packing (Zhang et al. 2013). Thus, they explain that, initially, the enzymatic attack occurs on the linear, long, and unstable chains that make up the amorphous zone of the granule at a high conversion rate, followed by depolymerization on the short and molecularly stable polymeric chains that make up the crystalline region at a lower hydrolysis rate (Li et al. 2004). However, a decrease in substrate concentration and an occurrence of product inhibition due to the formation of oligosaccharides may also explain a lower digestion rate observed at longer times, according to the results found in the digestion of rice starch using different amylolytic enzymes evaluated by NMR spectroscopy (Dona et al.

2010). Hydrolysis with AAM and AMG is characterized by a high rate of conversion of starch into reducing sugars compared to the enzymatic treatments of BAM and PUL, this behavior agrees with the enzyme activity values and the affinity of the enzymes to the substrate analyzed by the Michaelis-Menten constant (Table 2). Also, enzymatic hydrolysis involves a polypeptide material in solution acting on a solid starch substrate. Therefore, the surface area accessible to the enzyme and the adsorption efficiency of the enzyme to the surface are critical kinetic parameters (Yang et al. 2019). They could explain the poor enzymatic activity of BAM on native cassava starch (Kim et al. 2008).

**Table 2.** Enzyme activities and kinetic parameters on native cassava starch.

Enzyme	$U_a (\mu\text{M min}^{-1} \text{mL}^{-1})$	Protein ( $\text{mg mL}^{-1}$ )	$U (\mu\text{M min}^{-1} \text{mg}^{-1})$	$k_m (\mu\text{M}) \times 10^{-2}$	$V_{\max} (\mu\text{M s}^{-1})$
AAM	209.6±5.47 <sup>a</sup>	0.400±0.03 <sup>a</sup>	528.4±13.79 <sup>a</sup>	0.76±4×10 <sup>-4a</sup>	9.86±0.24 <sup>a</sup>
BAM	1856.3±28.89 <sup>b</sup>	22.83 ±1.87 <sup>b</sup>	81.3±1.27 <sup>b</sup>	4.92±6×10 <sup>-3b</sup>	2.75±0.27 <sup>b</sup>
AMG	1994.9±44.90 <sup>c</sup>	5.570±0.35 <sup>c</sup>	358.9±8.08 <sup>c</sup>	0.35±2×10 <sup>-4a</sup>	4.36±0.19 <sup>ac</sup>
PUL	360.7±6.57 <sup>d</sup>	3.220±0.60 <sup>d</sup>	112.1±2.04 <sup>d</sup>	1.59±5×10 <sup>-4c</sup>	3.85±0.12 <sup>c</sup>

AAM:  $\alpha$ -amylase; BAM:  $\beta$ -amylase; AMG: amyloglucosidase; PUL: pullulanase;  $U_a$ : enzyme activity;  $U$ : specific activity;  $k_m$ : Michaelis-Menten constant;  $v_{\max}$ : maximum velocity. Equal letters within a column do not differ statistically ( $P < 0.05$ ).

The behavior of the enzyme kinetics was adjusted to two-parameter nonlinear models, which presented a good fit with a coefficient of determination  $r^2 > 0.93$  and ( $P < 0.05$ ) and showed their suitability to describe and study polymeric degradation on native cassava starch (Table 3). In the hyperbolic model, AAM and AMG enzymes presented higher values in the maximum asymptote "A" and a longer time to reach 50% of maximum hydrolysis, indicating higher enzymatic activity

and higher depolymerization of starch granules. In the enzymatic action of BAM and PUL, the values of the maximum asymptote "A" were lower, as well as the time "t", indicating a higher molecular resistance of cassava starch granules to this type of enzyme. This model has also been suitable for studying the degree of resistance of waxy maize starches to enzymatic digestion with amylases (Lin et al. 2016). In relation to the exponential model, the hydrolysis coefficients "a" were different for

**Table 3.** Parameters derived from the hyperbolic fit and exponential model to fit the first-order kinetics during the hydrolysis of native cassava starch.

Enzyme	Hyperbolic model			Exponential model		
	$A[M] \times 10^{-2}$	B [h]	$r^2$	$a \times 10^{-2}$	$k [h^{-1}] \times 10^{-1}$	$r^2$
AAM	5.77±1×10 <sup>-3a</sup>	7.03±0.29 <sup>a</sup>	0.978	4.47±8×10 <sup>-4a</sup>	1.48±2×10 <sup>-4a</sup>	0.974
BAM	1.84±8×10 <sup>-4b</sup>	4.53±1.87 <sup>b</sup>	0.965	1.49±1×10 <sup>-3b</sup>	2.11±1×10 <sup>-3b</sup>	0.969
AMG	4.03±9×10 <sup>-4c</sup>	4.55±0.39 <sup>c</sup>	0.962	3.28±2×10 <sup>-3c</sup>	2.04±4×10 <sup>-3b</sup>	0.930
PUL	2.71±3×10 <sup>-4d</sup>	6.07±0.46 <sup>b</sup>	0.969	2.15±9×10 <sup>-4d</sup>	1.64±6×10 <sup>-4a</sup>	0.952

AAM:  $\alpha$ -amylase; BAM:  $\beta$ -amylase; AMG: amyloglucosidase; PUL: pullulanase. A is the maximum asymptote (M), and B is the time halfway through the maximum asymptote; k is the hydrolysis rate constant. Equal letters within a column do not differ statistically ( $P < 0.05$ ).

each enzyme, indicating a preferential and distinctive action on starch chains; these results are consistent with the behavior of the maximum asymptote values “A” and  $k_m$ . Lower values in the hydrolysis coefficient for BAM and PUL indicate a lower enzyme activity and a higher degree of molecular resistance of the starch granules. In addition, higher values in the hydrolysis constant “k” are consistent with the results of  $v_{max}$  estimated by the Michaelis-Menten model. The first-order exponential model was also used to evaluate biocatalysis processes on potato granules (Zhang et al. 2013), wheat, and waxy maize (Lin et al. 2016). In this study, the values of the maximum asymptote “A”, the biocatalysis coefficient “a”, and the constant  $k_m$ —which are characteristic parameters for each enzyme—presented a positive correlation with the decrease of amylose content after an enzymatic attack using amylolytic enzymes (AAM, BAM, and AMG) related to the preferential cleavage action on  $\alpha$ -(1,4) glycosidic bonds.

### Analysis of the enzymatic attack on the amorphous zones

Figure 3 shows the microphotographs of native and modified cassava starches. Native cassava starches (ANY by its Spanish acronym) exhibit smooth-surfaced spherical/oval geometric shapes with truncated ends associated with the grating process during extraction (Salcedo-Mendoza et al. 2018). As the granules undergo enzymatic treatment, significant changes in microstructure can be observed; the AAM starches presented significant morphological changes associated with the action of  $\alpha$ -amylase that caused the appearance of pores, cracks, and exo-erosions on the granular surface. In addition, microphotographs of AAM starches evidenced the presence of fragmented granules, overlapping layers resembling starch growth rings can be identified inside them (Figure 3; AAM-B). The amylolytic erosion of starch granules occurs in two ways: one is radial, from the surface towards the center of the granule, and another is superficial and acts peripherally (Das and Kayastha 2019). Consequently, it could be assumed that the degradation mechanism of  $\alpha$ -amylase on cassava granules starts with diffusion and adsorption processes, followed by a surface erosion phenomenon on overlapping layers, harshly attacking both weak and unstable zones (amorphous lamellae) composed of linear amylose chains, and slowing its enzymatic activity on ordered amylose regions (crystalline lamellae).

Similar morphological changes were observed in AMG starches, with a less severe effect on the exo-erosion phenomenon compared to AAM but causing a partial or total loss of the polymeric structure internally. This may imply that the action of amyloglucosidase shows a greater endogenous action on the amorphous and unstable zones, which is more noticeable in irregular granules that present damage associated with the extraction process and lead to obtaining slightly eroded fragmented granules with a hollow appearance (Figure 3, AMG-B). This result is congruent with Figuerola-Flórez et al. (2023), who argue that amyloglucosidase digestion on cassava starch was faster in the weakly packed inner region than in the densely packed peripheral zone, thus leaving granules with an empty/hollow structure. Meanwhile, BAM and PUL starches were characterized by the presence of slightly eroded and mostly fragmented granules, with a less severe effect in BAM starches; it could be associated with a lower affinity of the  $\beta$ -amylase catalytic sites for the polymeric chains of native cassava starch. The action of  $\beta$ -amylase and pullulanase on starch granules involves an exogenous action, whose hydrolytic processes start at the surface level in the amorphous zones and affect the amylose content with a subsequent stage that can lead to the fragmentation of granules into particles with noticeable morphological changes (Figure 3, BAM-B; PUL-B). Kim et al. (2008) hypothesized that enzyme-induced erosion of amorphous regions in starch granules leads to their fragmentation. Similar results have been reported on starches hydrolyzed from potatoes with plant  $\beta$ -amylase (Das and Kayastha 2019) and fungal pullulanase (Li et al. 2017), highlighting the presence of cracks and eroded areas on the surface after enzymatic action.

Moreover, the presence of undamaged granules is observed together with hydrolyzed granules as a result of non-homogeneous digestion. In this regard, Almeida et al. (2019) state that irregular granules with truncated areas are presumably more susceptible to enzymatic hydrolysis and, therefore, would show greater morphological changes with respect to whole granules of defined geometry. Likewise, in cereal starches hydrolyzed using various enzymes, the production of granules with porous structure stands out (Vajravijayan et al. 2018; Keeratiburana et al. 2020; Zhang et al. 2021; Davoudi et al. 2022; Semwal and Meera 2023); these results differ from those found

in the present study. Cereal starches present numerous pores on the surface, which widen and increase the access of hydrolyzing enzymes to the interior of the granule (Blazek and Gilbert 2010; Zhang et al. 2021). However, microscopic analysis under different magnification foci

reveals that ANY starches did not present surface holes or pores, which could restrict the access of amylolytic polypeptides and suggest that exogenous action governs the biocatalytic processes at the granular periphery, thus limiting the endo-erosion phenomenon.

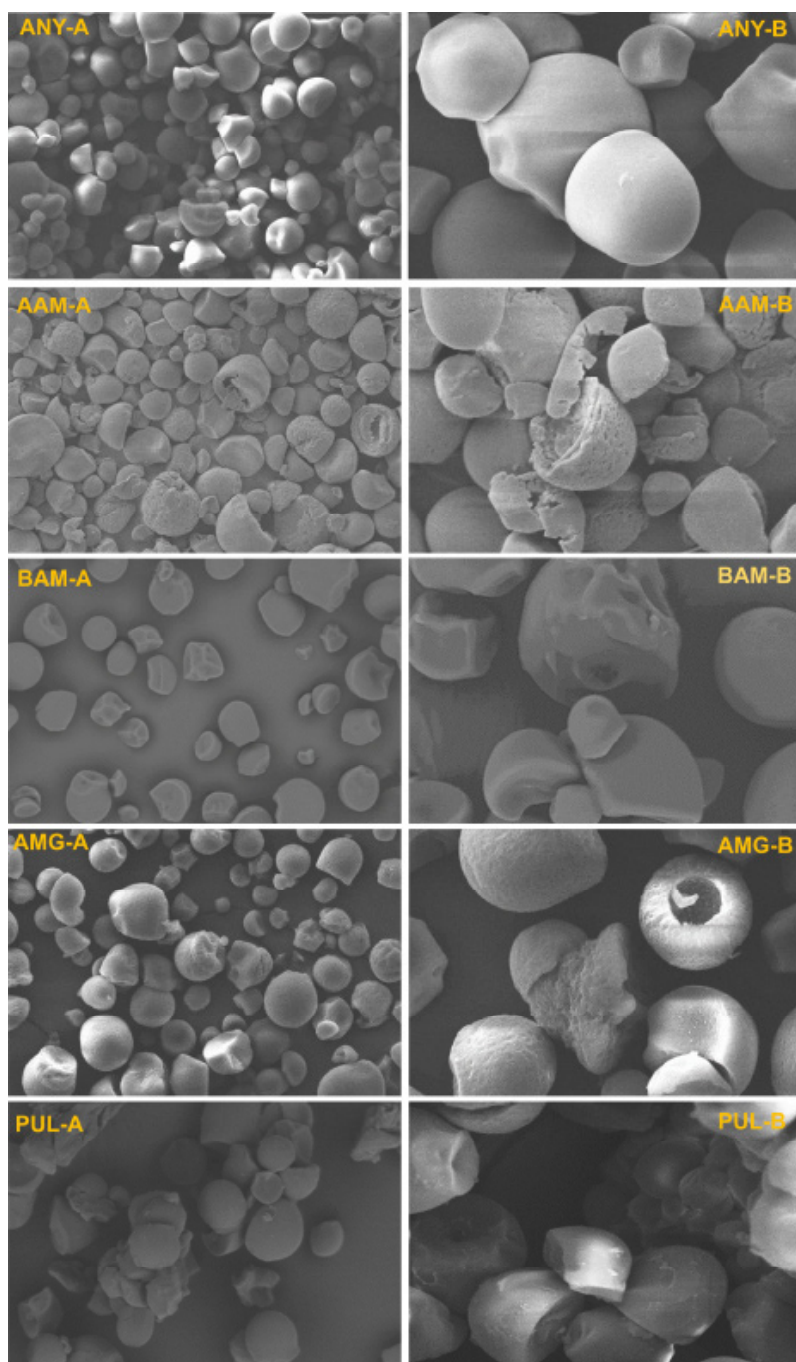


**Figure 3.** Morphological changes in the amorphous zones of starch after enzymatic hydrolysis. A) Magnification at 1,000X, B) Magnification at 3,000X. AAM:  $\alpha$ -amylase; BAM:  $\beta$ -amylase; AMG: amyloglucosidase; PUL: pullulanase.

Enzymatic action on cassava starch granules produced significant changes in amylose content (Table 4). The decrease in amylose content in AAM, BAM, and AMG treatments can be associated with depolymerization of the polymeric chains due to the cleavage of  $\alpha$ -(1,4) and glycosidic bonds, which subsequently induced variations in both morphological characteristics and semi-crystalline behavior evaluated from X-ray diffractogram (XRD) and infrared spectra analysis by FTIR. Native cassava starch exhibited a typical type-A diffraction pattern, with close peaks at Bragg angles ( $2\theta$ ) at 15.1, 17.2, 18.0, and 22.9° (Figure 4). Type-A starches are characterized by arrangements of the amylopectin double helices as a closed monoclinic structure with low interhelical water content; this behavior is characteristic of tuber starches with low amylose content (<20% w/w) (Zhou et al. 2021; Salcedo-Mendoza et al. 2018). Hydrolysis with  $\alpha$ - and

$\beta$ -amylase did not change the type-A diffraction pattern, which could indicate that hydrolysis occurred mainly in the amorphous region; results were congruent with SEM analyses. Meanwhile, the attack with AMG and PUL caused a significant decrease in diffraction intensity in the peaks at angles 17.2 and 18.0°, with partial loss of the peak at angle 18.0°. Studies have shown that peaks at angles ( $2\theta$ ) at 17.2 and 18.0° are characteristic of the amylopectin double helix arrangement (Wang et al. 2019). This may indicate that hydrolysis with AMG and PUL occurred mainly in the amorphous zone by surface action at the granular periphery, followed by degradation in the crystalline zones that affected morphological changes; for instance, the appearance of eroded granules of hollow structure using amyloglucosidase and eroded-fragmented granules after debranching action with pullulanase (Figure 3).

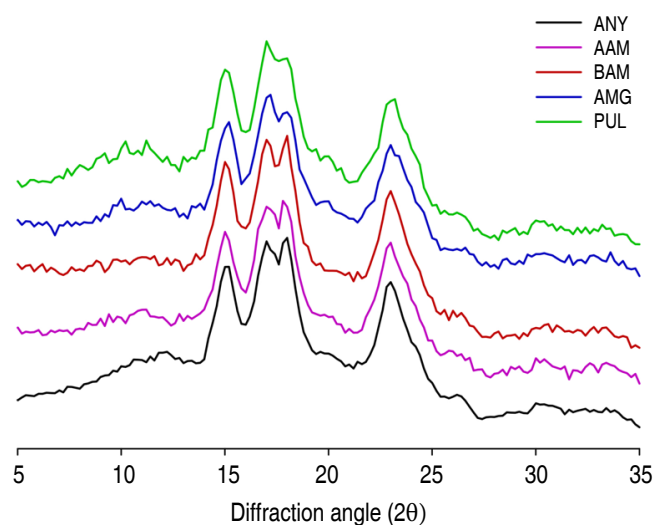


**Figure 4.** X-ray diffraction patterns of native and modified cassava starches. AAM:  $\alpha$ -amylase; BAM:  $\beta$ -amylase; AMG: amyloglucosidase; PUL: pullulanase.

Despite there was no change in A-type patterns after AAM and BAM attack, it is presumed that hydrolysis did not affect the long-range crystalline structure but did affect crystal melting, possibly because water gained greater accessibility in the crystalline regions after the amorphous regions were partially degraded (Gui et al. 2021; Li et al. 2023). This could explain the variation in the crystallinity degree (CD) in AAM and BAM starches relative to the native counterpart (ANY) (Table 4). The  $CD_1$  was estimated by the deconvolution method under

the definition of amorphous and crystalline zones in the X-ray diffractogram. A second method was proposed to estimate  $CD_2 = [(I_{max} - I_{am}) / I_{max}]$  from the intensity of the highest crystalline peak, as a quick comparison between treatments due to the partial loss of the peak at the Bragg angle ( $2\theta$ ) at 18.0°. In the performed calculations,  $I_{max}$  corresponds to the intensity of the maximum peak in the diffractogram, and  $I_{am}$  corresponds to the highest relative intensity between the zones with the highest contribution by the amorphous part (19~22°) (Foresti et al. 2014).

**Table 4.** Percentage of amylose, degree of crystallinity and molecular order.

Sample	Amylose (%)	<sup>1</sup> CD (%)	<sup>2</sup> CD (%)	<sup>3</sup> CD (%)	<sup>4</sup> OM <sub>1</sub>	<sup>5</sup> OM <sub>2</sub>
ANY	18.64±0.18 <sup>a</sup>	47.16±0.37 <sup>a</sup>	43.59±0.63 <sup>a</sup>	39.29±0.24 <sup>a</sup>	0.930±2x10 <sup>-3a</sup>	0.514±1x10 <sup>-3a</sup>
AAM	16.91±0.27 <sup>b</sup>	49.96±0.43 <sup>b</sup>	46.25±0.28 <sup>b</sup>	40.82±0.08 <sup>b</sup>	0.903±1x10 <sup>-3b</sup>	0.492±0x10 <sup>-2b</sup>
BAM	17.71±0.46 <sup>c</sup>	49.38±0.45 <sup>a</sup>	45.46±0.22 <sup>b</sup>	38.87±0.33 <sup>c</sup>	0.945±1x10 <sup>-3c</sup>	0.485±0x10 <sup>-3b</sup>
AMG	16.10±0.14 <sup>d</sup>	45.28±0.20 <sup>c</sup>	42.79±0.41 <sup>a</sup>	37.90±0.21 <sup>d</sup>	0.961±0x10 <sup>-3cd</sup>	0.519±2x10 <sup>-3c</sup>
PUL	20.08±0.40 <sup>e</sup>	41.22±0.50 <sup>d</sup>	41.37±0.56 <sup>c</sup>	36.65±0.10 <sup>d</sup>	0.950±2x10 <sup>-3d</sup>	0.547±1x10 <sup>-3d</sup>

AAM: α-amylase; BAM: β-amylase; AMG: amyloglucosidase; PUL: pullulanase. <sup>1</sup>CD: degree of crystallinity deconvolution method; <sup>2</sup>CD: degree of crystallinity "maximum height" method; <sup>3</sup>CD: degree of crystallinity estimated by FTIR; <sup>4</sup>OM<sub>1</sub>: molecular order based on the ratio 1,047/1,022 cm<sup>-1</sup>; <sup>5</sup>OM<sub>2</sub>: molecular order based on the ratio 995/1,022 cm<sup>-1</sup>. Equal letters within a column do not differ statistically (*P*<0.05).

Results showed that the CD variations by such techniques were low, although, for the maximum height method, the CD<sub>1</sub> values in AAM and BAM starches increased concerning the ANY sample. This could corroborate the preferential action of amylases on the amorphous zones in native cassava starch. In turn, the decrease of CD<sub>2</sub> in AMG and PUL starches presupposes a depolymerization in both amorphous and crystalline zones, thus causing a greater molecular disorganization in the granule, which is reflected in the morphological changes evaluated by SEM.

FTIR spectra in the mid-infrared region of native and enzymatically modified starches are presented in Figure 5. This method has been used to evaluate changes in starch structural organization at the short-range order molecular level (Gao et al. 2023). All the evaluated starches presented peaks at the 3,350 and 1,620 cm<sup>-1</sup> bands designated to

the stretching and angular deformation of O-H groups in tightly bound glucose units and water molecules, their width is attributed to the formation of inter- and intramolecular hydrogen bonds (Miao et al. 2015). The band at 2,940 cm<sup>-1</sup> is related to the stretching of C-H groups in glucose units; consequently, its intensity varies with the ratio of amylose/ amylopectin polymeric components (Almeida et al. 2019). The shifts and changes in band frequencies at 3,350, 2,940, and 1,620 cm<sup>-1</sup> in the hydrolyzed cassava starches with respect to the native counterpart allow us to suggest a possible molecular reorganization in the amorphous and crystalline lamellae after enzymatic treatments. In agreement with Ma et al. (2019), a helical realignment within the crystalline lamellae in modified starches is suggested due to shifts in the bands of C-H and O-H functional groups, which are structurally associated with glycosidic bonds and water strongly bound to the starch structure.

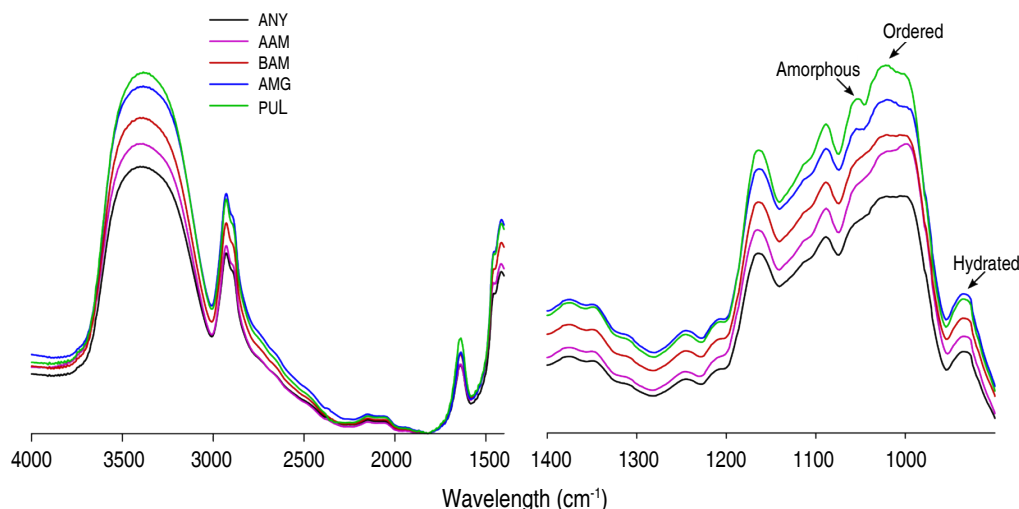


**Figure 5.** FTIR spectra of native and hydrolyzed cassava starches. AAM: α-amylase; BAM: β-amylase; AMG: amyloglucosidase; PUL: pullulanase.



The region between 1,200 and 900  $\text{cm}^{-1}$  represents the fingerprint of starch, in which a crystalline region is characterized by absorption peaks at 1,047 and 995  $\text{cm}^{-1}$ , while the absorption peak at 1,022  $\text{cm}^{-1}$  is linked to the amorphous region (Davoudi et al. 2022; Gao et al. 2023). In this region, the bands at 1,080 and 1,150  $\text{cm}^{-1}$  have been assigned to the bending and stretching vibrations of the C-O ring of anhydroglucose molecules (Wang et al. 2019). In turn, the ratio between bands at 1,047/1,022  $\text{cm}^{-1}$  were used to quantify the degree of molecular order (MO) in starch granules (Table 4). The MO values presented a decrease in AAM and BAM starches with respect to native cassava starch (ANY), but significantly increased in AMG and PUL starches. These results suggest irreversible changes in the semicrystalline order of granules after polymeric degradation. An increase in MO values is likely correlated to helical disruption within the crystalline lamellae (Ma et al. 2019), which may lead to disorganization at the molecular level, as evidenced in AMG and PUL starches where changes in crystalline peaks and  $\text{CD}_1$  were made based on X-ray diffraction spectra. From the amorphous and crystalline contributions defined by the ratio between the absorption peaks 1,047/1,022  $\text{cm}^{-1}$ , the maximum height method was applied assuming a baseline at the 1,065  $\text{cm}^{-1}$  band to propose an alternative method to estimate and evaluate the degree of crystallinity by FTIR. The results show that the  $\text{CD}_3$  evaluated by FTIR were lower than those estimated by X-ray diffraction with differences of less than 15% (Table 4). Likewise, the results reveal that the CD behavior in the different enzymatic treatments concerning the native counterpart maintains a similar trend independent of the implemented method. Therefore, it can be assumed that the maximum height method applied to FTIR spectra is a good approach to evaluate the semicrystalline order of cassava starch granules during enzymatic modification processes.

Additionally, the band in the peak at 995  $\text{cm}^{-1}$  has been assigned to the skeletal mode vibrations of the  $\alpha$ -(1,4) (C-O-C) glycosidic bond, while the sharp peak at 1,022  $\text{cm}^{-1}$  has been correlated to the stretching of C-O and C-O-C groups in  $\alpha$ -(1,6) glycosidic bonds (Das and Kayastha 2019). The ratio between the above bands was used as an approach to evaluate the differential enzymatic action of enzymes on glycosidic bonds ( $\text{OM}_2$ ) (Table 4).  $\text{OM}_2$  values decreased after amyolytic processes with  $\alpha$ - and

$\beta$ -amylase, indicating a possible higher activity on  $\alpha$ -(1,4) glycosidic bonds. Also, a slight decrease in  $\text{OM}_2$  value in AMG starches suggests a presumed hydrolytic action on different glycosidic bonds in a random manner. However, Keeratiburana et al. (2020) state that amyloglucosidase is an enzyme with preferential action on linear chains, followed by action on branched sites. In contrast, a preferential action of pullulanase on  $\alpha$ -(1,6)-glycosidic bonds can presumably be assigned due to increased  $\text{OM}_2$  values. Therefore, the behavior of  $\text{OM}_2$  values suggests that hydrolytic processes attacked linear and branched ones in native cassava starch, causing changes at the morphological and structural level, which have been previously verified through SEM and XRD analysis.

## CONCLUSION

The enzymatic activity of  $\beta$ -amylase and pullulanase on native cassava starch granules was lower than that presented by the enzymatic polypeptides of  $\alpha$ -amylase and amyloglucosidase, which had a higher rate of conversion to glucose, linked to a better biochemical affinity between the active site of the enzyme and the substrate. The morphological and structural results revealed that the hydrolysis was performed in two stages with different conversion rates depending on the polymeric packing and the crystallinity levels inside the granule. The correlation of structural analyses performed by XRD and FTIR suggest that  $\alpha$ - and  $\beta$ -amylase present a preferential action in the amorphous zones by selectively attacking internal and external  $\alpha$ -(1,4)-glycosidic bonds, respectively. Additionally, they lead to the formation of granules with an eroded or porous surface and a crystalline structure of higher molecular order. On the contrary, from a semicrystalline approach, the hydrolytic action of amyloglucosidase on polymeric chains seems to occur randomly, with a higher activity on truncated or previously eroded zones leading to fragmented granules of hollow structure. In turn, pullulanase presented a preferential action on the branched ends of amylopectin, decreasing the degree of crystallinity in eroded and highly fragmented granules.

## ACKNOWLEDGMENTS

Authors acknowledge the financial support to MINCIENCIAS through the National Program 776/2017, Doctorate National Scholarship 757/2016, and Investigation Project BPIN 2020000100035.



## REFERENCES

- Almeida RLJ, dos Santos TP, de Andrade VF et al (2019) Influence of enzymatic hydrolysis on the properties of red rice starch. *International Journal of Biological Macromolecules* 141: 1210-1219. <https://doi.org/10.1016/j.ijbiomac.2019.09.072>
- Almeida RLJ, Santos NC, de Brito-Lima WB et al (2022) Effect of enzymatic hydrolysis on digestibility and morpho-structural properties of hydrothermally pre-treated red rice starch. *International Journal of Biological Macromolecules* 222: 65-76. <https://doi.org/10.1016/j.ijbiomac.2022.09.089>
- Benavent-Gil Y and Rosell CM (2017) Morphological and physicochemical characterization of porous starches obtained from different botanical sources and amylolytic enzymes. *International Journal of Biological Macromolecules* 103: 587-595. <https://doi.org/10.1016/j.ijbiomac.2017.05.089>
- Blazek J and Gilbert EP (2010) Effect of enzymatic hydrolysis on native starch granule structure. *Biomacromolecules* 11(12): 3275-3289. <https://doi.org/10.1021/bm101124t>
- Chen A, Li Y, Nie J et al (2015) Protein engineering of *Bacillus acidopullulolyticus* pullulanase for enhanced thermostability using in silico data driven rational design methods. *Enzyme and Microbial Technology* 78: 74-83. <https://doi.org/10.1016/j.enzmictec.2015.06.013>
- De Schepper CF, Michiels P, Buvé C et al (2021) Starch hydrolysis during mashing: A study of the activity and thermal inactivation kinetics of barley malt  $\alpha$ -amylase and  $\beta$ -amylase. *Carbohydrate Polymers* 225: 117494. <https://doi.org/10.1016/j.carbpol.2020.117494>
- Das R and Kayastha AM (2019) Enzymatic hydrolysis of native granular starches by a new  $\beta$ -amylase from peanut (*Arachis hypogaea*). *Food Chemistry* 276: 582-590. <https://doi.org/10.1016/j.foodchem.2018.10.058>
- Davoudi Z, Azizi MH and Barzegar M (2022) Porous corn starch obtained from combined cold plasma and enzymatic hydrolysis: Microstructure and physicochemical properties. *International Journal of Biological Macromolecules* 223: 790-797. <https://doi.org/10.1016/j.ijbiomac.2022.11.058>
- Dona AC, Pages G, Gilbert RG et al (2010) Digestion of starch: *In vivo* and *in vitro* kinetic models used to characterise oligosaccharide or glucose release. *Carbohydrate Polymers* 80(3): 599-617. <https://doi.org/10.1016/j.carbpol.2010.01.002>
- Figuroa-Flórez J, Cadena-Chamorro E, Rodríguez-Sandoval E et al (2023) Hydrothermal processes and simultaneous enzymatic hydrolysis in the production of modified cassava starches with porous-surfaces. *Heliyon* 9(7): e17742. <https://doi.org/10.1016/j.heliyon.2023.e17742>
- Fitter J, Herrmann R, Dencher NA et al (2001) Activity and stability of a thermostable  $\alpha$ -amylase compared to its mesophilic homologue: Mechanisms of thermal adaptation. *Biochemistry* 40(35): 10723-10731. <https://doi.org/10.1021/bi010808b>
- Foresti ML, Williams MP, Martínez RG et al (2014) Analysis of a preferential action of  $\alpha$ -amylase from *B. licheniformis* towards amorphous regions of waxy maize starch. *Carbohydrate Polymers* 102: 80-87. <https://doi.org/10.1016/j.carbpol.2013.11.013>
- Frota EG, Sartor KB, Biduski B et al (2020) Co-immobilization of amylases in porous crosslinked gelatin matrices by different reticulations approaches. *International Journal of Biological Macromolecules* (165): 1002-1009. <https://doi.org/10.1016/j.ijbiomac.2020.09.220>
- Gao L, Wan C, Wang H et al (2023) Changes in the structural and physicochemical characterization of pea starch modified by *Bacillus*-produced  $\alpha$ -amylase. *Innovative Food Science & Emerging Technologies* 86: 103376. <https://doi.org/10.1016/j.ifset.2023.103376>
- Gui Y, Zou F, Li J et al (2021) Corn starch modification during endogenous malt amylases: The impact of synergistic hydrolysis time of  $\alpha$ -amylase and  $\beta$ -amylase and limit dextrinase. *International Journal of Biological Macromolecules* 190: 819-826. <https://doi.org/10.1016/j.ijbiomac.2021.09.052>
- Gupta K, Jana AK, Kumar S et al (2015) Solid state fermentation with recovery of amyloglucosidase from extract by direct immobilization in cross linked enzyme aggregate for starch hydrolysis. *Biocatalysis and Agricultural Biotechnology* 4(4): 486-492. <https://doi.org/10.1016/j.bcab.2015.07.007>
- Keeratiburana T, Hansen AR, Soontaranon S et al (2020) Porous high amylose rice starch modified by amyloglucosidase and maltogenic  $\alpha$ -amylase. *Carbohydrate Polymers* 230: 115611. <https://doi.org/10.1016/j.carbpol.2019.115611>
- Kikani B and Singh S (2015) Enzyme stability, thermodynamics and secondary structures of  $\alpha$ -amylase as probed by the CD spectroscopy. *International Journal of Biological Macromolecules* (81): 450-460. <https://doi.org/10.1016/j.ijbiomac.2015.08.032>
- Kim JY, Park DJ and Lim ST (2008) Fragmentation of waxy rice starch granules by enzymatic hydrolysis. *Cereal Chemistry Journal* 85(2): 182-187. <https://doi.org/10.1094/CCEM-85-2-0182>
- Lahmar I, Radeva G, Marinkova D et al (2018) Immobilization and topochemical mechanism of a new  $\beta$ -amylase extracted from *Pergularia tomentosa*. *Process Biochemistry* 64: 143-151. <https://doi.org/10.1016/j.procbio.2017.09.007>
- Li J, Vasanthan T, Hoover R et al (2004) Starch from hull-less barley: V. *In-vitro* susceptibility of waxy, normal, and high-amylose starches towards hydrolysis by  $\alpha$ -amylases and amyloglucosidase. *Food Chemistry* 84(4): 621-632. [https://doi.org/10.1016/S0308-8146\(03\)00287-5](https://doi.org/10.1016/S0308-8146(03)00287-5)
- Li P, He X, Dhital S et al (2017) Structural and physicochemical properties of granular starches after treatment with debranching enzyme. *Carbohydrate Polymers* 169: 351-356. <https://doi.org/10.1016/j.carbpol.2017.04.036>
- Li X, Zhao J, Fu J et al (2018) Sequence analysis and biochemical properties of an acidophilic and hyperthermophilic amylopullulanase from *Thermophilum pendens*. *International Journal of Biological Macromolecules* 114: 235-243. <https://doi.org/10.1016/j.ijbiomac.2018.03.073>
- Li Y, Cheng W, Qiu X et al (2023) Effects of  $\beta$ -amylase hydrolysis on the structural, physicochemical and storage properties of wheat starch. *Journal of Cereal Science* 109: 103605. <https://doi.org/10.1016/j.jcs.2022.103605>
- Lin L, Guo D, Huang J et al (2016) Molecular structure and enzymatic hydrolysis properties of starches from high-amylose maize inbred lines and their hybrids. *Food Hydrocolloids* 58: 246-254. <https://doi.org/10.1016/j.foodhyd.2016.03.001>
- Liu Y, Huang L, Jia L et al (2017) Improvement of the acid stability of *Bacillus licheniformis* alpha amylase by site-directed mutagenesis. *Process Biochemistry* 58: 174-180. <https://doi.org/10.1016/j.procbio.2017.04.040>
- Ma Z, Ma M, Zhou D et al (2019) The retrogradation characteristics of pullulanase debranched field pea starch: Effects of storage time and temperature. *International Journal of Biological Macromolecules* 134: 984-992. <https://doi.org/10.1016/j.ijbiomac.2019.05.064>

- Miao M, Li R, Huang C et al (2015) Impact of  $\beta$ -amylase degradation on properties of sugary maize soluble starch particles. *Food Chemistry* 177: 1-7. <https://doi.org/10.1016/j.foodchem.2014.12.101>
- Sagu ST, Nso EJ, Homann T et al (2015) Extraction and purification of beta-amylase from stems of *Abrus precatorius* by three phase partitioning. *Food Chemistry* 183: 144-153. <https://doi.org/10.1016/j.foodchem.2015.03.028>
- Semwal J and Meera MS (2023) Modification of sorghum starch as a function of pullulanase hydrolysis and infrared treatment. *Food Chemistry* 416: 135815. <https://doi.org/10.1016/j.foodchem.2023.135815>
- Salcedo-Mendoza J, Paternina-Urzola S, Lujan-Rhenals D et al (2018) Enzymatic modification of cassava starch (Corpoica M-Tai) around the pasting temperature. *DYNA* 85(204): 223-230. <https://doi.org/10.15446/dyna.v85n204.66620>
- Torabizadeh H, Tavakoli M and Safari M (2014) Immobilization of thermostable  $\alpha$ -amylase from *Bacillus licheniformis* by cross-linked enzyme aggregates method using calcium and sodium ions as additives. *Journal of Molecular Catalysis B: Enzymatic* 108: 13-20. <https://doi.org/10.1016/j.molcatb.2014.06.005>
- Vajravijayan S, Pletnev S, Mani N et al (2018) Structural insights on starch hydrolysis by plant  $\beta$ -amylase and its evolutionary relationship with bacterial enzymes. *International Journal of Biological Macromolecules*, 113, 329-337. <https://doi.org/10.1016/j.ijbiomac.2018.02.138>
- Wang X, Niu C, Bao M et al (2019) Simultaneous enhancement of barley  $\beta$ -amylase thermostability and catalytic activity by R115 and T387 residue sites mutation. *Biochemical and Biophysical Research Communications* 514: 301-307. <https://doi.org/10.1016/j.bbrc.2019.04.095>
- Yang Z, Xu X, Singh R et al (2019) Effect of amyloglucosidase hydrolysis on the multi-scale supramolecular structure of corn starch. *Carbohydrate Polymers* 212: 40-50. <https://doi.org/10.1016/j.carbpol.2019.02.028>
- Zareian S, Khajeh K, Ranjbar B et al (2010) Purification and characterization of a novel amylopullulanase that converts pullulan to glucose, maltose, and maltotriose and starch to glucose and maltose. *Enzyme and Microbial Technology* 46(2): 57-63. <https://doi.org/10.1016/j.enzmictec.2009.09.012>
- Zeng Y, Xu J, Fu X et al (2019) Effects of different carbohydrate binding modules on the enzymatic properties of pullulanase. *International Journal of Biological Macromolecules* 137: 973-981. <https://doi.org/10.1016/j.ijbiomac.2019.07.054>
- Zhang B, Dhital S and Gidley MJ (2013) Synergistic and antagonistic effects of  $\alpha$ -amylase and amyloglucosidase on starch digestion. *Biomacromolecules* 14(6): 1945-1954. <https://doi.org/10.1021/bm400332a>
- Zhang L, Zhong L, Wang J et al (2021) Efficient hydrolysis of raw starch by a maltohexaose-forming  $\alpha$ -amylase from *Corallococcus* sp. *LWT* 152: 112361. <https://doi.org/10.1016/j.lwt.2021.112361>
- Zhou X, Chang Q, Li J et al (2021) Preparation of V-type porous starch by amylase hydrolysis of V-type granular starch in aqueous ethanol solution. *International Journal of Biological Macromolecules*, 183, 890-897. <https://doi.org/10.1016/j.ijbiomac.2021.05.006>

# Coating of oxidized banana starch and olive oil for the preservation of cherry tomatoes (*Solanum lycopersicum* cv. Cerasiforme)

Recubrimiento de almidón oxidado de plátano y aceite de oliva para la conservación de tomates cherry (*Solanum lycopersicum* cv. Cerasiforme)

<https://doi.org/10.15446/rfnam.v77n3.109200>

Luis A. Cedeño Sares<sup>1</sup>, Alicia Casariego Año<sup>2</sup>, Mario A. García Pérez<sup>3\*</sup>, Ney D. Jumbo-Peña<sup>1</sup> and Jennifer V. Machuca Román<sup>1</sup>

## ABSTRACT

### Keywords:

Biodegradable coating  
*Musa paradisiaca*  
Starch  
*Solanum lycopersicum*  
Storage




Postharvest conservation of fresh fruits and vegetables is a constant challenge in the food industry. Biodegradable coatings represent an innovative and sustainable solution to extend their shelf life. In this context, this research evaluated the influence of a coating based on oxidized banana starch (*Musa paradisiaca* L. group AAA, cv. Cavendish) and olive oil on the conservation of cherry tomatoes (*Solanum lycopersicum* cv. Cerasiforme) during their storage at ambient conditions. Coating-forming emulsions were prepared using starch (4% m v<sup>-1</sup>) with a high degree of oxidation, glycerol, Tween 80, and olive oil. The products were dip coated. The starch extraction yield was 27.26% by the wet milling method. The contents of lipids, crude fiber, proteins, carbohydrates, and ashes tended to decrease in oxidized starches with increasing reaction time, the opposite behavior for humidity ( $P \leq 0.05$ ). Solubility and oil absorption capacity increased in oxidized starches, while water absorption and swelling power decreased ( $P \leq 0.05$ ). The best combination for the formulation of oxidized starch coatings was 3% (m v<sup>-1</sup>) of glycerol and 0.3% (m v<sup>-1</sup>) of oil. This coating reduced weight losses and delayed the ripening process. The results suggested that the use of coatings based on oxidized banana starch and olive oil is an effective strategy for maintaining the quality and freshness of the fruits during a longer storage period.

## RESUMEN


### Palabras clave:

Recubrimiento biodegradable  
*Musa paradisiaca*  
Almidón  
*Solanum lycopersicum*  
Almacenamiento

La conservación poscosecha de frutas y hortalizas frescas es un desafío constante en la industria alimentaria. Los recubrimientos biodegradables representan una solución innovadora y sostenible para prolongar su vida útil. En este contexto, esta investigación evaluó la influencia de un recubrimiento a base de almidón oxidado de plátano (*Musa paradisiaca* L. grupo AAA, cv. Cavendish) y aceite de oliva en la conservación de tomates cherry (*Solanum lycopersicum* cv. Cerasiforme) durante su almacenamiento en condiciones ambientales. Se prepararon emulsiones formadoras de recubrimiento usando almidón (4% m v<sup>-1</sup>) con alto grado de oxidación, glicerol, Tween 80 y aceite de oliva. Los productos se recubrieron mediante inmersión. El rendimiento de extracción del almidón fue de 27,26% por el método de molienda húmeda. Los contenidos de lípidos, fibra cruda, proteínas, carbohidratos y cenizas tendieron a disminuir en los almidones oxidados al aumentar el tiempo de reacción, comportamiento opuesto para la humedad ( $P \leq 0,05$ ). La solubilidad y capacidad de absorción de aceite aumentaron en los almidones oxidados, mientras que la absorción de agua y poder de hinchamiento disminuyeron ( $P \leq 0,05$ ). La mejor combinación para la formulación de los recubrimientos de almidón oxidado fue 3% (m v<sup>-1</sup>) de glicerol y 0,3% (m v<sup>-1</sup>) de aceite. Este recubrimiento redujo las pérdidas de masa y retrasó el proceso de maduración. Los resultados sugirieron que el uso de recubrimientos a base de almidón oxidado de plátano y aceite de oliva es una estrategia eficaz para mantener la calidad y frescura de los frutos durante un periodo de almacenamiento más prolongado.

<sup>1</sup>Faculty of Chemical and Health Sciences, Technical University of Machala, Ecuador. lcedeno@utmachala.edu.ec , njumbo1@utmachala.edu.ec , jmachuca3@utmachala.edu.ec 

<sup>2</sup>Department of Food, Pharmacy and Food Institute, University of Havana, Cuba. alicia@ifal.uh.cu 

<sup>3</sup>Universidad San Gregorio de Portoviejo, Manabí, Ecuador. marioifal@gmail.com 

\*Corresponding author

There are new packaging methods, among which, coatings are qualified as a promising technology due to their applicability and characteristics attributed to the different products involved in their matrix. Besides, these coatings are environmentally friendly, as they try to minimize the impact of traditional packaging by using natural and biodegradable biopolymers that are obtained from natural sources or extracted from industrial by-products (Fernández et al. 2017).

The coatings consist in coating a fruit or vegetable with one or several thin layers of a continuous matrix that fits around the product. They are usually applied by immersion in the coating-forming solution, to reduce quality loss and extend the shelf life of fruits and vegetables, either whole or minimally processed, in synergy with other treatments and ingredients (Fernández et al. 2017).

Among the polysaccharides of greatest interest for the formulation of coatings is starch, which forms cohesive molecular networks that confer good mechanical properties such as adhesion and flexibility, which depend on the composition and source of the starch. These coatings are tasteless, odorless, and transparent, having a minor impact on the coated product. However, they present poor barrier properties against water vapor, and their semi-crystallinity and rapid degradation affect their mechanical properties, so their structure must be modified to improve these properties (Ramos-García et al. 2018).

Oxidation is a feasible chemical modification route, in which sodium hypochlorite (NaOCl) acts as an oxidizing agent. This reaction consists of the introduction of carbonyl and carboxyl groups that hydrate and swell the molecule better, improve stability at high temperatures, and impart transparency and low viscosity compared to native starch. During starch oxidation, the primary hydroxyl groups are oxidized to carboxyl groups or aldehydes, depending on the conditions of oxidant concentration, pH, and starch origin, among others. Partial depolymerization of the polysaccharide chains also occurs and various degrees of oxidation are obtained; for example, when there is a low concentration of active chlorine in an alkaline medium, a greater number of carboxyl groups are formed (Bonilla et al. 2013; Ramos-García et al. 2018).

Starch oxidation is used in various applications due to its ability to enhance the properties of starch-based materials. Oxidation of starch modifies its chemical structure, improving its solubility and reducing its viscosity, which facilitates the formation of thin, uniform films and coatings. This modification is crucial in the food industry for creating effective edible coatings that improve food preservation. Oxidized starches provide better moisture and oxygen barrier properties, which are essential for extending the shelf life of perishable products. Studies have shown that oxidized starch coatings can reduce moisture loss and delay spoilage, which contributes to better preservation of fruits and vegetables, such as cherry tomatoes (Zamudio-Flores et al. 2010). Furthermore, these coatings often exhibit antimicrobial properties, which help in controlling microbial growth and reducing fungal decay, thereby enhancing the shelf life and safety of the food (Ungureanu et al. 2023). Overall, the use of oxidized starch in edible coatings is justified by its improved functional properties and effectiveness in food preservation.

Among these products, there is the cherry tomato (*Solanum lycopersicum* cv. Cerasiforme). The cherry tomato is a vegetable of importance due to its wide consumption, either as a fresh product or as raw material for the food industry and is characterized by a short shelf life (Pérez-Díaz et al. 2020); due to physiological changes during its postharvest stage. Its aw is 0.94, which is associated with the loss of water vapor during transpiration (Fich et al. 2020) and the subsequent weight loss due to dehydration. This, in turn, causes softening, flaccidity, and loss of turgidity and texture.

Previous studies have shown that edible coatings enhance the quality and shelf life of cherry tomatoes. For instance, the application of cornstarch coatings on tomato fruits has proven effective in maintaining postharvest quality by reducing weight loss and delaying ripening (Fitch-Vargas et al. 2019). Other studies have highlighted the use of various starch modifications, including oxidized and heat-moisture-treated starches, which enhance the mechanical and barrier properties of the coatings (Zavareze et al. 2012).

Considering the above, this research aimed to evaluate the influence of a coating based on banana (*Musa paradisiaca* L. AAA group, cv. Cavendish) oxidized starch and olive oil on the preservation of cherry tomatoes (*Solanum lycopersicum* cv. Cerasiforme) during their storage at ambient conditions.



## MATERIALS AND METHODS

### Isolation and chemical modification of banana starch

Green bananas (*Musa paradisiaca* L. AAA Group, cv. 'Cavendish') with a maturity grade of one according to the Von Loesecke scale and caliber of 39 to 42 cm (NTE INEN 2801, 2013), were acquired in the twelfth week of harvest, in a farm in La Iberia parish of El Guabo canton of El Oro province, Ecuador.

Starch isolation was carried out by the wet method (Hidalgo et al. 2020). For this, once the peel was removed, the fruit was cut into pieces 2 to 3 cm long. Wet grinding was achieved with a 3% (m v<sup>-1</sup>) citric acid solution at a ratio of 1:0.25 with a domestic blender at 3,600 rpm for 2 min. The product obtained was filtered through a 345 µm mesh and washed until the outlet liquid was free of apparent starch residues. Subsequently, the liquid was allowed to settle for 3 h. The sediment was centrifuged (Corning® LSE™, NY, USA) at 5,000 rpm and the supernatant was removed. The paste (native starch) was centrifuged again and oven-dried (Memmert, Schwabach, Germany) at 50 °C for 24 h to a constant mass. Finally, the dried product was ground and passed through a No. 60 mesh sieve (250 µm, ASTM E11, Gilson Co. Inc., USA) to obtain a uniform particle size. The yield (%) was calculated using Equation 1, Both masses were expressed in g.

$$\text{Yield}(\%) = \frac{\text{Mass of dry starch}}{\text{Mass of banana pulp}} \times 100 \quad (1)$$

### Starch oxidation

Starch oxidation was done according to the methodology proposed by Carhuallay et al. (2020) with some modifications. A starch solution (100 mL) was prepared at 30% (m v<sup>-1</sup>); this was then placed in a thermo-stirring plate (Cimarec+™ Thermo Fisher Scientific Inc., Waltham, Massachusetts, USA) at 525 min<sup>-1</sup> and heated to 30 °C. The pH was then adjusted to between 9 and 9.5 with NaOH at 2 N. Next, 100 mL of 1.5% (m v<sup>-1</sup>) NaClO was added dropwise for 30 min. During this time, the pH was maintained between 9 and 9.5 with H<sub>2</sub>SO<sub>4</sub> at 1 N. The solution was continuously stirred to promote the reaction according to the time evaluated in each treatment (40 and 90 min) and the pH was kept constant with a solution of NaOH at 1 N. When the reaction was finished, 1 g of sodium bisulfite was added and left to act for 1 min. The effluent

was filtered with Whatman® qualitative filter paper until a clear liquid was obtained. The retained product was placed in an oven at 45 °C for 16 h until constant mass and was then ground and sieved.

### Determination of carbonyl and carboxyl groups of starch

The carbonyl group was determined according to a volumetric method adapted by Fonseca et al. (2015). Four grams on a dry basis of oxidized starch was added to 100 mL of distilled water in a 500 mL beaker. The suspension was gelatinized in a boiling water bath for 20 min. The suspension was cooled until 40 °C and the pH was maintained at 3.2 with 0.1 N HCl. Following this, 15 mL of a hydroxylamine reagent were added to the mixture; the beaker was capped and placed in a water bath at 40 °C for 4 h with slow stirring on a thermostirring iron. For the preparation of the hydroxylamine reagent, a 500 mL volumetric flask was used in which 25 g of hydroxylamine hydrochloride were dissolved in 100 mL of NaOH at 0.5 N, completing the volume with distilled water. The reaction mixture was titrated to pH=3.2 with 0.1 N standardized HCl to determine excess hydroxylamine. The blank was titrated with native starch and hydroxylamine reagent following the same procedure. The carbonyl percentage was calculated according to Equation 2.

$$\text{Carbonyl}(\%) = \frac{V_{\text{Blank}} - V_{\text{Sample}}}{M_{\text{Dry base}}} \times C_{(\text{HCl})} \times 0.028 \times 100 \quad (2)$$

Where V is the volume consumed by the blank and sample, expressed in mL; M is the mass in g; and C is, the equivalent molar concentration of HCl.

The carboxyl group was quantified according to Ashwar et al. (2014). In a 100 mL beaker, 2 g (bs) of starch was placed, 25 mL of HCl at 0.1 N was added and continuously stirred in a thermostirring iron at 350 min<sup>-1</sup> for 30 min. The suspension was then filtered and washed with sufficient distilled water. The starch was then placed in a 600 mL beaker and 300 mL of distilled water was added; the solution was boiled for 10 min to achieve complete gelatinization and allowed to cool to 40 °C. Subsequently, it was titrated with NaOH at 0.1 N. This procedure was also performed with the native starch as blank. Equations 3 and 4 determined the carboxyl content (%):



$$\text{Carboxyl(\%)} = \frac{\text{meq acid}}{100 \text{ g of starch}} \times 0,00453 \times 100 \quad (3)$$

$$\frac{\text{meq acid}}{100 \text{ g of starch}} = \frac{V_{\text{Blank}} - V_{\text{Sample}}}{M_{\text{Dry base}}} \times C_{\text{NaOH}} \times 100 \quad (4)$$

Where V is the volume consumed by the blank and sample, expressed in mL; M is the mass in g; and C is the equivalent molar concentration of NaOH.

### Proximal composition of starches

The determination of the proximate composition of native and oxidized starches included the determination of protein content by the Dumas method (Mikó et al. 2023), crude fiber by the Weende method (Lopes et al. 2021); lipids and ash according to AOAC (2020). The moisture content was determined according to AOAC (2020). The total carbohydrate content was determined by difference.

### Functional characterization of starches

Water solubility index (ISA), water absorption index (IAA), and swelling power (PHi) values were determined (Salcedo-Mendoza et al. 2016). To 1 g (dry basis) of starch contained in a test tube, 25 mL of distilled water preheated to 60 °C was added. The suspension was kept in a water bath at 60 °C for 30 min and manually shaken for 10 min after the heating started. Subsequently, it was centrifuged at 2,500 min<sup>-1</sup> for 15 min and the supernatant (soluble starch) was recovered and the total volume was determined. Next, 10 mL of the supernatant was deposited in a Petri dish, previously weighed; it was dried in an oven at 70 °C for 16 h. The masses of the Petri dish with the material and the centrifuge tube containing the gel (insoluble starch) were recorded. The values of ISA, IAA, and Phi were calculated from Equations 5, 6, and 7, respectively.

$$\text{ISA} = \frac{\text{Mass}_{\text{Soluble starch}} * \frac{\text{Volume}_{\text{Supernatant}}}{10}}{\text{Mass}_{\text{Sample dry base}}} \quad (5)$$

$$\text{IAA} = \frac{\text{Mass}_{\text{Gel}}}{\text{Mass}_{\text{Sample dry base}}} \quad (6)$$

$$\text{PHi} = \frac{\text{Mass}_{\text{Gel}}}{\text{Mass}_{\text{Sample dry base}} - \text{Mass}_{\text{Soluble starch}}} \quad (7)$$

All masses were expressed in g and volumes in mL.

Oil absorption capacity (CAA) was determined using the methodology proposed by Olatunde et al. (2017) with modifications. In a centrifuge tube, previously weighed, 2 g of sample was deposited and mixed with 20 mL of edible oil. It was allowed to stand at room temperature for 30 min; then it was centrifuged at 2,000 min<sup>-1</sup> for 25 min and the supernatant oil was removed, finally, the tubes were weighed on an analytical balance and the results were expressed according to Equation 8.

$$\text{CAA} = \frac{\text{Mass}_{\text{Retained oil}}}{\text{Mass}_{\text{Sample}}} \times 100 \quad (8)$$

The CAA was expressed in %, and both masses in g.

For the determination of the gelling temperature, a 10% (m v<sup>-1</sup>) starch solution was prepared in a 150 mL beaker, which was placed in a water bath at 85 °C. A thermometer was then placed inside the beaker and stirred continuously. Finally, the reading was taken when a paste was formed and the temperature remained stable (Carhuallay et al. 2020).

### Selection of a coating based on the weight loss of cherry tomatoes

For the formulation of the coatings, an experimental design 2<sup>2</sup> completely randomized was applied using the Statgraphics Centurion XVI.I program (Statgraphics Technologies Inc., Virginia, USA), which was executed in three blocks, generating 12 runs that included eight replicates. The oxidized starch content was adjusted to 4% (m v<sup>-1</sup>) in all runs. The percentages of glycerol (3 and 3.5% m v<sup>-1</sup>) and olive oil (0.3 and 0.4% m v<sup>-1</sup>) were considered as design factors. The effect of the treatments on weight losses of cherry tomatoes (*S. lycopersicum* cv. Cerasiforme) was analyzed and a model was obtained for its estimation under the storage conditions studied. The results were expressed as percentage weight loss (WL) according to Equation 9.

$$\text{WL(\%)} = \frac{M_i - M_f}{M_i} \times 100 \quad (9)$$

Where WL is the weight loss (%);  $M_i$  is the initial mass (g); and  $M_f$ , the final mass (g).

### Preparation and application of coating-forming emulsions

For the preparation of the coating-forming emulsions, the methodology described by El Halal et al. (2015) was followed with some modifications. Starch with a high degree of oxidation was used to prepare the coating-forming emulsions. The oxidized starch solution (4% m v<sup>-1</sup>) for each of the treatments was heated with constant stirring to a temperature between 68 and 69 °C, corresponding to the gelatinization temperature (Schmiele et al. 2019). Next, the amount of glycerol was added according to the experimental design, and stirring was continued for 30 min maintaining the temperature constant. After cooling the solution to 35 °C, Tween 80 was added as an emulsifier considering a 1:1 ratio based on the amount of olive oil and stirring was continued for 1 min. Subsequently, the olive oil was added; this dispersion was homogenized (Homogenizer D-500, DLAB Scientific Instrument Inc., California, USA) at 15,000 rpm for 4 min.

To evaluate the effect of each of the coatings, selected cherry tomatoes were used, considering that they all presented similar sizes and ripening degrees of four (Saborío 2021) and without mechanical damage. The tomatoes were disinfected with a NaClO solution at 5 mg kg<sup>-1</sup> for 15 min, dried and coated by immersion in the film-forming emulsion for 4 min, and left to dry at ambient conditions for 48 h. The tomatoes were then dried at room conditions for 48 h. The tomato mass was then recorded, and the tomatoes were dried at 5 mg kg<sup>-1</sup>. The individual mass of the tomatoes was then recorded and considered as the initial mass; the final mass was determined after five days of storage at ambient conditions (20 to 25 °C and 70 to 85% relative humidity), dependent on time of day (Dovale-Rosabal et al. 2015).

### Preservation of cherry tomatoes with oxidized starch-based coatings

Based on the results on the effect of coatings on weight loss, a formulation was selected to verify its influence on the preservation of cherry tomatoes during storage under ambient conditions. The selected coating was applied by immersing the tomatoes in the emulsion for 4 min, followed by ambient drying for 48 h (Hoyos-Yela et al. 2019).

During 16 days of storage of cherry tomatoes, refractometric soluble solids (Al-Dairi et al. 2021), titratable acidity (Al-Dairi et al. 2021), pH (NTE INEN-ISO 1842, 2013), and percentage weight loss were determined. To compare the changes, a batch of uncoated tomatoes was kept under the same storage conditions.

### Statistical analysis

Analysis of variance was carried out to determine the statistical significance of the results of the different determinations. If there were significant differences, Duncan's multiple range test was applied to determine the differences between means ( $P \leq 0.05$ ). These differences were indicated with different letters for a determination.

## RESULTS AND DISCUSSION

### Yield of banana starch extraction

The banana starch extraction yield was  $27.26 \pm 3.95\%$ , applying wet milling, determined based on the weight of the peeled immature fruit. This value was similar to those reported by Hidalgo et al. (2020) for plantain (*Musa paradisiaca*) starch extraction. In these works, the influence of several variables of the wet milling process that affect this indicator, such as grinding speed and time, was explained.

### Chemical characteristics of oxidized starch

Table 1 shows the results of the effect of oxidation time on the degree of starch oxidation. An increase ( $P \leq 0.05$ ) of carbonyl and carboxyl groups formed was evident as the reaction time at constant temperature increased.

The reaction time of 90 min was more effective in obtaining a higher degree of oxidation, with values of  $0.107 \pm 0.1027\%$  for carbonyl groups (C=O) and  $0.071 \pm 0.0046\%$  for carboxyl groups (COOH), behavior similar to those described by Bonilla et al. (2013) and Sumardiono et al. (2021) for cassava and sago starch, respectively. This is related to the oxidizing agent initially converting hydroxyl groups to carbonyl groups (C=O). Subsequently, these are converted to carboxyl groups (COOH) that are selectively formed by the oxidation of hydroxyl groups on the carbons of positions 2, 3, and 6 of the glucose units that make up the starch molecule (Bonilla et al. 2013), defining the degree of substitution. Other factors such as pH, concentration of the oxidizing agent, and temperature influence this reaction.

**Table 1.** Effect of oxidation time on the oxidation degree of banana starch (*Musa paradisiaca* L. AAA group, cv. Cavendish).

Reaction time (min)	Carbonyl groups (%)	Carboxyl groups (%)
0	0.000±0.0000 <sup>a</sup>	0.000±0.0000 <sup>a</sup>
40	0.059±0.0036 <sup>b</sup>	0.048±0.0028 <sup>b</sup>
90	0.107±0.1027 <sup>c</sup>	0.071±0.0046 <sup>c</sup>

Mean ± standard error; n=3. Different letters in the same column indicate significant differences ( $P \leq 0.05$ ).

### Effect of oxidation on the proximal composition of banana starch

The protein and moisture contents of the native starch were  $2.06 \pm 0.0306$  and  $10.22 \pm 0.0833\%$ , respectively (Table 2), values close to those reported by Zamudio-Flores et al. (2015). For lipid, crude fiber, and carbohydrate contents, values of  $0.7 \pm 0.0379$ ,  $0.42 \pm 0.0264$ , and  $85.15 \pm 0.2685\%$ ,

respectively, were obtained. These values depend on factors such as the origin and variety of the banana, regional climate, cultural practices, harvesting conditions, isolation methods, and type of oxidizing agent used in extraction, among others (Helen et al. 2022; Olatunde et al. 2017). The ash percentage was  $1.46 \pm 0.0321\%$ , which could be due to the presence of minerals such as calcium, potassium, and magnesium.

**Table 2.** Effect of oxidation time on the proximal composition of banana starch (*Musa paradisiaca* L. AAA group, cv. Cavendish).

Reaction time (min)	Carbohydrates (%)	Lipids (%)	Proteins (%)	Crude fiber (%)	Ashes (%)	Humidity (%)
0	$85.15 \pm 0.2685^a$	$0.70 \pm 0.0379^a$	$2.06 \pm 0.0306^a$	$0.42 \pm 0.0264^a$	$1.46 \pm 0.0321^a$	$10.22 \pm 0.0833^a$
40	$84.50 \pm 0.0458^b$	$0.42 \pm 0.0346^b$	$1.35 \pm 0.0361^b$	$0.32 \pm 0.035^b$	$1.34 \pm 0.0416^b$	$12.06 \pm 0.0872^b$
90	$84.06 \pm 0.3164^c$	$0.30 \pm 0.0100^c$	$1.02 \pm 0.0964^c$	$0.22 \pm 0.0208^c$	$1.32 \pm 0.0945^c$	$13.10 \pm 0.0416^c$

Mean ± standard error; n=3. Different letters in the same column indicate significant differences ( $P \leq 0.05$ ).

The oxidation reaction time increased the moisture percentage ( $P \leq 0.05$ ) in oxidized starches from  $12.06 \pm 0.0872$  to  $13.1 \pm 0.0416\%$ , compared to native starches. This could have been due to the increase in the hydrophilic potential of oxidized starches because the carbonyl and carboxyl groups inserted in the molecule formed hydrogen bonds with water molecules (Zamudio-Flores et al. 2015). The contents of lipids, crude fiber, proteins, carbohydrates, and ash tended to decrease when the reaction time increased ( $P \leq 0.05$ ). This was related to the oxidative effect of chlorine on protein denaturation, lipid saponification, and chemical disintegration in the starch molecule, due to the exposure time to sodium hypochlorite, as well as to the leaching of minerals during the oxidation process (Olatunde et al. 2017).

### Effect of oxidation on the functional properties of starch

The technological behavior of starch is in correspondence with its functional properties, which are specific according to the starch origin and degree of modification (Cedeño-Sares et al. 2021). Table 3 shows the values of the functional

properties of starches. It is observed that the ISA increased with oxidation time, indicating greater solubility of the oxidized starch. On the other hand, both PHi and IAA decreased, suggesting a lower capacity of oxidized starch to absorb and retain water. CAA increased significantly, demonstrating a better ability of oxidized starch to interact with oils, which would be beneficial in some food applications. The gelation temperature decreased with oxidation time, implying that oxidized starch requires less energy to form a gel, an advantageous characteristic for certain industrial processes.

For native starch, these values were similar to those reported by Cedeño-Sares et al. (2021) and Correa et al. (2017) for starch from banana (*Musa* AAA cv. Cavendish) and Dominican plantain (*M. paradisiaca*), respectively. However, it was evidenced that increasing the reaction time, increased the ISA values ( $P \leq 0.05$ ), expressed as soluble starch, from  $0.031 \pm 0.0011$  to  $0.033 \pm 0.0016 \text{ g g}^{-1}$  sample, compared to that obtained for native starch

**Table 3.** Effect of oxidation time on functional properties of banana starch (*Musa paradisiaca* L. AAA group, cv. Cavendish).

Reaction time (min)	ISA (g soluble starch g <sup>-1</sup> sample)	PHi (g g <sup>-1</sup> )	IAA (g insoluble starch g <sup>-1</sup> sample)	CAA (%)	Gelling temperature (°C)
0	0.027±0.0011 <sup>a</sup>	2.07±0.0135 <sup>a</sup>	2.04±0.0142 <sup>a</sup>	103.2±2.0236 <sup>a</sup>	77.83±1.0408 <sup>a</sup>
40	0.031±0.0011 <sup>a</sup>	1.95±0.0141 <sup>b</sup>	1.92±0.0132 <sup>b</sup>	120.0±2.0216 <sup>b</sup>	71.5±0.5000 <sup>b</sup>
90	0.033±0.0016 <sup>b</sup>	1.89±0.0139 <sup>c</sup>	1.87±0.0141 <sup>c</sup>	124.3±2.8158 <sup>b</sup>	68.67±1.5275 <sup>b</sup>

ISA, water solubility index; IAA, water absorption index; PHi, swelling power; CAA, Oil absorption capacity. Mean ± standard error; n=3. Different letters in the same column indicate significant differences ( $P \leq 0.05$ ).

(0.027 g g<sup>-1</sup> sample). Olatunde et al. (2017) also obtained similar behavior in a study developed with bananas. According to Salcedo-Mendoza et al. (2018), ISA is related to the granule size and amylose content present in starch.

A contrary situation was observed for PHi and IAA values. As the reaction time increased, these values tended to decrease ( $P \leq 0.05$ ), compared to those of native starch. This could be due to the structural disintegration of the granules, which would cause a decrease in the amorphous region (Carhuallay et al. 2020), with a low capacity to retain water, decreasing its PHi and IAA, with an increase in solubility (Vanier et al. 2017).

Reaction time increased AAC, coinciding with that reported by De Barros et al. (2016). Among the factors related to this increase, is the presence of crystalline and amorphous regions that are affected by the oxidizing agent (Tovar-

Benítez et al. 2019). The native starch presented higher water and oil retention, but lower solubility because its structure remained intact.

Concerning the gelation temperature, the values obtained for native starch corresponded to those reported by Martínez et al. (2015). However, extending the reaction time decreased ( $P \leq 0.05$ ) the gelation temperature in oxidized starches. This was due to the early weakening and breaking of amylopectin double helix bonds and the introduction of negatively charged carbonyl and carboxyl groups, facilitating hydration, which would weaken the starch granule and cause it to gelatinize at a lower temperature (Carhuallay et al. 2020).

#### Influence of coatings on weight losses of cherry tomatoes

From the analysis of weight losses in cherry tomatoes for each of the treatments (Table 4), it was evidenced through

**Table 4.** Weight loss percentage of cherry tomatoes (*Solanum lycopersicum* cv. Cerasiforme) in each treatment.

Treatment	Glycerol (% m v <sup>-1</sup> )	Olive oil (% m v <sup>-1</sup> )	Weight loss (%)
1	3.5	0.4	9.32 (0.0141) <sup>a</sup>
2	3	0.4	10.97 (0.0282) <sup>b</sup>
3	3.5	0.3	9.32 (0.0141) <sup>a</sup>
4	3	0.3	7.50 (0.0708) <sup>c</sup>
5	3.5	0.3	9.81 (0.0138) <sup>d</sup>
6	3.5	0.4	9.33 (0.0141) <sup>a</sup>
7	3	0.4	10.24 (0.1414) <sup>e</sup>
8	3	0.3	7.73 (0.1555) <sup>f</sup>
9	3	0.3	7.87 (0.1414) <sup>f</sup>
10	3	0.4	10.65 (0.1555) <sup>h</sup>
11	3.5	0.4	9.41 (0.1535) <sup>a</sup>
12	3.5	0.3	9.69 (0.1272) <sup>d</sup>

Mean (Standard error); n=3. Different letters indicate significant differences ( $P \leq 0.05$ ).

the Pareto diagram (Figure 1A), that the percentage of olive oil and its interaction with the percentage of glycerol as components of the coating-forming emulsions, had an impact ( $P \leq 0.05$ ) on weight losses, evidencing a correct

functionality of the coating. Glycerol is a hydrophilic molecule that facilitates water vapor migration; fatty acids in the film matrix, on the other hand, impart hydrophobicity.

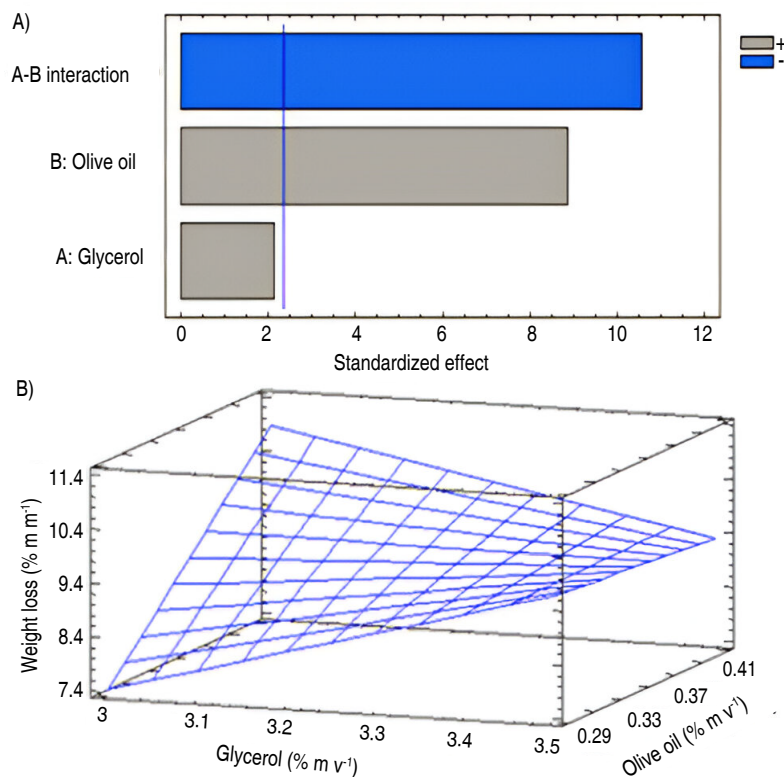


**Figure 1.** Influence of coatings based on banana oxidized starch and olive oil on weight losses of cherry tomatoes (*Solanum lycopersicum* cv. Cerasiforme): A) Pareto diagram; and B) estimated response surface.

The estimated response surface diagram (Figure 1B) shows the relationship between the factors studied and their combined effect on weight loss, in correspondence with the adjusted model that describes the behavior of this variable. Treatments with lower concentrations of olive oil ( $0.3\% \text{ m v}^{-1}$ ) generally exhibit slightly lower weight loss percentages compared to treatments with higher olive oil concentrations ( $0.4\% \text{ m v}^{-1}$ ), independently of the glycerol concentrations. This could be related to the influence of olive oil on the mechanical behavior of the coating, that is, the concentration of olive oil could affect its physical properties and increase the rate of weight loss during storage (Dovale-Rosabal et al. 2015). The variability in weight loss percentages across treatments indicates that factors other than olive oil concentration, such as glycerol concentration and other experimental

conditions, may also influence weight loss in cherry tomatoes.

The value of the coefficient of determination indicated that the adjusted model (Equation 10) was able to explain 96.52% of the variability in weight losses in coated cherry tomatoes, which allowed obtaining the best combination in the experimental region studied, for the formulation of a coating that would minimize weight losses during storage.

$$y = -69.6362 + 22.859 X_1 + 219.6 X_2 - 63.6487 X_1 X_2 \quad (10)$$

Where  $y$  is the weight loss;  $X_1$  is glycerol concentration; and  $X_2$  is olive oil concentration.

The olive oil concentration and its interaction with the glycerol concentration were significant ( $P \leq 0.05$ ). Thus,



it was obtained that for four oxidized starch coatings, it was necessary to add 0.3% (m v<sup>-1</sup>) olive oil and 3% (m v<sup>-1</sup>) glycerol. This formulation corresponded to the coating selected to evaluate its influence on the preservation of cherry tomatoes.

#### Influence of oxidized starch-based coatings on the preservation of cherry tomatoes

The pH and acidity values presented a characteristic behavior of the ripening of cherry tomatoes during storage

(Figure 2), without significant variations due to the coating. The increase in pH and decrease in acidity could be mainly due to the transformation of organic acids into sugars through cellular respiration (Hoyos-Yela et al. 2019), a process that consumes these acids and generates less acidic products, which could raise the pH of the fruit. Furthermore, water loss through transpiration and specific storage conditions, such as the use of the coating, can influence the enzymatic and metabolic activity of the product, facilitating the degradation of organic acids.

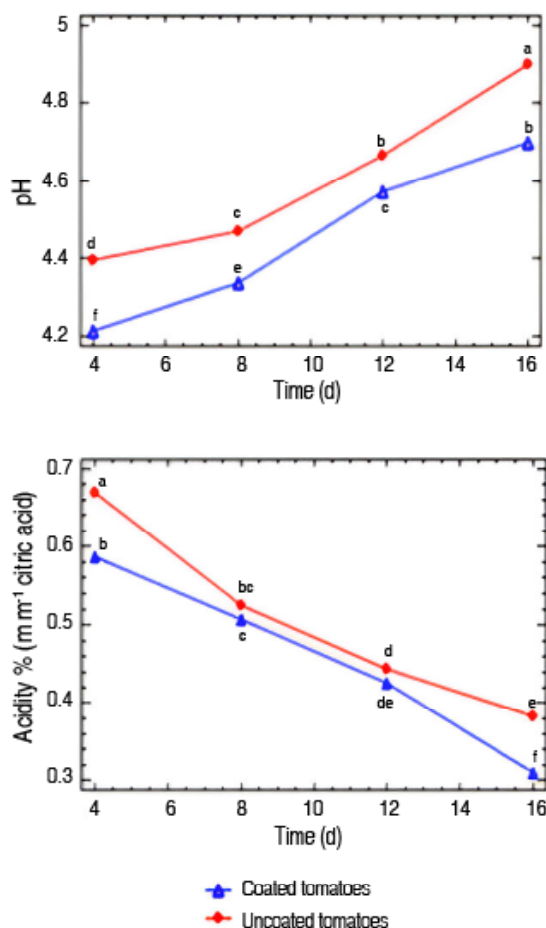


**Figure 2.** Evolution of pH and acidity in coated and uncoated cherry tomatoes (*Solanum lycopersicum* cv. Cerasiforme) during their storage at ambient conditions. Different letters indicate significant differences ( $P \leq 0.05$ ).

Figure 3 shows the gradual increase in soluble solids associated with the ripening process of cherry tomatoes with and without coating during storage. However, tomatoes with coating presented a lower rate of increase in soluble solids up to 12 days of storage, compared to tomatoes without coating, possibly due to the reduction in respiration and ethylene production

(Kumar and Saini 2021). The coatings form a physical barrier that limits the exchange of gases, including oxygen and carbon dioxide. This decreases the respiration rate of the tomatoes and slows down the ripening process and therefore the increase in soluble solids. Additionally, coatings, by reducing ethylene production, delay the conversion of starches to simple sugars,

one of the main causes of the increase in soluble solids in tomatoes during ripening.

The percentage of weight losses increased during storage (Figure 3); however, lower values were recorded for coated tomatoes. Osae et al. (2022) mentioned

that coatings act as a semi-permeable barrier against gas and moisture exchange, due to the hydrophobic character of the colloidal matrix, in this case, influenced by the addition of olive oil. Finally, it was evidenced that the coating reduced weight losses in cherry tomatoes by approximately 10%.

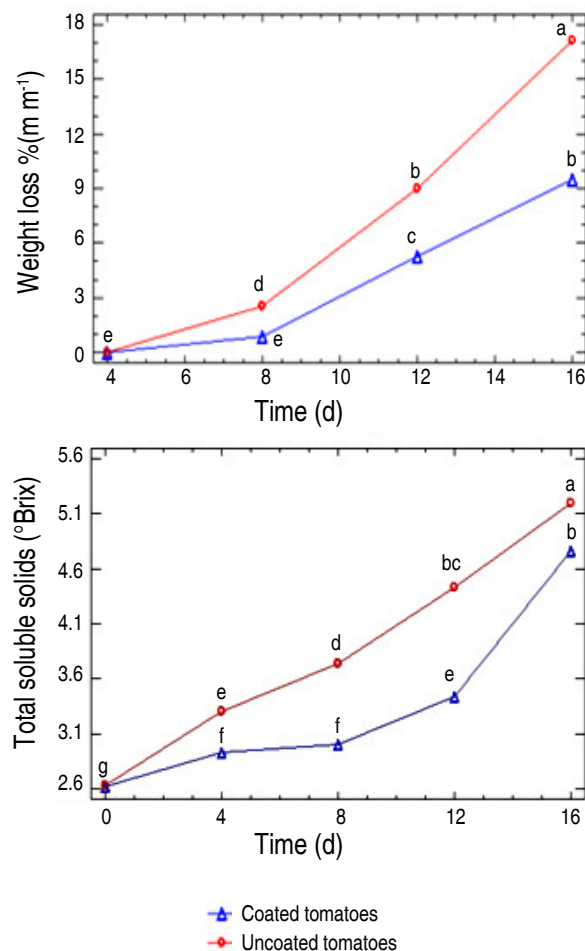


**Figure 3.** Evolution of weight loss and total soluble solids in coated and uncoated cherry tomatoes (*Solanum lycopersicum* cv. Cerasiforme) during their storage at ambient conditions. Different letters indicate significant differences ( $P \leq 0.05$ ).

## CONCLUSION

The research determined the best combination (4% m v<sup>-1</sup> oxidized starch coatings, 3% m v<sup>-1</sup> of glycerol, and 0.3% m v<sup>-1</sup> of olive oil), for the formulation for a coating based on oxidized banana starch and olive oil, offering valuable information on food preservation techniques. It demonstrated the potential of this coating to reduce weight loss and delay the ripening of cherry tomatoes during storage. By elucidating the effects of reaction

time on the properties of oxidized starch and identifying the best coating composition, the study contributes to the understanding of starch-based coatings for food preservation. The extraction yield of banana starch was 27.26% by the wet milling method. Lipid, crude fiber, protein, carbohydrate, and ash contents tended to decrease in oxidized starches as reaction time increased, the opposite behavior for moisture content ( $P \leq 0.05$ ). Solubility and oil absorption capacity increased in oxidized starches,

while water absorption and swelling power decreased ( $P \leq 0.05$ ). With the application of the coating, weight losses were reduced in cherry tomatoes stored for 16 days under ambient conditions, and lower soluble solids values were obtained, as an indicator of the delay in the ripening process. These results support sustainable food packaging solutions by utilizing natural materials such as banana starch and olive oil, potentially reducing reliance on synthetic additives. Additional research could explore the long-term effectiveness and scalability of the developed coating under storage conditions. Comparative studies with other preservation methods or coatings could provide information on the relative effectiveness and applicability of this technique.

## REFERENCES

- Al-Dairi M, Pathare P and Al-Yahyai R (2021) Chemical and nutritional quality changes of tomato during postharvest transportation and storage. *Journal of the Saudi Society of Agricultural Sciences* 20(6): 401-408. <https://doi.org/10.1016/j.jssas.2021.05.001>
- AOAC – Association of Official Analytical Chemists (2020) *Official Methods of Analysis*, Washington, D.C., EE.UU.
- Ashwar BA, Shah A, Gani A, Rather SA, Wani S Mohd et al (2014) Effect of gamma irradiation on the physicochemical properties of alkali-extracted rice starch. *Radiation Physics and Chemistry* 99: 37-44. <https://doi.org/10.1016/j.radphyschem.2014.02.002>
- Bonilla R, Hoyos L and Velasco R (2013) Efecto de oxidación de almidón de yuca sobre propiedades mecánicas y térmicas de películas biodegradables. *Biotecnología en el Sector Agropecuario y Agroindustrial* 11(1): 208-217. <https://revistas.unicauca.edu.co/index.php/biotecnologia/article/view/281/480>
- Carhuallay O, Cerna E, Polo J, Sandoval E and Salvador D (2020) Effect of sodium hypochlorite concentration and oxidation time on the degree of substitution of carboxyl groups, water absorption index and gelatinization temperature of Achira starch (*Canna edulis* Ker). *Agroindustrial Science* 10(2): 165-173. <http://doi.org/10.17268/agroind.sci.2020.02.07>
- Cedeño-Sares L, Díaz-Torres R, Casariego-Año A, Arias-Toro D and Yáñez-Romero M (2021) Efecto de la acetilación sobre propiedades físicas del almidón de banano (*Musa* spp. AAA subgrupo Cavendish). *Revista Cumbres* 7(1): 9-20.
- Correa D, Castaño M and Montoya J (2017) Influencia del método de extracción en las propiedades funcionales de almidón de plátano dominico hartón (*Musa paradisiaca* L.). *UGCiencia* 23: 88-91. <http://hdl.handle.net/11396/2254>
- De Barros C, Leonel M, Landi C, Leonel S, García E and Rodrigues T (2016) Characterization of banana starches obtained from cultivars grown in Brazil. *International Journal of Biological Macromolecules* 89: 632-639. <https://doi.org/10.1016/j.ijbiomac.2016.05.040>
- Dovale-Rosabal G, Casariego A, Forbes-Hernández TY and García MA (2015) Effect of chitosan-olive oil emulsion coating on quality of tomatoes during storage at ambient conditions. *Journal of Berry Research* 5(4): 207-218. <https://doi.org/10.3233/JBR-150103>
- El Halal SLM, Colussi R, Deon VG, Pinto VZ, Villanova FA et al (2015) Films based on oxidized starch and cellulose from barley. *Carbohydrate Polymers* 133: 644-653. <https://doi.org/10.1016/j.carbpol.2015.07.024>
- Fernández NM, Echeverría D, Mosquera S and Paz S (2017) Estado actual del uso de recubrimientos comestibles en frutas y hortalizas. *Biotecnología en el Sector Agropecuario y Agroindustrial* 15(2): 134-141. <http://www.scielo.org.co/pdf/bsaa/v15n2/v15n2a15.pdf>
- Fich EA, Fisher J, Zamir D and Rose JKC (2020) Transpiration from tomato fruit occurs primarily via trichome-associated transcuticular polar pores. *Plant Physiology* 184(4): 1840-1852. <https://doi.org/10.1104/pp.20.01105>
- Fitch-Vargas PR, Aguilar-Palazuelos E, Vega-García MO, Zazueta-Morales JJ et al (2019) Effect of a corn starch coating obtained by the combination of extrusion process and casting technique on the postharvest quality of tomato. *Revista Mexicana de Ingeniería Química* 18(3): 789-801. <https://doi.org/10.24275/uam/izt/dcbi/revmexingquim/2019v18n3/Fitch>
- Fonseca L, Gonçalves J, el Halal S, Pinto V et al (2015) Oxidation of potato starch with different sodium hypochlorite concentrations and its effect on biodegradable films. *LWT - Food Science and Technology* 60(2): 714-720. <https://doi.org/10.1016/j.lwt.2014.10.052>
- Helen A-O, Omotayo J, Olugbenga A and Timilehin O (2022) Physicochemical, functional, pasting properties and Fourier transform infrared spectroscopy of native and modified Cardaba banana (*Musa ABB*) starches. *Food Chemistry Advances* 1-36. <https://doi.org/10.1016/j.focha.2022.100076>
- Hidalgo J, Macas J, Pazmiño K and Chuiza M (2020) Obtención de almidón de plátano verde (*Musa paradisiaca* L.). En: *Book of Proceedings VII International congress application, transport and fluid storage in industrial process, hydrocarbons and environment. (VII ICATS 2020)*, Ecuador.
- Hoyos-Yela N, Pérez R, Mosquera S and Paz S (2019) Efecto de la aplicación de un recubrimiento de almidón de yuca modificado por vía ácida sobre el tomate larga vida. *Revista U.D.C.A Actualidad & Divulgación Científica* 22(2): 1-8. <https://doi.org/10.31910/rudca.v22.n2.2019.1388>
- Kumar A and Saini CS (2021) Edible composite bi-layer coating based on whey protein isolate, xanthan gum and clove oil for prolonging shelf life of tomatoes. *Measurement Food* 2: 100005. <https://doi.org/10.1016/j.meafoo.2021.100005>
- Lopes M, Roque MJ, Cavaleiro C and Ramos F (2021) Nutrient value of *Salicornia ramosissima* - A green extraction process for mineral analysis. *Journal of Food Composition and Analysis* 104: 104135. <https://doi.org/10.1016/j.jfca.2021.104135>
- Martínez O, Lapo B, Pérez J, Zambrano C and Maza F (2015) Mecanismo de gelatinización del almidón nativo de banano exportable del Ecuador. *Revista Colombiana de Química* 44(2): 16-21. <https://doi.org/10.15446/rev.colomb.quim.v44n2.55215>
- Mikó PP, Percze A, Kovács Á and Kende Z (2023) Effects of repeated replanting on yield, dry matter, starch, and protein content in different potato (*Solanum tuberosum* L.) genotypes. *Open Agriculture* 8(1): 20220246. <https://doi.org/10.1515/opag-2022-0246>
- NTE INEN 2801 (2013) Banano (Plátano). Instituto Ecuatoriano de Normalización. Ecuador.
- NTE INEN-ISO 1842 (2013) Productos vegetales y de frutas. Determinación de pH. Ecuador.
- Olatunde G, Arogundade L and Orija O (2017) Chemical, functional

and pasting properties of banana and plantain starches modified by pre-gelatinization, oxidation and acetylation. *Cogent Food and Agriculture* 3(1): 1-12. <https://doi.org/10.1080/23311932.2017.1283079>

Osae R, Apaliya M, Alolga R, Kwaw E, Otu P and Akaba S (2022) Influence of shea butter, bee wax and cassava starch coatings on enzyme inactivation, antioxidant properties, phenolic compounds and quality retention of tomato (*Solanum lycopersicum*) fruits. *Applied Food Research* 2(1): 1-6. <https://doi.org/10.1016/j.afres.2022.100041>

Pérez-Díaz F, Arévalo-Galarza ML, Pérez-Flores LJ, Lobato-Ortiz R and Ramírez-Guzmán ME et al (2020) Crecimiento y características postcosecha de frutos de genotipos nativos de tomate (*Solanum lycopersicum* L.). *Revista Fitotecnia Mexicana* 43(1): 89-99. <https://revistafitotecniamexicana.org/documentos/43-1/10a.pdf>

Ramos-García M, Romero C and Bautista S (2018) Almidón modificado: Propiedades y usos como recubrimientos comestibles para la conservación de frutas y hortalizas frescas. *Revista Iberoamericana de Tecnología Postcosecha* 19(1). <https://www.redalyc.org/articulo.oa?id=81355612003>

Saborío D (2021) Manual de manejo poscosecha del tomate fresco en Costa Rica (Comité Editorial INTA, Ed.; 1.a ed.). [http://www.platicar.go.cr/images/buscador/documents/pdf/2021/MANUAL%20POSCOSECHA\\_min\\_ed.pdf](http://www.platicar.go.cr/images/buscador/documents/pdf/2021/MANUAL%20POSCOSECHA_min_ed.pdf)

Salcedo-Mendoza J, García C and Salcedo D (2018) Propiedades funcionales de almidones de ñame (*Dioscorea alata*). *Biotechnología en el Sector Agropecuario y Agroindustrial* 16(2): 99-107. <http://scielo.org.co/pdf/bsaa/v16n2/1692-3561-bsaa-16-02-00099.pdf>

Salcedo-Mendoza J, Rodríguez M and Figueroa J (2016) Efecto de la acetilación en las propiedades estructurales y funcionales de almidones de yuca (*Manihot esculenta* Crantz) y ñame (*Dioscorea alata* cv. Diamante 22). *Revista Mexicana de Ingeniería Química* 15(3): 787-796. <http://www.redalyc.org/articulo.oa?id=62048168010>

Schmiele M, Sampaio UM and Pedrosa Silva Clerici MT (2019)

Chapter 1- Basic Principles. En *Starches for Food Application* (pp. 1-22). <https://doi.org/10.1016/B978-0-12-809440-2.00001-0>

Sumardiono S, Jos B, Pudjihastuti I, Yafiz A, Rachmasari M and Cahyono H (2021) Physicochemical properties of sago ozone oxidation: The effect of reaction time, acidity, and concentration of starch. *Foods* 10(6): 1-17. <https://doi.org/10.3390/2Foods10061309>

Tovar-Benítez T, Sánchez I, Porras J, Concepción N and Trejo I (2019) Aislamiento y caracterización parcial de un almidón a partir de semillas de girasol. *Revista de Ingeniería y Tecnologías Para El Desarrollo Sustentable* 5: 14-17. [http://reingtec.itsoeh.edu.mx/reingtec/docs/vol1\\_2019reingtec/Tovar\\_Beni%CC%81tez\\_2019\\_p14\\_17.pdf](http://reingtec.itsoeh.edu.mx/reingtec/docs/vol1_2019reingtec/Tovar_Beni%CC%81tez_2019_p14_17.pdf)

Ungureanu C, Tihan G, Zgârian R and, Pandelea G (2023) Bio-Coatings for Preservation of Fresh Fruits and Vegetables. *Coatings* 13(8): 2023:1420. <https://doi.org/10.3390/coatings13081420>

Vanier N, el Halal S, Dias A and da Rosa E (2017) Molecular structure, functionality and applications of oxidized starches: A review. *Food Chemistry* 221: 1546-1559. <https://doi.org/10.1016/j.foodchem.2016.10.138>

Zamudio-Flores PB, Ochoa-Reyes E, Ornelas-Paz J and Tirado-Gallegos J (2015) Caracterización fisicoquímica, mecánica y estructural de películas de almidones oxidados de avena y plátano adicionadas con betalainas. *Agrociencia* 49(5): 483-498. <https://www.scielo.org.mx/pdf/agro/v49n5/v49n5a2.pdf>

Zamudio-Flores PB, Torres AV, Salgado-Delgado R and Bello-Pérez LA (2010) Influence of the oxidation and acetylation of banana starch on the mechanical and water barrier properties of modified starch and modified starch/chitosan blend films. *Journal of Applied Polymer Science* 115(2): 991-998. <https://doi.org/10.1002/app.31047>

Zavareze EDR, Pinto VZ, Klein B, El Halal SLM, Elias MC et al (2012) Development of oxidised and heat-moisture treated potato starch film. *Food Chemistry* 132(1): 344-350. <https://doi.org/10.1016/j.foodchem.2011.10.090>

# Promoting food security and sustainability with a transportable indirect evaporative solar pre-cooler

Promoción de la seguridad alimentaria y la sostenibilidad con un preenfriador solar evaporativo indirecto transportable

<https://doi.org/10.15446/rfnam.v77n3.110667>

Nabil Shaban Mahmoud Elkaoud<sup>1\*</sup>, Ragab Kassem Mahmoud<sup>1</sup>, Hassan Hafiz Tarabye<sup>2</sup>  
and Mahmoud Saad Adam<sup>2</sup>

## ABSTRACT

### Keywords:

Food technology  
Pre-cooling  
Renewable energy  
Sustainability

Perhaps one of the most important goals of sustainable development for developing countries is to enhance the utilization of renewable energy sources in all sectors in general and the agricultural sector in particular. The pre-cooling process helps to maintain quality and extend the shelf life of the fruits and vegetables. The aim of this study was to fabricate an indirect evaporative solar pre-cooler (IESP) to reduce post-harvest loss for agricultural products. Tomato crop was chosen to be pre-cooled as an example of agricultural value chains. Experimental variables included three temperatures of cooling water (15, 10 and 5 °C) and two air velocities that passed through the cooling cabinet (1.5 and 2.5 m s<sup>-1</sup>). The results showed that at 1.5 m s<sup>-1</sup> air velocity, the actual coefficient of performance was 19.4, 25.5 and 34.7% at cooling water temperatures 15, 10 and 5 °C, respectively. At 2.5 m s<sup>-1</sup> air velocity, the actual coefficient of performance was 23.1, 28.8 and 37.2% at cooling water temperatures 15, 10 and 5 °C, respectively. The performance of the IESP under these conditions was 15.4 °C, 91.5% RH, 0.338 TR refrigeration load and 37.2% COP<sub>sys</sub>. Total energy consumption was 6.4 kWh day<sup>-1</sup>. The solar pre-cooler performance proved a very feasible solution to the demands of small and medium horticultural holdings, especially in cities with a very hot climate to keep vegetables and fruits from deteriorating after harvest.



## RESUMEN

### Palabras clave:

Tecnología de los alimentos  
Pre-enfriamiento  
Energía renovable  
Sostenibilidad

Quizás uno de los objetivos más importantes del desarrollo sostenible para los países en desarrollo es mejorar la utilización de fuentes de energía renovables en todos los sectores en general y en el sector agrícola en particular. El proceso de pre-enfriamiento ayuda a mantener la calidad y prolongar la vida útil de las frutas y verduras. Este estudio tuvo como objetivo fabricar un preenfriador solar evaporativo indirecto (IESP) para reducir las pérdidas posteriores a la cosecha de productos agrícolas. El cultivo de tomate fue elegido para ser preenfriado como ejemplo de cadenas de valor agrícolas. Las variables experimentales incluyeron tres temperaturas del agua de enfriamiento (15, 10 y 5 °C) y dos velocidades del aire que pasó por el gabinete de enfriamiento (1,5 y 2,5 m s<sup>-1</sup>). Los resultados mostraron que a una velocidad del aire de 1,5 m s<sup>-1</sup>, el coeficiente de rendimiento real fue de 19,4, 25,5 y 34,7% a temperaturas del agua de refrigeración de 15, 10 y 5 °C, respectivamente. A una velocidad del aire de 2,5 m s<sup>-1</sup>, el coeficiente de rendimiento real fue de 23,1, 28,8 y 37,2% a temperaturas del agua de refrigeración de 15, 10 y 5 °C, respectivamente. El desempeño del IESP bajo estas condiciones fue de 15,4 °C, 91,5% HR, 0,338 TR carga frigorífica y 37,2% COP<sub>sys</sub>. El consumo total de energía fue de 6,4 kWh día<sup>-1</sup>. El rendimiento del preenfriador solar resultó ser una solución muy viable para las demandas de las pequeñas y medianas explotaciones hortícolas, especialmente en ciudades con un clima muy cálido, para evitar que las verduras y frutas se deterioren después de la cosecha.

<sup>1</sup>Al-Azhar University, Faculty of Agricultural Engineering, Assiut, Egypt. [nabilelkaoud.50@azhar.edu.eg](mailto:nabilelkaoud.50@azhar.edu.eg) , [RagabKassem.50@azhar.edu.eg](mailto:RagabKassem.50@azhar.edu.eg) 

<sup>2</sup>Aswan University, Faculty of Agriculture and natural resources, Department of Agricultural and Bio-systems Engineering, Aswan, Egypt. [tarabye@agr.aswu.edu.eg](mailto:tarabye@agr.aswu.edu.eg) , [adam123@agr.aswu.edu.eg](mailto:adam123@agr.aswu.edu.eg) 

\*Corresponding author



Egypt is the Middle East and North Africa region's most populous country with over 92 million people and a projected 120 million by 2050 (FAO 2019). Rapid population growth, along with limited freshwater resources and arable land, is placing greater stress on Egypt's rural and urban food systems in terms of quantity and terms of changing food preferences towards high-value, more perishable fruits, and vegetables. While food needs are growing, Food Loss and Waste (FLW) in Egypt is high, especially for perishable products. Across the region, fruit and vegetable FLW is estimated to reach 45-55% of production annually (FAO 2019). Baseline data estimates for quantitative loss of over 45-50% over grapes and tomatoes, respectively, in the production, retail, and wholesale stages of the value chain alone, along with a serious loss of quality (Gustavsson et al. 2013). The pre-cooling process (Removing field heat) is considered one of the most important post-harvest processes that directly affect the quality and production. Pre-cooling reduces microbial activity, respiration rates, and vital heat. This process reduces water loss and decomposition; thus, it helps to maintain quality and extend the shelf life of the fruits (Elkaoud et al. 2024). The energy consumption for air-conditioning systems has recently been estimated to be 45% of households and commercial buildings. Moreover, the propagation of air-conditioning appliances reinforces peak electricity demand during summer. So, the consumption of electricity is a big problem for vapor compression refrigeration systems (Choudhury et al. 2013). Sorensen (2004) mentioned that in Egypt, the amount of incident solar radiation per square meter ranges between 5.0 and 8.0 kWh per day with about 3,500 sunshine hours per year. Solar energy has incredible potential to power our daily lives. The reduction in temperatures has the added advantage of decreasing the production and sensitivity of the produce to ethylene which accelerates ripening and senescence. Therefore, the quicker and more promptly the field heats, after harvest temperature is reduced, the faster these decay processes are restarted and hence the more of the initial quality can be maintained. However, with the increase the production of ethylene, enzymatic activity and higher respiration rate during ripening causes cell wall weakening and firmness loss (Senthilkumar et al. 2015). The pre-cooling system needs to consider the optimal temperature range for each fruit variety to prevent damage. Fresh fruits and vegetables need low temperatures (0 to 12.7 °C) and high relative humidities

(80 to 95%) to lower respiration and to slow metabolic and transpiration rates. By slowing these processes, water loss is reduced, and food value, quality, and energy reserves are maintained (Banerjee et al. 2021). Delay in pre-cooling of the product can cause a necessary loss of quality because field temperature can be up to 30 °C (Talbot and Chau 2002). For example, every 1-h delay in pre-cooling strawberries harvested at 54 °C will raise 10% low in shelf life (Brosnan and Sun 2001). Removing field heat from agricultural products could double shelf life (Lipinski et al. 2013). Sood and Kumari (2023) found that post-harvest losses of fruits occur due to a lack of proper techniques for harvesting, transportation, storage, and distribution. The freshness of fruits after harvest is controlled by water content, respiratory rate, ethylene production, endogenous plant hormones, and external factors such as microbial growth, temperature, relative humidity, and atmospheric compositions. Therefore, post-harvest loss of fruits can be considerably reduced and their shelf life increased by careful manipulation of these factors. Fruits can also benefit from controlled environment storage and regularization at low temperatures.

Elkaoud and Mahmoud (2022) are interested in the post-harvest operations of fruits in Egypt, especially small farms, they indicated that the total area under fruit cultivation in Egypt is about 700,854 hectares (7,008.54 million square meters). The post-harvest storage of perishable agricultural products is important to reduce the gap between demand and supply. Cold storage technologies are not popular in rural and remote areas due to the higher initial cost and the electrical energy requirement. Therefore, some low-cost technologies have been developed and, among these technologies, the evaporative cooling technology is gaining in popularity due to its simple design and lower initial cost (Kapilan and Patil 2023). Stand-alone cooling systems for the storage of perishables are needed in regions of the world lacking reliable electricity and the financial wherewithal to make sufficient investments in on-grid cold stores. To meet this need, an off-grid, batteryless solar refrigerated and evaporative cooled (SREC) was structured so that it can be self-built by smallholder farmers. Several innovative features have been incorporated including a "water battery" (a thermal reservoir) to provide nighttime cooling, a dual-use refrigeration coil to cool the thermal reservoir and interior air simultaneously, and a solar

adaptive controller to regulate power demand by refrigeration compressor based on available solar energy (Chopra et al. 2023). Vala (2022) reported that there are two principal methods of evaporative cooling: direct cooling and indirect cooling. Direct and indirect processes can also be combined. In the direct method of evaporative cooling outside unsaturated air is allowed to pass through a wet pad, due to evaporation of water air gets cooled and humidified. Whereas, in indirect method of evaporative cooling air is cooled as it flows outside the tubes of the heat exchanger in which cold water circulates. The combination of these two systems has obtained significantly enhanced cooling performance, with nearly 90% and a high energy efficiency ratio of up to 80. This system is energy efficient, environment friendly and having potential for cooling and storage of fruits and vegetables in countries where hot and dry weather prevails for most of the part. Sibanda and Workneh (2020) developed an indirect air-cooling combined with evaporative cooling (IAC + EC) system for temporary storage of fruit and vegetables (FV) to improve the shelf life of fresh produce under hot and humid climatic conditions. The study aimed to investigate the effect of IAC + EC in providing an optimum storage environment of temperature and relative humidity (RH) for the tomato fruit compared to storage under ambient conditions. The cooler efficiency varied from 88.04 to 95.6%. The results in this study are evidence that IAC + EC system can provide optimum storage conditions for FV as well as being a low-cost technology utilizable in hot and sub-humid to humid areas in sub-Saharan Africa. Accordingly, this study aimed to fabricate an indirect evaporative solar pre-cooler to reduce the post-harvest

loss for agricultural products and to enhance food security and sustainability.

## MATERIALS AND METHODS

The indirect evaporative solar pre-cooler (IESP) has been fabricated and tested under an hourly solar intensity of 7 kWh m<sup>-2</sup> per day or maximum solar intensity for a solar declination angle of 45°. All the experiments were carried out during October and November 2022 A.D.

### Agricultural product

Tomato is one of the most important horticultural crops. So, the tomato crop was chosen to be pre-cooled as an example of agricultural value chains. Fresh tomato fruits (*F1 commercial hybrid*) were obtained from a farm close to the test location on the same day of the harvest. The sample was collected in cages made of palm trees. Harvesting of the tomatoes was done before 10 o'clock in the morning. The field temperature was 27.5 °C. Fresh tomato fruits were immediately loaded in a car and transported to the test location. The sample was sorted manually and infected fruits that had mechanical damage were excluded. A sample of 50 kg was selected, packed, and kept under ambient conditions until the start of the experiment on the same day at 13:00 o'clock in the afternoon. The ambient temperature was 30.66 °C.

### Description of the indirect evaporative solar pre-cooler (IESP)

Figure 1 shows a a photograph of IESP during the experiments. IESP is fabricated from two solar photovoltaic panels (2×1 m, 550 W) connected in parallel as the power source.



**Figure 1.** The indirect evaporative solar pre-cooler (IESP) experimental setup.

A charge controller (MPPT) of 30 Amps was used to supply IESP with the optimum voltage and current. To store the electrical energy generated by the panels, two batteries (200 Ah, 12 v) were used to operate the IESP at night. An inverter (1.5 kW, 170 ~ 280 V) was used to power the pump and suction fan. A compressor (750 W) was utilized to generate a refrigerating effect in the refrigerator that also included a condenser, an expansion valve, an evaporator and a tank cooler. The pre-cooling cycle consisted of a buffer tank (100 L), a pump (19 W, 14 L min<sup>-1</sup>), a cooling cabinet (1,400×600×600 mm), a cooling coil (34 pipes with 160 fins), and a suction fan (12 m<sup>3</sup> min<sup>-1</sup>).

### Essential parts of the IESP

The IESP consists of a solar energy system (Power source), refrigerator, and pre-cooling cycle.

### Solar energy system (power source)

The power source included two photovoltaic panels, a solar charge controller, a battery, an inverter, and a control system. The panels were connected in parallel. For solar arrays to produce maximum power output, they must be at an optimal tilt angle to trap maximum radiation (Tripathy et al. 2017). According to Morales and Busch (2010), the optimum tilt angle correlates with latitude and is considered equal to the latitude or latitude ±15° (+ for winter and – for summer). This system is designed to operate all year round, so the tilt angle is set to be 30° to correspond to the latitude of the test location.

### Control system

This system is programmed to control the operation of the effective devices (Pump + Compressor) of IESP according to the temperature of either the buffer tank water or the cooling cabinet. The electronic system controls the operation of the hydraulic cycle of the pre-cooling mechanism. It consisted of an Arduino Uno R3, a waterproof temperature sensor, and a relay.

### The buffer tank

The buffer tank is considered one of the most important parts of the cooling system. It contains the refrigerant fluid that is cooled directly by the evaporator (The evaporator of the refrigeration cycle that operates with Freon). The tank is made of a thick material to resist rust and low coefficient of thermal conductivity so as not to lose the heat stored in the fluid. It is isolated from the outside by a

layer of glass wool with a thickness of 40 mm to maintain the temperatures inside the tank. The tank capacity was 100 L. The process of transferring the cooling water from the tank to the cooling coil is done by a pump. The water returns to the tank to equalize the degree of the cooling medium in the tank that (operates inside the direct cooling circuit).

### The cooling cabinet

The size of the cooling cabinet was chosen to accommodate 50 kg of tomatoes to carry out the experiments. However, it is possible to re-size the room to suit commercial purposes. The dimensions of the cabinet were 1,400×600×600 mm. The side walls and bottom of the cooling cabinet were insulated by two insulating materials, namely a carbon steel layer 2 mm thick and glass wool 50 mm thick.

### Experimental setup

The water flow rate was chosen at a limit that does not give temperatures less than required for pre-cooling. All experiments were carried out using a 6 L min<sup>-1</sup> water flow rate of cooling water that passes through the cooling coil. The time for each experiment was 4 h and temperature and humidity were recorded every 20 min. The initial temperature of the cabinet was 24 °C. As for the humidity, it was monitored after placing tomatoes in the cabinet. Variables of experiments are as follows: I) The temperature of the cooling water: Experiments were carried out using three temperatures of cooling water 15, 10 and 5 °C. II) Air velocity: IESP was tested under two air velocities that passed through cooling cabinets 1.5 and 2.5 m s<sup>-1</sup>.

### Measurements

#### Refrigeration load and Heat of respiration

The heat of respiration was calculated according to (Ashrae 2002) by the following Equation (1):

$$Q_{res.} = m \times h \times \frac{1}{3,600 \times n} \quad (1)$$

Where “Qres” is the Heat of respiration (W), “m” is the mass of tomatoes to be cooled (kg), “h” is the rate of respiration (J·kg<sup>-1</sup>), and “n” is the operation time (hours).

### Field heat

According to Sibanda (2019), field heat is the heat removed from freshly harvested tomatoes by introducing them into the cold store by reducing the field temperature

of the tomatoes to the desired storage temperature. Field heat in the case of this study, therefore, is the amount of heat removed from the tomatoes as they cool from initial harvest temperature to pre-cooling temperature. The mass of the tomatoes is 50 kg, and the operating time is assumed at 4 h. The specific heat of tomatoes is  $3.985 \text{ kJ} \cdot (\text{kg } ^\circ\text{C})^{-1}$ , according to Fellows (2000). The field heat calculated from the Equation (2):

$$Q_{fh} = \frac{m \times c_p (T_2 - T_1)}{3,600 \times n} \quad (2)$$

Where “ $Q_{fh}$ ” is the field heat (kW), “ $m$ ” is the mass of tomatoes to be cooled (kg), “ $C_p$ ” is the specific heat of tomatoes ( $\text{kJ} \cdot (\text{kg } ^\circ\text{C})^{-1}$ ), “ $T_2$ ” is the pre-cooling temperature ( $^\circ\text{C}$ ) of tomatoes and “ $T_1$ ” is the initial tomatoes in crates temperature ( $^\circ\text{C}$ ).

### Heat leakages

There is heat transfer because of leakages between the outside air and inside air through the walls and the roof as a result of the temperature gradient between the outside and inside temperature and is computed according to Ashrae (2002) by the following Equation (3):

$$Q_L = U_f \times A_f \times (T_a - T_c) \quad (3)$$

Where “ $Q_L$ ” is the heat leakages (W), “ $U_f$ ” is the overall heat coefficient =  $0.936 \text{ W} \cdot \text{m}^{-2} \cdot ^\circ\text{C}^{-1}$ , “ $A_f$ ” is the surface area of the cooling cabinet ( $4.08 \text{ m}^2$ ), “ $T_a$ ” is the ambient

temperature ( $^\circ\text{C}$ ) and “ $T_c$ ” is the temperature of material inside the refrigerator ( $^\circ\text{C}$ ). So, the refrigeration load was estimated by the following Equation (4):

$$\text{Refrigeration load} = (\text{Heat of respiration} + \text{Field heat} + \text{Heat leakages}) \times 1.1 \quad (4)$$

Where “1.1” is to compensate for the heat losses that may result from the frequent opening of the cooling cabinet door correspond to Thompson (2004).

### Actual coefficient of performance

The solar refrigerator’s efficiency is measured as the cooling capacity of solar energy absorbed by the solar collector (Mansoori and Patel 1979), following Equation (5):

$$(\text{COP}_{\text{cyc}})_{\text{actual}} = \frac{Q_{\text{Ref load}}}{P_{\text{Total}}} \quad (5)$$

Where  $P_{\text{Total}}$  is the total energy consumption (Refrigerator + Pump + Suction fan).

## RESULTS AND DISCUSSION

### Cooling cabinet temperature and humidity

#### At $1.5 \text{ m s}^{-1}$ air velocity:

It is noticeable that the cabinet temperature decreased by decreasing the cooling water temperature from 15 to  $5^\circ\text{C}$  at the same time, the cabinet humidity increased by decreasing the cooling water temperature as well. Figure 2 shows the effect of operating duration on temperature and humidity using  $15^\circ\text{C}$  cooling water temperature.

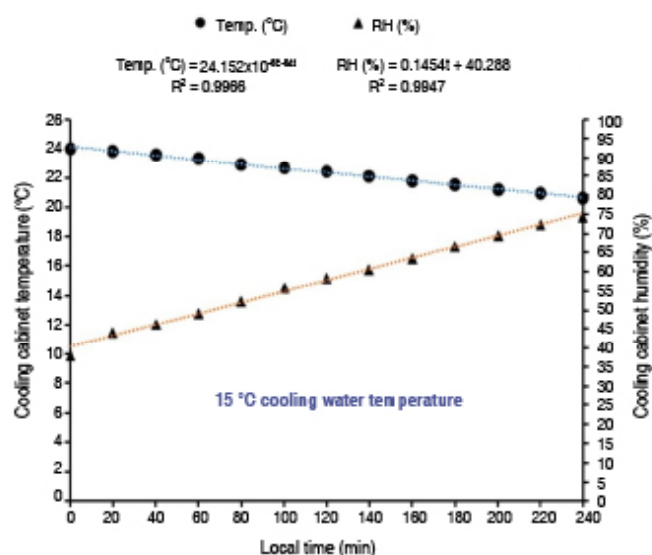


Figure 2. Effect of operating duration on temperature and humidity using  $15^\circ\text{C}$  cooling water temperature.

These results indicated that the cooling cabinet temperature dropped from 24 to 20 °C while the humidity (RH) inside the cooling cabinet increased from 38.72 to 75.3% during 4 h of operation using 15 °C cooling water temperatures. Under the same experimental conditions, the temperature and humidity can be estimated from the following Equations (6) and (7):

$$\text{Cabinet temperature (}^{\circ}\text{C)} = 24.152 \times 10^{-6} E^{-0.04t} \quad (6)$$

$$\text{Cabinet humidity (\%)} = 0.1454t + 40.288 \quad (7)$$

These relationships indicate that it is possible to calculate the temperature and relative humidity (RH) inside the cabinet by knowing time (t) and the coefficient of correlation is very high and closer to 1 ( $R^2=0.99$ ). So, the correlation between temperature and relative humidity and between the local time is a positive strong correlation as shown in Figure (2).

Figure 3 shows the effect of operating duration on temperature and humidity using 10 °C cooling water temperature.

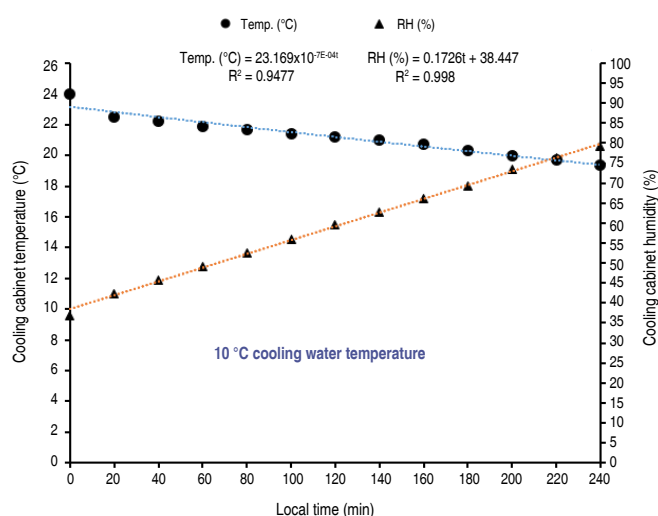


**Figure 3.** Effect of operating duration on temperature and humidity using 10 °C cooling water temperature.

The results showed that the cooling cabinet temperature dropped from 24 to 18.3 °C while the humidity inside the cooling cabinet increased from 37.52 to 81.2% during 4 h of operation with load using 10 °C cooling water temperatures. Under the same experimental conditions, the temperature and humidity can be estimated from the following Equations (8) and (9):

$$\text{Cabinet temperature (}^{\circ}\text{C)} = 22.788 \times 10^{-1} E^{-0.03t} \quad (8)$$

$$\text{Cabinet humidity (\%)} = 0.1754 + 39.256 \quad (9)$$

These relationships also indicate that it is possible to calculate the temperature and relative humidity (RH) inside the cabinet by knowing time (t) and the coefficient of correlation is very high and closer to 1 ( $R^2=0.9$ ).

Figure 4 shows the effect of operating duration on temperature and humidity using 5 °C cooling water temperature.

These results indicated that the cooling cabinet temperature dropped from 24 to 16.1 °C while the humidity inside the cooling cabinet increased from 39.9 to 89.8% during 4 h of operation with load using 5 °C cooling water temperatures. Under the same experimental conditions, the temperature and humidity can be estimated from the following Equations (10) and (11):

$$\text{Cabinet temperature (}^{\circ}\text{C)} = 21.205 \times 10^{-0.001t} \quad (10)$$

$$\text{Cabinet humidity (\%)} = 0.2118t + 41.481 \quad (11)$$



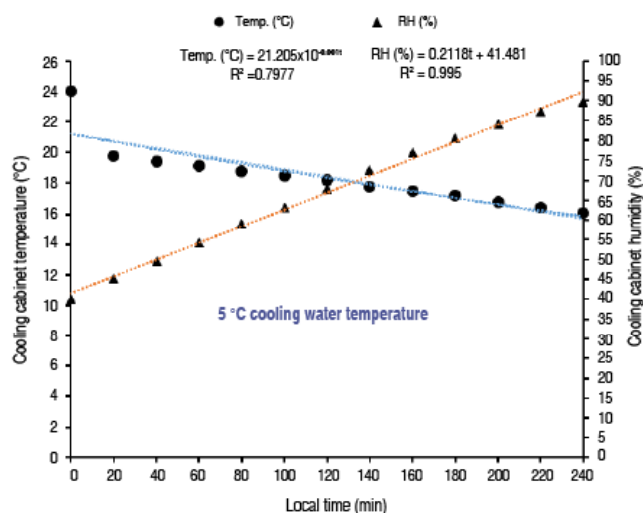


**Figure 4.** Effect of operating duration on temperature and humidity using 5 °C cooling water temperature.

#### At 2.5 m s<sup>-1</sup> air velocity:

Figure 5 shows the effect of operating duration on temperature and humidity using 15 °C cooling water temperature.

during 4 h of operation with a load using 15 °C cooling water temperatures. Under the same experimental conditions, the temperature and humidity can be estimated from the following Equations (12) and (13):

These results indicated that the cooling cabinet temperature dropped from 24 to 20 °C while the humidity inside the cooling cabinet increased from 38.72 to 75.3%

$$\text{Cabinet temperature (}^{\circ}\text{C)} = 23.816 \times 10^{-7} E^{-0.4t} \quad (12)$$

$$\text{Cabinet humidity (\%)} = 0.1477t + 40.975 \quad (13)$$

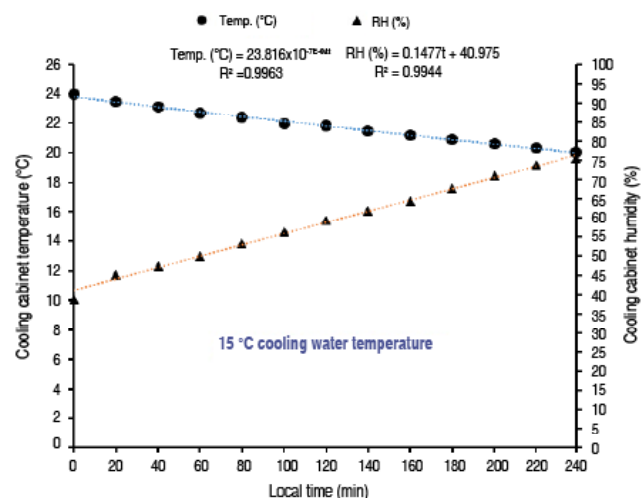


**Figure 5.** Effect of operating duration on temperature and humidity using 15 °C cooling water temperature.

These relationships also indicate that it is possible to calculate the temperature and relative humidity (RH) inside the cabinet by knowing time (t) and the coefficient of correlation is very high and closer to 1

( $R^2=0.99$ ). So, the correlation between temperature and relative humidity and between the local time is a positive strong correlation as shown in Figure (5).

Figure 6 shows the effect of operating duration on temperature and humidity using 10 °C cooling water temperature.

These results indicated that the cooling cabinet temperature dropped from 24 to 18.3 °C while the humidity inside the cooling cabinet increased from 37.52 to 81.2% during

4 h of operation with load using 10 °C cooling water temperatures. Under the same experimental conditions, the temperature and humidity can be estimated from the following Equations (14) and (15):

$$\text{Cabinet temperature (}^{\circ}\text{C)} = 22.788 \times 10^{-1E-03t} \quad (14)$$

$$\text{Cabinet humidity (\%)} = 0.1754t + 39.256 \quad (15)$$

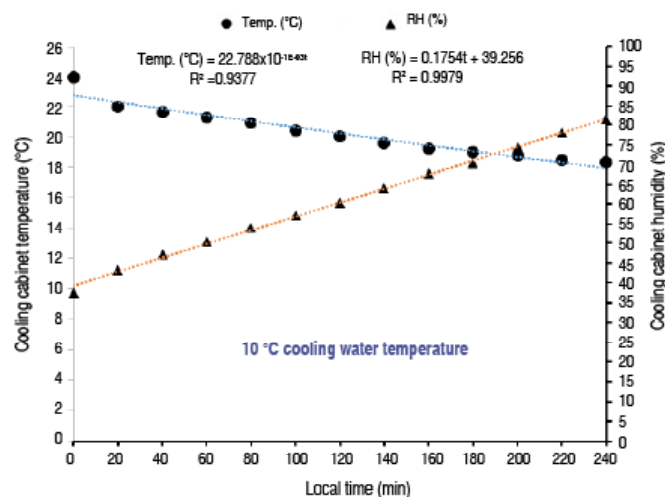


Figure 6. Effect of operating duration on temperature and humidity using 10 °C cooling water temperature.

Figure 7 shows the effect of operating duration on temperature and humidity using 5 °C cooling water temperature. These results indicated that the cooling cabinet temperature dropped from 24 to 15.4 °C while the humidity inside the cooling cabinet increased from 40 to 91.5% during 4 h of operation with load using 5 °C cooling water temperatures.

Under the same experimental conditions, the temperature and humidity can be estimated from the following Equations (16) and (17):

$$\text{Cabinet temperature (}^{\circ}\text{C)} = 20.9 \times 10^{-0.001t} \quad (16)$$

$$\text{Cabinet humidity (\%)} = 0.2162t + 41.851 \quad (17)$$

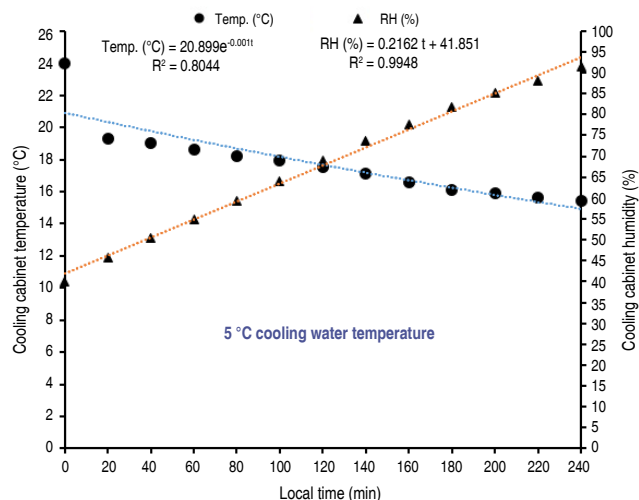


Figure 7. Effect of operating duration on temperature and humidity using 5 °C cooling water temperature.

From the results, it was found that the lowest temperature was 15.4 °C at the same time the highest relative humidity was 91.5% at 5 °C cooling water temperature.

From the previous results, it is notable that 5 °C cooling water temperature is considered optimal as it achieved the lowest temperature (16.1 and 15.4 °C) and, at the same time, it achieved the highest humidity (89.8 and 91.5%) of the cooling cabinet during 4 h of operation with load at air velocity 1.5 and 2.5 m s<sup>-1</sup>, respectively. These climatic conditions are suitable for the

pre-cooling process and correspond to the recommended temperature and humidity for tomato storage (From 12 to 15 °C and RH>85%), according to Beckles (2012).

#### Refrigeration load

#### Heat of respiration

According to Suslow and Cantwell (2009), the respiration rates of tomatoes change with the change in storage temperatures, so the respiration heat was calculated according to Table 1.

**Table 1.** Respiration heat using the recorded temperatures under the experimental variables.

Experimental variables		Pre-cooling temperature of tomatoes (°C)	Respiration rates* (J·kg <sup>-1</sup> )	Heat of respiration (kW)
Air velocities (m s <sup>-1</sup> )	Cooling water temperatures (°C)			
1.5	15	20.6	450	0.00160
	10	19.4	406	0.00141
	5	16.1	342	0.00120
2.5	15	20.0	427	0.00150
	10	18.3	384	0.00133
	5	15.4	320	0.00111

\*(Suslow and Cantwell 2009).

#### Field heat

Field heat was calculated using the recorded temperatures

under the variables of the experiments, as shown in Table 2.

**Table 2.** Field heat using the recorded temperatures under the experimental variables.

Experimental variables		(T <sub>2</sub> ) Pre-cooling temperature of tomatoes (°C)	(T <sub>1</sub> ) Initial tomatoes in crates temperature (°C)	The field heat (kW)
Air velocities (m s <sup>-1</sup> )	Cooling water temperatures (°C)			
1.5	15	20.6	28.50	0.110
	10	19.4	30.77	0.141
	5	16.1	30.35	0.197
2.5	15	20.0	29.47	0.131
	10	18.3	30.03	0.162
	5	15.4	30.66	0.211

#### Heat leakage

The heat leakage was calculated using the recorded

temperatures under the experimental variables as shown in Table 3.

**Table 3.** Heat leakage using the recorded temperatures under the experimental variables.

Experimental variables		(T <sub>2</sub> ) Pre-cooling temperature of tomatoes (°C)	(T <sub>1</sub> ) Initial tomatoes in crates temperature (°C)	The heat leakage (kW)
Air velocities (m s <sup>-1</sup> )	Cooling water temperatures (°C)			
1.5	15	20.6	28.50	0.030
	10	19.4	30.77	0.043
	5	16.1	30.35	0.054
2.5	15	20.0	29.47	0.036
	10	18.3	30.03	0.045
	5	15.4	30.66	0.058

From the previous results, the refrigeration load was calculated by the following Equation (18), as shown in Table 4.

$$\text{Refrigeration load} = (\text{Heat of respiration} + \text{Field heat} + \text{Heat leakages}) \times 1.1) \times 4 \text{ operation time} \quad (18)$$

**Table 4.** The refrigeration load under the experimental variables.

Experimental variables					The refrigeration load	
Air velocities (m s <sup>-1</sup> )	Cooling water temperatures (°C)	Heat of respiration (kW)	Field heat (kW)	The heat leakage (kW)	(kW)	(Ton R.)
1.5	15	0.00160	0.110	0.030	0.620	0.176
	10	0.00141	0.141	0.043	0.815	0.232
	5	0.00120	0.197	0.054	1.110	0.316
2.5	15	0.00150	0.131	0.036	0.740	0.210
	10	0.00133	0.162	0.045	0.920	0.260
	5	0.00111	0.211	0.058	1.190	0.338

#### Effect of Air velocity and cooling water temperatures on refrigeration load

The results indicated that the refrigeration load increased by decreasing the water temperature from 15 to 5 °C; it also, increased by increasing air velocity from 1.5 to 2.5 m s<sup>-1</sup>. At 1.5 m s<sup>-1</sup> air velocity, the refrigeration load was 0.176, 0.232, and 0.316 TR at cooling water temperatures of 15, 10, and 5 °C, respectively. At 2.5 m s<sup>-1</sup> air velocity, the refrigeration load were 0.21, 0.26, and 0.338 TR at cooling water temperatures 15, 10, and 5 °C, respectively.

#### Actual coefficient of performance (COP<sub>cyc</sub>)

A summary of the refrigeration load and the actual coefficient of performance under the experimental variables is shown in Table 5.

#### Effect of air velocity and cooling water temperatures on COP<sub>cyc</sub>

The actual coefficient of performance increased by decreasing the water temperature from 15 to 5 °C and also, increased by increasing air velocity from 1.5 to 2.5 m s<sup>-1</sup>.

At 1.5 m s<sup>-1</sup> air velocity, the actual coefficient of performance were 19.4, 25.5, and 34.7% at cooling water temperatures 15, 10, and 5 °C, respectively. At 2.5 m s<sup>-1</sup> air velocity, the actual coefficient of performance was 23.1, 28.8 and 37.2% at cooling water temperatures 15, 10, and 5 °C, respectively. The use of 5 °C cooling water temperature has achieved the highest COP<sub>cyc</sub> at 1.5 and 2.5 m s<sup>-1</sup> air velocities.

**Table 5.** A summary of the refrigeration load and the actual coefficient of performance under the experimental variables.

Experimental variables			The refrigeration load		
Air velocities (m s <sup>-1</sup> )	Cooling water temperatures (°C)	Total energy consumption (kW)	(kW)	(Ton R.)	COP <sub>sys</sub> (%)
1.5	15	3.2	0.620	0.176	19.4
	10		0.815	0.232	25.5
	5		1.110	0.316	34.7
2.5	15		0.740	0.210	23.1
	10		0.920	0.260	28.8
	5		1.190	0.338	37.2

## CONCLUSION

To achieve sustainable development of the agricultural sector, renewable energy should be relied upon to operate electrical energy-consuming systems, especially in developing countries. In this study, an IESP was successfully fabricated and tested to promote food security. It is completely powered by solar energy and is compact in size and transportable. The IESP performance proved a very feasible solution to the demands of small and medium horticultural holdings. From the experimental results, it can be observed that 5 °C cooling water temperature is considered optimal as it achieved the lowest temperature and at the same time it achieved the highest humidity. Based on the findings of this study, these climatic conditions are suitable for the pre-cooling process and correspond to the recommended temperature and humidity for tomato storage. So, the pre-cooling process is considered one of the most important techniques for handling horticultural crops to reduce post-harvest losses. However, choosing the appropriate pre-cooling technology is crucial to ensuring economical operation and sustainability.

## REFERENCES

- Ashrae Handbook (2002) Ashrae transactions. Atlanta: American Society of Heating, Refrigerating and Air-Conditioning Engineers, Inc.
- Banerjee S, Halder S, Skanda Kumar BN and Jayeeta Mitra (2021) Chapter 8 - Storage of fruits and vegetables: an overview. Packaging and storage of fruits and vegetables. 1<sup>st</sup> edition, New York, 157-181. <https://doi.org/10.1201/9781003161165>
- Beckles DM (2012) Factors affecting the postharvest soluble solids and sugar content of tomato (*Solanum lycopersicum* L.) fruit. Postharvest Biology and Technology 63(1): 129-140. <https://doi.org/10.1016/j.postharvbio.2011.05.016>
- Brosnan T and Sun DW (2001) Precooling techniques and applications for horticultural products—a review. International Journal of Refrigeration, 24(2): 154-170. [https://doi.org/10.1016/S0140-7007\(00\)00017-7](https://doi.org/10.1016/S0140-7007(00)00017-7)
- Chopra S, Müller N, Dhingra D, Pillai P, Kaushik T, Kumar A and Beaudry R (2023) Design and performance of solar-refrigerated, evaporatively-cooled structure for off-grid storage of perishables. Postharvest Biology and Technology, 197, 112212. <https://doi.org/10.1016/j.postharvbio.2022.112212>
- Choudhury B, Saha BB, Chatterjee PK and Sarkar JP (2013) An overview of developments in adsorption refrigeration systems towards a sustainable way of cooling. Applied Energy 104: 554-567 <https://doi.org/10.1016/j.apenergy.2012.11.042>
- Elkaoud NSM and Mahmoud RK (2022) Design and implementation of sequential fruit size sorting machine. Brazilian Journal of Agricultural and Environmental Engineering 26 (10): 722-728. <http://doi.org/10.1590/1807-1929/agriambi.v26n10p722-728>
- Elkaoud NSM, Mahmoud RK, Tarabye HH and Adam MS (2024) Optimal design of a solar precooling system for small-scale producers. CIGR Journal 26(1): 148-161. <https://cigrjournal.org/index.php/Ejournal/article/view/9063/4189>
- FAO (2019) Food and Agriculture Organization, Food loss and waste reduction and value chain development for food security in Egypt and Tunisia - Egypt Component. <https://www.fao.org/egypt/programmes-and-projects/food-loss-waste-reduction/fr/>
- Fellows PJ (2000) Principles and practice. Food processing technology, 2nd edition. Ed. Ellis Horwood, Chichester, Woodhead Publishing Limited and CRC Press LLC, 369-380.
- Gustavsson J, Cederberg C, Sonesson ULF and Emanuelsson A (2013) The methodology of the FAO study: "Global Food Losses and Food Waste—extent, causes and prevention"—FAO, 2011. <https://www.diva-portal.org/smash/get/diva2:944159/FULLTEXT01.pdf>
- Kapilan N and Patil VK (2023) Development and evaluation of a low-cost evaporative cooling system for agricultural product storage. Research in Agricultural Engineering 69(1): 48–53. <https://doi.org/10.17221/41/2021-RAE>
- Lipinski B, Hanson C, Waite R, Searchinger T and Lomax J (2013) Creating a Sustainable Food Future, Installment Two:



reducing food loss and waste. World Resources Institute. <https://www.wri.org/research/reducing-food-loss-and-waste>

Mansoori A and Patel V (1979) Thermodynamic basis for the choice of working fluids for solar absorption cooling systems. *Solar Energy* 22(6): 483-491. [https://doi.org/10.1016/0038-092X\(79\)90020-3](https://doi.org/10.1016/0038-092X(79)90020-3)

Morales TD and Busch J (2010) Design of small photovoltaic (PV) solar-powered water pump systems. United States Department of Agriculture (USDA), Natural Resources Conservation Service (NRCS), Technical Note 28: 1-64. [https://www.aeei.bse.vt.edu/wp-content/uploads/2014/05/nrcs142p2\\_046471.pdf](https://www.aeei.bse.vt.edu/wp-content/uploads/2014/05/nrcs142p2_046471.pdf)

Senthilkumar S, Vijayakumar RM and Kumar S (2015) Advances in precooling techniques and their implications in horticulture sector: A Review. *International Journal of Environmental & Agriculture Research (IJOEAR)* 1(1): 24-30. [https://ijoeear.com/assets/articles\\_menuscripts/file/IJOEAR-MAY-2015-5.pdf](https://ijoeear.com/assets/articles_menuscripts/file/IJOEAR-MAY-2015-5.pdf)

Sibanda S (2019) Development of a solar-powered indirect air cooling combined with direct evaporative cooling system for storage of fruits and vegetables in Sub-Saharan Africa (Doctoral dissertation). <http://doi.org/10.13140/RG.2.2.13604.60808>

Sibanda S and Workneh TS (2020) Performance evaluation of an indirect air cooling system combined with evaporative cooling. *Heliyon* 6(1). <https://doi.org/10.1016/j.heliyon.2020.e03286>

Sood M and Kumari D (2023) Hybridization: Importance, techniques and consequences; recent trends in agriculture. Chapter

4 - Post-harvest technology for fruits. *Recent Trends in Agriculture* 53.

Sorensen B (2004) *Renewable Energy Its physics, engineering, use, environmental impacts, economy and planning aspects*, 3<sup>rd</sup>. Elsevier Academic Press, Roskilde Univ. Energy & Environment Group, Ins, 2.

Suslow T and Cantwell M (2009) *Tomato: recommendations for maintaining postharvest quality*. Produce Facts. Davis: Postharvest Technology Research & Information Center. <https://postharvest.ucdavis.edu/produce-facts-sheets/tomato>

Talbot MT and Chau KV (2002) *Precooling strawberries*. Gainesville: IFAS, Univ. of Florida, 8p. (Circular 942). <https://ufdcimages.uflib.ufl.edu/IR/00/00/45/22/00001/AE13600.pdf>

Thompson JF (2004) *The commercial storage of fruits, vegetables and florist and nursery stocks*. A revised draft of Agriculture Handbook No. 66, USDA, ARS.

Tripathy M, Yadav S, Sadhu PK and Panda SK (2017) Determination of optimum tilt angle and accurate insolation of BIPV panel influenced by adverse effect of shadow. *Renewable Energy* 104: 211-223. <https://doi.org/10.1016/j.renene.2016.12.034>

Vala KV (2022) Environment friendly indirect-direct type evaporative cooling technology: A review. *International Journal of Environment and Climate Change* 12(10): 494-503. <https://doi.org/10.9734/ijec/2022/v12i1030823>

# Artificial neural networks in the retention of anthocyanins and total phenolics in the osmotic pre-treatment of Biloxi variety blueberry (*Vaccinium corymbosum* L.) jam

Redes neuronales artificiales en la retención de antocianinas y fenoles totales en el pre-tratamiento osmótico de mermelada de arándano (*Vaccinium corymbosum* L.) variedad Biloxi

<https://doi.org/10.15446/rfnam.v77n3.107488>

Jesús Alfredo Obregón Domínguez<sup>1\*</sup>, Carlos Alberto Minchón Medina<sup>2</sup>  
and Gabriela del Carmen Barraza-Jáuregui<sup>2</sup>

## ABSTRACT

### Keywords:

Artificial intelligent  
Machine learning  
Multiple-response  
Single-response

Blueberries are a fruit that is an important source of bioactive components beneficial to the human diet, such as anthocyanins and total phenolics, which are altered by the use of high temperatures during processing. This study aimed to evaluate the use of artificial neural networks in the optimization of sucrose concentration and time for the osmotic pre-treatment of blueberries of the Biloxi variety, to retain the greatest amount of anthocyanins and total phenolics in the subsequent preparation of jam. Artificial neural networks of the feedforward type were used, with a Backpropagation training algorithm with Levenberg-Marquardt weight adjustment, to achieve the optimal predicted combination that maximizes the retention of these bioactive components. The model achieved its best performance with 11 neurons in the hidden layer, achieving an  $R^2$  coefficient of 0.98 and a mean square error of 4.76, indicating a strong ability for generalization. Artificial neural networks allowed to obtain the best optimal combination of predicted multiple responses of factors consisting of a sucrose concentration of 1.64 M and a time of 211.52 min, which retained a higher content of total monomeric anthocyanins with 70.98 mg cyanidin-3-O-glucoside 100 g<sup>-1</sup> of jam and total phenolics with 110.54 mg GAE g<sup>-1</sup> of jam. On the other hand, through single-response optimization was obtained that the combination of experimental factors that maximized total anthocyanins (71.59 mg cyanidin-3-O-glucoside 100 g<sup>-1</sup> of jam) was 1.54 M of sucrose and 232.73 min and for total phenols (111.06 mg GAE g<sup>-1</sup> of jam) 1.79 M of sucrose and 196.36 min. The use of artificial neural networks is an excellent alternative for modeling phenomena, compared to traditional methods.

## RESUMEN

### Palabras clave:

Inteligencia artificial  
Aprendizaje de máquina  
Múltiple-respuesta  
Simple-respuesta

El arándano es un fruto que posee una fuente importante de componentes bioactivos beneficiosos para la dieta humana, como las antocianinas y fenoles totales, que se ven alterados por el uso de temperaturas altas durante el procesamiento. El objetivo de este estudio fue evaluar el uso de redes neuronales artificiales en la optimización de la concentración de sacarosa y el tiempo para el pretratamiento osmótico de arándanos de la variedad Biloxi, con la finalidad de retener la mayor cantidad de antocianinas y componentes fenólicos totales en la elaboración posterior de mermelada. Se utilizó redes neuronales artificiales del tipo feedforward, con algoritmo de entrenamiento de Backpropagation con ajuste de pesos de Levenberg-Marquardt para lograr la combinación óptima predicha que maximice la retención de estos componentes bioactivos. El modelo logró su mejor rendimiento con 11 neuronas en la capa oculta, logrando un coeficiente  $R^2$  de 0,98 y un error cuadrático medio de 4,76; lo que indica una gran capacidad de generalización. Las redes neuronales artificiales permitieron obtener la mejor combinación de los factores experimentales –concentración de sacarosa (1,64 M) y tiempo (211,52 min)- que maximizaron los contenidos de antocianinas monoméricas totales (70,98 mg cianidina-3-O-glucósido 100 g<sup>-1</sup>) y fenoles totales (110,54 mg AGE g<sup>-1</sup>) presentes en mermelada. En cambio, mediante optimización de respuesta se obtuvo que la combinación de factores experimentales que maximizó las antocianinas totales (71,59 mg cianidina-3-O-glucósido 100 g<sup>-1</sup> de mermelada) fue 1,54 M de sacarosa y 232,73 min y para fenoles totales (111,06 mg GAE g<sup>-1</sup> de mermelada) 1,79 M y 196,36 min. El uso de redes neuronales artificiales es una excelente alternativa para modelar fenómenos, en comparación con los métodos tradicionales.

<sup>1</sup>Data Engineering, Mz "M" Lote 12-A Urbanización San Andrés V-Etapa, Peru. [gerencia@dataengineeringperu.com](mailto:gerencia@dataengineeringperu.com) 

<sup>2</sup>Universidad Nacional de Trujillo, Peru. [cminchon@unitru.edu.pe](mailto:cminchon@unitru.edu.pe) , [gbarraza@unitru.edu.pe](mailto:gbarraza@unitru.edu.pe) 

\*Corresponding author

In the current environment, the execution of any industrial operation sans the application of machine learning is nearly implausible (Chhajjer et al. 2022; Chang et al. 2022; Liao et al. 2023). Artificial Neural Networks (ANNs) are one of the most widely used machine learning techniques for modeling, regression analysis, and classifying agricultural products (Çetin and Sağlam 2022). The capacity to develop prediction models utilizing ANNs has been a significant contribution of artificial intelligence and machine learning (Rodríguez-Hernández et al. 2021; Soumyabrata et al. 2022).

Due to the complex relationship between molecular structure and activity, linear models often fall short in capturing all sources of variation. Artificial Neural Networks (ANNs) are particularly effective for modeling non-linear interactions. Among these, the multi-layer perceptron (MLP), a type of ANN, offers near-perfect estimates compared to linear models (Çetin and Sağlam 2022; Vidra and Németh 2022).

ANN is an algorithm meant to grasp complex difficulties that basic machine learning algorithms cannot. ANNs are constructed in a more sophisticated and intricate network of interconnectedness than the human brain (Costa et al. 2022). The approach is based on algebraic equations and is intended to channel data to a model (Chhajjer et al. 2022).

In the most basic terms, ANNs are a network of numerical equations. A sequence of equations is used to process one or more input variables, resulting in one or more outputs. Every network has three layers: an input layer, a hidden layer, and an output layer. The independent variables or predictors are represented by the input layer, the hidden layer is where the mapping between input and output occurs, and the output layer is the dependent variable. The precise prediction of weights is critical to obtaining a decent model. This aim is accomplished by the backpropagation algorithm; it is this algorithm that distinguishes ANN as a learning model (Chhajjer et al. 2022; Rodríguez-Hernández et al. 2021).

The benefit of ANNs is that they can learn from historical data and have a general framework. In addition, when compared to the response surface technique (RSM), the key advantages of ANNs are: ANNs do not require any prior definition of an adequate fitting function, and

they are capable of universal approximation. They can estimate practically any nonlinear function, including quadratic functions; RSM, on the other hand, can only estimate quadratic functions. To create an efficient model, ANN is expected to need a significantly greater number of experiments (number of patterns) than RSM. Indeed, ANNs may perform well even with limited data as long as the data is statistically properly distributed in the input domain, as is the case with Design of Experiments. As a result, RSM experimental data should be sufficient to build an effective ANN model (Vidra and Németh 2022). ANNs are presently the most widely used artificial learning techniques in biotechnology, with applications ranging from pattern detection in chromatographic spectra to functional studies of genomic and proteomic sequences (Hesami et al. 2020).

Fruits are frequently high in bioactive chemicals like vitamins, phenolic compounds, carotenoids, flavonoids, and so on, which are heat-labile components whose rate of degradation varies depending on the process conditions used. The loss of bioactive substances throughout the manufacturing process can be accelerated or slowed by the product composition (jam), such as pectin type and concentration, sugar, fruit and cultivar, and pH. These are ready-to-eat, shelf-stable goods that can be transferred to any location (Shinwari and Rao 2018).

*Vaccinium corymbosum* (blueberry) is one of the most commonly consumed soft fruits and is recognized as an important source of bioactive components in the human diet, playing an important role in maintaining a healthy lifestyle; bioactive chemicals found in blueberries, such as flavonoids, stilbenes, phenolic compounds and tanins, may protect against degenerative illnesses, and their health benefits are frequently linked to antioxidant qualities (Dias et al. 2023; Dong et al. 2023; Barraza-Jáuregui et al. 2017). The health advantages of antioxidant activity and phenolics are mostly connected to their ability to scavenge free radicals. Excessive reactive oxygen species generation can cause oxidative stress in cellular lipids, proteins, and nucleic acids, which has been linked to the development of cancer, cardiovascular disease, diabetes, central nervous system illnesses, and chronic obstructive pulmonary disease (Çetin and Sağlam 2022). Furthermore, taste is the most essential element driving customer preferences, making flavor a key aim. Blueberry flavor

perception has been linked mostly to the mix of sugars, acids, and volatile organic chemicals that, when recognized by taste and olfactory receptors, provide a wide range of flavor sensations (Dias et al. 2023).

Although these fruits may be eaten fresh, preserving them in processed goods like jellies, jams, and cakes extends their shelf-life and enables year-round enjoyment. However, making jam has a number of obstacles, one of which is preserving the healthy components in the fresh fruit while preventing spoiling. Heat treatment duration, component identity and quantity, and fruit pre-treatment are all suitable preparation stages to optimize. Heat treatment, as well as the addition of sugar and citric acid, can all affect jam quality and final flavone and anthocyanin concentrations (Barraza-Jáuregui et al. 2017).

Osmotic dehydration (OD) pre-treatment is a method that involves immersing items in an aqueous solution containing salt or sugar. It is commonly used on fruits and vegetables (Alabi et al. 2022). By lowering water activity in the fruit, this approach may preserve the quality of the fruit that is later used in jam production. The difference in solute concentration between the solution and the interstitial fluid drives the process, causing water to depart and solutes to enter the cells until osmotic equilibrium is reached (Ahmed et al. 2016; Barraza-Jáuregui et al. 2017).

According to research, prior to jam manufacture, osmotic dehydration pre-treatment of strawberries with sucrose stabilizes anthocyanin better than just adding sucrose during jam preparation (Watanabe et al. 2011). The main anthocyanins involved in blueberry color are delphinidin and cyanidin 3-glucoside and to a lesser extent malvidin, petunidin, and peonidin. However, the variety, maturity, storage conditions, and other components of the blueberry affect these anthocyanins and phenolic compounds (Barraza-Jáuregui et al. 2017). Sugars' impacts, including not just monosaccharides but also oligo and polysaccharides, in the manufacture of jam on the anthocyanin content have been studied (Skrede et al. 2008). However, the solute's identity and concentration (often sucrose), immersion time, temperature, pressure, raw food structure, food-to-solution ratio, permeability, size, and shape of the fruit, all have an effect on the osmotic dehydration process (Barraza-Jáuregui et al. 2017).

This study aimed to optimize, through the use of artificial neural networks, the sucrose concentration and the osmotic pre-treatment time of blueberries of the Biloxi variety, to retain the greatest amount of anthocyanins and total phenolic components for the subsequent preparation of jam.

## MATERIALS AND METHODS

### Raw material

Blueberry fruits (*Vaccinium corymbosum* L.) Biloxi variety, from the district of Virú, province of Virú, department of La Libertad, Peru. The content of soluble solids ( $13.49 \pm 0.10\%$ ), titratable acidity ( $0.49 \pm 0.09\%$ ), and pH ( $3.47 \pm 0.12$ ) were evaluated. Fruits were picked at commercial ripeness and chilled before being sent to the National University of Trujillo's Department of Agro-industrial Engineering. The blueberry fruits were received verifying their good condition, such as intense blue color, spherical shape with an approximate diameter of  $20 \pm 2$  mm, and firmness to the touch; and that they have not presented the development of microorganisms. The Fruit was kept in 1,000 kg clamshell packaging in the dark at  $3.0 \pm 0.5$  °C and  $94 \pm 3\%$  RH (Barraza-Jáuregui et al. 2017).

### Jam preparation

Blueberry fruits were washed using drinking water with sodium hypochlorite at 50 ppm, to remove foreign particles and reduce the microbial load, subsequently, the fruits were cut in half. To create a data matrix input for the ANN that is statistically well distributed, a rotational composite central design was applied, consisting of twelve experimental units (Vidra and Németh 2022). The osmotic pre-treatment (Figure 1) was carried out with concentrations of sucrose solution (between 0.88-2.04 M) and immersion times (between 60-360 min), with a ratio of fruit: syrup of 1:10 (w/w), maintaining constant agitation (vertical stirrer IKA® EUROSTAR 20 Digital, Königswinter, Germany) at 48 rpm (at 20 °C), subsequently the dehydrated blueberry fruits were removed from the osmotic solution, for which were placed in a strainer for a time of 10 min, to eliminate the excess of solution (Barraza-Jáuregui et al. 2017; Watanabe et al. 2011; Rahman et al. 2022). For the preparation of the jam, the proportion used of dehydrated blueberries was 60% and sucrose 40%, the cooking was carried out by initially adding 10% of the amount of sucrose calculated, later

when this came to 50 °Brix the rest of the sucrose when the jam came to 62 °Brix, it was removed from cooking and finally brought to 64 °Brix. The filling in cylindrical glass jars (220 mL capacity, transparent, 74.6 mm wide, 67 mm high and 70 mm twist-off metal cap) was done hot at a temperature not lower than 85 °C (this temperature improved the fluidity of the product during

filling and at the same time allowed the formation of an adequate vacuum inside the container), hermetically sealed jars and chilled to 20 °C for at least 1.5 h to achieve thermal shock, that guarantees the safety of the product. Before being employed in the study, samples were maintained in total darkness at 5 °C for at least 24 h (Lu-Lu et al. 2016; Shinwari and Rao 2018).

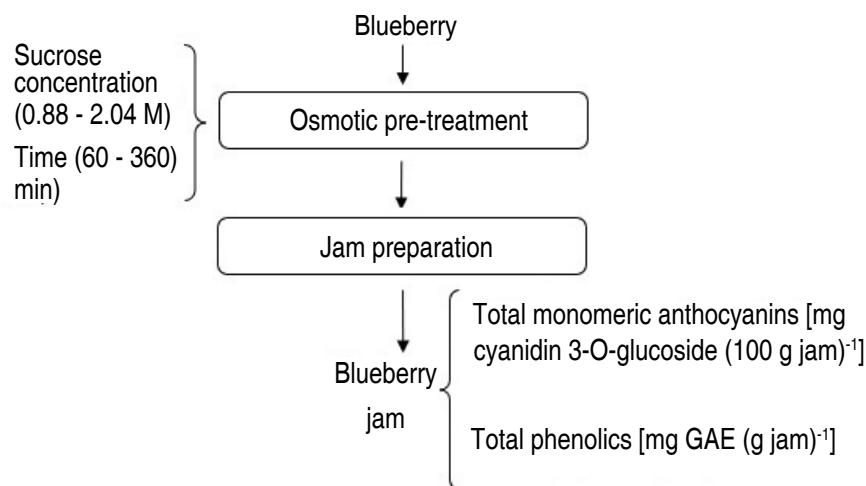


**Figure 1.** Experimental scheme for osmotic pre-treatment and preparation of Biloxi variety blueberry jam.

### Total monomeric anthocyanins

To 10 g homogenized jam was treated with acidified ethanol (0.01 M HCl solution in ethanol; 40 mL). The extract was chilled overnight before being filtered the next day through S&S 520 (Schleicher and Schuell - Whatman filter paper grade 520, Maidstone, United Kingdom) (Wicklunda et al. 2005; Barraza-Jáuregui et al. 2017). The total monomeric anthocyanins (TA) in the extracts were calculated using the pH-differential technique (Lee et al. 2005), using hydrochloric acid/potassium chloride buffer (0.025 M, pH=1.0) and sodium acetate buffer (0.4 M, pH=4.5) as the buffers. In brief, 0.2 mL of the filtrate was mixed with 1.8 mL of one of the buffer solutions, and absorbance was measured on a UV-VIS spectrophotometer at 510 and 700 nm (GENESYS™ 10, THERMO, USA). The anthocyanin content in the extract was determined and represented as cyanidin-3-O-glucoside equivalent per 100 g of jam using Equation 1 (Giusti and Wrolstad 2001).

$$TA \left( \frac{\text{mg}}{100 \text{ g jam}} \right) = \frac{A \cdot Mw \cdot DF}{Ma \cdot L} \times 100 \quad (1)$$

Where:  $A = (A_{510} - A_{700})_{\text{pH}=1.0} - (A_{510} - A_{700})_{\text{pH}=4.5}$ ; Mw= molecular weight (449.2 g mol<sup>-1</sup>); DF= dilution factor (50); Ma = extinction coefficient 26,900 L cm<sup>-1</sup> mol<sup>-1</sup>; L= path length (1 cm).

### Total phenolics

In a flask, homogenized jam was diluted with ethanol (2 g jam 10 mL<sup>-1</sup> solution). The extract was chilled overnight before being filtered (S&S 520) the next day. The Folin-Ciocalteu test was used to evaluate the phenolic component content (Çetin and Sağlam 2022). Briefly, 20 µL of diluted extract was combined with 100 µL of Folin-Ciocalteu reagent and 1,580 µL of distilled water.

The mixtures were vortexed (Thermo Scientific™ A LP Vortex Mixer, FBKT17302, Darmstadt, Germany), held in the dark at room temperature for 20 min, and then transferred into a 40 °C water bath with 300 µL addition of 20% sodium carbonate (w/v) for another 20 min. The samples were promptly chilled in an ice bath for 3 min, and the  $A_{765}$  was quantified using a UV-VIS spectrophotometer (UV-VIS GENESYS™ 10, THERMO,



USA). A calibration curve was created using gallic acid as the standard ( $\text{Absor} = 3.3167 \times Q + 0.0044$ ;  $R^2 = 0.9936$ ; Absor: absorbance; Q: amount of gallic acid) was armed with 0.05, 0.10, 0.15, 0.20, 0.25, 0.30, 0.35, 0.40, 0.45 and 0.50 mg mL<sup>-1</sup> gallic acid solutions, and the findings were reported as gallic acid equivalents (mg GAE g<sup>-1</sup> jam) (Barraza-Jáuregui et al. 2017; Piljac-Zegarac et al. 2009).

### Data processing

MLP-type ANN was employed in this investigation to estimate anthocyanins and total phenolics (Çetin and Sağlam 2022). In the first instance, the input and output data were normalized (center=min, scale=max-min) (Costa et al. 2022; Yu et al. 2022; Vidra and Németh 2022). The number of inputs was taken as two, the number of neurons in the hidden layer as 11, and the number of outputs as two. The logistic activation function was used in the hidden layer and the linear function in the output layer. Backpropagation was used with Levenberg-Marquardt adjustment, in addition to the learning ratio of 0.01 and threshold of 0.01. The training data was given in supervised learning as a sequence of labeled outputs, each of which was a feature collection set (tagged with

the correct output corresponding to the feature set) (Chhajjer et al. 2022; Rodríguez-Hernández et al. 2021). The coefficient of determination  $R^2$  (maximization) and the mean square error MSE (minimization) were used to evaluate model performance (Yu et al. 2022; Vidra and Németh 2022; Soumyabrata et al. 2022). For data processing, the R version 4.2.1 software was used, with the libraries: "rsm", "MASS", "neuralnet", "ggplot2" and "colorRamps".

### RESULTS AND DISCUSSION

ANN were trained in 1,000 cycles with the Brackpropagation algorithm, where the highest performance of the model was achieved with 11 neurons in the hidden layer (Figure 2), having a coefficient of determination  $R^2$  of 0.988 and a mean square error of 4.760, presenting a good capacity for generalization. Çetin and Sağlam (2022) determined the performance of ANN presenting  $R^2$  value of 0.916 in the modeling of total phenols in dehydrated apples. ANN is the most effective dataset modeling approach. It is used for data fitting and prediction, which have a non-linear connection. It is a self-organizing map and a multi-layer perceptron (Chhajjer et al. 2022).

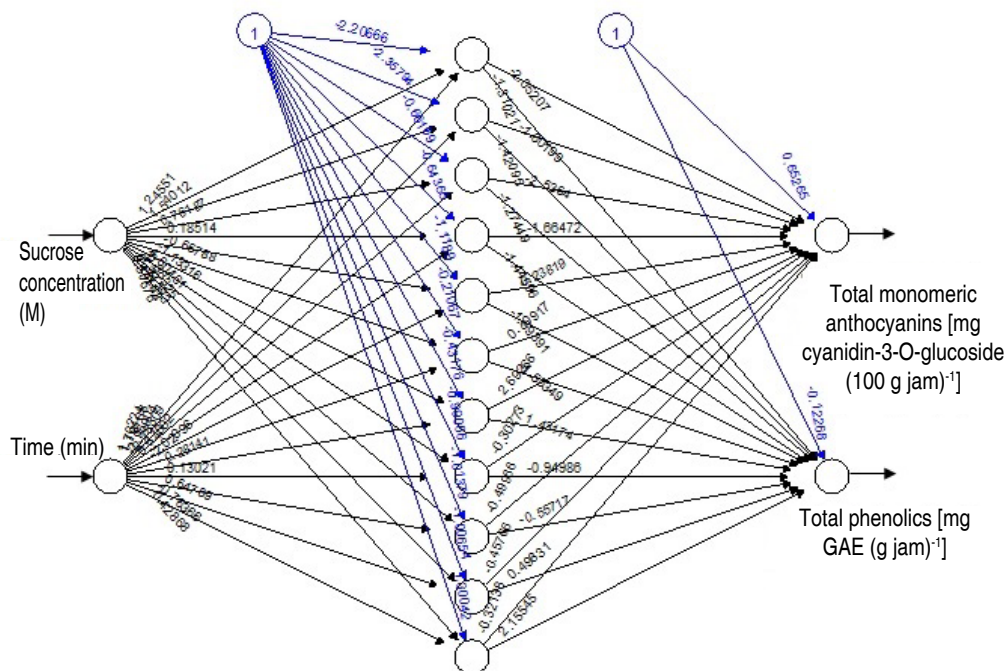


**Figure 2.** Artificial neural networks in the retention of anthocyanins and total phenolics in the osmotic pre-treatment of Biloxi variety blueberry jam.

Before the osmotic pre-treatment, the content of total monomeric anthocyanins and total phenolic compounds were  $104.47 \pm 3.89$  mg cyanidin-3-O-glucoside  $100 \text{ g}^{-1}$  and  $161.04 \pm 23.24$  mg GAE  $\text{g}^{-1}$  in variety Biloxi blueberry fresh, respectively. After osmotic pre-treatment and the preparation of the jam, ANN allowed to obtain (Table 1) the best optimal combination predicted multiple-response (Figure 3) of factors made up of a sucrose concentration of 1.64 M and a time of 211.52 min, which retained a higher content of total monomeric anthocyanins with 70.98 mg cyanidin-3-O-glucoside  $100 \text{ g}^{-1}$  of jam (confidence interval at 95% between 70.88 and 71.08 mg cyanidin-3-O-glucoside

$100 \text{ g}^{-1}$  of jam) and total phenolics with 110.54 mg GAE  $\text{g}^{-1}$  of jam (95% confidence interval between 110.40 and 110.68 mg GAE  $\text{g}^{-1}$  of jam), similar trends were observed by Barraza-Jáuregui et al. (2017), where the greatest phenolic and anthocyanin contents were determined to produce blueberry jam pretreatment conditions of 1.65 M and 242 min and strawberry jam pre-treatment conditions of 1.46 M and 219 min. Osmotic treatments for impregnation with sucrose in solution, before making the jam, at concentrations of 0.29 to 2.34 M, for 5 to 60 min, are effective for the efficacy of anthocyanins (Watanabe et al. 2011).

**Table 1.** Multiple-response and single-response values for optimization through artificial neural networks in the retention of anthocyanins and total phenolics in the osmotic pre-treatment of Biloxi variety blueberry jam.

Prediction	Factors		Total monomeric anthocyanins [mg cyanidin-3-O-glucoside ( $100 \text{ g jam}^{-1}$ )]			Total phenolics [mg GAE ( $\text{g jam}^{-1}$ )]		
	Sucrose concentration (M)	Time (min)	Point estimate	(95%) CI		Point estimate	(95%) CI	
				Lower	Upper		Lower	Upper
Multiple-response	1.64	211.52	70.98	70.88	71.08	110.54	110.40	110.68
Single-response	1.54	232.73	71.59	71.50	71.69	-	-	-
	1.79	196.36	-	-	-	111.06	110.92	111.20

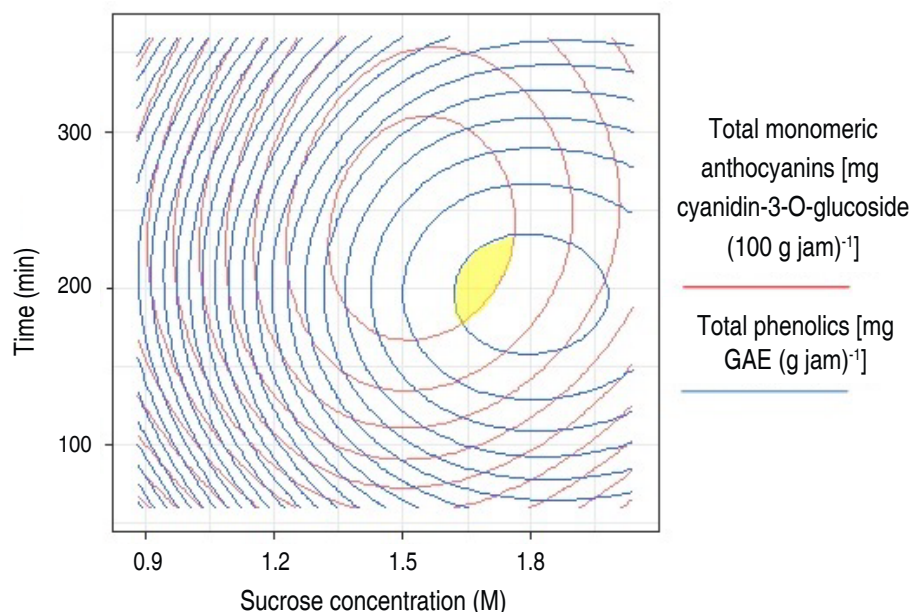


**Figure 3.** Contour overlap for multiple-response optimization in the retention of anthocyanins in the osmotic pre-treatment of Biloxi variety blueberry jam.

Regarding the single-response optimization for total monomeric anthocyanins (Table 1 and Figure 4) the combination of factors of sucrose concentration of 1.54 M and time of 232.73 min allowed to retain 71.59 mg cyanidin-3-O-glucoside  $100 \text{ g}^{-1}$  of jam (confidence interval at 95% between 71.50 and 71.69 mg cyanidin-3-O-glucoside  $100 \text{ g}^{-1}$  of jam); and for total phenolics (Table 1 and Figure 5) the combination of sucrose concentration of 1.79 M and time of 196.36 min allowed the retention of 111.06 mg GAE  $\text{g}^{-1}$  of jam (95% confidence interval between 110.92 and 111.20 mg GAE  $\text{g}^{-1}$  of jam). It should be noted that the retention of anthocyanins and phenolic compounds was low when the sucrose concentration and immersion time moved away from the optimization zone (maximization of retention), either towards a lower or higher value of the levels of work factors. Barraza-Jáuregui et al. (2017) reported a similar tendency, with an island of high phenolic component or anthocyanin content surrounded by lower expected quantities; lengthy times and/or high sucrose concentrations, as well as short periods and/or low osmotic concentrations, may lower the concentration of phenolic chemicals and anthocyanins in the jam. Because anthocyanins are water-soluble pigments found in most fruits, sugars suppress water activity and protect the flavylium cation from nucleophilic attack at the C-2 position by water, resulting in colorless carbinol base. At low quantities; however, sugar breakdown products

(furfurals) from processes such as the Maillard reaction promote anthocyanin destruction (Shinwari and Rao 2018). Osmotic dehydration inhibits water activity in fruit, which has been shown to preserve phenolic components and anthocyanins during jam production (Watanabe et al. 2011). Furthermore, reduced water activity may impede enzymes that hydrolyze pigments, such as polyphenol oxidase and  $\beta$ -glucosidase. Sucrose may also act as a steric inhibitor, blocking anthocyanin-ascorbate or anthocyanin-phenolic condensation. Furthermore, due to colligative effects, the oxygen solubility of high osmotic solutions is limited, providing a partial oxygen barrier that can shield the pigments from oxidation (Barraza-Jáuregui et al. 2017; Wrolstad et al. 2005). Significant losses occur when they are kept and transported in unsuitable settings. Preservation techniques such as drying, freezing, pickling, sugaring, and salting may provide a considerable answer to these challenges (Çetin and Sağlam 2022; Shinwari and Rao 2018). During osmotic dehydration, the concentration of the osmotic agent is an important factor in mass transfer kinetics (Shukla et al. 2018). Low sugar concentrations result in little water loss and solid gain ratios (Figures 4 and 5, low sucrose concentrations) (Cichowska et al. 2019). As osmolarity rises, so does water loss and hypertonic solution absorption. However, as concentration increases, water loss becomes less efficient. Due to case hardening and viscosity fluctuations,

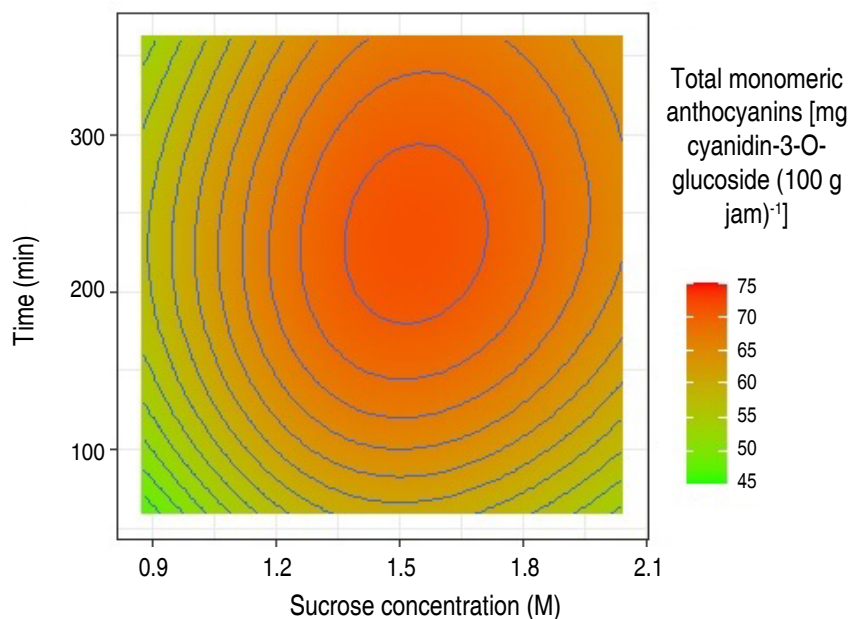


**Figure 4.** Contours surface in the retention of anthocyanins in the osmotic pre-treatment of Biloxi variety blueberry jam.

fruit cell membranes and pericarp are projected to become less permeable in severely hypertonic solutions, lowering penetration (Figures 4 and 5, high concentrations) (Ahmed et al. 2016; Winkler et al. 2019; Brüggewirth and Knoche

2016). Furthermore, prolonged exposure to the osmotic pre-treatment conditions may cause anthocyanin and other chemicals in the hypertonic solution to leach (Barraza-Jáuregui et al. 2017) (Figures 4 and 5, longer time points).

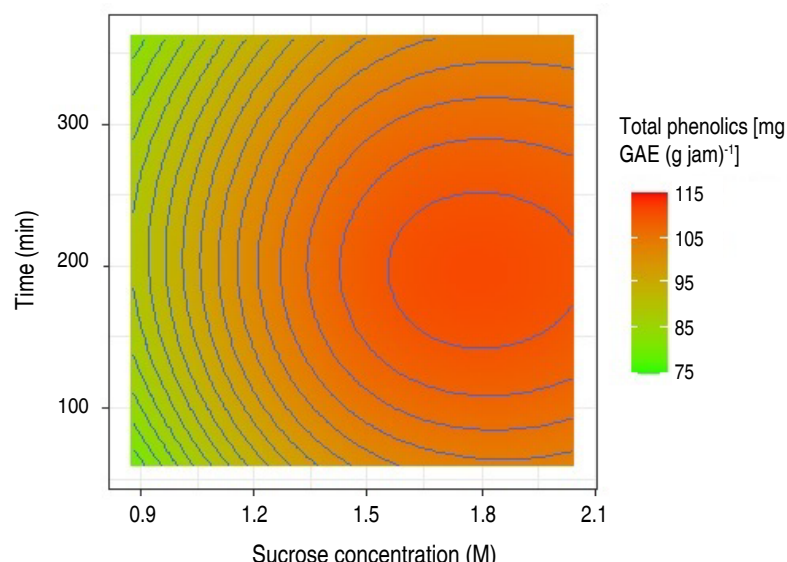


**Figure 5.** Contours surface in the retention of total phenolics in the osmotic pre-treatment of Biloxi variety blueberry jam.

## CONCLUSION

The artificial neural networks allowed to obtain the optimal combination of multiple-response factors consisting of a sucrose concentration of 1.64 M and a time of 211.52 min, which maximized the content of total monomeric anthocyanins and total phenols; corresponding concentrations of 70.98 mg cyanidin-3-O-glucoside 100 g<sup>-1</sup> of jam and 110.54 mg AGE g<sup>-1</sup> of jam, respectively. From the perspective of simple-response optimization for total monomeric anthocyanins, the combination of experimental factors was sucrose concentration of 1.54 M and time of 232.73 min, allowed to retain 71.59 mg cyanidin-3-O-glucoside 100 g<sup>-1</sup> of jam. For total phenols, the combination of experimental factors was a sucrose concentration of 1.79 M and time of 196.36 min, which corresponded to total phenolic retention of 111.06 mg of AGE g<sup>-1</sup> of jam. The use of artificial neural networks is an excellent alternative to model phenomena, compared to traditional methods.

## REFERENCES

Ahmed I, Qazi I and Jamal S (2016) Developments in osmotic dehydration technique for the preservation of fruits and vegetables. *Innovative Food Science and Emerging Technologies* 34:29-43. <https://doi.org/10.1016/j.ifset.2016.01.003>

[doi.org/10.1016/j.ifset.2016.01.003](https://doi.org/10.1016/j.ifset.2016.01.003)

Alabi K, Olalusi A, Olaniyan A, Fadeyibi A and Gabriel L (2022) Effects of osmotic dehydration pretreatment on freezing characteristics and quality of frozen fruits and vegetables. *Journal of Food Process Engineering* 45(8):e14037. <https://doi.org/10.1111/jfpe.14037>

Barraza-Jáuregui G, Vega G, Valeriano J, Obregón J, Siche R and Miano A (2017) Osmotic pretreatment to assure retention of phenolics and anthocyanins in berry jams. *Food Bioscience* 17: 24–28. <https://doi.org/10.1016/j.fbio.2016.12.001>

Brüggewirth M and Knoche M (2016) Factors affecting mechanical properties of the skin of sweet cherry fruit. *Journal of the American Society for Horticultural Science. American Society for Horticultural Science* 141:45–53. <https://doi.org/10.21273/JASHS.141.1.45>

Chang V, Rupa V, Qianwen A and Hossain MA (2022) An artificial intelligence model for heart disease detection using machine learning algorithms. *Healthcare Analytics* 2:100016. <https://doi.org/10.1016/j.health.2022.100016>

Chhajer P, Shah M and Kshirsagar A (2022) The applications of artificial neural networks, support vector machines, and long-short term memory for stock market prediction. *Decision Analytics Journal* 2:100015. <https://doi.org/10.1016/j.dajour.2021.100015>

Çetin N and Sağlam C (2022) Rapid detection of total phenolics, antioxidant activity and ascorbic acid of dried apples by chemometric algorithms. *Food Bioscience* 47:101670. <https://doi.org/10.1016/j.fbio.2022.101670>

Cichowska J, Figiel A, Stasiak-Róžańska L and Witrowa-Rajchert D (2019) Modeling of osmotic dehydration of apples in sugar alcohols and dihydroxyacetone (DHA) solutions. *Foods* 8: 20. <https://doi.org/10.3390/foods8020020>



org/10.3390/foods8010020

Costa E, Hess A, Finger C, Schons C, Klein D et al (2022) Enhancing height predictions of brazilian pine for mixed, uneven-aged forests using artificial neural networks. *Forests* 13: 1284. <https://doi.org/10.3390/f13081284>

Dias R, Johnson T, Ferrão F, Munoz P, de la Mata P and Harynuk J (2023) Improved sample storage, preparation and extraction of blueberry aroma volatile organic compounds for gas chromatography. *Journal of Chromatography Open* 3: 100075. <https://doi.org/10.1016/j.jcoa.2022.100075>

Dong R, Tian J, Huang Z, Yu Q, Xie J et al (2023) Intermolecular binding of blueberry anthocyanins with water-soluble polysaccharides: Enhancing their thermostability and antioxidant abilities. *Food Chemistry* 410: 135375. <https://doi.org/10.1016/j.foodchem.2022.135375>

Giusti M and Wrolstad R (2001) Characterization and measurement of anthocyanins by UV–visible spectroscopy. *Current Protocols in Food Analytical Chemistry*. <http://doi.org/10.1002/0471142913.faf0102s00>

Hesami M, Condori-Apata J, Valencia M and Mohammadi M (2020) Application of artificial neural network for modeling and studying *in vitro* genotype-independent shoot regeneration in wheat. *Applied Sciences* 10(15): 5370. <https://doi.org/10.3390/app10155370>

Lee J, Durst R and Wrolstad R (2005) Determination of total monomeric anthocyanin pigment content of fruit juices, beverages, natural colorants, and wines by the pH differential method: collaborative study. *Journal of AOAC International* 88(5): 1269–1278. <https://doi.org/10.1093/jaoac/88.5.1269>

Liao W, Shen J, Manickam S, Li S, Tao Y, Li D, Liu D and Han Y (2023) Investigation of blueberry juice fermentation by mixed probiotic strains: Regression modeling, machine learning optimization and comparison with fermentation by single strain in the phenolic and volatile profiles. *Food Chemistry* 405: 134982. <https://doi.org/10.1016/j.foodchem.2022.134982>

Lu-Lu Z, Jing-Nan R, Yan Z, Jia-Jia L, Ya-Li L et al (2016) Effects of modified starches on the processing properties of heat-resistant blueberry jam. *LWT - Food Science and Technology* 72: 447–456. <https://doi.org/10.1016/j.lwt.2016.05.018>

Piljac-Zegarac J, Valek L, Martinez S and Belšcak A (2009) Fluctuations in the phenolic content and antioxidant capacity of dark fruit juices in refrigerated storage. *Food Chemistry* 113: 394–400. <https://doi.org/10.1016/j.foodchem.2008.07.048>

Rahman S, Sharma P and Said Z (2022) Application of response surface methodology based D-optimal design for modeling and optimization of osmotic dehydration of zucchini. *Digital Chemical Engineering* 4: 100039. <https://doi.org/10.1016/j.dche.2022.100039>

Rodríguez-Hernández C, Musso M, Kyndt E and Cascallar E (2021) Artificial neural networks in academic performance prediction: Systematic implementation and predictor evaluation. *Computers and Education: Artificial Intelligence* 2: 100018. <https://doi.org/10.1016/j.caeai.2021.100018>

Shinwari K and Rao P (2018) Stability of bioactive compounds in fruit jam and jelly during processing and storage: A review. *Trends in Food Science & Technology* 75: 181–193. <https://doi.org/10.1016/j.tifs.2018.02.002>

Shukla R, Khan M and Srivastava A (2018) Mass transfer kinetics during osmotic dehydration of banana in different osmotic agent. *International Journal of Agricultural Engineering* 11: 108–122. <https://doi.org/10.15740/HAS/IJAE/11.1/108-122>

Skrede G, Wrolstad E and Durst W (2008) Changes in anthocyanins and polyphenolics during juice processing of highbush blueberries (*Vaccinium corymbosum* L.). *Journal of Food Science* 65(2): 357–364. <https://doi.org/10.1111/j.1365-2621.2000.tb16007.x>

Sourmyabrata D, Hewei W, Chidozie S, Nishtha J, Bharadwaj V and Deepu J (2022) A predictive analytics approach for stroke prediction using machine learning and neural networks. *Healthcare Analytics* 2: 100032. <https://doi.org/10.1016/j.health.2022.100032>

Vidra A and Németh A (2022) Applicability of neural networks for the fermentation of propionic acid by propionibacterium acidipropionici. *Periodica Polytechnica Chemical Engineering* 66: 10–19. <https://doi.org/10.3311/PPCh.18283>

Watanabe Y, Yoshimoto K, Okada Y and Nomura M (2011) Effect of impregnation using sucrose solution on stability of anthocyanin in strawberry jam. *LWT – Food Science and Technology* 44: 891–895. <https://doi.org/10.1016/j.lwt.2010.11.003>

Winkler A, Grimm E and Knoche M (2019) Sweet cherry fruit: ideal osmometers?. *Frontiers in Plant Science* 10: 164. <https://doi.org/10.3389/fpls.2019.00164>

Wicklunda T, Rosenfeldb H, Martinsenc B, Sundforb M et al (2005) Antioxidant capacity and colour of strawberry jam as influenced by cultivar and storage conditions. *LWT – Food Science and Technology* 38: 387–391. <https://doi.org/10.1016/j.lwt.2004.06.017>

Wrolstad R, Durst R and Lee J (2005) Tracking color and pigment changes in anthocyanin products. *Trends in Food Science & Technology* 16(9): 423–428. <https://doi.org/10.1016/j.tifs.2005.03.019>

Yu Z, Gong H, Li M and Tang D (2022) Hollow prussian blue nanozyme-richened liposome for artificial neural network-assisted multimodal colorimetric-photothermal immunoassay on smartphone. *Biosensors and Bioelectronics* 218: 114751. <https://doi.org/10.1016/j.bios.2022.114751>





# Starch from *Colocasia esculenta* (L.) Schott of purple and white esculenta varieties: Thermal, technological properties, and morphological study

Almidón de *Colocasia esculenta* (L.) Schott de variedades esculenta morada y blanca: Estudio de propiedades térmicas, tecnológicas y morfológicas

<https://doi.org/10.15446/rfnam.v77n3.111574>

José Trujillo-Ccanahuire<sup>1</sup>, Elizabeth S. Ordoñez<sup>2</sup>, Darlym Reategui<sup>3</sup> and Melchor Soria Iturri<sup>1\*</sup>

## ABSTRACT

### Keywords:

Food industry  
Gelatinization  
Microstructure  
Taro



The high demand for starch in the food industry drives the search for new alternative sources for extraction. In this regard, *Colocasia esculenta* (L.) Schott, an edible root, is a promising alternative source for starch extraction. This study focused on correlating the technological and thermal properties with the microstructure and size distribution of starch from white and purple varieties. Starch granules with high thermal stability ( $132\text{--}258.3\text{ }^{\circ}\text{C}$ ) and good digestibility based on granule size ( $0.79\text{--}4.05\text{ }\mu\text{m}$ ) were obtained. It was demonstrated that larger starch granules exhibit higher water absorption capacity (WAC) ( $139\pm 0.53\%$ ). Moreover, the increase in WAC results in a higher gelatinization temperature ( $76.1\pm 0.3\text{ }^{\circ}\text{C}$ ), which is favorable as it allows the use of this starch in food processing at high temperatures.


## RESUMEN


### Palabras clave:

Industria de alimentos  
Gelatinización  
Microestructura  
Taro

La alta demanda de almidón en la industria alimentaria provoca la búsqueda de nuevas fuentes alternativas para su extracción. En este sentido, *Colocasia esculenta* (L.) Schott es una raíz comestible que demuestra ser una buena fuente alternativa para la extracción de almidón. Este estudio se centró en relacionar las propiedades tecnológicas y térmicas con la microestructura y la distribución de tamaño del almidón de las variedades blanca y morada. Se obtuvieron gránulos de almidón con una alta estabilidad térmica ( $132\text{--}258,3\text{ }^{\circ}\text{C}$ ) y buena digestibilidad basada en el tamaño de los gránulos ( $0,79\text{--}4,05\text{ }\mu\text{m}$ ). Se demostró que los gránulos de almidón más grandes originan mayor capacidad de absorción de agua (WAC) ( $139\pm 0,53\%$ ), además el aumento de WAC genera una mayor temperatura de gelatinización ( $76,1\pm 0,3\text{ }^{\circ}\text{C}$ ), este comportamiento es favorable, pues permite el uso de este almidón en el procesamiento de alimentos a altas temperaturas.

<sup>1</sup>Laboratorio Central de Investigación - Universidad Nacional Agraria de la Selva, Tingo María, Perú. [jose.trujillo@unas.edu.pe](mailto:jose.trujillo@unas.edu.pe) , [soriamelchor127@gmail.com](mailto:soriamelchor127@gmail.com) 

<sup>2</sup>Departamento académico de Ciencia y Tecnología de Alimentos - Facultad de Ingeniería en Industrias Alimentarias, Universidad Nacional Agraria de la Selva, Tingo María, Perú. [Elizabeth.ordonez@unas.edu.pe](mailto:Elizabeth.ordonez@unas.edu.pe) 

<sup>3</sup>Biocentro - Universidad Nacional Agraria de la Selva, Tingo María, Perú. [Darlym.reategui@unas.edu.pe](mailto:Darlym.reategui@unas.edu.pe) 

\*Corresponding author

**G**lobal production of native starch is projected to reach 156.5 million tons by 2025, driven primarily by its extensive use in the food industry (Compart et al. 2023). However, traditional sources such as maize, potato, wheat, cassava, and sweet potato are being overexploited, highlighting the urgent need to investigate new botanical sources of starch (Singh et al. 2024). Research and characterization of novel or alternative starches could alleviate pressure on these limited sources.

Taro (*Colocasia esculenta* L.), a perennial herbaceous plant native to Asia and widespread in tropical and subtropical regions of the Americas has garnered increasing interest due to its technological and nutritional properties. Thriving in climates with annual precipitation between 1,800 and 2,500 mm and temperatures ranging from 12 to 35 °C, taro benefits from high solar luminosity (Nagar et al. 2021; Gupta et al. 2023). The edible corm of taro, which can be spherical, ellipsoidal, or conical in shape, typically contains 27% starch on a dry weight basis, with starch granules ranging from 1 to 6.5 µm (Legesse and Bekele 2021; Huang et al. 2024). Its high moisture and carbohydrate content promotes microbial activity, leading to post-harvest losses. Although research has been conducted on taro, most of it has focused on the characterization of fresh corms, with less attention given to the study of taro flour and starch (Boahemaa et al. 2024).

Starch, owing to its functional properties and diverse applications in the industry, stands out as the most commercially significant carbohydrate. These properties are closely linked to the composition, morphology, and molecular structure of amylose and amylopectin within starch granules, factors influenced by genetic, agronomic, and environmental conditions (Saraiva et al. 2020; Choque-Quispe et al. 2024). Technological properties assessed for starches in the food industry include gelatinization, solubility index, swelling capacity, water absorption capacity, syneresis/retrogradation, and emulsification capacity (Hui et al. 2024). Understanding these functional properties is critical for predicting starch behavior when incorporated into food products. Marboh and Mahanta (2021) highlighted the interrelationship between these technological properties. For instance, higher water absorption capacity correlates with reduced syneresis, thereby enhancing stability during the freezing and thawing

cycles of foods. Additionally, gelatinization alters the starch structure, leading to enhanced water separation in certain starches post-freezing and thawing (Moorthy et al. 2024). In Peru, particularly in the Huánuco region, the climatic conditions are favorable for the cultivation of taro, where both white and purple varieties are grown. However, the lack of scientific studies on the technological properties of taro has limited its economic exploitation. The aim was to study the morphology, color, techno-functional properties, and thermal behavior of starch extracted from taro (white and purple).

## MATERIALS AND METHODS

This study was carried out in the Laboratorio Central de Investigación at the UNAS, located in the city of Tingo María, Rupa Rupa district, Leoncio Prado province, Huánuco region, Peru which is geographically located at 9°17'08" south latitude and 75°59'52" west longitude, at a height of 660 meters above sea level (masl), with a relative humidity of 80%, and an average annual temperature of 25 °C.

### Raw material

Approximately 5 kg of fresh roots from the two taro varieties, white and purple, were collected from the CIPTALD (Figure 1); geographically situated at the coordinates: 9°51" south longitude and 75°00" longitude, in the Huánuco department (Peru). For the identification of the varieties, a cross-sectional cut was made in the roots to identify the color of the pulp. The purple variety was coded as **PTS**, and the white variety as **WTS**.

### Starch extraction

The extraction was done according to the methodology of Naidoo et al. (2015). The roots were selected according to their variety and the first washing was done to eliminate impurities. Later the roots were peeled, and a second washing using distilled water was done, then the pulp was cut into 3 mm thick slices. These slices were dried at 50 °C for 8 h in an electric stove (MMM Group, EC 222 ECO, Germany), then the dry matter was ground and sifted (mesh=180 µm). Distilled water was added to the powder that was obtained at a proportion of 1:10 (powder mass: distilled water mass) at room temperature, and it was put in constant agitation for 6 h. Then it was left to sediment for 24 h, and later it was centrifuged at 14,000 g for 20

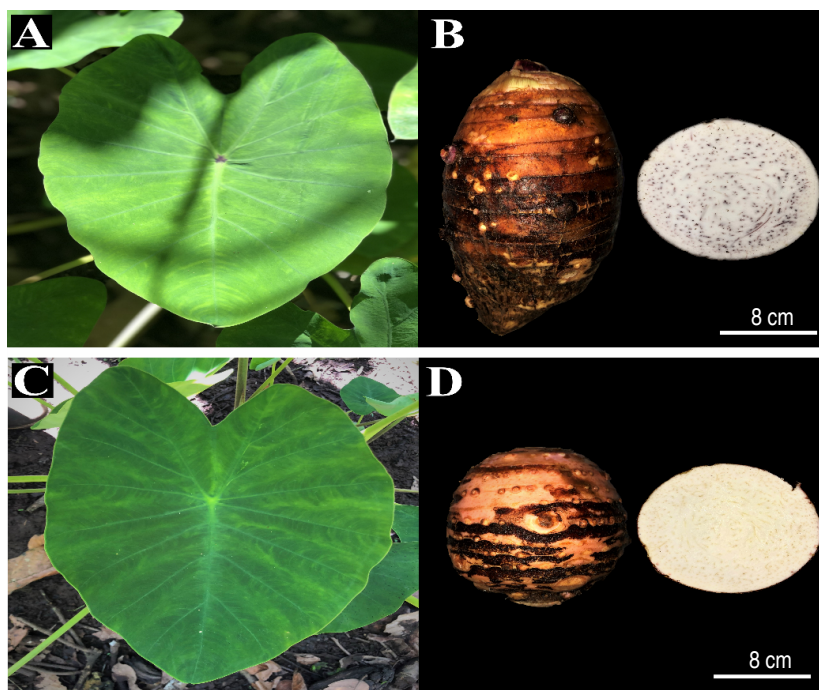


**Figure 1.** Plant and root. PTS (A, B) and WTS (C, D).

min (HETTICH, MIKRO 22 R, Germany). Finally, the solid fraction was dried at 50 °C for 24 h and the starch obtained was packaged in glass recipients with a screw-on top.

#### Analysis of the starch microstructure

The methodology described by Liu et al. (2018) was used, and the microstructures were observed using a scanning electron microscope (SEM) (Phenom-World B.V., Phenom ProX, Netherlands). The starches were fixed to the aluminum specimen holders with carbon tape, and they were covered with a gold film in a metallizer (Leica, EM ACE200, USA) for 5 min, with a 5 nm thickness. The micrographs were observed with increments from 4,000 and 4,500x, with an acceleration voltage of 15 kV while the images were obtained.

#### Chromaticity analysis

The color measurements were done using a colorimeter (Konica Minolta, Chroma meters CR-400, Japan); the basis for the measures was: luminosity ( $L^*$ ), red-green chroma ( $a^*$ ), and yellow-blue chroma ( $b^*$ ). The measurements were taken by placing the starches in a glass cell, focalizing the sources of the light, and covering the base of the glass cell with a white plaque.

The whiteness index (WI) was determined using Equation 1, reported by Guo et al. (2019).

$$WI = 100 - \sqrt{(100 - L^*)^2 + (a^*)^2 + (b^*)^2} \quad (1)$$

#### Analysis of the starch technological properties

##### Water absorption capacity (WAC)

The method proposed by Ashri et al. (2014) was utilized. For this, a suspension of starch with distilled water was prepared in a proportion of 1:15 (starch mass: water volume); it was agitated for 1 h and was centrifuged at 1,006 g for 15 min to eliminate the supernatant. The mass of the wet starch was recorded, and the WAC was expressed as a percentage using Equation 2.

$$WAC(\%) = \frac{\text{wet starch mass (g)}}{\text{dry starch mass (g)}} \times 100 \quad (2)$$

##### Solubility in cold water (S)

This was estimated according to the method recommended by Zhu et al. (2017a). To do this, the starch was dispersed in water at a concentration of 1% (w/w) and it was agitated at 100 rpm for 30 min at 25 °C, utilizing a magnetic agitator (Ultra-Turrax, IKA®, USA);

later the mix was centrifuged at 1,372 g for 10 min. The supernatant was poured onto a plaque and was dried at 105 °C for 4 h; finally, the dissolved solids were weighed, and the solubility was expressed as a percentage, according to Equation 3:

$$S(\%) = \frac{\text{dry supernatant mass (g)}}{\text{dispersed starch mass (g)}} \times 100 \quad (3)$$

#### Stability during freezing-thawing (Si)

The methodology described by Salgado-Ordosgoitia et al. (2018) was utilized. For this, a starch suspension was prepared at 5% (w/v); this was heated at 95 °C for 30 min in a water bath with constant agitation (MEMMERT, WNB 22, Germany). The gel obtained was cooled at 26±2 °C, from which, 2 g was placed in centrifuge tubes and was stored at 4 °C for 24 h. Later, they were frozen (LG, GR-5392QLC, South Korea) at -20 °C for 48 h. The thawing was done at 25 °C for 3 h and the samples were centrifuged at 2,360 g for 15 min. Finally, the separated water was weighed and the percentage of syneresis was calculated using Equation 4:

$$Si(\%) = \frac{\text{mass of the separated liquid water(g)}}{\text{mass of the starch from the gel (g)}} \quad (4)$$

#### Analysis of the starch thermal behavior

##### Thermal stability (TG/DTG)

For the thermogravimetric analysis, a calorimeter was used (SETARAM, Labsys EVO robot option, USA), following the methodology described by Londoño-Restrepo et al. (2014). For this, 5 mg of starch was weighed in an aluminum crucible and the samples were heated from 25 to 550 °C; the best heating velocity was 10 °C min<sup>-1</sup> with a nitrogen flow of 50 mL min<sup>-1</sup>. The mass loss was processed using Calisto software incorporated into the equipment. The maximum temperature for each thermal event was calculated on the DTG curve.

##### Analysis of gelatinization by DSC

The method proposed by Iturri et al. (2021) was used. For this, 10 mg of starch was weighed in an aluminum crucible, and to create the suspension, distilled water was added at a 1:3 ratio (starch mass: distilled water mass). The crucible was sealed and stored between 25 and 27 °C for 1 h. The calorimeter (SETARAM, Labsys EVO robot option, USA) was calibrated with indium (99.99%

purity, fusion temperature of 126.63 °C). The heating was programmed from 25 to 110 °C; the best heating velocity was 5 °C min<sup>-1</sup> in an inert environment with a nitrogen flow of 30 mL min<sup>-1</sup>. The gelatinization temperatures (onset, To; peak, Tp; and conclusion, Tc) and gelatinization enthalpy (ΔH) were calculated with the Calisto SETARAM software.

#### Statistical Analysis

All analyses were performed in triplicate and the values are reported as mean ± standard deviation. The t-student statistical analysis with paired variables proposed by Flores-Ruiz et al. (2017) was utilized to evaluate if a statistically significant difference existed between the two **taro varieties** concerning the size, WAC, S, Si, WI, and thermal behavior of the starch granules. The statistical test was performed using the Statistical software version 13 (StatSoftInc, Tulsa, OK, USA.) with 95% confidence.

## RESULTS AND DISCUSSION

### Morphological characterization and size distribution

The starches from both varieties of taro proved to be similar morphologically, presenting characteristics of irregular polyhedral granules with central cavities (Figure 2 and Table 1); this same morphology was also reported by Andrade et al. (2017) and Martins et al. (2020) in *C. esculenta* starch granules. Nonetheless, this morphological similarity is not common among the starch sources, for example, Zhu (2016) found differences in the morphology of starches due to the genetic variations between *Alocasia macrorrhiza*, *Amorphophallus campanulatus*, *Cyrtosperma merkusii*, and *Xanthosoma sagittifolium*.

The granules of PTS and WTS had similar size ranges in the inferior as well as superior limits; moreover, there was no proven significant statistical difference between them for the average arithmetic size (Table 1), nor did they prove to have the same size distribution (Figures 2C and 2D). For granules of PTS, a large percentage was in the size intervals of 1.13–1.47 μm (22.1%) and 1.81–2.14 μm (20.7%), while for granules of WTS, the greatest percentage was found in the size intervals of 1.21–1.57 μm (20.7%), 1.57–1.93 μm (23.6%) and 1.93–2.29 μm (18.6%). The difference in the size distribution between the PTS and WTS also was evidenced by the values difference of the diameter representative of the sample ( $D_{[3,2]}$ ). The interval for the diameters of the starch granules (Table 1) was within the range reported by Zhu et



**Table 1.** Morphologic characterization, size, chromaticity, technological and thermal properties of taro starch.

Morphology and Size	PTS*	WTS*
Form	Polyhedric with cavities and roundedness	Polyhedric with cavities and fissures
Size range ( $\mu\text{m}$ )	0.79-3.84	0.85-4.05
Average ( $\mu\text{m}$ )	1.97 $\pm$ 0.66 <sup>a</sup>	1.90 $\pm$ 0.63 <sup>a</sup>
$D_{[3,2]}$ ( $\mu\text{m}$ )	2.41	2.31
<b>Chromaticity</b>		
L*	99.72 $\pm$ 0.13 <sup>a</sup>	96.43 $\pm$ 0.08 <sup>b</sup>
a*	-0.59 $\pm$ 0.01 <sup>b</sup>	0.29 $\pm$ 0.02 <sup>a</sup>
b*	8.87 $\pm$ 0.04 <sup>a</sup>	8.92 $\pm$ 0.05 <sup>a</sup>
WI	91.10 $\pm$ 0.04 <sup>a</sup>	90.39 $\pm$ 0.06 <sup>b</sup>
<b>Technological properties</b>		
WAC (%)	127.8 $\pm$ 1.61 <sup>b</sup>	1.39 $\pm$ 0.53 <sup>a</sup>
S (%)	1.33 $\pm$ 0.21 <sup>b</sup>	3.20 $\pm$ 0.12 <sup>a</sup>
Si (%)	6.92 $\pm$ 1.22 <sup>a</sup>	6.24 $\pm$ 1.13 <sup>a</sup>
<b>Thermogravimetry</b>		
	$\Delta T$ ; (% m m <sup>-1</sup> )	$\Delta T$ ; (% m m <sup>-1</sup> )
$\Delta m_1$ (stage 1)	30-139 °C; (7.9%)	30.3-132.8 °C; (7.1%)
Stability (stage 2)	139-258.3 °C; (0.0%)	132.8-229.6 °C; (0.0%)
$\Delta m_2$ (stage 3)	258.3-360.1 °C; (54.8%)	229.6-380.0 °C; (64.4%)
$\Delta m_3$ (stage 4)	362.4-554.3 °C; (10.0%)	381.7-554.1 °C; (7.4%)
<b>Gelatinization (DSC)</b>		
T <sub>o</sub> (°C)	74.9 $\pm$ 0.4 <sup>b</sup>	76.1 $\pm$ 0.3 <sup>a</sup>
T <sub>p</sub> (°C)	78.6 $\pm$ 0.2 <sup>b</sup>	81.5 $\pm$ 0.5 <sup>a</sup>
T <sub>c</sub> (°C)	83.2 $\pm$ 0.3 <sup>b</sup>	88.0 $\pm$ 0.7 <sup>a</sup>
$\Delta H$ (J g <sup>-1</sup> )	2.7 $\pm$ 0.0 <sup>b</sup>	3.1 $\pm$ 0.1 <sup>a</sup>

Values in the same row with different super indices have statistically significant differences according to the t-student test ( $P < 0.05$ ). PTS\*: Purple taro starch, WTS\*: White taro starch.  $D_{[3,2]}$ : Sauter diameter; WI: Whiteness Index; WAC: Water retention capacity; S: Solubility; Si: Syneresis;  $\Delta T$ : Thermal decomposition temperature range; % m m<sup>-1</sup>: Percentage mass loss.

al. (2017b) (0.39–5.02  $\mu\text{m}$ ) in starch granules in three *C. esculenta* varieties originating from the Jiangsu province of China; in that study, the difference in granule sizes was also subjected to the *C. esculenta* varieties, as reported by Zhu (2016). According to Aboubakar et al. (2008), the size of starch granules that are highly digestible for kids and the elderly is between  $3 \leq d \leq 20 \mu\text{m}$ , which indicates that PTS and WTS are highly metabolized.

The size distribution of the starch granules had an important effect on the WAC since large granules have greater swelling causing greater water absorption, this can be visualized in Figure 2D, where the granules of WTS had a high percentage of larger granules and generated an elevated WAC (Table 1).

The increase in the WAC influenced the delay of the gelatinization process, increasing the typical temperatures for the process; for example, for the granules of WTS, the WAC was 139% with To, Tp, and Tc greater than for the granules of WTS which had a WAC of 127.8%. Also, the gelatinization enthalpy (Table 1) was affected by the increase in the WAC; this behavior was also reported by Calle et al. (2021) in starch of *Xanthosoma sagittifolium*.

#### Whiteness index

This parameter is related to starch purity; the chromaticity values are in Table 1. According to Sit et al. (2014), a value superior to 90.0 for this index reflects a high purity for the extracted starch. Consequently, the starches from the two varieties of this study (PTS and WTS) had

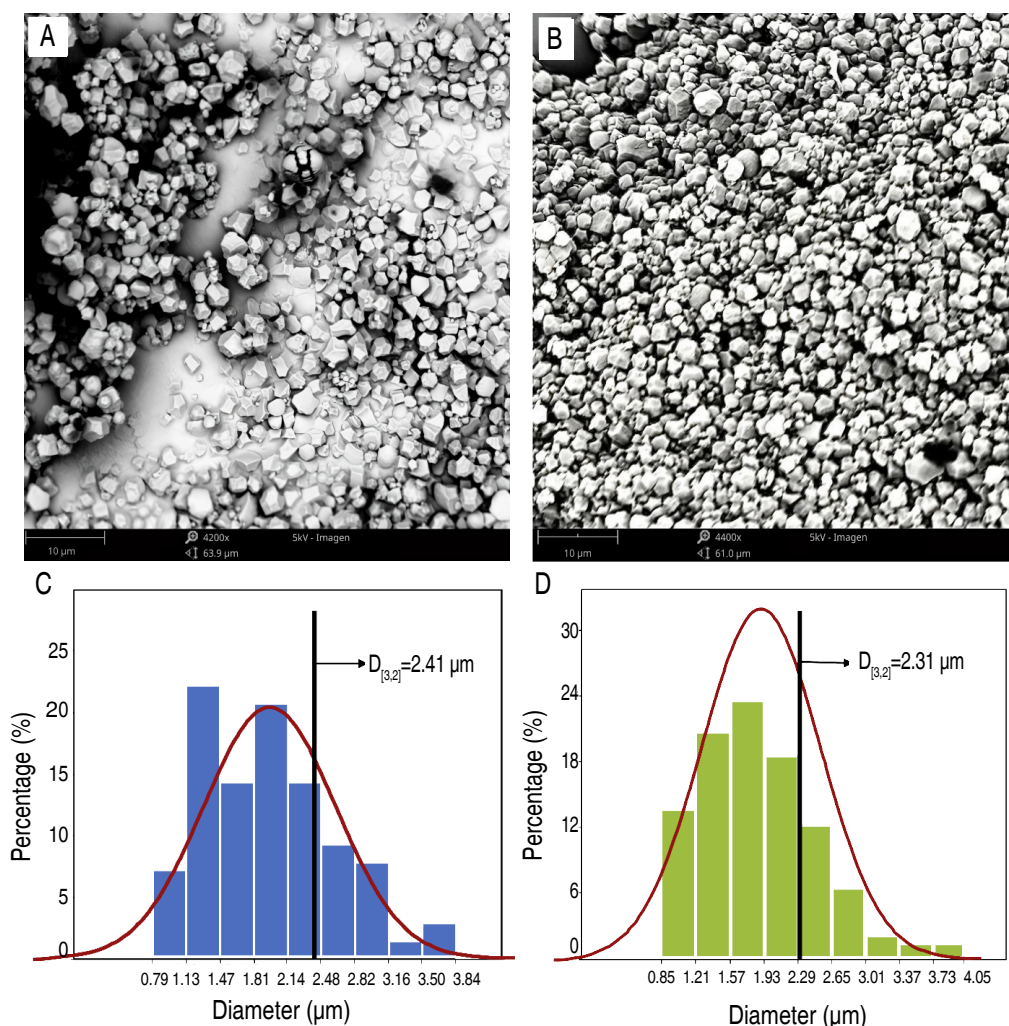


**Figure 2.** Morphology and size distribution of the starch granules. PTS (A, C) and WTS (B, D).

acceptable purities for their use in the food industry, as mentioned by Guo et al. (2019), given that they are framed within the acceptable range (PTS:  $WI=91.10\pm0.04$  and WTS:  $WI=90.39\pm0.06$ ). The differences in the  $a^*$  chroma between the varieties were due to the intensity of the non-enzymatic browning (Maillard reaction), which is related to the humidity content of the starch (Kim et al. 2013; Deka and Sit 2016). For example, the TG analysis for the PTS revealed a higher humidity, of 7.9%, with  $a^*=-0.59$ , and in the WTS it was 7.1% with  $a^*=0.29$ . Greater humidity content generates a greater WI due to the water reflection effect; this was corroborated by the data (PTS: 7.9% with  $WI=91.10$  and WTS: 7.1% with  $WI=90.39$ ).

On the other hand, a greater amylopectin content generates a greater opacity (less luminosity) in the starch, as was mentioned by Bultosa and Taylor (2003); this was corroborated by the DTG analysis (Figure 3), where the PTS presented a more acute area under the degradation curve and it had a greater luminosity, which is characteristic of the lower amylopectin content.

### Technological properties

#### Water absorption capacity

To establish the starch functionality when submitted to the thermal process it is necessary to quantify the WAC, which allows for the prediction of the capacity to be used as an emulsifier and in the formation of gels. According

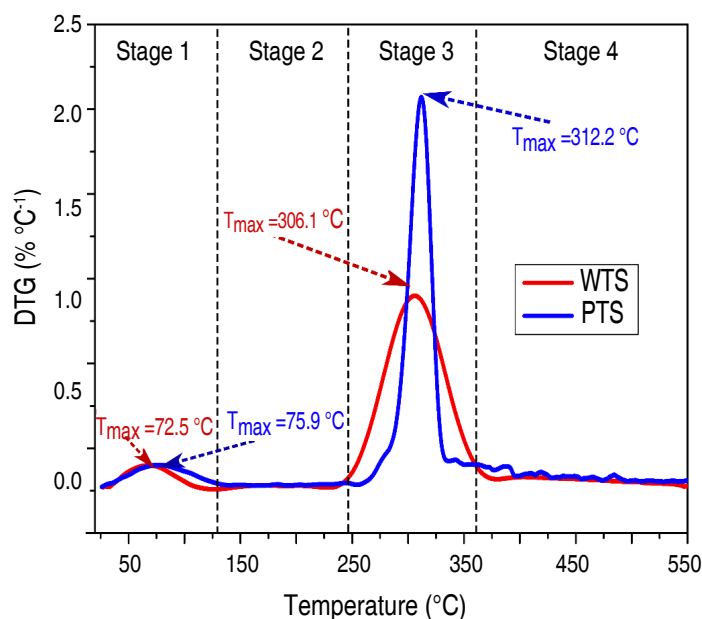


**Figure 3.** DTG of the starch from purple (PTS) and white taro (WTS).

to the results of the WAC, a statistical difference existed ( $P < 0.05$ ) between the PTS with  $1.28 \text{ g g}^{-1}$  (127.8%) and the WTS with  $1.39 \text{ g g}^{-1}$  (139.0%). These values were inferior to those reported by Calle et al. (2021) for *Colocasia* spp. Flour ( $1.75 \pm 0.15 \text{ g g}^{-1}$ ); this difference is related to the larger average size of the granules reported by these authors ( $117.24 \pm 8.62 \mu\text{m}$ ), which influences the greater WAC. The differences in the WAC between the PTS and WTS can also be explained because of the white variety's high percentage of larger-sized granules (Figure 2). On the other hand, the relationship proposed by Amon et al. (2014), as it presented a greater WAC, it is possible to consider that the WTS presents a greater quantity of hydrophilic constituents on the external surface of the granule (polysaccharides).

#### Solubility in cold water

Solubility is the capacity that the starch has to bond with the water, indicating the degree of association between amylose-amylopectin, crystallinity, and granule size (Rafiq et al. 2015; Wang et al. 2018). The greatest percentage of solubility was for the WTS, in comparison to the PTS; this is explained due to the greater amylopectin content (branched chain, more hydrogen bonds) (Figure 3) and

the smaller granule size of the starch ( $D_{[3,2]} = 2.31 \mu\text{m}$ ), making that the water gets in the starch granules. Studies done for other starch sources reported similar values for solubility, such as 2.67–3.86% for three varieties of *C. esculenta* (Falade and Okafor 2013), 1.25% for *Dioscorea alata* L., 3.70% for *Manihot esculenta*, and 2.97% for *Solanum tuberosum* (Alvis et al. 2008).

#### Stability during freezing-thawing

This parameter is important because it predicts a possible microbiological degradation (increase in water activity) and decreases in the sensory quality of the frozen foods after thawing due to the thermal variations, and the water changes phase, provoking the liberation of liquid water during storage (Gupta et al. 2021).

During the freezing and thawing process of the starches, the phenomenon evidenced is "syneresis," which is related to the loss of water due to exudation. The syneresis values did not reveal a statistical difference (Table 1); this can be attributed to the fact that during the freezing-thawing process, both samples had the same size of ice crystals, analogous to the average granule sizes of the starch (Table 1), and the same amylose-amylopectin crystalline structure as also reported by Liu et al. (2019).

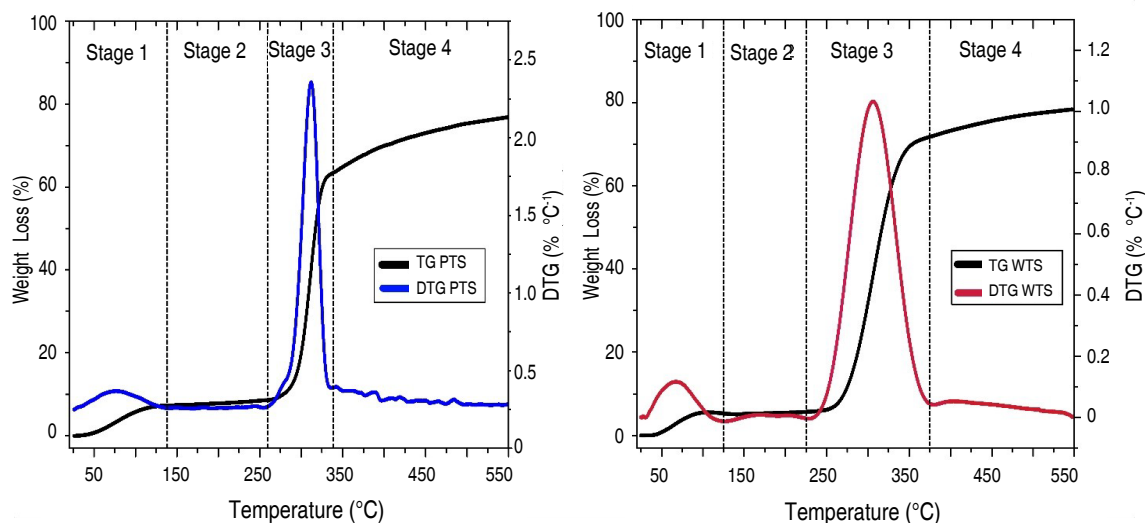
### Thermogravimetry (TG/DTG)

Table 1 shows the percentages of mass loss and the degradation temperature intervals, and in Figure 4 the TG and DTG are recorded with the stages of thermal degradation. The principal event of the first stage was water loss and volatile compounds; likewise, according to Liu et al. (2010), during this stage, there is rapid dehydration and decomposition of glucose hydroxyl groups which form water molecules, which are evaporated in this same stage of decomposition. The PTS presented a greater percentage of mass loss in comparison to the WTS, and the maximum decomposition temperatures were 75.9 and 72.5 °C, respectively (Figure 3). Andrade et al. (2017) and Elmi Sharlina et al. (2017), found similar weight loss percentages in the starch associated with the first stage.

In the second stage, the starch granules showed thermal stability, with no mass loss occurring (Table 1 and Figure 4). The PTS presented greater thermal stability in this stage, reaching a  $\Delta T$  range of 119.3 °C; while for the WTS, the  $\Delta T$  range was 96.8 °C. This behavior is explained by

the greater amylose content present in the PTS (Figure 3); curve with a slim base and greater height in stage 3, which generated a higher internal energy demand during the thermal destructuring in this stage. Moreover, the amylose-amylopectin proportion is 20/80, as reported by Singla et al. (2020), and the amylose has a linear chemical structure that generates greater resistance to thermal degradation. According to Martins et al. (2020), the differences in the temperature range during this stage are related to the crystallinity of the starch as a function of the disposition of amylose and amylopectin; these authors reported that the average typical temperature at the end of this stage is 251.9 °C; in this study, similar temperatures were found.

Londoño-Restrepo et al. (2014) indicated that the widening of the peak with a lower height in the third stage of thermal decomposition corresponds to a greater amylopectin content in the starch (Figure 3). In the third stage, a greater decomposition occurred, related to the loss of mass for the majority compound (amylose for the PTS and amylopectin for WTS); there was also a difference in the



**Figure 4.** TG/DTG thermogram of starch from purple (PTS) and white (WTS) Taro.

degradation temperature range of the starches (Figure 4 and Table 1). Studies related to the thermal behavior of the *C. esculenta* starch revealed similar values in the loss of mass and temperature range for this stage; the same which are associated in this stage with the degradation

of amylose and the breaking of the amylopectin chain (Liu et al. 2010; Andrade et al. 2017; Martins et al. 2020).

The fourth stage corresponded to the formation of inert carbonaceous waste and a slow decomposition

existed due to the formation of  $\text{CO}_2$  originating from the separation of oxygen from the amylose-amylopectin complex; the final waste from the pyrolysis process, with an absence of external oxygen flow, reached 27.3% for the PTS and 21.1% for WTS; according to Mukurumbira et al. (2017) and Xu et al. (2014), this difference can be attributed to the crystalline structure and the increase of the intermolecular interactions during the thermal decomposition of the starch's polymeric structure.

### Analysis of the gelatinization by DSC

The PTS and WTS presented a zone for endothermal energy exchange, corresponding to the gelatinization process (Figure 5). The typical temperatures for the endothermal peak,  $T_o$ ,  $T_p$  (peak temperature), and  $T_c$  revealed significant statistical differences between the

samples (Table 1). On top of presenting the greater amylose content, the WTS also had a greater  $T_p$ ; which generated a greater energy demand ( $3.1 \text{ J g}^{-1}$ ), given that the amylose acts as a dilutant (greater absorption of water molecules in the starch granules during the gelatinization). Coronell-Tovar et al. (2019) and Elmi Sharlina et al. (2017), also indicated that the different typical temperatures and the enthalpy during the gelatinization were associated with the amylose and amylopectin content, crystallinity degree, morphology, size distribution, and the water absorption capacity of the starch granules. The gelatinization enthalpy presented statistical differences between the PTS and the WTS (Table 1); these values for the enthalpy were similar to those reported by Jiang et al. (2012) in starch granules of *C. esculenta* and *D. bulbifera*, respectively.

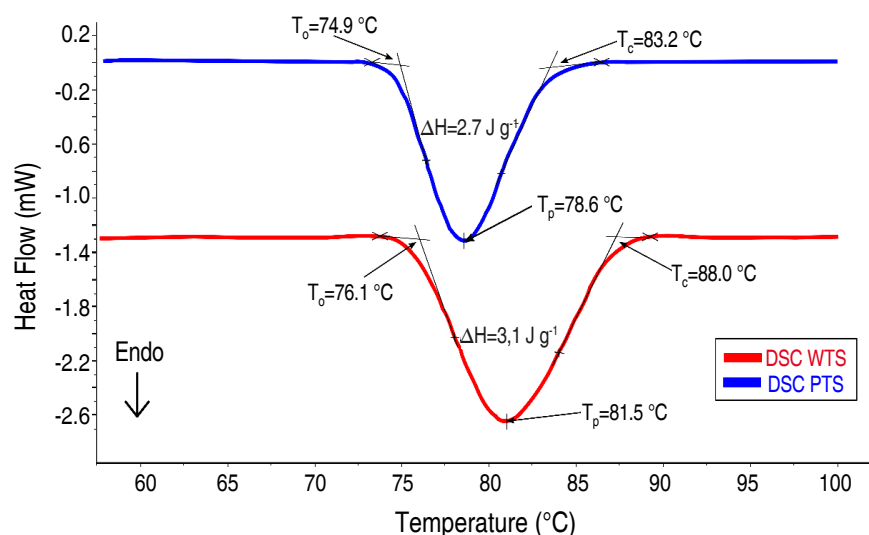


Figure 5. Endothermic peak during gelatinization of purple (PTS) and white (WTS) taro starches.

### CONCLUSION

The comparative study of purple (PTS) and white (WTS) sweet potato starches revealed significant similarities and differences in their morphological, technological, and thermal properties. Both varieties exhibited similar morphology, with polyhedral granules and cavities; however, WTS stood out for having larger granules, resulting in higher water-holding capacity (WHC) and opacity. Thermogravimetry showed higher thermal stability for PTS, whereas WTS differential scanning calorimetry exhibited a higher peak temperature ( $T_p$ )

and greater gelatinization enthalpy, suggesting higher energy requirements. These findings underscore the importance of considering the specific characteristics of each starch variety for effective application in the food industry and other technological areas.

### ACKNOWLEDGMENTS

This study was financed in part by the Universidad Nacional Agraria de la Selva (UNAS) in Peru. The authors thank the Laboratorio Central de Investigación at the UNAS for the opportunity to carry out the analyses for this study.



## REFERENCES

- Aoubakar, Njintang YN, Scher J and Mbofung CMF (2008) Physicochemical, thermal properties and microstructure of six varieties of taro (*Colocasia esculenta* L. Schott) flours and starches. *Journal of Food Engineering* 86: 294–305. <https://doi.org/10.1016/j.foodeng.2007.10.006>
- Alvis A, Vélez CA, Villada HS and Rada-Mendoza M (2008) Análisis físico-químico y morfológico de almidones de ñame, yuca y papa y determinación de la viscosidad de las pastas. *Información Tecnológica* 19: 19–28. <https://doi.org/10.4067/s0718-07642008000100004>
- Amon AS, Soro RY, Assemmand EF et al (2014) Effect of boiling time on chemical composition and physico-functional properties of flours from taro (*Colocasia esculenta* cv fouê) corm grown in Côte d'Ivoire. *Journal of Food Science and Technology* 51: 855–864. <https://doi.org/10.1007/s13197-011-0578-7>
- Andrade LA, Barbosa NA and Pereira J (2017) Extraction and properties of starches from the non-traditional vegetables Yam and Taro. *Polímeros* 27: 151–157. <https://doi.org/10.1590/0104-1428.04216>
- Ashri A, Yusof MSM, Jamil MS et al (2014) Physicochemical characterization of starch extracted from Malaysian wild yam (*Dioscorea hispida* Dennst.). *Emirates Journal of Food and Agriculture* 26: 652–658. <https://api.semanticscholar.org/CorpusID:12901363>
- Boahemaa LV, Dzandu B, Amissah JGN et al (2024) Physicochemical and functional characterization of flour and starch of taro (*Colocasia esculenta*) for food applications. *Food Humanity* 2: 100245. <https://doi.org/10.1016/j.foohum.2024.100245>
- Bultosa G and Taylor JRN (2003) Chemical and physical characterisation of grain tef [*Eragrostis tef* (Zucc.) Trotter] starch granule composition. *Research Paper. Starch* 55: 304–312. <https://doi.org/10.1002/star.200390065>
- Calle J, Benavent-Gil Y and Rosell CM (2021) Use of flour from cormels of *Xanthosoma sagittifolium* (L.) Schott and *Colocasia esculenta* (L.) Schott to develop pastes foods: Physico-chemical, functional and nutritional characterization. *Food Chemistry* 344: 128666. <https://doi.org/10.1016/j.foodchem.2020.128666>
- Choque-Quipe D, Obregón Gonzales FH, Carranza-Oropeza MV et al (2024) Physicochemical and technofunctional properties of high Andean native potato starch. *Journal of Agriculture and Food Research* 15: 100955. <https://doi.org/10.1016/j.jafr.2023.100955>
- Compart J, Singh A, Fetteke J and Apriyanto A (2023) Customizing starch properties: A review of starch modifications and their applications. *Polymers (Basel)* 15: 3491. <https://doi.org/10.3390/polym15163491>
- Coronell-Tovar DC, Chávez-Jáuregui RN, Bosques-Vega Á and López-Moreno ML (2019) Characterization of cocoyam (*Xanthosoma* spp.) corm flour from the nazareno cultivar. *Food Science and Technology* 39: 349–357. <https://doi.org/10.1590/fst.30017>
- Deka D and Sit N (2016) Dual modification of taro starch by microwave and other heat moisture treatments. *International Journal of Biological Macromolecules* 92: 416–422. <https://doi.org/10.1016/j.ijbiomac.2016.07.040>
- Elmi Sharlina MS, Yaacob WA, Lazim AM et al (2017) Physicochemical Properties of Starch from *Dioscorea pyriformis* tubers. *Food Chemistry* 220: 225–232. <https://doi.org/10.1016/j.foodchem.2016.09.196>
- Falade KO and Okafor CA (2013) Physicochemical properties of five cocoyam (*Colocasia esculenta* and *Xanthosoma sagittifolium*) starches. *Food Hydrocolloids* 30: 173–181. <https://doi.org/10.1016/j.foodhyd.2012.05.006>
- Flores-Ruiz E, Miranda-Novales M and Villasis-Keever M (2017) El protocolo de investigación VI: cómo elegir la prueba estadística adecuada. *Estadística inferencial. Revista Alergia México* 64: 364–370. <https://doi.org/10.29262/ram.v64i3.304>
- Guo J, Kong L, Du B and Xu B (2019) Morphological and physicochemical characterization of starches isolated from chestnuts cultivated in different regions of China. *International Journal of Biological Macromolecules* 130: 357–368. <https://doi.org/10.1016/j.ijbiomac.2019.02.126>
- Gupta RK, Guha P and Srivastav PP (2023) Effect of high voltage dielectric barrier discharge (DBD) atmospheric cold plasma treatment on physicochemical and functional properties of taro (*Colocasia esculenta*) starch. *International Journal of Biological Macromolecules* 253: 126772. <https://doi.org/10.1016/j.ijbiomac.2023.126772>
- Gupta V, Thakur R and Das AB (2021) Effect of natural deep eutectic solvents on thermal stability, syneresis, and viscoelastic properties of high amylose starch. *International Journal of Biological Macromolecules* 187: 575–583. <https://doi.org/10.1016/j.ijbiomac.2021.07.099>
- Huang G, Wang F, Yang R, Wang ZC, Fang Z et al (2024) Characterization of the physicochemical properties of Lipu *Colocasia esculenta* (L.) Schott starch: A potential new food ingredient. *International Journal of Biological Macromolecules* 254: 127803. <https://doi.org/10.1016/j.ijbiomac.2023.127803>
- Hui G, Zhu P and Wang M (2024) Structure and functional properties of taro starch modified by dry heat treatment. *International Journal of Biological Macromolecules* 261:129702. <https://doi.org/10.1016/j.ijbiomac.2024.129702>
- Iturri MS, Calado CMB and Prentice C (2021) Microparticles of *Eugenia stipitata* pulp obtained by spray-drying guided by DSC: An analysis of bioactivity and *in vitro* gastrointestinal digestion. *Food Chemistry* 334: 127557. <https://doi.org/10.1016/j.foodchem.2020.127557>
- Jiang Q, Gao W, Li X et al (2012) Characterizations of starches isolated from five different *Dioscorea* L. species. *Food Hydrocolloids* 29: 35–41. <https://doi.org/10.1016/j.foodhyd.2012.01.011>
- Kim J, Ren C and Shin M (2013) Physicochemical properties of starch isolated from eight different varieties of Korean sweet potatoes. *Starch* 65: 923–930. <https://doi.org/10.1002/star.201200217>
- Legesse T and Bekele T (2021) Evaluation of improved taro (*Colocasia esculenta* (L.) Schott) genotypes on growth and yield performance in North-Bench woreda of Bench-Sheko zone, South-Western Ethiopia. *Heliyon* 7: e08630. <https://doi.org/10.1016/j.heliyon.2021.e08630>
- Liu C, An F, He H et al (2018) Pickering emulsions stabilized by compound modified areca taro (*Colocasia esculenta* (L.) Schott) starch with ball-milling and OSA. *Colloids Surfaces A: Physicochemical Engineering Aspects* 556: 185–194. <https://doi.org/10.1016/j.colsurfa.2018.08.032>
- Liu X, Yu L, Xie F et al (2010) Kinetics and mechanism of thermal decomposition of cornstarches with different amylose/amylopectin ratios. *Starch* 62: 139–146. <https://doi.org/10.1002/star.200900202>
- Liu Y, Yang L, Ma C and Zhang Y (2019) Thermal behavior of sweet potato starch by non-isothermal thermogravimetric analysis. *Materials (Basel)* 12: 699. <https://doi.org/10.3390/ma12050699>
- Londoño-Restrepo SM, Rincón-Londoño N, Contreras-Padilla M et al (2014) Physicochemical, morphological, and rheological characterization of *Xanthosoma robustum* Lego-like starch. *International Journal of Biological Macromolecules* 65: 222–228. <https://doi.org/10.1016/j.ijbiomac.2014.05.006>

org/10.1016/j.ijbiomac.2014.01.035

Marboh V and Mahanta CL (2021) Physicochemical and rheological properties and in vitro digestibility of heat moisture treated and annealed starch of sohphlang (*Flemingia vestita*) tuber. International Journal of Biological Macromolecules 168: 486–495. <https://doi.org/10.1016/j.ijbiomac.2020.12.065>

Martins A, Beninca C, Bet CD et al (2020) Ultrasonic modification of purple taro starch (*Colocasia esculenta* B. Tini): structural, psychochemical and thermal properties. Journal of Thermal Analysis and Calorimetry 142: 819–828. <https://doi.org/10.1007/s10973-020-09298-3>

Moorthy SN, Sajeev MS and Anish RJ (2024) Chapter 14 - Functionality of tuber starches. Starch in Food 14: 327–375. <https://doi.org/10.1016/b978-0-323-96102-8.00022-x>

Mukurumbira A, Mariano M, Dufresne A et al (2017) Microstructure, thermal properties and crystallinity of amadumbe starch nanocrystals. International Journal of Biological Macromolecules 102: 241–247. <https://doi.org/10.1016/j.ijbiomac.2017.04.030>

Nagar CK, Dash SK, Rayaguru K et al (2021) Isolation, characterization, modification and uses of taro starch: A review. International Journal of Biological Macromolecules 192: 574–589. <https://doi.org/10.1016/j.ijbiomac.2021.10.041>

Naidoo K, Amonsou EO and Oyeyinka SA (2015) In vitro digestibility and some physicochemical properties of starch from wild and cultivated amadumbe corms. Carbohydrate Polymers 125: 9–15. <https://doi.org/10.1016/j.carbpol.2015.02.066>

Rafiq SI, Jan K, Singh S and Saxena DC (2015) Physicochemical, pasting, rheological, thermal and morphological properties of horse chestnut starch. Journal of Food Science and Technology 52: 5651–5660. <https://doi.org/10.1007/s13197-014-1692-0>

Salgado-Ordosgoitia RD, Rodríguez-Manrique JA, Cohen-Manrique CS and Mendoza-Ortega GP (2018) Characterization of the techno-functional properties of starch from purple yam (*Dioscorea alata*), Hawthorn yam (*Dioscorea rotundata*) and Diamante 22-type yam. DYNA 85: 143–152. <https://doi.org/10.15446/dyna.v85n207.72869>

Saraiva SC, da Silva AS, de Carvalho LH et al (2020) Morphological,

structural, thermal properties of a native starch obtained from babassu mesocarp for food packaging application. Journal of Materials Research and Technology 9: 15670–15678. <https://doi.org/10.1016/j.jmrt.2020.11.030>

Singh AK, Lee M, Jang D and Lee YS (2024) Non-conventional starch nanoparticles: Novel avenues towards improving sustainability of the food packaging sector. Trends in Food Science & Technology 143: 104273. <https://doi.org/10.1016/j.tifs.2023.104273>

Singla D, Singh A, Dhull SB et al (2020) Taro starch: Isolation, morphology, modification and novel applications concern - A review. International Journal of Biological Macromolecules 163: 1283–1290. <https://doi.org/10.1016/j.ijbiomac.2020.07.093>

Sit N, Deka SC and Misra S (2014) Combined effect of ultrasound and enzymatic pretreatment on yield and functional properties of taro (*Colocasia esculenta*) starch. Starch 66: 959–967. <https://doi.org/10.1002/star.201400085>

Wang X, Reddy CK and Xu B (2018) A systematic comparative study on morphological, crystallinity, pasting, thermal and functional characteristics of starches resources utilized in China. Food Chemistry 259: 81–88. <https://doi.org/10.1016/j.foodchem.2018.03.121>

Xu Y, Sismour EN, Grizzard C et al (2014) Morphological, structural, and thermal properties of starch nanocrystals affected by different botanic origins. Cereal Chemistry 91: 383–388. <https://doi.org/10.1094/CCEM-10-13-0222-R>

Zhu B, Liu J and Gao W (2017a) Process optimization of ultrasound-assisted alcoholic-alkaline treatment for granular cold water swelling starches. Ultrasonics Sonochemistry 38: 579–584. <https://doi.org/10.1016/j.ultsonch.2016.08.025>

Zhu F (2016) Structure, properties, and applications of aroid starch. Food Hydrocolloids 52: 378–392. <https://doi.org/10.1016/j.foodhyd.2015.06.023>

Zhu J, Zhang S, Zhang B et al (2017b) Structural features and thermal property of propionylated starches with different amylose/ amylopectin ratio. International Journal of Biological Macromolecules 97: 123–130. <https://doi.org/10.1016/j.ijbiomac.2017.01.033>



# Broiler feed proposal with vinasse

Propuesta de alimento con vinaza para pollos de engorde

<https://doi.org/10.15446/rfnam.v77n3.111204>

Nicolle Giraud<sup>1\*</sup> and María Alejandra Rodríguez<sup>1</sup>

## ABSTRACT

### Keywords:

Distilled must  
Metabolizable energy  
Nutritional contribution  
Particle size  
Poultry feed  
Production process

Considering previous studies on the potential use of vinasse in the agricultural sector, this study seeks to design a feed for broilers in three presentations according to the stages of the animal's feeding program (start 1-14, growth 15-30 and end 31-42 days) that includes vinasse in the formulation. To this end, soybeans were considered as a source of protein, a diet with metabolizable energy between 12,351.06 and 14,025.78 kJ·kg<sup>-1</sup>. The granulometry was determined according to the broiler management manuals, and the feed manufacturing process was specified in a block diagram and a flow diagram; in the same way, a test protocol for the use of the feed formulated in a sample of broilers of the Cobb breed. This research suggests that using vinasse in feed formulations for broilers could provide significant benefits to the agricultural sector.

## RESUMEN

### Palabras clave:

Mosto destilado  
Energía metabolizable  
Aporte nutricional  
Tamaño de partícula  
Alimento avícola  
Proceso de producción

Considerando estudios previos sobre el potencial uso de la vinaza en el sector agropecuario, este estudio busca diseñar un alimento para pollos de engorde en tres presentaciones de acuerdo con las etapas del programa de alimentación del animal (inicio 1-14, crecimiento 15-30 y finalización 31-42 días) que incluya vinaza en la formulación. Para ello, se consideró el grano de soya como fuente de proteína, una dieta con energía metabolizable entre 12.351,06 a 14.025,78 kJ·kg<sup>-1</sup>. Se determinó la granulometría de acuerdo con los manuales de manejo de pollos de engorde, y se especificó el proceso de fabricación del alimento en un diagrama de bloques y un diagrama de flujo; de igual forma se propone un protocolo de prueba para el uso del alimento formulado en una muestra de pollos de engorde de la raza Cobb. Esta investigación sugiere que el uso de la vinaza en las fórmulas de los beneficios para pollos de engorde podría aportar importantes beneficios al sector agrícola.

<sup>1</sup>Universidad Metropolitana, Caracas, Venezuela. [nicollegp05@gmail.com](mailto:nicollegp05@gmail.com) , [marodriguezded@unimet.edu.ve](mailto:marodriguezded@unimet.edu.ve) 

\*Corresponding author

Vinasse is a liquid residue resulting from the distillation process from molasses or fermented sugarcane juice (*Saccharum officinarum*) to obtain ethanol in the production of rum, tequila, brandy, cachaça or bioethanol (Aristizábal 2015). In the liquor industry, for every liter of ethanol produced, 12 to 15 L of vinasse is obtained as a residue. Vinasse is a brown liquid with a low pH, sweet odor, and high content of dissolved and suspended organic matter (Conadesuca 2016).

García and Rojas (2006) indicate that vinasse contains soluble inorganic substances such as potassium and calcium, organic substances resulting from the metabolic process of yeasts and other microorganisms, alcohol and residual sugars, some insoluble organic substances, and volatile organic substances. The presence of high content of organic matter, potassium, and calcium, as well as moderate amounts of nitrogen and phosphorus, make it a highly polluting waste for water (Rajagopal et al. 2014), and its effects include a decrease in luminosity, photosynthetic activity and dissolved oxygen. It also causes eutrophication of water, contributes to an increase in insect and vector populations, resulting in the development of diseases.

There are different types of technologies for the handling and use of distillery vinasse. García and Rojas (2006) and Leal et al. (2003) studied the potential use of vinasse and concluded that, due to the presence of elements such as calcium, magnesium, sodium, potassium, zinc, and copper in adequate quantities, in addition to compounds and plant constituents such as free fatty acids, carbohydrates, amino acids, proteins, lipids, sugars among others, it can be combined with raw materials in order to produce animal feed.

Giraud and Rodríguez (2023) physicochemically characterized the vinasse and evaluated some alternative uses using the Hierarchical Analytical Process Method (AHP), where they considered the evaluated physicochemical potential, ease of production, utility in the market, and environmental contribution of the possible products as criteria; in the same way, they took into account as alternatives for the use of vinasse, liquid fertilizer (fertigation), pellet fertilizers, organic matter for the production of biogas and feed for livestock. The alternative recommended by consensus of the experts according to the AHP methodology was the feed for small animals and birds, accrediting as a

key factor the high potential of the vinasse at the level of its physical-chemical characterization, particularly for its contribution of vegetable protein, fat, nutrients, and organic acids.

Likewise, previous studies indicate that the use of vinasse as part of the feed formulation for broilers increases their live weight and the efficiency of nutrient utilization by increasing digestibility and absorption, the latter attributed in part to the high contribution of B vitamins (Hidalgo et al. 2009; Rodríguez and Garcés 2015).

The design of feed for broilers is based on two aspects: 1) the need in Venezuela for an accessible source of protein such as chicken meat (Encovi 2022), and 2) the study by Hidalgo et al. (2009) shows that vinasse improves the immune system of chickens, which can be an important contribution since December 2022, Venezuelan poultry production has been impacted by a crisis of avian influenza (OPS 2023).

The Venezuelan poultry sector consists mainly of private companies that operate medium to large facilities for the production of chicken meat and eggs. On the other hand, within the diversity of breeds for broilers, there is the Cobb breed. In this breed, it is important to differentiate according to the commercial purpose between the male (meat production) and the female (egg production). They are characterized by their excellent growth rate with low-cost diets. Broiler diets are formulated to provide the energy and nutrients essential for broiler health and production efficiency. The basic nutritional components that birds require are water, amino acids, energy, vitamins, and minerals (Pronavicola 2018).

Based on what has been indicated, this study seeks to design a feed for broilers as an alternative use for vinasse. This approach would contribute to less management of this material as an environmental benefit and provide a lower-cost feed as an agro-industrial benefit.

## MATERIALS AND METHODS

The study proposes the design of a feed for broilers considering vinasse in its formulation, including: 1) the formulation of the product, 2) the design of the production process for the feed, and 3) a proposal to evaluate the efficacy of the product in the bird growth.



### Product formulation for broilers

Three formulations were designed according to the stage of the bird's feeding plan (Table 1), taking as a reference the diet for a) EB 34 hybrid chickens used in

the study by Hidalgo et al. (2009), b) laying hens of the Lohmann-Brown genetic line of Organización El Tunal (2023), and c) Japanese quails from the trial by Martins et al. (2017).

**Table 1.** Formulations designed for broiler feeding according to their different stages in the feeding program.

Raw materials (%)	Beginning (1-14 days)	Growth (15-30 days)	Finalized (31-42 days)
Ground corn	61.0	55.0	42.0
Soy	27.0	26.5	33.0
Wheat bran	3.0	4.5	6.0
Vinasse	5.0	10.0	15.0
Dicalcic phosphate	1.3	1.4	1.5
Calcium carbonate	1.3	1.2	1.2
Will	0.2	0.2	0.2
Vitamin and mineral premix (Hidalgo et al. 2009)	1.0	1.0	1.0
DL-Methionine	0.2	0.2	0.1

The broiler feed formulation was developed based on an extensive literature review and consultations with experts on the subject, resulting in a formulation for each stage of the poultry feeding program that meets the nutritional requirements of broilers, as shown in Table 1.

The amount of vinasse in the formulation is increased as the bird grows. The main physicochemical characteristics of this ingredient being those presented in Table 2. The amount of nutrients such as nitrogen, potassium, phosphorus, calcium,

iron, and manganese, which are required in broiler feed for its proper development, stand out in the composition of the vinasse used in the study (Vásquez 2018).

According to Hidalgo et al. (2009), the inclusion of vinasse in the feed favors the feed conversion ratio, which means a reduction in costs by substituting ingredients such as molasses and cane juice. Additionally, vinasse is easy to produce and does not require any prior treatment before its inclusion in the preparation of the food.

**Table 2.** The main characteristics of the vinasse considered for the formulation of broiler feed.

Physicochemical characteristic	Value
Humidity (%)	92.50
Protein (% w/w)	1.09
Carbohydrates (% w/w)	1.70
Ashes (% w/w)	1.20
Grease (ppm)	7,787.00
Total Nitrogen (ppm)	1,061.00
Potassium (ppm)	3,410.00
Phosphorus (ppm)	366.00
Calcium (ppm)	2,157.00
Manganese (ppm)	29.50
Iron (ppm)	19.06

Conversely, nitrogen-adjusted metabolizable energy (ME) was calculated for each formulation to quantify the total energy contribution (Table 3). The results indicate

that the reported values remain within the recommended range for achieving optimal broiler growth performance, as reported by Torres (2018).

**Table 3.** Energy input of broiler feed formulations at different stages of the feeding program.

Energy intake of macronutrients (kJ·kg <sup>-1</sup> )	Beginning (1-14 days)	Growth (15-30 days)	Finalized (31-42 days)
Ground corn	8,926.26	8,048.29	6,146.22
Soy	4,908.19	4,817.33	5,999.27
Wheat bran	90.43	135.65	180.45
Vinasse	66.99	133.98	200.97
<b>Metabolizable energy (adjusted for nitrogen)</b>	<b>13,991.87</b>	<b>13,135.25</b>	<b>12,526.91</b>

### Design of the production process for food

The broiler feed production process involves eight phases: raw material reception, storage, raw material cleaning, grinding, mixing, sieving, pelletizing, and packaging. To test this design, future researchers must consider the bromatological analysis of the product in its different presentations, then verify the nutritional composition, and the presence of possible contaminants, to know its physicochemical properties, and rule out any microbiological contamination.

Figure 1 shows the diagram of the proposed manufacturing process of a broiler feed.

### Process description

The process begins with the receipt and storage of dry macro ingredients and vitamins in separate silos, while the vinasse is received in tanker trucks and stored in a closed tank. The macro ingredients are cleaned to remove impurities and then screened to optimize the grinding process. Material with a size between 1.0 and 3.5 mm is transported directly to the weighing hopper, while larger particles of this size are crushed in a hammer mill. Material smaller than 1.0 mm in size is stored in a flour silo, as recommended for crumb and pellet feeds (Arbor Acres 2018). Vitamins and minerals are ground to a particle size of less than 3.5 mm, except for calcium carbonate which is supplied in particles of 2.0 to 4.0 mm (ISA Poultry 2010).

The macro-ingredients, vitamins, and vinasse are weighed and added to the industrial mixer according to the feed in

the feeding stage to be produced to obtain a homogeneous mixture of the feed. If the feed is produced in crumbs, it goes directly to a packing scale (feed for the initiation stage), in case the feed is required in mini pellets or pellets, it continues the production line. In the latter case, the coarse powder is heat-treated (maximum 80 °C) by adding steam to a spiral conveyor belt. The increase in temperature reduces the percentage of moisture in the powder and additionally, together with the pressure of the pelletizer, the pellet is compacted in a better way, increasing its density and therefore its quality.

Once heat-treated, the hot powder is turned into pellets in the pellet machine to the desired diameter and then left to stand in a counter-current cooler. The final product is passed through a rotary sieve to ensure the desired particle size, weighed, and packaged in bird feed bags.

### Proposal to evaluate the efficacy of the product in the growth of birds

The testing phase aims to provide an assessment of broiler feed that includes vinasse in its formulation, based on its impact on growth, feed conversion ratio, and overall health of the birds.

It is proposed to carry out the test in a chicken farm located in the state of Carabobo, Venezuela, where the average temperature is 31 °C, and there is a relative humidity of 59% (González 2017); the lighting and ventilation of the shed must be adequate (Pronavicola 2018). It includes a manual three-phase feeding system, *ad libitum*, with

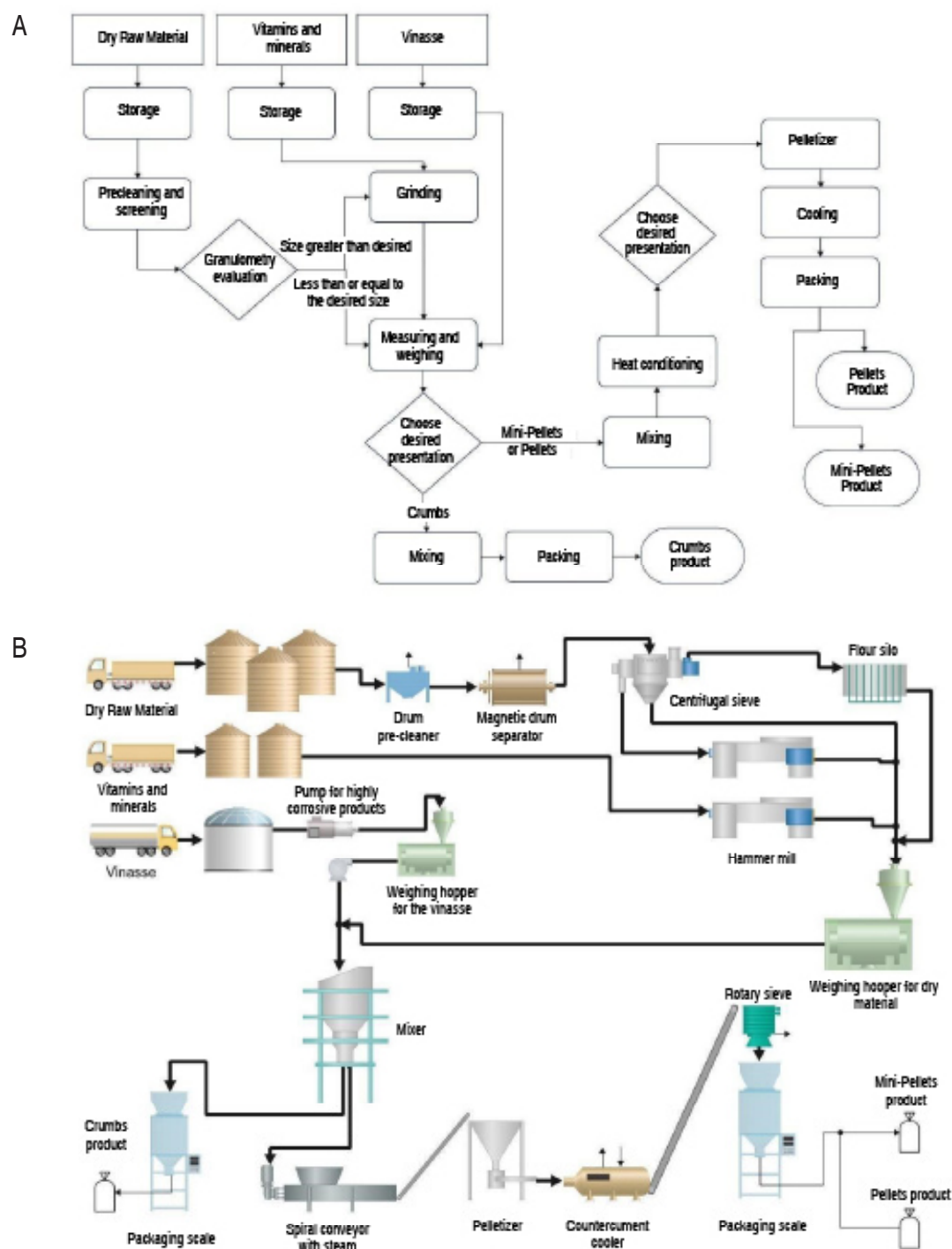


**Figure 1.** Diagram of the manufacturing process of a broiler feed. A) Block diagram and B) Flow diagram.

60 male chicks of the Cobb breed, and an experimental design of completely randomized blocks (Gutiérrez 2015), distributed in two equal groups: a control group and another

with the formulated feed. Each group is subdivided into three (subgroups of 10 chickens) to consider the repetitions of the trial covering the three stages of the poultry feeding

program: initiation from 1 to 14 days, growth from 15 to 30 days, and termination from 31 to 42 days (Vásquez 2018).

During the trial, the supply of vinasse is proportional to the percentage indicated according to the stage of the feeding program in Table 1 and the amount of feed is fixed according to the nutritional needs of the breed, distributed in four daily rations. Before starting the trial, both groups of animals (control and formulated feed) are weighed to determine the average starting weight, and the feeding carcass is cleaned to ensure accuracy in the evaluation. Throughout the trial, feed is weighed before and after feeding to the animals to measure product acceptance and calculate the feed conversion ratio. At the end of each growth stage and before changing the feed ratio, the animals are weighed again on an empty stomach to determine the final weight. It is recommended at the end of the trial (42 days) to slaughter ten animals from each group to determine the total yield in carcass, breast, thighs and legs, viscera, and abdominal fat.

In Venezuela, poultry farms are located in the coastal area (western, central, and eastern) due to their proximity to both the ports through which most inputs arrive and the cities that are centers of consumption (Álvarez 2014). Based on this, the state of Carabobo is proposed as a site to carry out the testing phase of the formulated food. Additionally, the farm must have adequate lighting and ventilation conditions that allow the desired development of the broiler.

Before starting the feed testing phase, researchers must select 60 healthy chicks with 1 day of life. Likewise, during the development of the test, they must consider the vaccination plan required to maintain the birds' health (Pronavicola 2018). Variables of interest are 1) the weight of the chicken before and after eating, 2) the weight of the chicken at the beginning and end of each feeding stage, and 3) the weight of the food consumed; With these variables, the aim is to calculate the acceptance of the product, the feed conversion ratio, and the growth of the chicken in the different stages of feeding, with which it can be defined as whether or not the formulated product meets the desired objective, that is, that the vinasse within the formulation of the feed for broiler feeding is beneficial.

## CONCLUSION

The study shows that it is possible to design a broiler feed containing vinasse that meets the essential nutritional

requirements. The amount of vinasse used in the feed aligns with the recommended daily dietary intake for broilers, which falls between 12,351.06 to 14,025.78 kJ•kg<sup>-1</sup>. A production process was developed for the feed in three different forms (initiation, growth, and completion), integrated into the standard broiler feed production line, and made ready for introduction to the market.

For future research, it is suggested to conduct a test phase to evaluate the effectiveness of the feed, as well as an economic study to assess its feasibility for broilers. It is also recommended to carry out field trials with varying proportions of vinasse in broiler feed, involving different genetic lines and/or other poultry species, to expand the scope of the study and provide practical application insights.

## ACKNOWLEDGMENTS

To Universidad Metropolitana, for its academic support and help during this research. To the organization El Tunal C.A. for providing valuable information and perspectives for this research.

## REFERENCES

- Álvarez R (2014) Sistemas de producción de aves en Venezuela. Departamento de Producción Animal. Universidad Central de Venezuela. [http://www.ucv.ve/fileadmin/user\\_upload/facultad\\_agronomia/PDI/2014/Clase\\_VI\\_Aves.pdf](http://www.ucv.ve/fileadmin/user_upload/facultad_agronomia/PDI/2014/Clase_VI_Aves.pdf)
- Arbor Acres (2018) Manual de manejo del pollo de engorde. Aviagen. [https://eu.aviagen.com/assets/Tech\\_Center/BB\\_Foreign\\_Language\\_Docs/Spanish\\_TechDocs/AA-BroilerHandbook2018-ES.pdf](https://eu.aviagen.com/assets/Tech_Center/BB_Foreign_Language_Docs/Spanish_TechDocs/AA-BroilerHandbook2018-ES.pdf)
- Aristizábal CE (2015) Caracterización físico-química de una vinaza resultante de la producción de alcohol de una industria licorera, a partir del aprovechamiento de la caña de azúcar. Ingenierías USBMed 6(2): 36–41. <https://doi.org/10.21500/20275846.1729>
- Conadesuca - Comité Nacional para el Desarrollo Sustentable de la Caña de Azúcar (2016) Vinazas, alternativas de uso. [https://www.gob.mx/cms/uploads/attachment/file/171932/Nota\\_Informativa\\_Septiembre\\_Vinazas.pdf](https://www.gob.mx/cms/uploads/attachment/file/171932/Nota_Informativa_Septiembre_Vinazas.pdf)
- Cortés A, Águila R and Ávila E (2002) La utilización de enzimas como aditivos en dietas para pollos de engorda. Veterinaria México 33(1): 1-9. Universidad Nacional Autónoma de México. <https://www.redalyc.org/articulo.oa?id=42333101>
- Encovi (2022) Condiciones de vida de los venezolanos Proyecto ENCOVI 2022. Universidad Católica Andrés Bello. [https://assets.website-files.com/5d14c6a5c4ad42a4e794d0f7/636d0009b0c59ebfd2f24acd\\_Presentation%20ENCOVI%202022%20completa.pdf](https://assets.website-files.com/5d14c6a5c4ad42a4e794d0f7/636d0009b0c59ebfd2f24acd_Presentation%20ENCOVI%202022%20completa.pdf)
- García A and Rojas C (2006) Posibilidades del uso de la vinaza en la agricultura de acuerdo con su modo de acción en suelos. Tecnicaña. 10: 125-145. <https://www.siiiba.conadesuca.gob.mx/siiaca/Consulta/verDoc.aspx?num=655>
- García H and Gómez J (2013) Propuesta para el consumo de Glycine max L (Soya), cultivado en la comunidad Nueva Esperanza, Jiquilisco

Usulután y tres alimentos derivados [Trabajo de Grado]. Universidad de El Salvador. <https://repositorio.ues.edu.sv/items/07a246ad-2fca-4b4a-a8e7-64d858ba6149>

Giraud N and Rodríguez M (2023) Evaluación de las alternativas de uso de la vinaza utilizando el método del proceso analítico jerárquico (AHP). *Revista Tekhné* 26(1): 59–78. <https://doi.org/10.62876/tekhn.v26i1.6118>

Gómez R, Cortés A, López C and Ávila E (2011) Evaluación de tres programas de alimentación para pollos de engorda con base en dietas sorgo-soya con distintos porcentajes de proteína. *Veterinaria México* 42(4): 299-309. [http://www.scielo.org.mx/scielo.php?script=sci\\_arttext&pid=S0301-50922011000400005&lng=es&tlng=es](http://www.scielo.org.mx/scielo.php?script=sci_arttext&pid=S0301-50922011000400005&lng=es&tlng=es).

González L (2017) Efecto del tiempo de restricción de alimento en pollos de engorde comerciales en condiciones tropicales. [Trabajo de Maestría]. Universidad Central de Venezuela. [http://saber.ucv.ve/bitstream/10872/16574/1/T026800017172-0-Final\\_Defensa-000.pdf](http://saber.ucv.ve/bitstream/10872/16574/1/T026800017172-0-Final_Defensa-000.pdf)

Gutiérrez J (2015) Diseños de bloques al azar. Universidad Autónoma del Estado de México. <http://ri.uaemex.mx/bitstream/handle/20.500.11799/31401/secme-17390.pdf?sequence=1#:~:text=la%20aleatorización%20de>

Hidalgo K, Rodríguez B, Valdivié M et al (2009) Utilización de la vinaza de destilería como aditivo para pollos en ceba. *Revista Cubana de Ciencia Agrícola* 43(3): 281-284. ISSN:0034-7485. <https://www.redalyc.org/articulo.oa?id=193015481011>

Ibarra-Camacho R and León-Duarte L (2018) Caracterización químico-física de vinazas de destilerías. *Ciencia en su PC* 1(2): 1–13. <https://www.redalyc.org/journal/1813/181358410001/html/>

ISA Poultry (2010) ISA BROWN Guía de manejo de la nutrición de ponedoras comerciales. Genética Hendrix. <https://www.avicolatoscana.com/wp-content/uploads/2020/02/Guia-de-Manejo-General-de-ponedoras-comerciales-ISA-Brown.pdf>

Leal I, Chirinos E, Leal M et al (2003) Caracterización fisicoquímica de la vinaza del Agave cocui y su posible uso agroindustrial. *Multiciencias* 3(2): 1317-2255. <https://www.redalyc.org/articulo.oa?id=90430202>

Martins PC, de Oliveira MC, da Silva DM et al (2017) Use of liquid vinasse as a feed additive for Japanese quails *Revista Colombiana de Ciencias Pecuarias* 30(4). <https://doi.org/10.17533/udea.rccp.v30n4a03>

Mex-Álvarez R, Garma-Quen P, Bolívar-Fernández N et al (2016) Análisis proximal y fitoquímico de cinco variedades de maíz del Estado de Campeche (México). *Revista Latinoamericana de Recursos Naturales*, 12(2), 76.

NRC - Consejo Nacional de Investigación (1994) *National Research Council Nutrient Requirements of Poultry – Ninth Revised Edition* (1994) 3(1): 101. <https://doi.org/10.1093/japr/3.1.101>

Organización El Tunal (2023) Dieta formulada FGPP-3320 [Conjunto de datos].

OPS - Organización Panamericana de la Salud (2023) OPS emite alerta ante brotes de influenza aviar en aves de diez países de las Américas. <https://www.paho.org/es/noticias/17-1-2023-ops-emite-alerta-ante-brotes-influenza-aviar-aves-diez-paises-americas>

Pronavicola (2018) Pollo de engorde, Guía de manejo. Cobb Una familia Un propósito. <https://pronavicola.com/manuales/manualcoob.pdf>

Rajagopal V, Paramjit SM, Suresh KP et al (2014) Significance of vinasses waste management in agriculture and environmental quality-Review. *African Journal of Agricultural Research* 9(38): 2862–2873. <https://doi.org/10.5897/ajar2014.8819>

Rodríguez AM and Solarte S (2019) Análisis proximal del salvado de trigo, Guías, Proyectos, Investigaciones de Análisis de Ingeniería. Universidad del Valle. Análisis proximal del salvado de trigo | Guías, Proyectos, Investigaciones de Análisis de Ingeniería | Docsity

Rodríguez H and Garcés DE (2015) Parámetros productivos y digestibilidad de proteínas al incluir vinaza de achicoria en dietas para pollos de carne en etapa de engorda. Universidad de Concepción.

Torres DM (2018) Exigencias nutricionales de proteína bruta y energía metabolizable para pollos de engorde. *Revista de Investigación Agraria y Ambiental* 9(1): 106–113. <https://doi.org/10.22490/21456453.2052>

Vásquez E (2018) Fases de alimentación en pollos de engorde [Trabajo de Grado]. Universidad Autónoma Agraria Antonio Narro. México. <https://oai.uaan.mx/bitstream/handle/123456789/45221/V%c3%a1zquez%20Mendoza%20Eduardo.pdf?sequence=1&isAllowed=y>

Velasco V and Soto V (2015) Rendimiento y parámetros de calidad de carne de pollos alimentados con vinaza de achicoria (*Cichorium intybus*) en su etapa de engorda [Trabajo de Grado]. Universidad de Concepción.





# Leaf spectrum analysis of three tropical timber species: Diomate (*Astronium graveolens*), Choibá (*Dipteryx oleifera*), and Algarrobo (*Hymenaea courbaril*)

Análisis del espectro foliar de tres especies tropicales maderables:  
Diomate (*Astronium graveolens*), Choibá (*Dipteryx oleifera*), y  
Algarrobo (*Hymenaea courbaril*)

<http://doi.org/10.15446/rfnam.v77n3.112180>

Estefany Johana Alzate-Marin<sup>1</sup>, Luis Jairo Toro-Restrepo<sup>1</sup> and July Andrea Suárez-Gómez<sup>1</sup>

## ABSTRACT

### Keywords:

Classification  
Leaves  
Separability  
Spectral signature  
Spectroradiometry  
Tropical forest




This study analyzed the leaf spectral response of three native timber forest species in the tropical dry forest: Diomate (*Astronium graveolens* Jacq.), Choibá (*Dipteryx oleifera* Benth.), and Algarrobo (*Hymenaea courbaril* L.). The study was conducted at the León Morales Soto Arboretum and Palmetum, at the Universidad Nacional de Colombia in Medellín, Antioquia, Colombia. Spectral data from the leaves were collected *in situ* using the portable spectroradiometer ASD FieldSpec HandHeld-2, which operates with a spectral resolution of 1 nm (resampled to 10 nm) and covers a spectral range between 325 and 1,075 nm (limited to 400-900 nm). Based on the measurements, the behavior and spectral variability of the species were evaluated. One-factor Analysis of Variance and Mann-Whitney-Wilcoxon U-test were implemented in reflectance spectra to select the optimal narrow bands for species discrimination. The classification capacity of the selected narrow bands was assessed using the K-nearest neighbors' algorithm. It was found that *A. graveolens* and *H. courbaril* exhibited spectral signatures typical of healthy vegetation, while *D. oleifera* showed spectral changes during the early stages of senescence. Regarding spectral separability, 23 narrow bands in the visible region and near-infrared region were identified as optimal for distinguishing the plant species. The supervised classification algorithm applied to these 23 narrow bands achieved an overall accuracy of 95.8%. In conclusion, these findings provide valuable insights into the spectral response of important tropical species and contribute to their conservation efforts by enhancing understanding of their unique spectral characteristics in diverse and heterogeneous ecosystems like tropical forests.

## RESUMEN

### Palabras clave:

Clasificación  
Hojas  
Separabilidad  
Firma espectral  
Espectrorradiometría  
Bosque tropical

Esta investigación analizó la respuesta espectral foliar de tres especies forestales maderables nativas del bosque seco tropical, Diomate (*Astronium graveolens* Jacq.), Choibá (*Dipteryx oleifera* Benth.) y Algarrobo (*Hymenaea courbaril* L.). El estudio se efectuó en el Arboretum y Palmetum León Morales Soto de la Universidad Nacional de Colombia, sede Medellín, Antioquia, Colombia. Los datos espectrales de las hojas se colectaron *in situ* con el espectrorradiómetro portátil ASD FieldSpec HandHeld-2, que trabaja con una resolución espectral de 1 nm (remuestreada a 10 nm) y un rango espectral entre 325 y 1.075 nm (acotado entre 400 y 900 nm). A partir de las mediciones, se evaluó el comportamiento y la variabilidad espectral de las especies. Se implementó el Análisis de Varianza de un factor y la prueba U de Mann – Whitney – Wilcoxon en los espectros de reflectancia con el fin de seleccionar las bandas estrechas óptimas para discriminar las especies. Se evaluó la capacidad de clasificación de las especies en las bandas estrechas seleccionadas, utilizando el algoritmo de los K vecinos más cercanos. Encontrando que *A. graveolens* e *H. courbaril* presentaron firmas espectrales típicas de la vegetación saludable y *D. oleifera* evidenció cambios espectrales en el período inicial de la senescencia. Respecto a la separabilidad espectral, se encontraron 23 bandas estrechas en la región visible e infrarrojo cercano óptimas para diferenciar las especies vegetales. El algoritmo de clasificación supervisada aplicado en las 23 bandas estrechas, tuvo una precisión general del 95,8%. En conclusión, estos hallazgos proporcionan valiosos conocimientos sobre la respuesta espectral de importantes especies tropicales y contribuyen a sus esfuerzos de conservación al mejorar la comprensión de sus características espectrales únicas en ecosistemas diversos y heterogéneos como el bosque tropical.

<sup>1</sup>Facultad de Ciencias Agrarias, Departamento de Ciencias Forestales, Universidad Nacional de Colombia, Medellín, Colombia. [ejalzatem@unal.edu.co](mailto:ejalzatem@unal.edu.co) , [ljtoro@unal.edu.co](mailto:ljtoro@unal.edu.co) , [jasuarezgom@unal.edu.co](mailto:jasuarezgom@unal.edu.co) 

\*Corresponding author

Aggarwal (2004) explains that every object possesses a distinct spectral response, which is determined by the energy reflected or emitted at different wavelengths. In the realm of remote sensing, artificial sensors capture radiation within specific contiguous bands and convert it into either multi or hyperspectral images, or numerical data that can be processed using computers. Through digital manipulation of this information, reflectance curves or spectral signatures can be generated, which have found widespread application in local and regional vegetation studies.

Remote sensing involves the use of aerial and satellite sensors to capture images of the Earth's surface, and these images can have different spectral resolutions, such as multi or hyperspectral (Nalepa 2021). On the other hand, spectroradiometry is a field within remote sensing that utilizes portable devices known as spectroradiometers. These instruments can measure the radiant energy flux at the surface of objects, specifically focusing on leaf samples in this particular investigation.

In tropical regions, the majority of spectral investigations have primarily focused on analyzing the canopy level through the processing of aerial and satellite imagery. This approach is driven by the complex structure and diversity of tropical forests, which present challenges in acquiring and analyzing spectral data at the leaf level. Consequently, remote sensing emerges as a valuable tool for gathering information in these ecosystems, offering advantages in terms of efficiency and cost-effectiveness compared to direct data collection methods.

Spectral investigations conducted at the leaf level using the spectroradiometry technique find greater applicability in extratropical forests. These ecosystems exhibit a higher degree of species homogeneity, making fieldwork for capturing spectral readings more feasible. Additionally, the measuring instrument used typically possesses a high spectral resolution, enabling precise quantification of even minor variations in reflectance across the electromagnetic spectrum (O'Shaughnessy and Rush 2014). This enhanced spectral resolution significantly enhances the predictive capabilities during data analysis.

In recent years, spectroradiometry has found applications in various areas such as species identification, phenology

tracking, and monitoring the phytosanitary status of vegetation (Clark et al. 2005; Clark and Roberts 2012; Lu et al. 2017). Most of these studies have been conducted in the Americas, Southeast Asia, and the western fringe of Europe. Spectral signatures have been documented in the tropical dry forest for species such as Diomite (*Astronium graveolens*), Cedro Rojo (*Cedrela odorata*), Ceiba (*Ceiba pentandra*), Nogal Cafetero (*Cordia alliodora*), Algarrobo (*Hymenaea courbaril*), and Caoba (*Swietenia macrophylla*). In the tropical rainforest, species like Caucho (*Castilla elastica*), Choibá (*Dipteryx oleifera*), Olla de Mono (*Lecythis ampla*), Surá (*Terminalia oblonga*) and Suribio (*Zygia longifolia*) have been studied. Genera such as *Quercus*, *Pinus*, and *Acer* have been investigated in temperate forests. Spectral studies have also focused on the Rhizophoraceae family in the mangrove ecosystem (Clark and Roberts 2012; Papeş et al. 2013; Prasad and Gnanappazham 2014; Ferreira et al. 2016; Miyoshi et al. 2020).

The tropical ecosystem is recognized as a significant source of species with valuable characteristics such as hardness, strength, and durability, making them highly sought after in both the market and scientific communities, leading to numerous studies focusing on the spectral characterization of leaves and wood. However, the findings reported so far lack generalizability due to the adoption of different methodologies (Clark and Roberts 2012), limiting comparisons with other studies (Rasaiah et al. 2014). It is important to research the spectral behavior of plant species at different phenological stages, particularly in the case of *D. oleifera*, and to explore data processing techniques, especially supervised classification with K-nearest neighbors, which have been underutilized in spectroradiometry.

This study aims to analyze the leaf spectra of three timber forest species (*A. graveolens*, *H. courbaril*, and *D. oleifera*) native to tropical dry forests using spectroradiometry, a technique commonly applied in ecosystems with higher homogeneity. The study had the following specific aims: a) to examine the spectral characterization of leaf samples using spectroradiometry, b) to identify the narrow bands that exhibit the best discriminatory power for distinguishing between the species, c) to evaluate the spectral discrimination ability of the species in the selected narrow bands. The hypothesis evaluated in this research is that spectroradiometry is a reliable technique

for separating and classifying leaves from different forest species.

## MATERIALS AND METHODS

### Study area

The research was conducted at the León Morales Soto Arboretum and Palmetum of the Universidad Nacional

de Colombia, located in Medellín, Antioquia, Colombia (Figure 1). The study area climate is characterized by a mean annual air temperature of 19 °C and a mean annual precipitation of 1,752 mm (IDEAM 2010). These climatic conditions classify the area as belonging to the Premontane Rainforest (bh-PM) life zone, according to the Holdridge classification system.

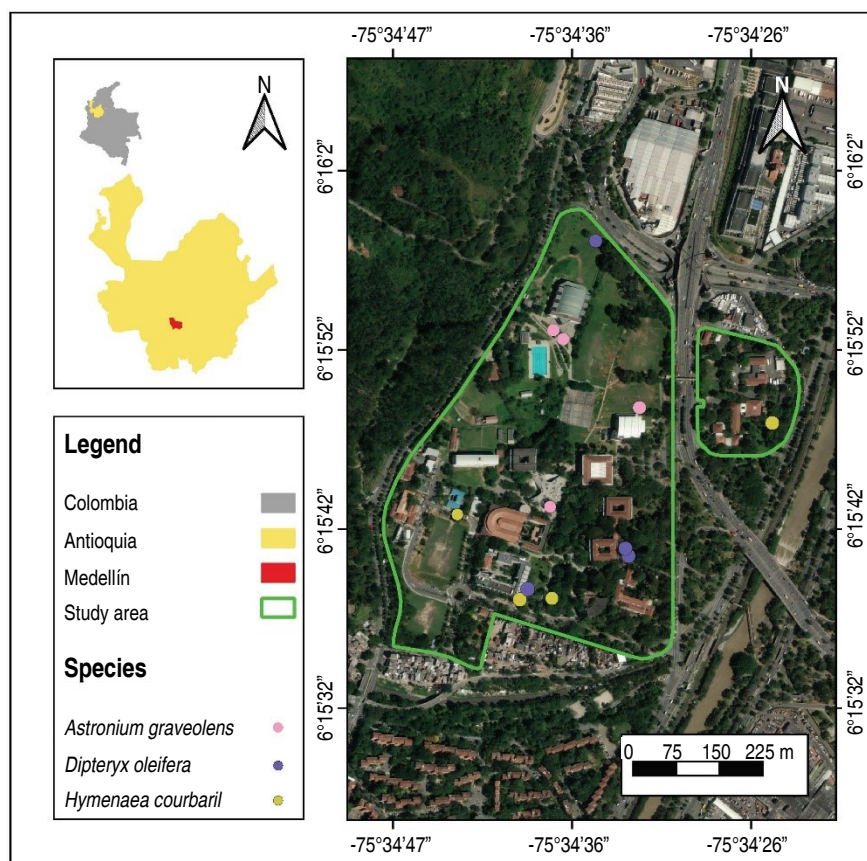


**Figure 1.** Location of tree species in the León Morales Soto Arboretum and Palmetum of the Universidad Nacional de Colombia, Medellín, Antioquia, Colombia.

### Selection of forest species

A literature review was conducted to identify tropical timber tree species that have undergone spectral analysis. The studies indicate that sample size varies depending on the number of available individuals at each site, such as at the Arboretum and Palmetum León Morales Soto, where, despite species diversity, the collection has a limited number of individuals. Sample size recommendations range from one to five individuals per species and from 3 to 15 leaves per tree (Castro-Esau et al. 2006; Féret and

Asner 2011). Based on this review, four individuals per species and three leaves per tree were selected at the Universidad Nacional de Colombia, Medellín Headquarters. The selected species are listed in Table 1.

Diomate (*A. graveolens*) is a forest species belonging to the Anacardiaceae family (Figure 2A). It is characterized by compound, alternate, imparipinnate leaves that are arranged spirally. The leaves are composed of 11 to 15 lanceolate, acuminate, and serrate leaflets (Gómez and



**Table 1.** List of forest species with their abbreviations, identification codes in the León Morales Soto Arboretum and Palmetum, common names, scientific names, and references consulted.

Abbreviation	Codes	Common name	Scientific name	References
Asg	760, 761, 933, 1911	Diomate	<i>Astronium graveolens</i> Jacq.	Castro-Esau et al. 2006; Ferreira et al. 2016
Dip	425, 1397, 1408, 1785	Choibá	<i>Dipteryx oleifera</i> Benth.	Clark et al. 2005; Clark and Roberts 2012
Hyc	165, 282, 422, 1105	Algarrobo	<i>Hymenaea courbaril</i> L.	Papeş et al. 2013; Ferreira et al. 2016; Miyoshi et al. 2020

Toro 2008). According to the IUCN Red List, Diomate holds a classification of Least Concern (LC) (Machuca et al. 2022) and plays a vital role in the ecological restoration of the tropical dry forest in Colombia.

Choibá (*D. oleifera*) is a member of the Fabaceae family (Figure 2B) and is characterized by compound, alternate, imparipinnate leaves. The petiole is smooth, winged, and grooved, while the rachis is winged and bears 4-8 pairs of elliptic leaflets (Cogollo et al. 2004).

Choibá is classified as a Vulnerable Species (VU) in the Colombian Red Book of Plants (Cárdenas and Salinas 2007). On the other hand, Algarrobo (*H. courbaril*) is a forest species belonging to the Fabaceae family (Figure 2C). It exhibits compound, alternate, and paripinnate leaves, with a pair of elliptical leaflets 3–12 cm long and 1.5–7 cm wide (Gómez and Toro 2008). According to the IUCN Red List, Algarrobo is classified as Least Concern (LC) (Bachman 2023) and plays a crucial role in the restoration of the tropical dry forest in Colombia.

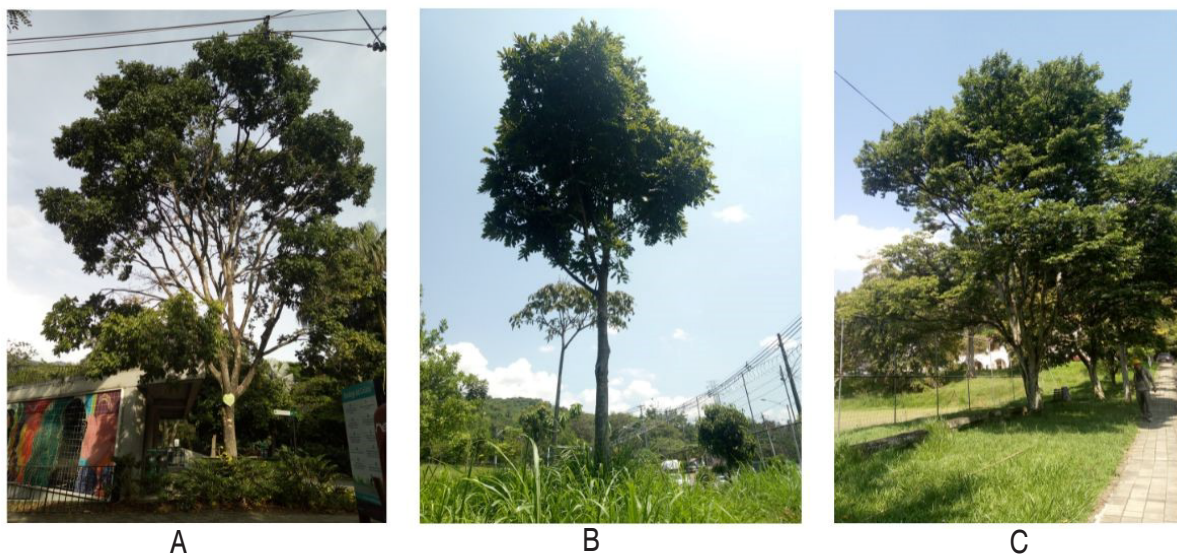


**Figure 2.** Forest species selected for foliar sampling: A) *A. graveolens*, B) *D. oleifera*, and C) *H. courbaril*.

### Foliar sampling

In this study, a total of four individuals from each of the three tree species were selected. Branches were extracted from the middle third of the canopy of each tree, specifically, those directly exposed to solar radiation. A minimum of three leaflets were collected

from these branches to capture the spectral reflectance data (Figure 3).

The collected leaves were carefully wiped with gauze, and then placed in moist cotton and polyester towels. They were subsequently stored in labeled polyethylene



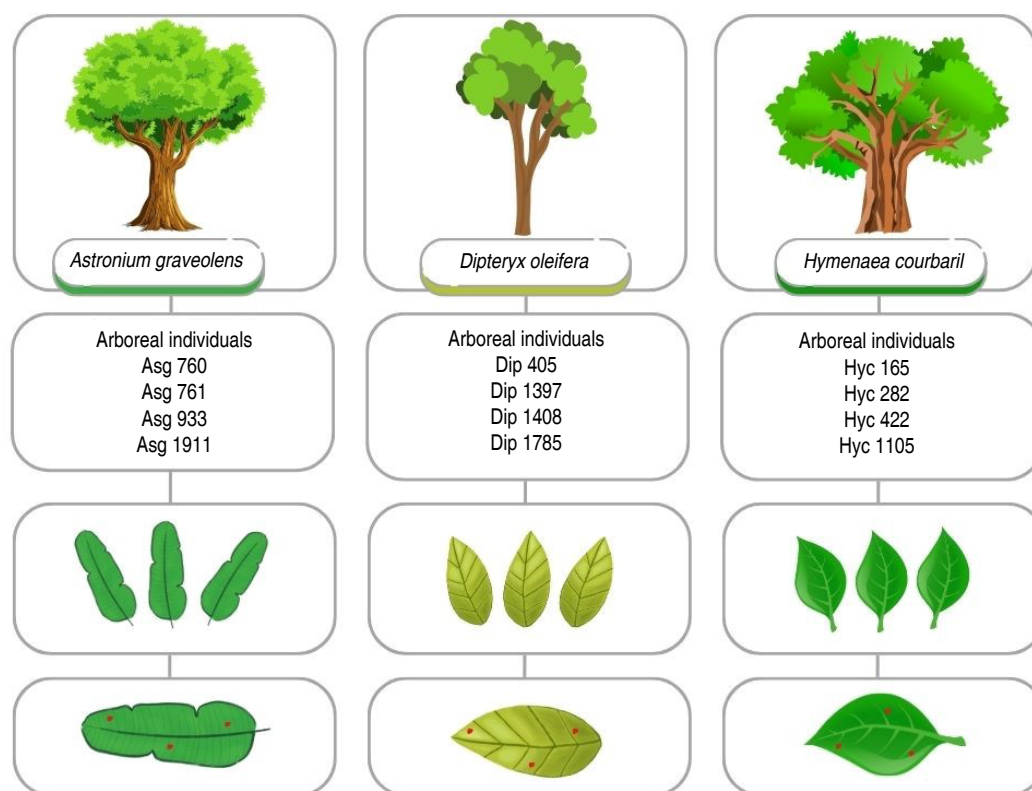


**Figure 3.** Experimental design for the acquisition of spectral signatures.

bags, with each bag bearing the abbreviation and code corresponding to the respective arboreal individual. The leaves were stored in these bags for approximately 2 h, until the leaf sampling was completed. Subsequently, the spectral measurements of the three species were taken *in situ* under uniform conditions.

### Spectral measurements

The spectroradiometer used in this study was the ASD FieldSpec HandHeld-2, a portable device that employs firmware for internal hardware management and desktop software for configuring data recording and processing. This instrument offers a high spectral resolution of 3 nm (interpolated to 1 nm) and a minimum scan time of 17 ms. Used to capture spectral signatures in the ultraviolet (UV) and near-infrared (NIR) regions, covering a wavelength range from 325 nm to 1,075 nm.

The approximate size of the leaves, excluding the petiole, ranged from 8 to 20 cm in length. For this reason, a field

of view (FOV) of approximately 14 cm in diameter was chosen by placing the sensor with a 25° optic at a distance of 30 cm from the nadir. In this way, the influence of surrounding materials on the spectral measurements of the leaves was reduced.

To ensure accuracy and account for any potential variation in solar radiation, the data were collected within a  $\pm 30$  min interval from solar noon. Three points on each leaf were scanned, evenly distributed, and perpendicular to the main rib of the leaf blade (Figure 3). For this purpose, a field spectroradiometer was used, calibrated every 15 min using the spectral signature of a 3.6" reference white panel, which exhibits nearly 100% reflectance across the electromagnetic spectrum.

The spectral signatures were collected on clear days in April when solar elevation angles ranged between 87 and 89°, which minimized the effects of atmospheric conditions and variations in the sun's position. To reduce

the influence of external factors, a matte black plastic material was utilized to absorb direct solar radiation from the wavelengths of the visible and near-infrared spectrum.

It is highlighted that the *D. oleifera* samples were in an early stage of senescence in April, which could have influenced their spectral characteristics. The senescence process can affect the cellular structure and chemical composition of leaves, altering their ability to reflect energy at different wavelengths. To ensure the validity of the comparison, spectral samples were collected under standardized conditions, and potential influences of the senescence state were considered in the analysis.

### Spectral characterization

The spectral records (a total of 36 records per species) were processed using spectral interpretation software. This software allowed for the calculation of the mean and standard deviation of these records. Subsequently, spectral signatures were plotted using the ggplot2 package in RStudio 1.1.463, covering a wavelength range between 400 and 900 nm of the electromagnetic spectrum.

### Extraction of optimal spectral bands

Considering previous research on the similarity in reflectance between contiguous bands and the advantages of using narrow bands, this study reduced the dataset by applying a simple averaging function every 10 nm. Originally, the data were distributed at 1 nm intervals between 400 and 900 nm. To obtain narrowbands every 10 nm, wavelengths were grouped into 10 nm ranges (for example, from 400 to 410 nm, from 410 to 420 nm, and so on). Within each of these ranges, the reflectance data were averaged to obtain the mean value of the corresponding narrowband, ranging from 405 to 895 nm. This process resulted in a reduced dataset where each narrowband represents an average reflectance within a specific wavelength interval.

To determine the appropriate statistical analysis for each species's reflectance patterns, an initial assessment of distribution normality and variance homogeneity was conducted. For datasets exhibiting normal distribution and homoscedasticity, analysis of variance (ANOVA) was applied. Conversely, datasets that showed deviation from normal distribution were subjected to the Mann-Whitney-Wilcoxon U Test. The statistical analyses were conducted using the base package in RStudio 1.1.463 software.

ANOVA is a statistical method used to assess the equality of population means. Specifically, a one-factor ANOVA is employed, which involves utilizing a single characteristic, referred to as the treatment or factor, to categorize the populations (Triola 2009). The primary aim of this test is to evaluate the null hypothesis, which states that the population means of the two groups of reflectance values are equal (Equation 1). This null hypothesis is then compared against the alternative hypothesis, which suggests a significant difference between the two population means (Equation 2).

$$H_0: \theta_{sp1} = \theta_{sp2} \quad (1)$$

$$H_0: \theta_{sp1} \neq \theta_{sp2} \quad (2)$$

Where  $\theta_{sp}$  is the mean reflectance of each tree species to be compared in each spectral band.

The test statistic used by ANOVA has a Snedecor F distribution (Equation 3). According to Triola (2009), the numerator of the F-statistic measures the variance between sample means  $\sigma_1^2$  and the denominator of the F-statistic depends on the variability within the samples  $\sigma_2^2$ :

$$F = \frac{\sigma_1^2}{\sigma_2^2} = \frac{\frac{SCR}{k}}{\frac{SCE}{n - k - 1}} \quad (3)$$

Where SCR is the sum of squares of the regression, SCE is the sum of squares of the residuals, n is the number of observations in the sample and k is the degrees of freedom.

The Mann-Whitney U test assesses whether two populations have different means or medians, especially with non-normal data (Yue and Wang 2002). The null hypothesis proposes that the means or medians are equal (Equation 1), while the alternative suggests they are different (Equation 2).

To conduct the Mann-Whitney U test, the two samples are merged, and the observations are arranged in ascending order from lowest to highest (Equation 4). According to Yue and Wang (2002), the U-test statistic can be computed using the following Equation:

$$U = \min \left\{ n_1 n_2 + \frac{n_1(n_1 + 1)}{2} - R_1, n_1 n_2 + \frac{n_2(n_2 + 1)}{2} - R_2 \right\} \quad (4)$$

Where  $n_1$  and  $n_2$  are the sizes of the two samples, and  $R_1$  and  $R_2$  correspond to the sum of each of the samples.

### Species discrimination algorithm

The supervised K-nearest neighbor (K-NN) classification method was employed on the dataset consisting of 108 records, which represents the total spectral records obtained from the combination of three points on every leaf, three leaflets, four individuals, and three forest species. These data were extracted from narrow bands that exhibited statistically significant differences ( $P < 0.05$ ) across all combinations of forest species. In this analysis, 70% of the data (76 records) were randomly selected as the training set, while the remaining 30% (32 records) were used for testing. The class package in RStudio 1.1.463 was utilized for data processing.

The K-NN (K-nearest neighbors) algorithm estimates the value of an unknown point based on similarity with neighboring points (Cover and Hart 1967). In this approach, the Euclidean distance between observations is calculated (Equation 5). According to Amat (2016), to ensure accurate estimates, it is necessary to normalize predictor values when their scales differ, as shown in Equation (6).

$$d(x_i, x_j) = \sqrt{\sum_{r=1}^p (x_{ri} - x_{rj})^2} \quad (5)$$

$$dN(x_i, x_j) = \frac{|x_{ri} - x_{rj}|}{\max(x_r) - \min(x_r)} \quad (6)$$

Where  $d$  is the Euclidean distance between the points  $x_i$  and  $x_j$  evaluated at the  $r$ -th input feature,  $\max(x_r)$  and  $\min(x_r)$  are the maximum and minimum values observed in the training set of  $x_r$ .

The K-nearest neighbor (K-NN) classification method classifies objects based on the number of neighboring observations, denoted as  $K$ . In this study,  $K$  is set to one, meaning that the category of an object is determined by the value of its nearest neighbor.

## RESULTS AND DISCUSSION

### Spectral signatures

Figure 4 displays the average leaf spectral signatures  $\pm$  standard deviation (S.D) of the forest species Diomate, Choibá, and Algarrobo within the wavelength range of 400 to 900 nm. This range corresponds to the visible (VIS, 400-700 nm) and near-infrared (NIR, 700-900 nm) regions of the electromagnetic spectrum.

Figure 4 presents the spectral characteristics of forest species, illustrating a distinctive pattern of low reflectance in the visible (VIS) range and high reflectance in the near-infrared (NIR) range. The spectral signatures showed an increase in reflectance within the green region (500-600 nm), peaking around the 555 nm band with average reflectance ranging from 14 to 31%. Additionally, there was a notable rise in reflectance from the visible (VIS) to the near-infrared (NIR) range, especially within the red edge position (REP) segment (680-730 nm), ranging from 9 to 16% at 680 nm and from 14 to 19% at 730 nm. In contrast, reflectance remained consistently high in the NIR range (730-900 nm) and tended to stabilize at longer wavelengths.

The spectral signature of *A. graveolens* (Figure 4A) showed low reflectance ( $<15\%$ ) in the ranges of 400-500 nm and 600-680 nm. The highest reflectance was observed in the visible region of the electromagnetic spectrum, specifically around the 553 nm band ( $18 \pm 3\%$ ). Reflectance sharply increased from the 685 nm band ( $16 \pm 3\%$ ) onwards, reaching its maximum in the near-infrared (NIR) region at the 765 nm band ( $34 \pm 4\%$ ), followed by a relatively stable trend.

The spectral signature of *D. oleifera* (Figure 4B) exhibited the highest average reflectance values among the three species. Reflectance in the 430-500 nm range was notably high and gradually increased until reaching its peak at the 554 nm band ( $31 \pm 10\%$ ). Subsequently, there was a significant decrease in reflectance until the 687 nm band ( $10 \pm 2\%$ ). In the red edge position (REP) segment (687-730 nm), reflectance showed an increasing trend with considerable variability before stabilizing at longer wavelengths.

The leaf spectrum of *H. courbaril* (Figure 4C) exhibited less variability in the visible (VIS) region compared to the other species. Reflectance in the 400-500 nm segment was low ( $<9\%$ ). It reached its maximum in the

green region, specifically in the 554 nm band ( $14\pm4\%$ ). It then showed a gradual increase in the 682 nm band and reached its peak in the near-infrared (NIR) region,

specifically in the 755 nm band ( $39\pm10\%$ ). From there, reflectance remained relatively constant until the 900 nm band.

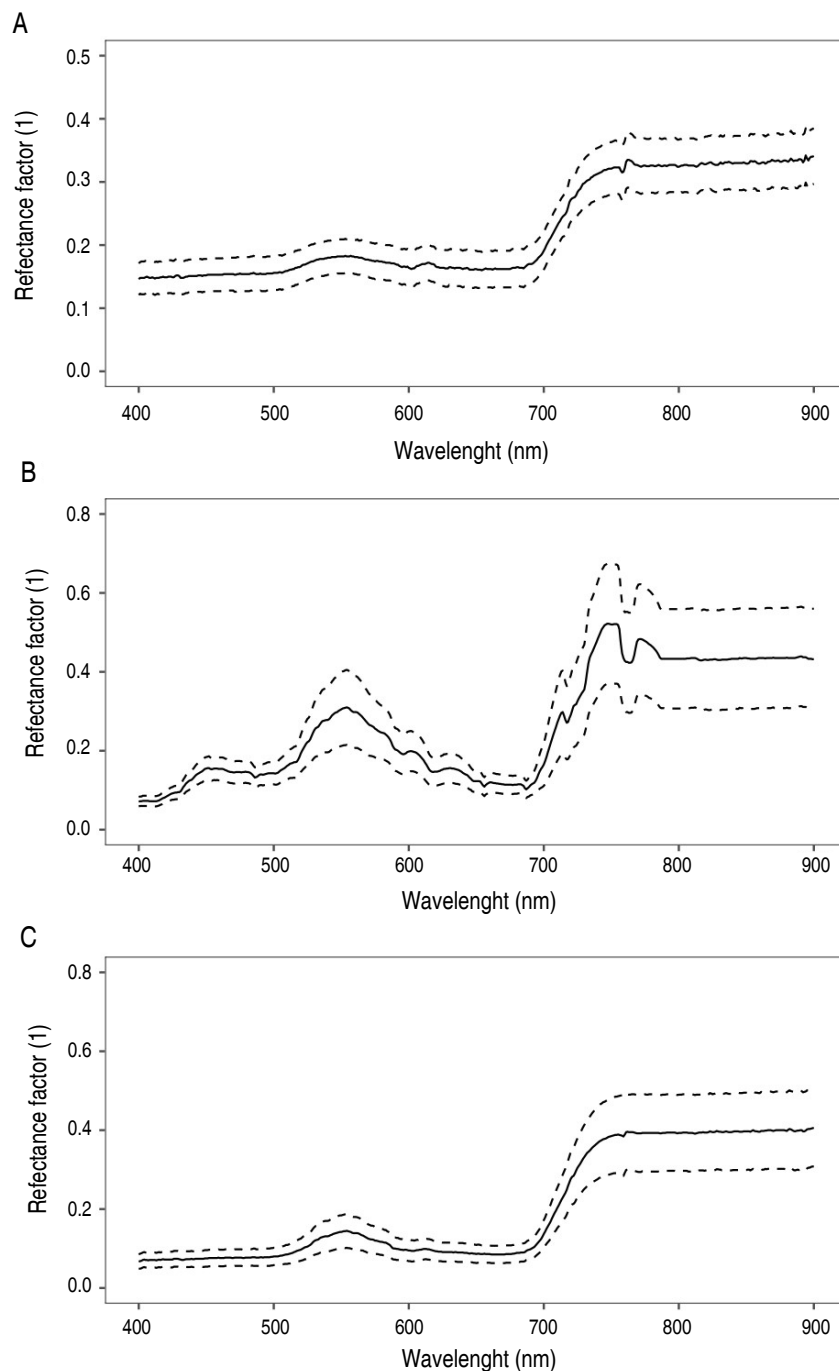


**Figure 4.** Leaf spectral signatures of mean reflectance (solid line) and standard deviation ( $\pm S.D.$ , dotted line) of A) *A. graveolens*, B) *D. oleifera*, and C) *H. courbaril*.

The results show a notable difference in average reflectance between the visible and near-infrared spectra of *D. oleifera* leaves compared to *H. courbaril* and *A. graveolens*. This variation is due to *D. oleifera* being in an early senescence stage in April when spectral records were taken. During this phase, deciduous trees typically exhibit changes in reflectance spectra, such as increases in the visible spectrum and decrease in the near-infrared spectrum (Clark et al. 2005). However, there have been no specific studies on the spectral variability of *D. oleifera* across different phenological stages.

*H. courbaril* and *A. graveolens* exhibited typical spectral signatures of healthy vegetation, characterized by low reflectance in the visible spectrum and high reflectance in the near-infrared spectrum. Despite a notable increase in reflectance from the red edge to the near-infrared, previous research confirms that *H. courbaril* and *A. graveolens* maintain low reflectance in the visible and near-infrared spectra (Papeş et al. 2013; Ferreira et al. 2016; Miyoshi et al. 2020). These findings highlight the consistency in the spectral response of these plant

species, suggesting that low reflectance in the visible and the near-infrared are useful distinctive characteristics for the identification and characterization of *H. courbaril* and *A. graveolens*.

The study showed minimal variation in reflectance for *H. courbaril* and *A. graveolens* compared to the spectral signatures reported for the tropical dry forest (Papeş et al. 2013; Ferreira et al. 2016; Miyoshi et al. 2020). It is important to note that the life zone, which includes environmental factors such as rainfall and temperature, influences the spectral response of species and physiological stress. However, in this experiment, the impact of this variable was not significant, as the spectral signatures obtained in the premontane rainforest were similar to those of the tropical dry forest.

### Spectral separability

Figure 5 shows the number of species pairs that can be distinguished from each other (Asg vs Dip, Asg vs Hyc, and Dip vs Hyc). Significant differences were found in most spectral bands among all species pairs, except for the bands centered at 715 and 725 nm, corresponding

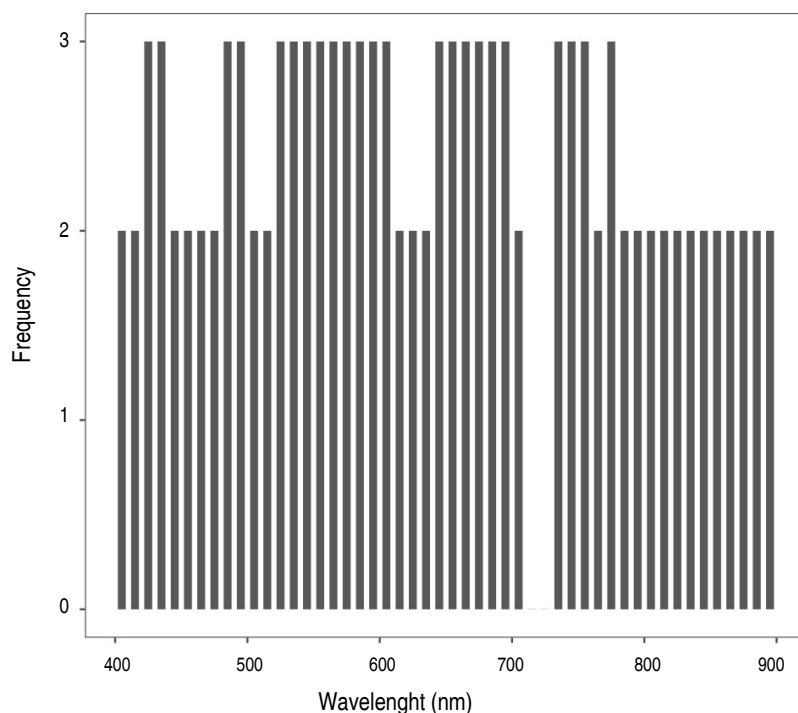


**Figure 5.** Frequency of occurrence of narrow bands with  $P < 0.05$ , according to U-test and ANOVA.



to the red edge position (REP). The analysis revealed that 23 narrow bands effectively classified all species combinations, 25 narrow bands differentiated between two pairs of species, and only two narrow bands were able to distinguish one or fewer pairs of species.

Table 2 shows the optimal narrow bands for distinguishing plant species. Within each pair of species, significant

variations were observed across a range of 33 to 48 narrow bands, demonstrating statistically significant differences ( $P < 0.05$ ). Notably, when comparing *A. graveolens* to *H. courbaril* and *A. graveolens* to *D. oleifera*, over 38 bands in the visible and near-infrared spectrum proved to be distinguishing factors. However, in the case of *D. oleifera* and *H. courbaril*, the disparity was limited to 33 bands primarily within the visible range.

**Table 2.** Potentially optimal narrow bands for the discrimination of each pair of plant species, identified using ANOVA and Mann-Whitney-Wilcoxon U test ( $P < 0.05$ ).

Pair of species	Narrow bands	
	Visible (400-700 nm)	NIR (701-900 nm)
Asg vs Dip	405, 415, 425, 435, 485, 495, 525, 535, 545, 555, 565, 575, 585, 595, 605, 645, 655, 665, 675, 685, 695	735, 745, 755, 765, 775, 785, 795, 805, 815, 825, 835, 845, 855, 865, 875, 885, 895
Asg vs Hyc	405, 415, 425, 435, 445, 455, 465, 475, 485, 495, 505, 515, 525, 535, 545, 555, 565, 575, 585, 595, 605, 615, 625, 635, 645, 655, 665, 675, 685, 695	705, 735, 745, 755, 765, 775, 785, 795, 805, 815, 825, 835, 845, 855, 865, 875, 885, 895
Dip vs Hyc	425, 435, 445, 455, 465, 475, 485, 495, 505, 515, 525, 535, 545, 555, 565, 575, 585, 595, 605, 615, 625, 635, 645, 655, 665, 675, 685, 695	705, 735, 745, 755, 775

Table 2 indicates that *A. graveolens* and *D. oleifera* exhibited moderate separability in the electromagnetic spectrum, with 38 out of 50 (76%) significant narrow bands. This differentiation was observed consistently across both the visible and near-infrared spectra. In the case of *A. graveolens* and *H. courbaril*, their spectral reflectance diverges in almost all narrow bands, except for the bands centered at 715 and 725 nm in the near-infrared range, as indicated in Table 2. The analysis revealed a high level of separability between these species, with 48 out of 50 (96%) bands effectively distinguishing them.

On the other hand, the spectral signatures of *D. oleifera* and *H. courbaril* showed lower separability compared to the other species pairs, with a total of 33 out of 50 (66%) significant narrow bands (Table 2). Additionally, the differentiation between these two species is slightly more fragmented and is predominantly limited to the visible spectrum (425-695 nm). According to Table 2, the separability between *A. graveolens* and *H. courbaril* shows a broader range of significant narrow bands, achieving 96% spectral differentiation. In contrast, the separability

between *D. oleifera* and *H. courbaril*, as well as between *A. graveolens* and *D. oleifera*, ranges from 66 to 76% of significant narrow bands. This pattern suggests that the early senescence stage of *D. oleifera* may have reduced the effectiveness of some narrow bands in distinguishing this species from others, affecting the overall interpretation of the spectral results.

Figure 6 shows the average reflectance curves and highlights the spectral regions (shaded areas) where the three pairs of species exhibit statistically significant differences. The analysis revealed that a total of 23 narrow bands contributed to the spectral separability of the three species. This study identified the most sensitive narrow bands for accurately identifying tree species, which were predominantly located in the blue (425, 435, 485, 495 nm), green (525, 535, 545, 555, 565, 575, 585, 595 nm), red (605, 645, 655, 665, 675, 685, 695 nm), and near-infrared (735, 745, 755, 775 nm) spectral regions.

In the study, five wavelengths matched the optimal bands recommended by Thenkabail et al. (2004) for 350 to

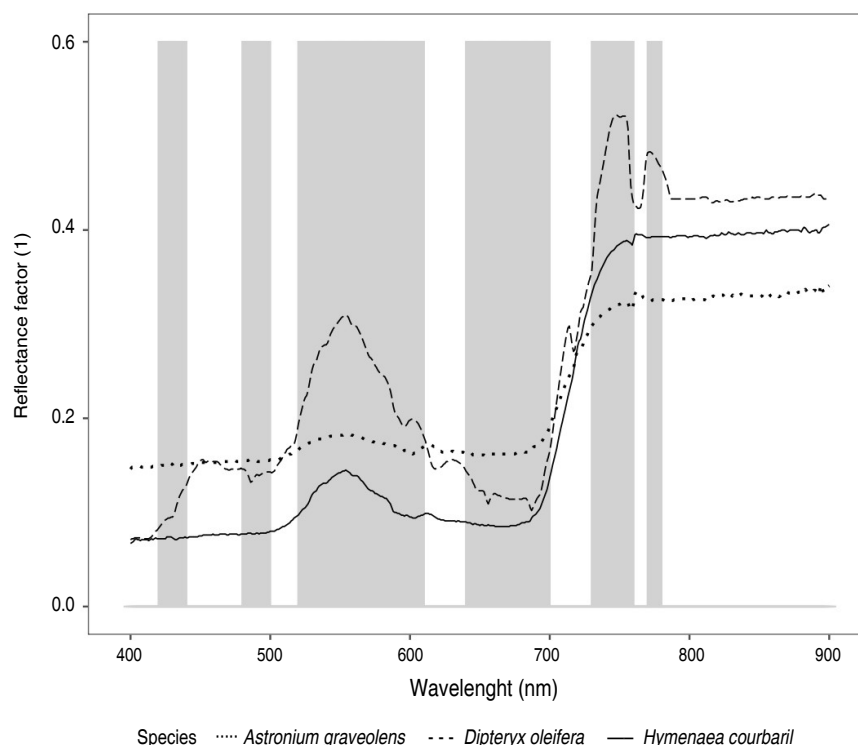


**Figure 6.** Distribution of the significant narrow bands (in gray) that best discriminate the three pairs of species, identified from ANOVA and the Mann Whitney - Wilcoxon U test, whose  $P < 0.05$ .

2,500 nm. Kumar et al. (2013) demonstrated the differentiation of tea plantations using bands in the blue, green, red, and near-infrared spectra. Zulfa et al. (2020) found that species in the Rhizophoraceae family were effectively discriminated against using the visible and mid-infrared spectra. These studies indicate that the best separation of plant species occurs in the green, red edge, and near-infrared regions. The presence of 14 out of the 23 selected bands in these segments highlights their importance for accurate discrimination.

### Spectral discrimination

The spectral classification was performed on the 23 narrow bands that exhibited statistically significant differences. The results of the K-NN test are presented in Table 3, which shows the confusion matrix. The rows represent the true class, while the columns indicate the classifier output. The total count and the corresponding accuracy percentage are provided at the end of each row.

**Table 3.** Confusion matrix obtained from the supervised K-NN classification of the three forest species *A. graveolens*, *D. oleifera*, and *H. courbaril*.

Species	<i>A. graveolens</i>	<i>D. oleifera</i>	<i>H. courbaril</i>	Total	Accuracy (%)
<i>A. graveolens</i>	12	0	0	12	100
<i>D. oleifera</i>	0	12	0	12	100
<i>H. courbaril</i>	1	0	7	8	88
<b>Total</b>				32	95.8

Furthermore, out of the eight data samples for *H. courbaril*, the classifier accurately classified seven instances, resulting in an 88% effectiveness. On average, the accuracy across

the test dataset reached 95.8%. These results highlight the exceptional accuracy achieved in discriminating between different species using the significant narrow bands.

Although KNN achieved perfect accuracy in identifying *D. oleifera*, differences during the early senescence stage of this species may have caused overlaps in the spectral signatures of other species. This overlap is reflected in the confusion matrix (Table 3), where the spectral signature of *H. courbaril* was incorrectly assigned to *A. graveolens*. This suggests that variations in the phenological state of the species can influence the model's accuracy, indicating the need to consider these factors to improve spectral differentiation between species.

In previous studies, Maxwell et al. (2018) used KNN to classify the Indian Pines dataset with an accuracy of 78.6 to 82.1%, which is lower than that of this study. In contrast, Castillo et al. (2008) achieved 100% accuracy when classifying Eucalyptus leaves using near-infrared spectroscopy, which is close to the 95.8% accuracy obtained in this study.

Research on the K-NN model in vegetation has tended to focus on disease detection and crop nutritional status, with a notable gap in its application for spectral discrimination of species in tropical forests. The K-NN model is valuable in this context for its ability to classify based on the spectral similarity between samples (Lu et al. 2017; Karadağ et al. 2020), which is particularly relevant in complex environments like tropical forests, where spectral variability is high and species differences are subtle.

The phenological state of *D. oleifera*, especially during the early senescence stages, is crucial for spectral data analysis. This phenomenon shows that the results are influenced both by the intrinsic characteristics of the species and its phenological state. Therefore, it is essential to consider this factor in future studies to improve the accuracy of classification and interpretation of spectral data.

This research suggests that spectroradiometry is highly useful for species classification, as it allows capturing fine details of leaf reflectance. Despite the challenges associated with the time and resources required for data acquisition in tropical environments, its application remains essential for advancing the understanding of biodiversity and the functioning of tropical ecosystems.

## CONCLUSION

The findings suggest that the leaves of *A. graveolens* and *H. courbaril* were in good physiological condition since they exhibited a spectral pattern characterized by low reflectance in the visible spectrum and high reflectance in the near-infrared spectrum. However, the leaves of *D. oleifera* showed changes in their reflectance spectrum, as they were in the early stages of leaf senescence. At an interspecific level, significant variations in leaf reflectance were observed across different wavelengths, which were crucial for identifying specific narrow bands in the blue (425, 435, 485-495 nm), green (525-595 nm), red (605, 645-695 nm), and near-infrared (735-775 nm) regions. These bands proved ideal for the accurate classification of the studied species, as validated by the K-NN algorithm achieving a classification accuracy of 95.8%. For future studies, it is recommended to consider the phenology of species in the acquisition of spectral data. The study provides valuable information in the field of remote sensing by demonstrating the effective use of hyperspectral data to classify forest species and highlights the need to consider phenological states in spectral studies. These approaches have practical implications for biodiversity monitoring, conservation efforts, and ecological research in tropical forest environments.

## ACKNOWLEDGMENTS

We extend our gratitude to the Geomatics laboratory of the Facultad de Ciencias Agrarias at the Universidad Nacional de Colombia, Medellín Headquarters, for generously providing us with the FieldSpec HandHeld 2 device and offering us access to their facilities during the challenging period of COVID-19 confinement. We would also like to express our appreciation to Rodrigo Betancur, the operator of the Vivero Universidad Nacional, for his valuable assistance in collecting foliar samples.

## REFERENCES

- Aggarwal S (2004) Earth resources satellites. pp 39–65. In: Sivakumar MVK, Roy PS, Harmsen K and Saha SK. (eds.). Satellite remote sensing and GIS applications in agricultural meteorology. World Meteorological Organization, Dehra Dun. 44 p.
- Amat J (2016) Comparación entre Regresión Logística, Linear Discriminant Analysis (LDA), Quadratic Discriminant Analysis (QDA) y K-Nearest-Neighbors. In: RPubS. [https://rpubs.com/Joaquin\\_AR/236130](https://rpubs.com/Joaquin_AR/236130)
- Bachman S (2023) *Hymenaea courbaril*. In: IUCN - Red list of threatened species. <https://www.iucnredlist.org/es/species/19891869/68101847>
- Cárdenas D and Salinas R (2007) Libro rojo de plantas de Colombia. SINCHI - Instituto Amazónico de Investigaciones Científicas, Bogotá.

75-78 p. [https://sinchi.org.co/files/publicaciones/publicaciones/pdf/LR\\_MADERABLES.pdf](https://sinchi.org.co/files/publicaciones/publicaciones/pdf/LR_MADERABLES.pdf)

Castillo R, Contreras D, Freer J et al (2008) Supervised pattern recognition techniques for classification of *Eucalyptus* species from leaves NIR spectra. Journal of the Chilean Chemical Society 53: 1709–1713. <https://doi.org/10.4067/S0717-97072008000400016>

Castro-Esau KL, Sánchez-Azofeifa, Rivard B et al (2006) Variability in leaf optical properties of mesoamerican trees and the potential for species classification. American Journal of Botany 93: 517–530. <https://doi.org/10.3732/ajb.93.4.517>

Clark ML and Roberts DA (2012) Species-level differences in hyperspectral metrics among tropical rainforest trees as determined by a tree-based classifier. Remote Sensing 4: 1820–1855. <https://doi.org/10.3390/rs4061820>

Clark ML, Roberts DA and Clark DB (2005) Hyperspectral discrimination of tropical rain forest tree species at leaf to crown scales. Remote Sensing of Environment 96: 375 – 398. <https://doi.org/10.1016/j.rse.2005.03.009>

Cogollo A, Castrillón J and Vélez L (2004) Manejo *in situ* y *ex situ* del Almendro (*Dipteryx oleífera* Benth) como base para un modelo de uso sostenible de productos vegetales no maderables en la región del Bajo Cauca antioqueño. Jardín Botánico de Medellín Joaquín Antonio Uribe, Medellín. 11 p.

Cover T and Hart P (1967) Nearest neighbor pattern classification. IEEE Transactions on Information Theory 13: 21–27. <https://doi.org/10.1109/TIT.1967.1053964>

Féret JB and Asner GP (2011) Spectroscopic classification of tropical forest species using radiative transfer modeling. Remote Sensing of Environment 115: 2415–2422. <https://doi.org/10.1016/j.rse.2011.05.004>

Ferreira MP, Zortea M, Zanotta DC et al (2016) Mapping tree species in tropical seasonal semi-deciduous forests with hyperspectral and multispectral data. Remote Sensing of Environment 179: 66–78. <https://doi.org/10.1016/j.rse.2016.03.021>

Gómez M and Toro J (2008) Manejo de las semillas y la propagación de diez especies forestales del bosque seco tropical. First edition. CORANTIOQUIA - Corporación Autónoma Regional del Centro de Antioquia, Medellín. 5-43 p. <http://hdl.handle.net/20.500.12324/1106>

IDEAM - Instituto de Hidrología, Meteorología y Estudios Ambientales de Colombia (2010) Promedios climatológicos 1981-210. In: Tiempo y Clima. <http://www.ideam.gov.co/web/tiempo-y-clima/clima>

Karadağ K, Tenekeci ME, Taşaltın R and Bilgili A (2020) Detection of pepper fusarium disease using machine learning algorithms based on spectral reflectance. Sustainable Computing Informatics and Systems 28: 1-8. <https://doi.org/10.1016/j.suscom.2019.01.001>

Kumar A, Manjunath K, Meenakshi et al (2013) Field hyperspectral data analysis for discriminating spectral behavior of tea plantations under various management practices. International Journal of Applied

Earth Observation and Geoinformation 23: 352–359. <https://doi.org/10.1016/j.jag.2012.10.006>

Lu J, Ehsani R, Shi Y et al (2017) Field detection of anthracnose crown rot in strawberry using spectroscopy technology. Computers and Electronics in Agriculture 135: 289–299. <https://doi.org/10.1016/j.compag.2017.01.017>

Machuca K, Martínez E and Samain M (2022) *Astronium graveolens*. In: IUCN - Red List of Threatened Species. <https://www.iucnredlist.org/es/species/61530992/61531208>

Maxwell AE, Warner TA and Fang F (2018) Implementation of machine-learning classification in remote sensing: An applied review. International Journal of Remote Sensing 39: 2784–2817. <https://doi.org/10.1080/01431161.2018.1433343>

Miyoshi G, Imai N, Tommaselli AM and Honkavaara E (2020) Spectral differences of tree species belonging to Atlantic forest obtained from UAV hyperspectral images. Remote Sensing and Spatial Information Sciences 49–54. <https://doi.org/10.1109/LAGIRS48042.2020.9165616>

Nalepa J (2021) Recent advances in multi-and hyperspectral image analysis. Sensors 21: 1-7. <https://doi.org/10.3390/s21186002>

O'Shaughnessy SA and Rush C (2014) Precision agriculture: irrigation. Encyclopedia of Agriculture and Food Systems 4: 521–535. <https://doi.org/10.1016/B978-0-444-52512-3.00235-7>

Papeş M, Tupayachi R, Martínez P et al (2013) Seasonal variation in spectral signatures of five genera of rainforest trees. Journal of Selected Topics in Applied Earth Observations and Remote Sensing 6: 339–350. <https://doi.org/10.1109/JSTARS.2012.2228468>

Prasad K and Gnanappazham L (2014) Species discrimination of mangroves using derivative spectral analysis. Remote Sensing and Spatial Information Sciences 2: 45–52. <https://doi.org/10.5194/isprsannals-ii-8-45-2014>

Rasaiah BA, Jones SD, Bellman C and Malthus TJ (2014) Critical metadata for spectroscopy field campaigns. Remote Sensing 6: 3662–3680. <https://doi.org/10.3390/rs6053662>

Thenkabail P, Enclona E, Ashton M and Van Der Meer B (2004) Accuracy assessments of hyperspectral waveband performance for vegetation analysis applications. Remote Sensing of Environment Journal 91: 354–376. <https://doi.org/10.1016/j.rse.2004.03.013>

Triola M (2009) Estadística. Tenth edition. Pearson Educación, México. 634–673 p.

Yue S and Wang C (2002) The influence of serial correlation on the Mann–Whitney test for detecting a shift in median. Advances in Water Resources 25: 325–333. [https://doi.org/10.1016/S0309-1708\(01\)00049-5](https://doi.org/10.1016/S0309-1708(01)00049-5)

Zulfa AW, Norizah K, Hamdan O et al (2020) Discriminating tree species from the relationship between spectral reflectance and chlorophyll contents of mangrove forest in Malaysia. Ecological Indicators 111: 1-9. <https://doi.org/10.1016/j.ecolind.2019.106024>





## ÍNDICE DE AUTORES

- Adam Mahmoud Saad.** Promoting food security and sustainability with a transportable indirect evaporative solar pre-cooler. 77(3): 10865-10876. 2024.
- Almaguer-Vargas Gustavo.** Sulfuric acid as a germination stimulator in forage soybean seeds (*Neonotonia wightii*). Vol. 77(3): 10833-10838. 2024.
- Alzate-Marin Estefany Johana.** Leaf spectrum analysis of three tropical timber species: Diomate (*Astronium graveolens*), Choibá (*Dipteryx oleífera*), and Algarrobo (*Hymenaea courbaril*) 77(3): 10907-10919. 2024
- Barraza-Jáuregui Gabriela del Carmen.** Artificial neural networks in the retention of anthocyanins and total phenolics in the osmotic pre-treatment of Biloxi variety blueberry (*Vaccinium corymbosum* L.) jam. 77(3): 10877-10885. 2024.
- Cadena-Chamorro Edith.** Enzymatic biocatalysis processes on the semicrystalline and morphological order of native cassava starches (*Manihot esculenta*). Vol. 77(3): 10839-10852. 2024.
- Casariogo Año Alicia.** Coating of oxidized banana starch and olive oil for the preservation of cherry tomatoes (*Solanum lycopersicum* cv. Cerasiforme). 77(3): 10853-10864. 2024
- Castañeda-Vildozola Álvaro.** Sulfuric acid as a germination stimulator in forage soybean seeds (*Neonotonia wightii*). Vol. 77(3): 10833-10838. 2024.
- Cedeño Sares Luis A.** Coating of oxidized banana starch and olive oil for the preservation of cherry tomatoes (*Solanum lycopersicum* cv. Cerasiforme). 77(3): 10853-10864. 2024
- Ciro-Velásquez Héctor.** Enzymatic biocatalysis processes on the semicrystalline and morphological order of native cassava starches (*Manihot esculenta*). Vol. 77(3): 10839-10852. 2024.
- Cruz-Castillo Juan Guillermo.** Sulfuric acid as a germination stimulator in forage soybean seeds (*Neonotonia wightii*). Vol. 77(3): 10833-10838. 2024.
- Figuerola-Flórez Jorge.** Enzymatic biocatalysis processes on the semicrystalline and morphological order of native cassava starches (*Manihot esculenta*). Vol. 77(3): 10839-10852. 2024.
- García Pérez Mario A.** Coating of oxidized banana starch and olive oil for the preservation of cherry tomatoes (*Solanum lycopersicum* cv. Cerasiforme). 77(3): 10853-10864. 2024
- Giraud Nicolle.** Broiler feed proposal with vinasse. 77(3): 10899-10905. 2024.
- Guerra-Ramírez Diana.** Sulfuric acid as a germination stimulator in forage soybean seeds (*Neonotonia wightii*). Vol. 77(3): 10833-10838. 2024.
- Huamán Vela María.** Influence of indole-butyric acid and substrate type on vegetative propagation of native Peruvian blueberry (*Vaccinium* sp.). Vol. 77(3): 10827-10832. 2024.
- Jumbo-Peña Ney D.** Coating of oxidized banana starch and olive oil for the preservation of cherry tomatoes (*Solanum lycopersicum* cv. Cerasiforme). 77(3): 10853-10864. 2024
- Lizarazo-Forero Luz Marina.** First report of bacteria associated with soft rot in yellow pitahaya (*Selenicereus megalanthus* haw.) in Colombia crops. Vol. Vol. 77(3): 10797-10809. 2024.
- Machuca Román Jennifer V.** Coating of oxidized banana starch and olive oil for the preservation of cherry tomatoes (*Solanum lycopersicum* cv. Cerasiforme). 77(3): 10853-10864. 2024
- Mahmoud Elkaoud Nabil Shaban.** Promoting food security and sustainability with a transportable indirect evaporative solar pre-cooler. 77(3): 10865-10876. 2024.
- Mahmoud Ragab Kassem.** Promoting food security and sustainability with a transportable indirect evaporative solar pre-cooler. 77(3): 10865-10876. 2024.
- Másmela-Mendoza Julián Esteban.** First report of bacteria associated with soft rot in yellow pitahaya (*Selenicereus megalanthus* haw.) in Colombia crops. Vol. Vol. 77(3): 10797-10809. 2024.
- Minchón Medina Carlos Alberto.** Artificial neural networks in the retention of anthocyanins and total phenolics in the osmotic pre-treatment of Biloxi variety blueberry (*Vaccinium corymbosum* L.) jam. 77(3): 10877-10885. 2024.
- Noreña-Grisales Jorge Mario.** Soil quality indicators related to the deterioration of Kikuyu grass *Cenchrus clandestinus* (Hochst. ex Chiov.) Morrone. Vol. 77(3): 10811-10825. 2024.
- Obregón Domínguez Jesús Alfredo.** Artificial neural networks in the retention of anthocyanins and total phenolics in the osmotic pre-treatment of Biloxi variety blueberry (*Vaccinium corymbosum* L.) jam. 77(3): 10877-10885. 2024.
- Ordoñez Elizabeth S.** Starch from *Colocasia esculenta* (L.) Schott of purple and white esculenta varieties: Thermal, technological properties, and morphological study. 77(3): 10887-10897. 2024.
- Osorio Vega Nelson Walter.** Soil quality indicators related to the deterioration of Kikuyu grass *Cenchrus clandestinus* (Hochst. ex Chiov.) Morrone. Vol. 77(3): 10811-10825. 2024.
- Ramírez Pisco Ramiro.** Soil quality indicators related to the deterioration of Kikuyu grass *Cenchrus clandestinus* (Hochst. ex Chiov.) Morrone. Vol. 77(3): 10811-10825. 2024.
- Reategui Darlym.** Starch from *Colocasia esculenta* (L.) Schott of purple and white esculenta varieties: Thermal, technological properties, and morphological study. 77(3): 10887-10897. 2024.
- Reina-García Jhusua David.** Sulfuric acid as a germination stimulator in forage soybean seeds (*Neonotonia wightii*). Vol. 77(3): 10833-10838. 2024.

---

---

**Rodríguez María Alejandra.** Broiler feed proposal with vinasse. 77(3): 10899-10905. 2024.

**Soria Iturri Melchor.** Starch from *Colocasia esculenta* (L.) Schott of purple and white esculenta varieties: Thermal, technological properties, and morphological study. 77(3): 10887-10897. 2024.

**Rodríguez-Sandoval Eduardo.** Enzymatic biocatalysis processes on the semicrystalline and morphological order of native cassava starches (*Manihot esculenta*). Vol. 77(3): 10839-10852. 2024.

**Suárez-Gómez July Andrea.** Leaf spectrum analysis of three tropical timber species: Diomate (*Astronium graveolens*), Choibá (*Dipteryx oleifera*), and Algarrobo (*Hymenaea courbaril*) 77(3): 10907-10919. 2024

**Salcedo-Mendoza Jairo.** Enzymatic biocatalysis processes on the semicrystalline and morphological order of native cassava starches (*Manihot esculenta*). Vol. 77(3): 10839-10852. 2024.

**Tarabye Hassan Hafiz.** Promoting food security and sustainability with a transportable indirect evaporative solar pre-cooler. 77(3): 10865-10876. 2024.

**Sanchez-Santillan Tito.** Influence of indole-butyric acid and substrate type on vegetative propagation of native Peruvian blueberry (*Vaccinium* sp.). Vol. 77(3): 10827-10832. 2024.

**Toro-Restrepo Luis Jairo.** Leaf spectrum analysis of three tropical timber species: Diomate (*Astronium graveolens*), Choibá (*Dipteryx oleifera*), and Algarrobo (*Hymenaea courbaril*) 77(3): 10907-10919. 2024

**Santillan-Culquimboz Henry.** Influence of indole-butyric acid and substrate type on vegetative propagation of native Peruvian blueberry (*Vaccinium* sp.). Vol. 77(3): 10827-10832. 2024.

**Trujillo-Ccanahuire José.** Starch from *Colocasia esculenta* (L.) Schott of purple and white esculenta varieties: Thermal, technological properties, and morphological study. 77(3): 10887-10897. 2024.

**Serna-Fadul Tiana.** Enzymatic biocatalysis processes on the semicrystalline and morphological order of native cassava starches (*Manihot esculenta*). Vol. 77(3): 10839-10852. 2024.

---

---